Experimental and numerical characterizations of the hydro-mechanical behavior of a heterogeneous material : pellet/powder bentonite mixture

Agustin Molinero Guerra

Thèse présentée pour obtenir le grade de

Docteur de l'Université Paris-Est

Spécialité : Géotechnique

par

Agustín Molinero Guerra

Ecole Doctorale : SCIENCES, INGENIERIE ET ENVIRONNEMENT

Caractérisations expérimentale et numérique du comportement hydro-mécanique d'un matériau hétérogène : mélange de poudre/pellets de bentonite

JURY

Mr Philippe Cosenza	*Président*	Université de Poitiers
Mr Sebastià Olivella	*Rapporteur*	Universitat Politècnica de Catalunya
Mr Olivier Cuisinier	*Rapporteur*	Université de Lorraine
Mr Maarten Van Geet	*Examinateur*	Organisme national des déchets radioactifs et des matières fissiles enrichies
Mme Nadia Mokni	*Examinateur*	Institut de Radioprotection et de Sûreté Nucléaire
Mr Pierre Delage	*Examinateur*	Ecole des Ponts ParisTech
Mr Frédéric Bernier	*Invité*	Agence Fédérale de Contrôle Nucléaire
Mr Patrick Aimedieu	*Invité*	Centre National de la Recherche Scientifique
Mr Yu-Jun Cui	*Directeur de thèse*	Ecole des Ponts ParisTech

Thèse présentée pour obtenir le grade de

Docteur de l'Université Paris-Est

Spécialité : Géotechnique

par

Agustín Molinero Guerra

Ecole Doctorale : SCIENCES, INGENIERIE ET ENVIRONNEMENT

Caractérisations expérimentale et numérique du comportement hydro-mécanique d'un matériau hétérogène : mélange de poudre/pellets de bentonite

JURY

Mr Philippe Cosenza	*Président*	Université de Poitiers
Mr Sebastià Olivella	*Rapporteur*	Universitat Politècnica de Catalunya
Mr Olivier Cuisinier	*Rapporteur*	Université de Lorraine
Mr Maarten Van Geet	*Examinateur*	Organisme national des déchets radioactifs et des matières fissiles enrichies
Mme Nadia Mokni	*Examinateur*	Institut de Radioprotection et de Sûreté Nucléaire
Mr Pierre Delage	*Examinateur*	Ecole des Ponts ParisTech
Mr Frédéric Bernier	*Invité*	Agence Fédérale de Contrôle Nucléaire
Mr Patrick Aimedieu	*Invité*	Centre National de la Recherche Scientifique
Mr Yu-Jun Cui	*Directeur de thèse*	Ecole des Ponts ParisTech

Dissertation presented for the degree of

Doctor of University of Paris-Est

Specialty: Géotechnique

by

Agustín Molinero Guerra

Doctoral school: Science, Engineering and Environment

Experimental and numerical characterizations of the hydro-mechanical behavior of a heterogeneous material: pellet/powder bentonite mixture

REVIEWERS

Mr Philippe Cosenza	Université de Poitiers
Mr Sebastià Olivella	Universitat Politècnica de Catalunya
Mr Olivier Cuisinier	Université de Lorraine
Mr Maarten Van Geet	Organisme national des déchets radioactifs et des matières fissiles enrichies
Mrs Nadia Mokni	Institut de Radioprotection et de Sûreté Nucléaire
Mr Pierre Delage	Ecole des Ponts ParisTech
Mr Frédéric Bernier	Agence Fédérale de Contrôle Nucléaire
Mr Patrick Aimedieu	Centre National de la Recherche Scientifique
Mr Yu-Jun Cui	Ecole des Ponts ParisTech

Ce travail de thèse a été réalisé dans le cadre d'une collaboration entre l'Ecole des Ponts ParisTech (ENPC), l'Institut de Radioprotection et de Sûreté Nucléaire (IRSN) et l'Agence Fédérale de Contrôle Nucléaire (AFCN).

The presented PhD work has been carried out in the framework of a collaboration between Ecole des Ponts ParisTech (ENPC), the French Institute for Radiation Protection and Nuclear Safety (IRSN) and Agence Fédérale de Contrôle Nucléaire (AFCN), in Belgium.

REMERCIEMENTS

RESUME

Cette thèse porte sur le comportement hydromécanique d'un mélange de poudre et pellets de bentonite MX80 avec une proportion 80/20 en masse sèche. Il s'agit d'un matériau étudié par l'Institut de Radioprotection et de Sûreté Nucléaire (IRSN) dans le cadre du projet SEALEX qui a pour objectif principal la vérification de l'efficacité des dispositifs de scellement ou des barrières ouvragées dans le system du stockage géologique des déchets radioactifs. Le comportement hydromécanique du matériau à différentes échelles a été étudié par différents essais en laboratoire. Premièrement, les changements à l'échelle microstructurale d'un seul pellet de bentonite durant l'hydratation a été abordé à l'aide de deux techniques : la porosimétrie au mercure et la tomographie aux rayons-X. Les résultats ont montré que le gonflement d'un pellet peut être expliqué par deux mécanismes : la création des fissures surtout à des succion entre 38 et 9 MPa, et le gonflement des grains de bentonite, correspondant à l'hydratation des smectites à l'échelle nano. A des succions inférieures à 9 MPa, une diminution de l'épaisseur des feuillets d'argile et une augmentation du désordre des ceux-ci sont observées. Des essais de rétention d'eau, de pression de gonflement et de compression à l'oedomètres à succion contrôlée ont été effectués sur le mélange de poudre et pellets. Les propriétés de rétention d'eau sous conditions de volume constant et pour un seul pellet sous conditions de gonflement libre apparaissent similaires pour des valeurs de succion supérieures à 4 MPa. Cela implique que la succion physico-chimique est prédominante devant la succion capillaire. Pour des valeurs de succions plus basses, une capacité de rétention plus faible a été observée sous conditions de volume constant, à relier à la disparition des macro-pores par le gonflement des grains de bentonite. Des valeurs de pression de préconsolidation plus petites que celles des mélanges de bentonite pure ont été obtenues pour des succions non-nulles, montrant l'effet granulaire des pellets dans le mélange. Deux colonnes d'infiltration ont été réalisés afin d'étudier deux cas extrêmes avec une densité sèche globale identique ($1.49\ Mg/m^3$). Avec la première colonne, un mélange de poudre et pellets relativement homogène, fabriqué en suivant un protocole spécial a été étudié. En revanche, un mélange fortement hétérogène a été fabriqué dans la deuxième colonne d'infiltration. Les résultats montrent que la pression de gonflement radiale dépend fortement de la distribution des pellets et de la poudre ainsi que de l'évolution du front d'hydratation. Une anisotropie de gonflement a été observée dans les deux cas, avec la pression de gonflement axiale inférieure à celle radiale. De plus, la valeur finale de pression de gonflement axiale est différente pour les deux colonnes, bien que les deux échantillons aient fabriquées avec la même densité sèche globale. En parallèle, plusieurs observations à la

tomographie aux rayons-X ont été réalisées sur le mélange de pellets et poudre pendant l'hydratation. Un mélange complètement homogène a été observé après 100 jours d'hydratation à l'échelle étudiée (50 µm/voxel). Un nouveau modèle d'endommagement qui prend en compte des fissures observées au sein du pellet pendant hydratation a été développé en adaptant le Barcelona Expansive Model (BExM). L'essai d'infiltration sur l'échantillon relativement homogène a été simulé avec succès en utilisant le modèle développé. L'hétérogénéité initiale de la porosité a été aussi considérée dans la simulation afin de reproduire l'anisotropie de gonflement.

Les résultats expérimentaux obtenus dans le cadre de cette étude permettent de mieux comprendre la réponse des ouvrages de scellement avec le mélange de pellets et poudre de bentonite dans le projet SEALEX. De plus, le modèle développé, qui prend en compte des fissures observées au sein du pellet et l'hétérogénéité initiale du matériau, permettra d'améliorer la prévision du comportement hydromécanique des ouvrages avec ce type de mélanges.

Mots clés : mélange de poudre/pellets de bentonite, observations microstructurales, essais oedométriques, colonnes d'infiltration, modélisation.

ABSTRACT

The present investigation deals with the hydro-mechanical behavior of a mixture composed of pellets and powder of MX80 bentonite with a proportion of 80/20 in dry mass. This is one of the studied materials by the French Institute for Radiation protection and Nuclear Safety (IRSN) within the SEALEX project, which aims at investigating the long-term performance of swelling clay-based sealing systems in the context of geological high-level radioactive waste disposal. This study has been conducted by following an experimental program covering different scales. Firstly, the microstructure changes while wetting of a single pellet was investigated by combining MIP results with µ-CT observations. Results revealed that swelling of a pellet is due to the development of cracks, with significant development between 38 and 9 MPa of suction, combined to swelling of bentonite grains, which is governed by the hydration mechanisms of smectite at nano-scale. The application of suctions below 9 MPa leads to a significant decrease of the platelet thickness and to an increase in the disorder of the platelet assembly. Water retention tests, swelling pressure tests and suction controlled oedometer tests on the pellet/powder mixture were performed. Similar water retention properties were observed for the mixture under constant-volume condition and pellet under free swelling condition under suctions higher than 4 MPa, suggesting that physico-chemical suction prevails on capillary suction. At lower suctions, constant-volume condition defined a lower water retention capacity because of the disappearance of macro-pores. Lower yield stress values than the common pure bentonite mixtures were found for the pellet/powder mixture for non-zero suctions, showing that the volume change behavior is governed by the rearrangement and crushing of pellets, and the loss of the granular structure in the case of zero suction. Two mock-up tests were performed, aiming at studying two extreme cases at a global dry density of 1.49 Mg/m^3: a homogeneous pellet/powder mixture fabricated by following a special protocol, and a strong heterogeneous sample. Results revealed that the radial swelling pressure depends strongly on the local pellet/powder distribution combined with the evolution of the hydration front. An anisotropy swelling was found in both cases, being the axial swelling pressure lower than the radial one. Moreover, different values of axial pressure were found between the two tests, even though they have the same global dry density of samples. In parallel, µ-CT observations were carried out on the mixture while wetting, revealing a homogeneous sealed sample after 100 days of hydration. No density gradients were identified at the investigated resolution (50 µm/voxel) after this long time of hydration. A new damage model, which takes into account the development of fissures within a pellet while wetting, was proposed an included to the well-

known double porosity Barcelona Expansive Model (BExM) to carry out numerical simulations of one mock-up test. The initial heterogeneous porosity distribution was also considered to reproduce the anisotropy swelling.

The experimental results obtained in this study will greatly help well understand the response of seals made up of pellets/powder bentonite mixture in the SEALEX *in situ* experiment. Moreover, the constitutive model developed taking into account the pellet cracking damage and the initial sample heterogeneity allows significantly improving the prediction of hydomechanical behavior of seals/plugs made up of this mixture, constituting thus an useful tool for the safety assessment of the nuclear waste disposal system.

Key words: pellet/powder bentonite mixture, microstructural observations, oedometer tests, mock-up tests, numerical modelling.

PUBLICATIONS

Journal Papers

1. Molinero-Guerra, A., Mokni, N., Delage, P., Cui, Y. J., Tang, A. M., Aimedieu, P., Bernier, F., Bornert, M., (2016). In-depth characterisation of a mixture composed of powder/pellets MX80 bentonite. Applied Clay Science (135), 538 – 546.

2. Molinero-Guerra, A., Delage, P., Mokni, N., Cui, Y. J., Tang, A. M., Aimedieu, P., Bernier, F., Bornert, M., (2017). Water retention properties and microstructure changes of a bentonite pellet upon wetting/drying; application to radioactive waste disposal. Submitted to Géotechnique.

3. Molinero-Guerra, A., Cui, Y.J., He, Y., Delage, P., Mokni, N., Tang, A. M., Aimedieu, P., Bornert, M., Bernier, F., (2018). Characterization of water retention, compressibility and swelling properties of a pellet/powder bentonite mixture. Submitted to Engineering Geology.

4. Molinero-Guerra, A., Cui, Y.J., Delage, P., Mokni, N., Tang, A. M., Aimedieu, P., Bernier, F., Bornert, M., (2018). Investigation of the hydro-mechanical behavior of a pellet/powder MX80 bentonite mixture using an infiltration column. Engineering Geology (243), 18 - 25.

5. Molinero-Guerra, A., Aimedieu, P., Bornert, M., Cui, Y.J., Tang, A. M., Sun, Z., Mokni, N., Delage, P., Bernier, F., (2018). Analyses of the structural changes of a pellet/powder bentonite mixture upon wetting by X-ray computed microtomography. Applied Clay Science (165), 164 - 169.

6. Molinero-Guerra, A., Mokni, N., Cui, Y.J., Delage, P., Tang, A. M., Aimedieu, P., Bernier, F., Bornert, M., (2018). Impact of initial heterogeneity on long term swelling behavior of MX80 bentonite pellet/powder mixtures. Submitted to Canadian Geotechnical Journal.

7. Mokni, N., Molinero-Guerra, A., Cui, Y.J., Delage, P., Aimedieu, P., Bornert, M. and Tang, A.M., (2018). Modelling the long term hydro-mechanical behavior of a bentonite pellet/powder mixture with consideration of initial structural heterogeneities. Submitted to Géotechnique.

Conference communications

1. Molinero-Guerra, A., Mokni, N., Delage, P., Cui, Y. J., Tang, A. M., Aimedieu, P., Bernier, F., Bornert, M., (2016). Experimental and digital characterizations of the hydro-mechanical behavior of a heterogeneous material, powder/pellets bentonite mixture. PhD conference on Radioactive Waste Management and Geological Disposal. Delft – Netherlands. (Poster).

2. Molinero-Guerra, A., Mokni, N., Delage, P., Cui, Y. J., Tang, A. M., Aimedieu, P., Bernier, F., Bornert, M., (2017). In-depth characterization of the hydro-mechanical behavior of a mixture composed of pellets/powder MX80 bentonite. Proceedings of Pan-An UNSAT 2017, Dallas – US.

3. Molinero-Guerra, A., Mokni, N., Delage, P., Cui, Y. J., Tang, A. M., Aimedieu, P., Bernier, F., Bornert, M., (2018). Experimental characterizations of the hydro-mechanical behavior of a pellet/powder bentonite mixture. Proceedings of UNSAT 2018, Hong Kong – China.

4. Molinero-Guerra, A., Cui, Y. J., Delage, P., Aimedieu, P., Bernier, F., Bornert, M., Mokni, N., Tang, A. M., (2018). Digital characterizations of the swelling behavior of a pellet/powder bentonite mixture. Clay Conference 2017, Davos – Switzerland. (Poster).

CONTENTS

Introduction

INTRODUCTION

Context

Nuclear energy is used in many fields, as electricity production by nuclear power plants, nuclear medicine and scientific research, among others. From these activities, wastes are inevitably generated, which can be classified into different categories depending on their activity levels and the half-life period of their radioactive isotopes (IAEA, 2009). Among these wastes, High-level (HLW) and intermediate-level (ILW) ones are the most adverse to human-being and environment. Therefore, the safe long-term storage of these wastes has become an important issue for nuclear energy industry and government in many countries.

Deep geological disposal is considered as the most propitious solution for safe storage of high-level and intermediate-level wastes in many countries (OECD/NEA, 1995; NEA, 2008). Depending on the country, different configurations are considered (Sellin and Leupin, 2013). In France, the concept is based on the multi-barrier system consisting of the natural barrier (host rock) and the engineered barriers (waste container, buffer and sealing elements).

In many countries such as France, Sweden, Spain and Switzerland, bentonite-based materials are considered as the most appropriate materials for the sealing elements. These bentonite-based materials have been selected due to their favorable properties for ensuring the safety of the disposal, as follows (Pusch, 1979; Yong *et al.*, 1986; Villar and Lloret, 2008):

(i) High swelling capacity: the bentonite seal, initially unsaturated, will be subjected to hydration from the surrounding saturated host rock. While wetting, it will swell and fill the technological gaps between the engineered barrier and the host rock. Swelling pressures will be developed once in contact with the host rock. As a result, fractures and the excavation damaged zone will be sealed. Moreover, preferential pathways will be significantly reduced.

(ii) Low permeability: the radionuclides migration will be delayed thanks to the pretty low permeability of the seal. Furthermore, water flow will be limited from the host rock to the canister, which will retard the corrosion of the canister.

(iii) High retention capacities: this property, together with the low permeability, will limit the release of radionuclides to the biomass.

A number of laboratory studies has been conducted to investigate the hydro-mechanical behavior of compacted bentonite-based materials (e.g. Delage *et al.*, 1998; Lloret *et al.*, 2003; Agus and Schanz, 2005; Romero *et al.*, 2005; Lloret and Villar, 2007; Wang *et al.*, 2013; Saba

et al., 2014). Various experiments were also performed in underground research laboratories (URL) such as FEBEX at Grimsel (Switzerland), RESEAL at Mol (Belgium), KEY at Bure (France). However, few works have been conducted to investigate the effects of initial heterogeneity and microstructure evolution on the hydro-mechanical behavior of seal, particularly in the case of use of pellets.

In this context, the French Institute for Radiological Protection and Nuclear Safety (IRSN) has launched the SEALEX (SEALing performance EXperiments) project, within which this work has been undertaken. It consists on a series of *in situ* experiments emplaced in IRSN's Underground Research Laboratory (URL) in Tournemire, located in a Mesozoic sedimentary basin on the western edge of the French Causses (south of France) (Mokni and Barnichon, 2016; Mokni, 2016; Mokni *et al.*, 2016). This project focuses on the long-term performance of the sealing systems. Specifically, the project aims (i) to test the long-term hydraulic performance of sealing systems in normal conditions for different core compositions (mixtures made up bentonite pellets with bentonite powder or sand/bentonite mixtures) and for different configurations (precompacted bentonite blocks or *in situ* compacted bentonite), (ii) to quantify the impact of construction joints (namely technological voids also) on the hydraulic properties of the sealing system, (iii) to investigate the long term homogenisation of bentonite-based seals and, (iv) to test the robustness of seals in altered scenarios, such as a decrease of swelling pressure due to the failure of the confining plugs. To install the experiments, horizontal boreholes ($0 \pm 2°$), with a 60 cm diameter and 540 cm long were prepared by excavation from recent drift (Mokni *et al.*, 2016). Each experiments consists of a bentonite-based core mechanically confined at both ends and artificially hydrated by water injection through hydration systems installed at both ends of the core. The present investigation focuses on the mixtures made up of MX80 bentonite powder and pellets with a proportion of 20/80 in dry mass.

Problematics and objectives of the investigation

Once the unsaturated pellet/powder mixture is installed in the repository, the material will be subjected to coupled hydro-mechanical loadings. Initially, the mixture is emplaced in the repository at its hygroscopic water content under constant-volume conditions. While wetting, one of the primary functions of bentonite is to seal voids created during the construction of the barrier and the inter-pellet voids within the mixture. At the same time, the progressive saturation results in the development of swelling pressures. Obviously, during the saturation process, the soil macrostructure will not stop to evolve, leading to a long-term evolution of the hydro-

2

mechanical behavior of the material, which is crucial issue in the assessment of the safety of whole disposal system.

It is well known that the swelling pressure depends on the dry density of the material (Imber and Villar, 2006). As a consequence, a change in density significantly influences the swelling pressure. Previous studies revealed that there is a well-defined relationship between the swelling pressure and the dry density of bentonite (Börgesson *et al*., 1996; Dixon *et al*., 1996; Lloret *et al*., 2003; Karnland *et al*., 2008; Gens *et al*., 2011; Villar *et al*., 2012; Wang *et al*., 2013; Saba *et al*., 2014; Schanz & Al-Badran, 2014). This implies that a uniform distribution of swelling pressure is equivalent to a uniform dry density. Thereby, the evolution of microstructure in terms of dry density can be monitored through the measurements of swelling pressure in different position of the bentonite-based material.

The process of homogenization under saturation can be take long time. For instance, the Engineered Barrier emplacement experiment (EB) in which two types of bentonite with different dry densities were emplaced (blocks and pellets), some heterogeneities in terms of dry density and water content distribution were observed after almost ten years of hydration (Wieszorek *et al*., 2017).

As the macroscopic behavior of bentonite-based materials is closely related to their microstructure (e.g. Alonso *et al*., 2011; Gens and Alonso, 1992). Several investigations have been performed on the microstructure of these materials by different methods, including Mercury Intrusion Porosimetry (MIP) and/or Scanning Electron Microscopy (SEM) (Wang *et al*., 2012, 2013, 2014; Saba *et al*., 2014a, 2014b; Romero *et al*., 2011). The hydration mechanisms of the smectite minerals and the evolution of interlayer porosity were also analysed (e.g. Saiyouri *et al*., 1998; Villar *et al*., 2007; Bestel *et al*., 2013). However, there is a few available data on pellets and powder/pellets mixtures. Hoffmann *et al*. (2007) performed MIP tests on samples of pellets of FEBEX bentonite under different conditions and observed a multimodal distribution of a single pellet. For a pellet/powder distribution, a trimodal distribution was identified.

The techniques described previously require a preliminary dehydration of the samples, which is commonly carried out by freeze-drying. Moreover, they provide local observations of the investigated specimens. Results given by these techniques could be complemented by the use of X-ray computed microtomography (µ-CT) observations, which allows investigating the long term homogenization of the mixture. Van Geet *et al*. (2005) performed µ-CT observations to

3

investigate the significant changes and homogenisation process of a 50/50 pellet/powder mixture during hydration. From a qualitative analysis, the sample was found to be homogeneous at the end of the saturation process. For the pellet/power mixture considered in this study, considering the large-size of inter-pellets pores, the µ-CT observation technique seems particular promising in visualizing the evolution of microstructure in the course of saturation.

This thesis was motivated by the challenging task of better understanding and modelling the long-term hydro-mechanical behavior of a 80/20 pellet/powder bentonite mixture. The main objectives include:

- At a microscopic scale, the understanding of the swelling behavior and structural changes of the material during the saturation process. To this end, MIP tests combined with µ-CT observations were carried out on a single pellet of bentonite while wetting. For the pellet/powder mixture, a special PMMA (Polymethyl methacrylate) cell was designed in order to perform µ-CT observations of the mixture with monitoring of axial swelling pressure during the saturation process. Two extreme cases were investigated with the same global dry density: a homogeneous 80/20 pellet/powder mixture and a heterogeneous case. The results obtained allowed examination of the density gradients evolution which corresponds to the homogenisation process.

- At a macroscopic scale, the swelling, compressibility and water retention properties of the pellet/powder mixture were investigated by means of a series of laboratory tests. The water retention curves of a single pellet of bentonite hydrated under free swelling conditions as well as the pellet/powder mixture under constant volume conditions were determined. The hydro-mechanical behavior of the mixture was investigated through two mock-up tests, which represent the SEALEX *in situ* tests at a scale 1/10. Special attention was paid to the effect of initial structural heterogeneities induced by the installation processes on the hydromechanical behavior of the mixture. To this end, two different mixtures were also investigated (a homogeneous and a heterogeneous case). Emphasis was put on the anisotropy swelling behavior.

- The results from laboratory tests were compared with some results from the SEALEX *in situ* experiments, allowing the effects of test conditions and test scales to be assessed.

- A hydro-mechanical model was developed to describe the mechanical behavior identified experimentally. The model takes into account the multimodal nature of the porous network of the mixture, which governs the global hydro-mechanical behavior. This aspect has been described in several existing constitutive models (e.g. Gens &

Alonso, 1992, Alonso *et al.* 1999, Sanchez *et al.* 2005, Gens *et al.*, 2011, Alonso *et al*, 2011) for double structure materials. In this work, the model includes the initial heterogeneous distribution and transient microstructural features characterizing the high density bentonite pellets. The proposed model has been outlined and applied to describe the results from the mock-up of SEALEX test. The long term behavior of the mixture has been also predicted.

Outline of the thesis

The results of this work have allowed seven journal articles to be published/submitted. The dissertation is organized with these articles in their original form within five chapters.

The first chapter presents, firstly, the microstructure of the pellet/powder mixture at its initial state before hydration. Pore size distribution curves (PSD) of both pellet and powder of bentonite are presented, together with µ-CT observations of a single pellet of bentonite at its initial state. Moreover, µ-CT observations were performed on the pellet/powder mixture in order to characterize its initial heterogeneous distribution, which is responsible of its multimodal porous network and complex HM behavior. A special protocol was stablished for preparing representative pellet/powder mixtures. Secondly, the water retention properties and swelling behavior of a single pellet of bentonite was investigated. To this end, several MIP results combined with µ-CT observations of a single pellet of bentonite submitted to different suctions were analysed. The water retention curve under free swelling conditions was presented and changes of void ratio, water content and degree of saturation with suction were analysed.

The second chapter is devoted to the swelling, compressibility and water retention properties of the pellet/powder mixture. The swelling pressure and potential of the material was studied with different techniques. Suction controlled oedometer tests were performed in order to investigate the compressibility properties. Finally, the water retention curve under constant-volume conditions was obtained; to this end, a special device was designed which allows vapor exchanges in all directions, accelerating the hydration process.

The third chapter is devoted to physical modeling, aiming at investigating the complex hydro-mechanical behavior of the pellet/powder mixture. Two mock-up tests of the SEALEX *in situ* experiments were performed. Two different samples were studied, representing two extreme cases: a homogeneous 80/20 pellet/powder distribution and a heterogeneous sample. In parallel, µ-CT observations were performed on two samples fabricated by following the same protocol as that used for the mock-up tests. The structural changes while wetting the mixtures were

investigated by both qualitative and quantitative observations. Finally, the results were compared to those from the SEALEX *in situ* experiments.

The fourth chapter presents the development of a coupled HM model which allows for the multimodal porous network of the mixture, as well as the initial heterogeneity of the material and transient microstructural features characterizing the bentonite pellets. This model was validated based on the experimental results from the mock-up test.

Chapter 1

Microstructural characterization of the pellet/powder mixture

INTRODUCTION

Several investigations have been carried out on the microstructure of bentonite-based materials by using several methods including Mercury Intrusion Porosimetry (MIP) and/or Scanning Electron Microscopy (SEM) (Wang *et al.*, 2012, 2013, 2014; Saba *et al.*, 2014; Romero *et al.*, 2011). These techniques require a preliminary dehydration of the samples, often carried out by freeze-drying. Due to the size of the sample investigated, these techniques provide local observations of a part of millimetric samples. These results may fruitfully be complemented by the use of X-ray computed microtomography (µ-CT), a non-destructive 3D technique that provides high-resolution observations of samples at a larger scale without any pre-treatment.

This chapter deals, firstly, with an experimental program aiming to study the microstructural features of a pellet/powder mixture at various scales by using µ-CT observations coupled to MIP and SEM investigations. A special protocol was stablished in order to obtain a representative pellet/powder bentonite mixture, to be used later to design mock-up tests in the laboratory, which simulate the SEALEX *in situ* tests at a reduced scale (1/10). Then, the water retention properties and microstructure changes of a bentonite pellet under wetting/drying paths were investigated. The changes in microstructure of the samples submitted to various controlled suctions by means of the vapor control technique were studied by MIP tests and complemented X-ray µCT observations.

The first part of this chapter was published in "Applied Clay Science"; the article is presented here in its original version. The second part was submitted to "Géotechnique".

In-depth characterisation of a mixture composed of powder/pellets MX80 bentonite

Agustín Molinero Guerra[1,2], Nadia Mokni[2], Pierre Delage[1], Yu-Jun Cui[1], Anh Minh Tang[1], Patrick Aimedieu[1], Frédéric Bernier[3], Michel Bornert[1]

[1]Ecole des Ponts ParisTech, Laboratoire Navier, Marne la Vallée, France
[2]Institut de Radioprotection et de Sûreté Nucléaire (IRSN), Fontenay-aux-Roses, France
[3]Agence Fédérale de Contrôle Nucléaire (AFCN), Belgique

Abstract: Mixtures made up of bentonite powder and pellets are a possible candidate for making sealing plugs used in deep radioactive waste disposal due to their low permeability, high swelling capacity, favourable properties with respect to radionuclide retention and operational advantages in terms of placement *in situ*, that is much easier than that of pre-compacted bricks of bentonite/sand mixture. It is therefore essential to better understand their hydro-mechanical behavior to optimize the design of the repository. In this context, the French Institute for Radiation Protection and Nuclear Safety (IRSN) has launched the SEALEX project (SEALing performance EXperiments) in which this work has been conducted.

Once the initially heterogeneous unsaturated powder/pellet (80/20) MX80 bentonite mixture is put in place, these sealing materials will be subject to coupled hydro-mechanical loadings: hydration due to the infiltration of pore water from the natural barrier and mechanical confinement resulting from the engineered barriers. The present work focuses on the different scales of the material: at the macroscopic scale, it is characterized by a heterogeneous distribution of pellets and powder of bentonite; at the microscopic scale, it is studied by several techniques (MIP, µ-CT observations and SEM). From MIP results, a typical bimodal distribution was found for both pellet and powder. From µ-CT and SEM observations, a heterogeneity was revealed in the internal structure of the pellet: heterogeneous density distribution of the clay minerals and presence of several high density elements.

Keywords: heterogeneous pellet/powder bentonite mixture; sealing plug; radioactive waste disposal; microstructure; mercury intrusion porosimetry; X-ray computed microtomography; scanning electron microscopy.

1. Introduction

In the French concept of deep geological disposal for High Level and Intermediate Level Long Lived radioactive Wastes (HLW & ILLLW), the wastes are emplaced within large diameter boreholes (HLW) and galleries (ILLLW) excavated at great depths in a low-permeability host-rock (Callovo-Oxfordian argillite, ANDRA, 2005). Sealing of theses underground works to

10

prevent potential pathways for water, gas and radionuclides migration is one of the key points to ensure the long-term safety of the repository.

Mixtures made up of bentonite powder and pellets are a candidate sealing material for deep underground radioactive waste repositories. In addition to their low permeability, high swelling capacity and high radionuclide migration retardation properties, powder/pellet mixtures have obvious operational advantages in terms of emplacement and reduction of the gaps between the rock and the seal. Once installed in the repository, powder/pellet mixtures will be submitted to coupled hydro-mechanical loadings comprising hydration due to the infiltration of pore water from the host rock and mechanical confinement resulting from the constrained volume condition imposed in the galleries. It is therefore essential to better understand their hydro-mechanical behavior when assessing the overall repository safety.

In this context, and as part of the overall IRSN (French Institute for Radiological Protection and Nuclear Safety) R&D program that provides scientific background for its expertise on disposal safety, the SEALEX (SEALing performance Experiments) project was launched to specifically focus on long-term performance of sealing systems. The SEALEX project is dedicated (i) to test the long-term hydraulic performance of sealing systems in normal conditions for different core compositions (mixtures composed of bentonite pellets with bentonite powder or of sand with bentonite powder) and for different configurations (pre-compacted bentonite blocks or bentonite compacted *in situ*), (ii) to quantify the impact of construction joints (also called technological voids) on the hydraulic properties of the sealing system, and (iii) investigate the concept of robustness by considering altered scenarios, such as an incidental decrease of the swelling pressure (for instance originating from the failure of the confining plugs). This project relies on a series of *in situ* experiments emplaced in IRSN´s Underground Research Laboratory (URL) at Tournemire located in a Mesozoic sedimentary basin on the western edge of the French Causses (South France) (Mokni & Barnichon., 2016). To install the experiments, horizontal boreholes ($0 \pm 2°$), with a 60 cm diameter and 540 cm long have been excavated from recent drifts (2008). Each experiment consists of a bentonite-based core mechanically confined at both ends corresponding to a generic seal mock-up except in terms of saturation that will be an artificial one carried out by water injection through porous filters installed at both ends of the core (Barnichon *et al*., 2012; Mokni & Barnichon., 2016). Various materials are being considered as seals in the SEALEX project. The present work focuses on a mixture made up of MX80 bentonite powder and pellets with a proportion of 20/80 in dry mass.

The use of high-density bentonite pellets combined with bentonite powder has also been proposed in Salo & Kukkola (1989), Dereeper *et al*. (2001), Ab (2002). A characterisation of the fundamental properties of the MX80 bentonite pellets used in the Prototype Repository test is reported in Sugita *et al*. (2005). At a larger scale, a series of infiltration tests on a 50/50% FoCa bentonite pellet/powder mixture compacted at different dry densities were performed by Imbert & Villar (2006) to investigate the swelling capacity of the material.

It is well documented that the macroscopic behavior of expansive soils is related to its microstructure (e.g. Alonso *et al*., 2011; Gens & Alonso, 1992). For this reason, several investigations have been carried out on the microstructure of bentonite-based materials by using several methods including Mercury Intrusion Porosimetry (MIP) and/or Scanning Electron Microscopy (SEM) (Wang *et al*., 2012, 2013, 2014; Saba *et al*., 2014; Romero *et al*., 2011). There is less available data on pellets and powder-pellets mixtures. Hoffmann (2005) carried out MIP tests on samples of pellets of FEBEX bentonite under different conditions and observed a bimodal distribution on a single pellet with a dry unit mass $\rho_d = 1.95$ Mg/m^3. For a non-compacted pellet mixture, a trimodal distribution was identified with two populations of pores corresponding to the intra and inter-aggregate pores and the third one related to the inter-pellet pores.

The microstructure investigation techniques require a preliminary dehydration of the samples, often carried out by freeze-drying. Due to the size of the sample investigated, these techniques provide local observations of a part of millimetric samples. These results may fruitfully be complemented by the use of X-ray computed microtomography (µ-CT), a non-destructive 3D technique that provides high-resolution observations of samples at a larger scale without any pre-treatment. The changes in microfabric during hydration under constant volume conditions of a 50/50 pellet/powder mixture of FoCa clay at a dry unit weight of 1.36 Mg/m^3 were observed by Van Geet *et al*. (2005) using µ-CT. The significant changes of the pellet/powder mixture during hydration could be observed but the technique did not allow investigating the microstructure of an elementary pellet itself because the resolution of the images obtained was not enough in order to study the material at this scale.

This paper deals with an experimental program aiming to study the microstructural features of a pellet/powder mixture at various scales by using µ-CT observations coupled to MIP and SEM investigations. This mixture will afterwards be used to develop a mock-up test in the laboratory,

to simulate SEALEX *in situ* tests at reduced scale (1/10) by considering a column of 60 mm in diameter and 120 mm in height.

2. Materials and methods

2.1. Materials

The materials investigated are on the one hand the basic pellet made of MX80 bentonite and on the other hand a mixture of MX80 bentonite powder and pellets at a proportion of 20/80 in dry mass (Figure 1). The bentonite used comes from Wyoming, USA, and was provided by the Laviosa-MPC company under the commercial name Expangel (Expangel SP7 for pellets and Expangel SP32 for the powder). To make things clear, the name MX80 will however be used here. The MX80 bentonite has a high smectite content (80%) with some inclusions of non-clayey minerals (see Table 1) and a cation exchange capacity (CEC) of 98 meq/100g. The major exchangeable cation is Na^+, with a value of 52 meq/100g (Table 2). The liquid limit is 560%, the plastic limit is 53% and the unit mass is of 2.77 Mg/m^3 (Saba *et al*., 2014, Table 3).
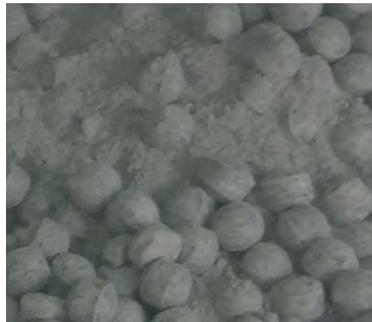
Figure 1. Mixture of MX80 bentonite powder and pellets with a proportion of 20/80 in dry mass.

Table 1. Results from the X-ray diffractometer (XRD) of the MX80 bentonite. The results are expressed as a percent of the total mass (Laviosa Minerals SpA)

Mineral	% of the total mass
Pyrite	<1%
Smectite	80%
Albite	2%
Anorthite	8%
Quartz	4%
Muscovite	4%

Table 2. Cation exchange capacity (CEC) and original exchangeable cations of the MX80 bentonite (Laviosa Minerals SpA)

Property	
CEC Capacity	*98 meq/100g*
Na conversion	52 meq/100g
K conversion	1.2 meq/100g
Mg conversion	10 meq/100g
Ca conversion	37 meq/100g

Pellets were industrially produced in Laviosa-MPC company by instantaneously compacting a powder of MX80 bentonite in a mould of 7 mm of diameter and 7 mm of height (Laviosa Minerals). The fabrication was done at water content w = 5% - 7% and at dry unit mass ρ_d = 1.998 Mg/m^3 - 2.12 Mg/m^3. Pellets were received in packages of 25 kg and stored in the laboratory at 20°C. The pellet initial suction was measured in the laboratory with a chilled mirror dew point tensiometer (Decagon WP4), providing a value s = 132.4 MPa at initial water content w = 7.25% (determined after drying in the oven at 105°C during 24h). More details about the initial properties of the pellets and the powder are presented in Table 3.

Figure 2 shows a typical pellet with a radius of 7.14 mm and a height of 7.27 mm. It appears that the pellet has a quasi-cylindrical shape with two spherical poles on top and bottom. The lengths measured in the laboratory were larger than those just after the fabrication (7 mm), indicating swelling due to hydration in the course of storage. Indeed, higher water contents (7.25% - 6.69%) were measured on pellets located at the top of the bucket stored in the laboratory, compared to that located at the bottom (6.06% - 6.00%).
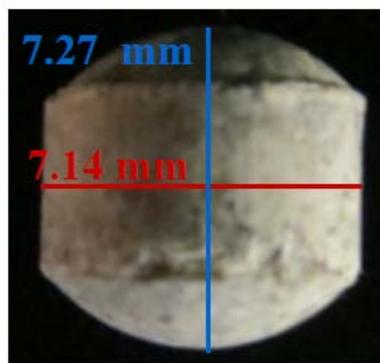
Figure 2. Pellet of bentonite at initial state. Dry unit mass ρ_d = 2.12 Mg/m^3.

The MX80 bentonite powder was produced by crushing pellets. The characteristics at initial state is presented in Table 3 and Table 4. Compared to the fabrication value of water content (between 5% and 7%), a value of 3.17% was found in the laboratory (after drying at 105°C for 24h) corresponding to an initial suction $s = 190.9$ MPa, measured with a chilled mirror dew point tensiometer (Decagon WP4). The grain size distribution of the powder, obtained by dry sieving is presented in Figure 3 together with the size of a pellet. The average diameter is $D_{50} = 0.65$ mm.
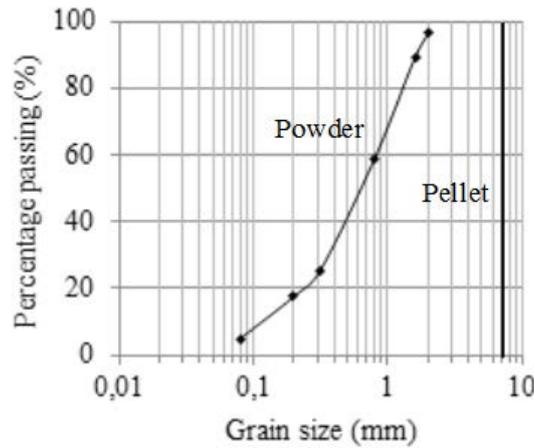
Figure 3. Grain size distribution of the MX80 bentonite powder.

Table 3. Initial properties and conditions of pellets and powder of bentonite

	Pellet	*Powder*
Initial suction, s_0	132.4 MPa	190.9 MPa
Initial water content, w_0	7.25%	3.17%
Initial dry density, ρ_0	2.12 Mg/m^3	
Initial porosity, φ_0	0.25	
Unit mass of bentonite particles, ρ_s*	2.77 Mg/m^3	

*(Saba *et al.*, 2014)

Table 4. Properties of powder of MX80 bentonite.

Atterberg limits	
Liquid limit, LL	560%
Plasticity limit, PL	62%
Shrinkage index, SI	498%

2.2. Testing procedures

Mercury intrusion porosimetry (MIP)

The pore size distribution of both pellet and powder of MX80 bentonite was obtained on freeze dried samples using an Autopore IV 9500 mercury intrusion porosimeter (Micromeritics) that operates at a maximum pressure of 230 MPa. Instantaneous freezing was carried out by plunging small samples (a pellet of bentonite) in slush nitrogen (-210°C) obtained by previously submitting it to vacuum (Delage *et al.*, 1996). In such conditions, there is no nitrogen boiling around the samples when plunging them into nitrogen, resulting in an optimized quick freezing and good microstructure preservation. The pore size distribution was obtained assuming parallel, cylindrical nonintersecting pores of different radii, using the Autopore IV 9500 V1.09 standard software package. The total void ratio was obtained by standard methods and compared to the total volume of mercury intruded into the sample at a pressure of 230 MPa.

X-ray computed microtomography (µ-CT)

The µ-CT scans were carried out using an "Ultratom" microtomograph (RX Solutions, France). Images were reconstructed using the software Xact (RX Solutions). The source is a microfocus X-ray tube Hamamatsu L10801 and the imager is a Paxscan Varian 2520V (1960x1536 square pixels 127µm in size).

Several µ-CT observations were carried out on a pellet of bentonite at initial state and on the powder/pellet MX80 bentonite mixture with a proportion of 80/20 in dry mass. For a single pellet of bentonite, the X-ray source parameters were 80 kV and 40 µA; the voxel size was 4.4 µm. The samples were scanned using 1440 projections equally spread on 360°. After reconstruction, 1292 horizontal slices were calculated (16bit images; 1644x1292 pixels). For the powder/pellet mixture, the X-ray source parameters were 100 kV and 25 µA; the voxel size was 59 µm. The mixture was scanned using 2880 projections in helical mode and after reconstruction 2472 horizontal slices were obtained (16 bit images, 1735x1735 pixels).

Scanning electron microscopy (SEM) and Energy-Dispersive X-ray spectroscopy (EDS)

SEM combined to EDS was performed in order to carry out a chemical characterization of a pellet of bentonite at initial state. Instantaneous freezing was carried out by plunging the samples in slush nitrogen (-210°C). After freeze-drying, the pellet of bentonite was carefully cut at mid-height, separating the upper and the lower poles. Once cut, the specimens were immersed into a resin and polished with abrasive papers with decreasing fineness from grade

800 to 4000 in order to obtain a smooth surface. Finally, the samples were metallized under vacuum with gold and palladium. Observations in conventional SEM require a high vacuum condition to allow a precise focusing of the incident electrons on the sample and to prevent the emitted electrons from interacting with the atmosphere.

2.3.   The pellet/bentonite mixture

Two SEALEX performance tests with core made of MX80 bentonite powder/pellets (20/80) have been installed in Tournemire URL, in February and October 2013, to investigate the impact of core composition and conditioning on the long term performance of sealing systems. To ensure the feasibility of injecting within a large diameter and compacting *in situ* a seal made of pellet/powder mixture so as to obtain a reasonably homogeneous core with the target dry unit mass of 1.49 Mg/m^3, a series of preliminary full scale mock up tests were carried out using a plastic tube with transparent windows to allow the observation of the distribution of the mixture within the emplacement borehole. The bentonite was introduced by means of an auger conveyor measuring 5 m in length and 60 mm in outer diameter. The auger measures 50 mm in diameter and is driven by a 1.5 kW geared motor. The tube features a loading hoper and has a flanged connection in its midpoint, so that despite its length it can be easily mounted in the gallery with its back end already inserted in the borehole, as the auger inside is flexible.

It is however important to prepare an homogeneous powder/pellet MX80 bentonite mixture at the required target dry unit mass (1.49 Mg/m^3) because the dry unit mass governs both the saturated permeability (k_w) and the swelling pressure of the mixture (Saba *et al*., 2014; Hoffmann *et al*., 2007). In this study, the challenge was to obtain a reasonably homogeneous powder/pellet mixture to be placed in a reduced scale mock-up test of the SEALEX *in situ* tests. This mock-up test is planned to be carried out at a scale of 1/10 of the SEALEX tests, corresponding to a cylinder of 60 mm in diameter and 120 mm in height.

Three protocols were considered aiming at identifying the one that provides the best homogeneity. The first protocol consisted in filling the cell by packets corresponding to one layer of pellets spread over the base of the 60 mm diameter cylinder and by adding the corresponding amount of powder (80% pellets and 20% powder). The second protocol was comparable but involved two layers of pellets. Finally, the third protocol consisted in filling a quantity of pellets corresponding to three layers, but that has been previously mixed with the powder.

3. Results

3.1. X-ray computed microtomography

Case of Pellet

Further information about the microstructure of a pellet of bentonite at initial state (suction s = 132.4 MPa, water content w = 7.25% and dry unit mass ρ_d = 2.12 Mg/m^3) was obtained using µ-CT observations.

Figure 4 and Figure 5 show horizontal and vertical slices, respectively, taken at different positions as indicated in the photo of the pellets presented on top left in the figures. Grey levels depend on the density and atomic number of the components, with darker grey levels typically corresponding to lower densities and black zones to voids. Several higher density elements (light grey levels) are observed in both cases. Several cracks are identified in the sections located in the upper part of the pellet (horizontal sections I and II, and vertical sections I, II and III). It can be deduced from Figure 4 that they coincide with the upper spherical part, close to the contact with the cylindrical section. Such fissures are not observed on the same zone at the bottom of the pellet.
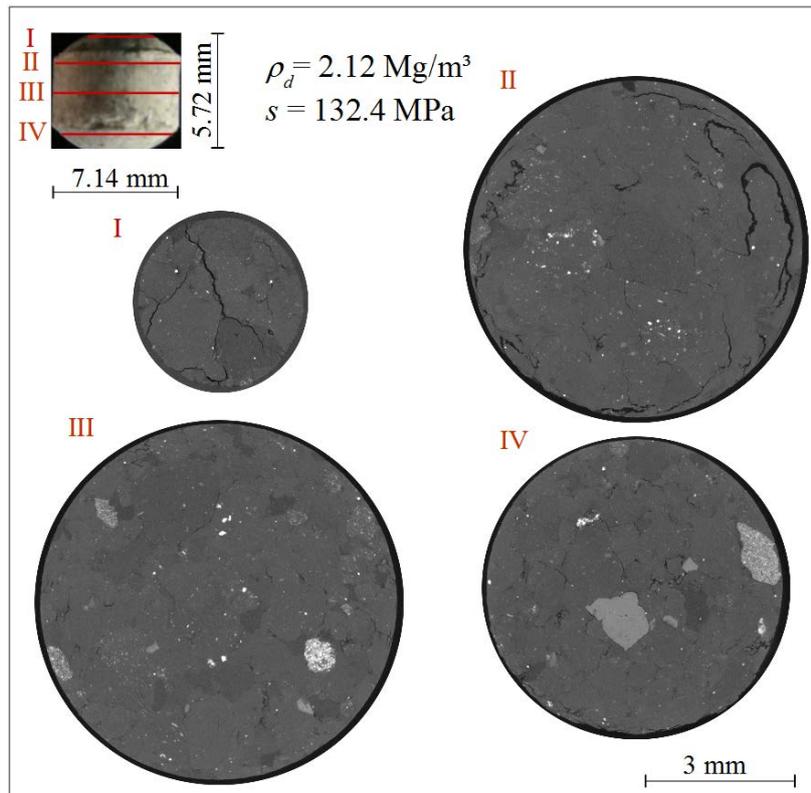
Figure 4. X-ray computed microtomography (µ-CT) observations - horizontal sections - of a pellet of bentonite at its initial state.
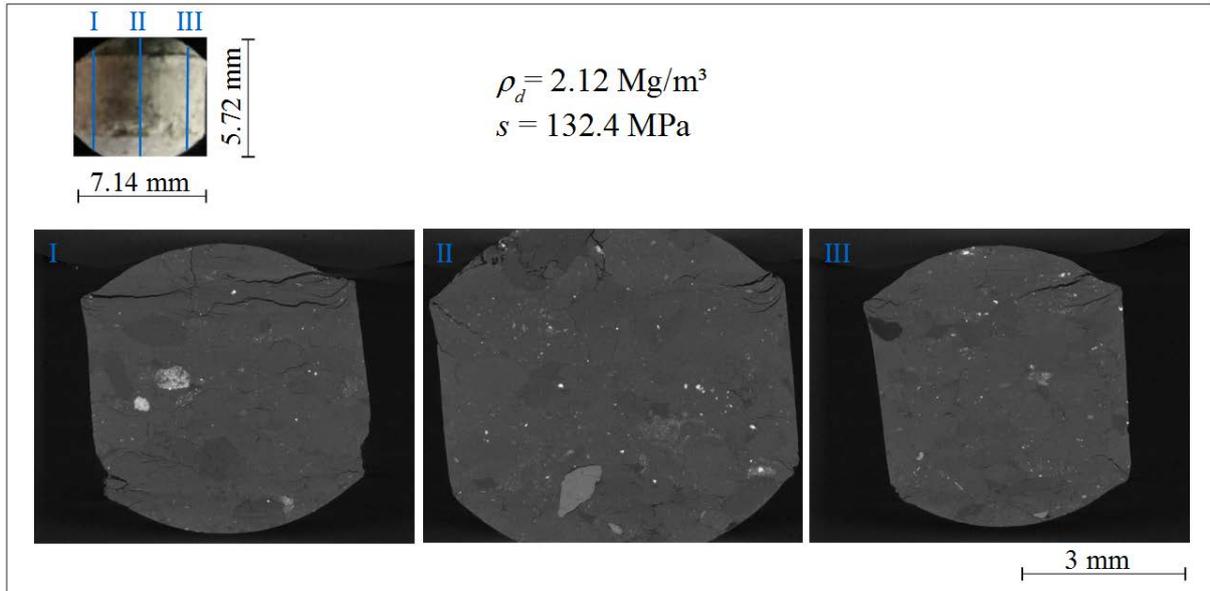
Figure 5. X-ray computed microtomography (µ-CT) observations - vertical sections - of a pellet of bentonite at initial state.

Further information about the fissure network is obtained by a 3D rendering of the surfaces defined by the cracks within a region of interest of the pellet at initial state presented in Figure 6. Cracks are defined as the voxels with a grey level below some threshold. It is observed that crack networks are located on both the upper and bottom part of the pellet; however, as it was revealed by horizontal and vertical slices, there are more cracks in the upper part. The 3D rendering was performed by means of the Avizo image analysis software.
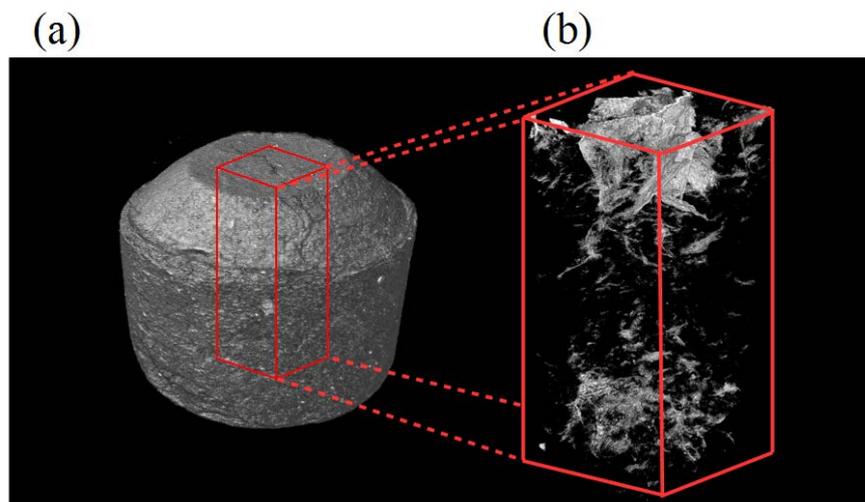
Figure 6. 3D rendering of a pellet of bentonite at initial state (a) and of the crack network in a region of interest (b).
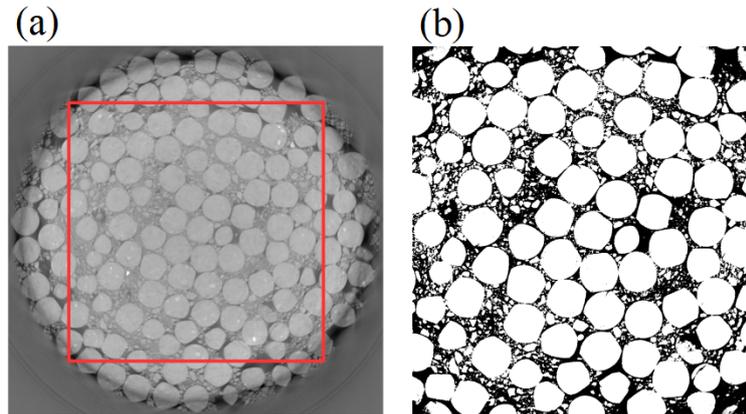
Figure 7. Horizontal slice with the selected ROI (a) and segmented image (b).

Further investigation on a single pellet and on the respective distribution of pellets and powder within the mixture was done by means of image analysis. In a first step, a region of interest (ROI) in the sample was selected (Figure 7). Then, a segmentation of the image was made to separate the voids from the other phases (i.e. the pellets and the powder grains). This step was completed using the ImageJ image analysis software. This method is a variation of the IsoData algorithm (Ridler & Calvard, 1978), an iterative procedure that divides the image into an object and a background by adopting an initial threshold. Then the averages of the pixels at or below the threshold and pixels above are computed, the threshold is incremented and the process is repeated until the threshold is larger than the composite average. Figure 7 shows the initial state with the selected ROI (a) and the segmented image (b). It is noted that such a procedure does not give access to an accurate evaluation of the actual total porosity of the sample, as the result strongly depends on the selected threshold, is strongly sensitive to partial volume effects and other image artefacts, and does not allow to detect the smaller pores. It provides however a way to characterize, at least qualitatively, the spatial distribution of the larger voids within the sample.

An investigation of the porosity was conducted on a single pellet of bentonite with this approach. The porosity was calculated for each horizontal slice obtained by μ-CT observations by dividing the number of black voxels (below some threshold, corresponding to voids) by the total number of voxels within the pellet. Figure 8 and Figure 9 present the calculated values of void ratio for horizontal and vertical sections respectively. It is confirmed from Figure 8 that the value of void ratio increases at the upper part of the pellet (for a level higher than 5 mm) because of the presence of the fissures. In Figure 9 (calculated void ratio for each vertical section), the highest values of void ratio are located at both edges and in the centre of the pellet.

Note that this porosity corresponds to that detected by image analysis with a resolution of 4.4 µm/voxel and for a particular choice of grey level threshold; hence, it provides a first evaluation of the porosity associated with the cracks (see for instance the 3D representation of the fissure network of Figure 6).
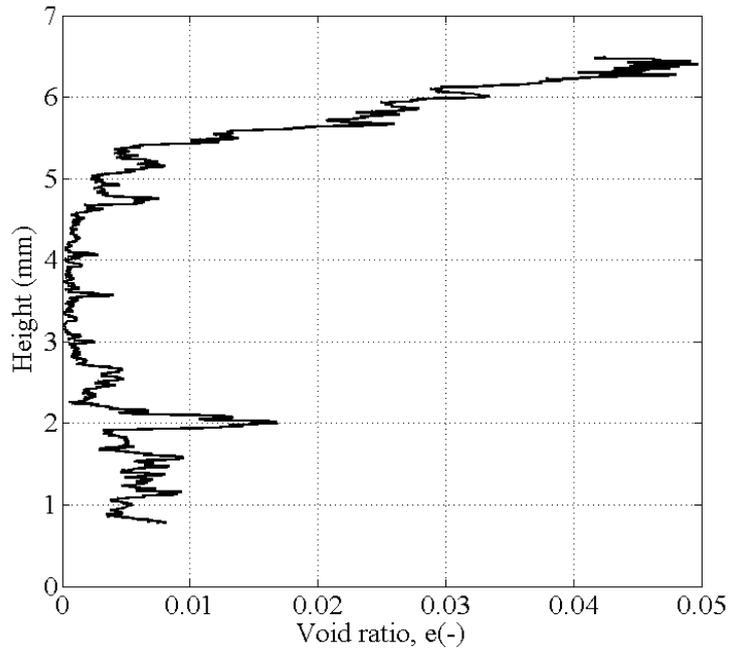
Figure 8. Evolution of the void ratio with height of a pellet of bentonite at initial state (Y direction – horizontal sections).
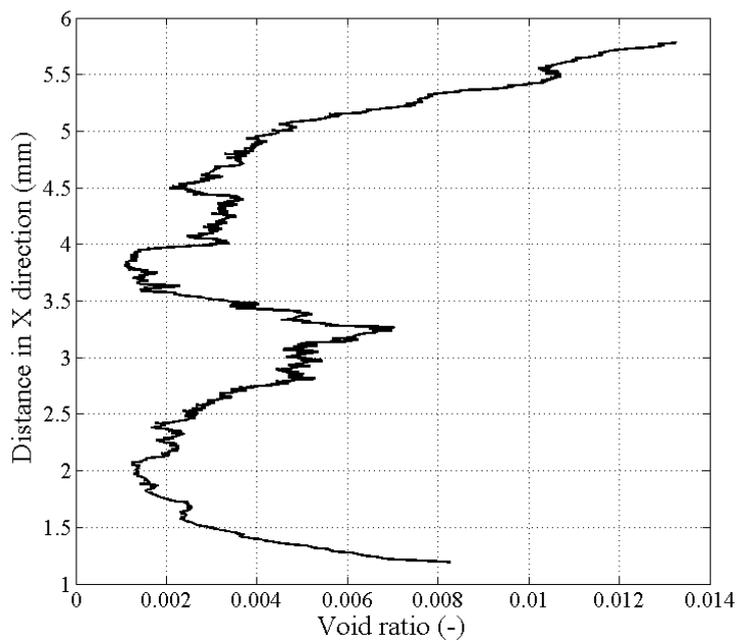
Figure 9. Evolution of the void ratio of a pellet of bentonite at initial state (X direction – vertical sections).

Case of Pellet-powder mixture

The homogeneity of the specimens obtained by using each of the three protocols was examined by using X-ray computed microtomography, the results of which are presented in Figure 10. Observation of Figure 10a shows that the first protocol (1 layer) provided a reasonably good homogeneity of the mixture, with regular scattering of the powder grains within the pores located between the pellets. Several voids between the pellets are however observed at the top of the sample. Inspection of Figure 10b shows that the homogeneity is not ensured with the second protocol (2 layers) with much more inter-pellets pores that are not filled with powder, particularly in the peripheral part of the specimen. Note also the presence of large inter-pellets voids completely filed with powder, in the middle of the sample at 1/3 of the height. The same problem is observed with the third protocol (Figure 10c). The target dry unit mass ($\rho_d = 1.49$ Mg/m^3) was obtained with the first protocol only, while a unit mass of $\rho_d = 1.41$ Mg/m^3 and 1.43 Mg/m^3 is found for the second and third protocols respectively.
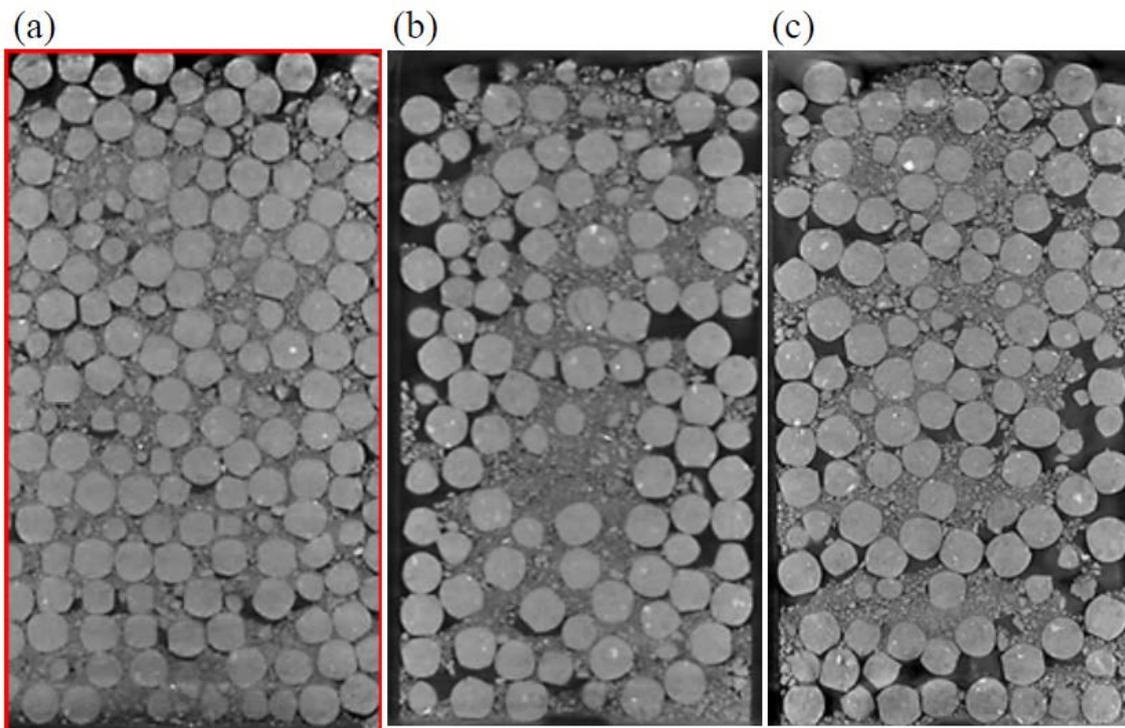
Figure 10. Vertical cross section of X-ray computed microtomography images of a mixture of powder/pellets of bentonite with a proportion of 20/80 in dry mass obtained by three different protocols. (a) First protocol of mixture, (b) Second protocol and (c) third protocol.

An investigation of the porosity was conducted on the three protocols in the same way as detailed previously for a single pellet of bentonite. To this end, the porosity was estimated for each horizontal slice obtained by μ-CT observations, using the same threshold for all slices. Figure 11 presents the evolution of the obtained porosity along the height of the sample for the

three protocols. One can observe an oscillation of the value of porosity for all three protocols. In the first one, the minimum and maximum void ratios are 0.18 and 0.63 respectively. Oscillations are more remarkable and they correspond to one layer of pellets. In the second protocol, the minimum and maximum void ratio values are 0.15 and 0.33 respectively, oscillating around a value of 0.2. Finally, for the third protocol, void ratio goes from 0.08 to 0.55, and the oscillations correspond to three layers of pellets.
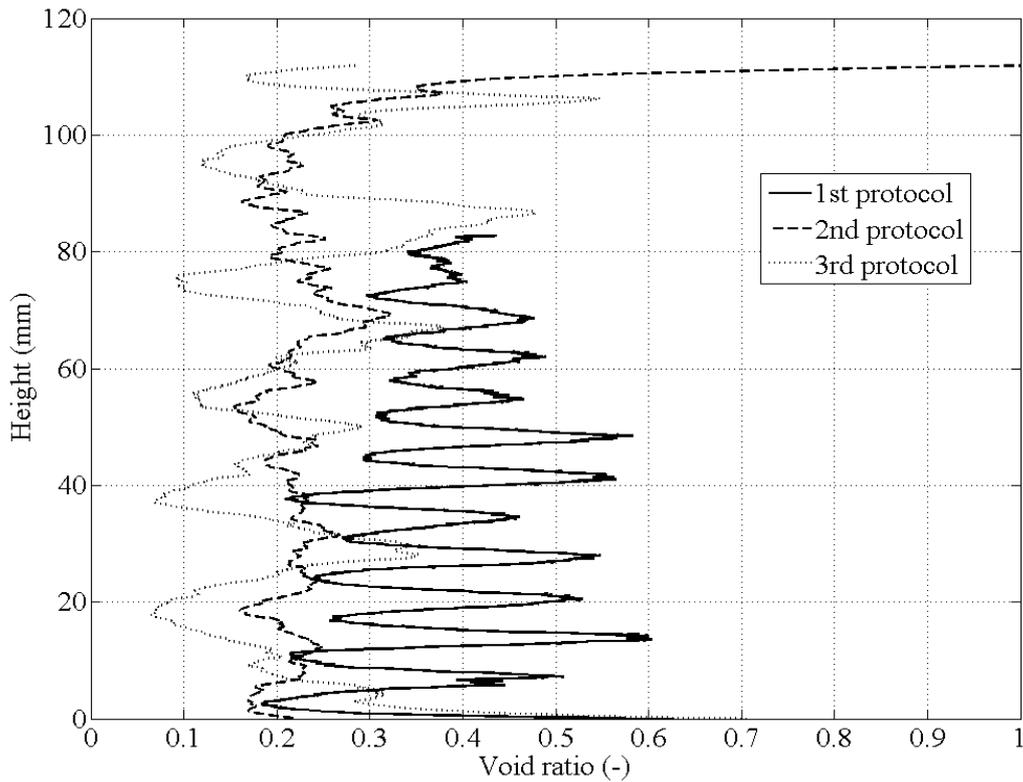
Figure 11. Evolution of the void ratio along height of a pellet/powder MX80 bentonite mixture (80/20) fabricated by three protocols.

Taking into account the target dry density, the homogeneity observed in Figure 10 and the data of image analysis, the first protocol should be selected in order to prepare the pellet/powder mixture samples of MX80 bentonite. Note however that the best result corresponds to the second protocol according to the image analysis, because the values of void ratio oscillate around a value of 0.2 for all the sections. This low fluctuation along the vertical direction of the apparent average porosity within a section does however not reflect the strong heterogeneity of the pore distribution within a section, which is observed in the vertical slice represented in Figure 12b. Furthermore, the target dry density (1.49 Mg/m^3) was only obtained with the first protocol.

3.2. Mercury intrusion porosimetry

Figure 12 shows the results of MIP tests carried out on a pellet (w = 6.7%, s = 138.4 MPa) and on the bentonite powder (w = 3.1%, s = 190.9 MPa). The cumulative curve (Figure 12a) shows that the final value of intruded mercury void ratio of the pellet (e = 0.23) is lower than its total void ratio (eT = 0.34), indicating a significant porosity with an average diameter smaller than 5.5 nm, corresponding to the maximum mercury pressure applied (230 MPa). This is well known for compacted smectite (Lloret *et al*., 2003; Delage *et al*., 2006; Ridley *et al*., 2010).

A typical bimodal porosity distribution is observed for the bentonite powder, with an intruded void ratio of 0.9 at maximum mercury pressure (230 MPa). Actually, this void ratio is conditioned by the isotropic compression exerted by the mercury prior to penetrating the powder. The density function curve indicates that this penetration occurs at an average entrance diameter of 207 µm between powder grains with an average diameter of 0.65 mm. This configuration is not far from the standard ratio between the diameter of spherical grains and the inter-grains pores of their dense assembly, known to be close to 1/3. The second pore population is defined by an average entrance of 16.6 nm, to relate to a suction of 190.9 MPa of the powder. The PSD curve of the pellet has a population of micro-pores quite comparable with an average entrance diameter of 13.3 nm, recalling that the powder was obtained from crushed pellets. Another less clearly defined porosity is observed with an average entrance diameter of 5 µm, that will be described in more details later on. The intruded void ratio represents 67.6% of the total void ratio. The void ratio of the population of large pores represents around 5.6% of the total void ratio.
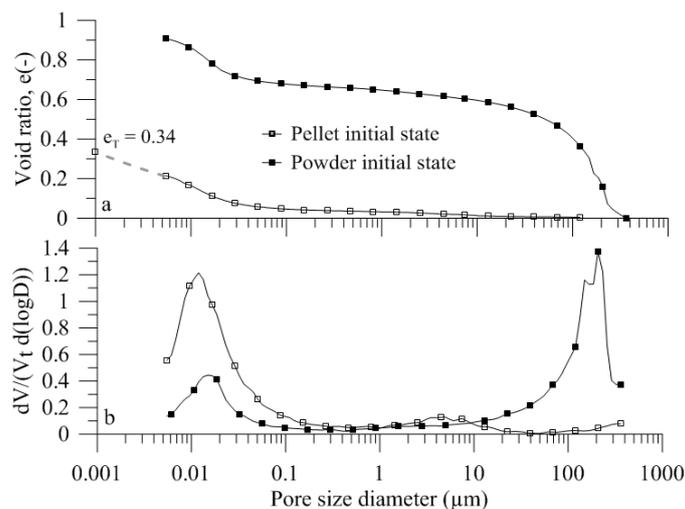
Figure 12. Cumulative porosity curve (a) and derivative curve (b) for a pellet and powder of bentonite at their initial state.

3.3. EDS characterisation

Figure 13 presents SEM photos along with the corresponding EDS chemical analysis of the inclusions of different minerals observed within the pellet of bentonite. These inclusions correspond to the high density elements found by µ-CT observations and are included in the mineralogical composition of the MX80 bentonite given in Table 1. These minerals are identified based on the chemical composition detected by EDS: a high concentration of silicon indicate an inclusion of quartz (see the two inclusions observed in Figure 13a and b); a concentration in sulphur/iron indicate a pyrite inclusion (see Figure 13c). Note that the dimensions of these inclusions are significant (137.3 µm and 70.4 µm for the quartz inclusions) compared to the size of the pellet. An inclusion of calcite is also observed in Figure 14 which was not identified in the X-ray diffractometer (XRD) analyses of MX80 bentonite (Table 1).
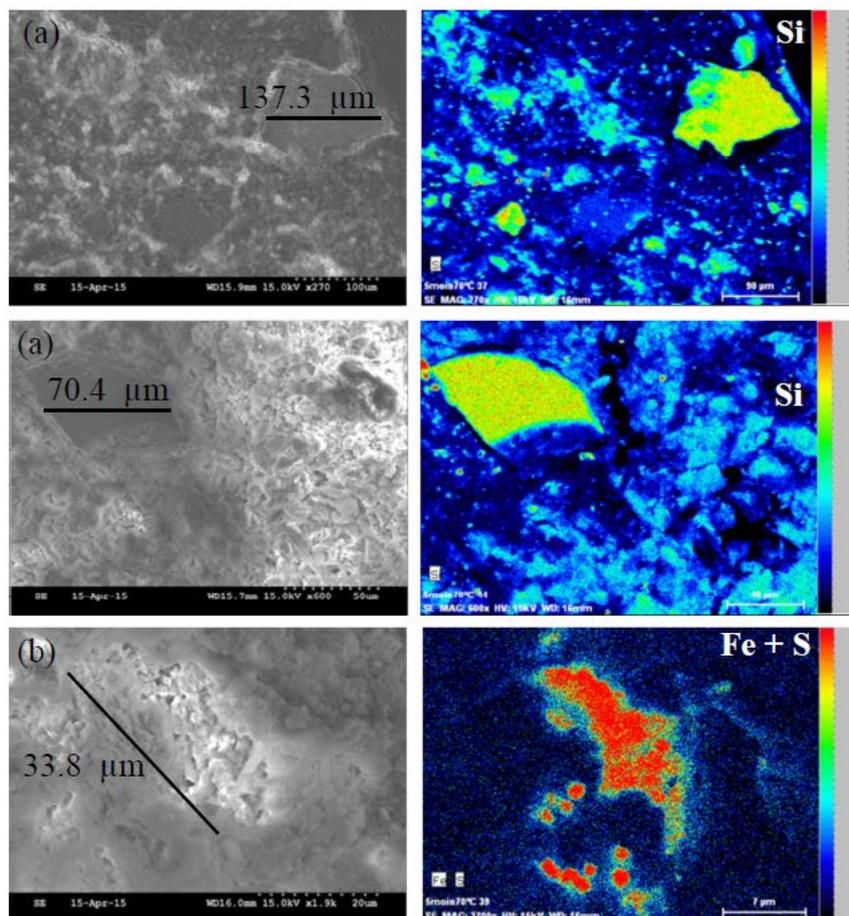
Figure 13. SEM pictures taken on a pellet of bentonite at its initial state (132.38 MPa of suction) + EDS results. Mineral inclusions of quartz (a, b) and pyrite (c). Dry unit mass $\rho_d =$ 2.12 Mg/m^3.
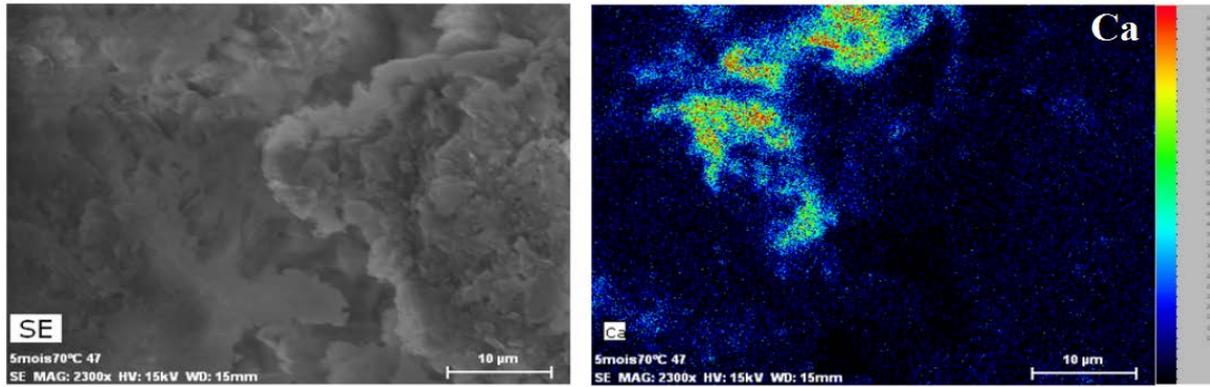
Figure 14. SEM picture taken on a pellet of bentonite at its initial state (132.38 MPa of suction) + EDS results. Mineral inclusion of calcite. Dry unit mass $\rho_d = 2.12$ Mg/m^3.

4. Discussion

Most of the investigations carried out up to now on bentonite-based materials have been based on the use of MIP and SEM (e.g. Saba *et al*., 2014; Wang *et al*., 2013, 2014; Romero *et al*., 2011). These techniques, that require preliminary dehydration of the samples and that concern specimen volumes smaller than about 1 cm^3 can be fruitfully complemented by more recent techniques like X-ray computed microtomography (Van Geet *et al*., 2005) that investigate specimens at larger scale and do not require any preliminary treatment.

In this paper, the microstructure of a pellet of bentonite at its initial state was studied by the pore size distribution curve, obtained by MIP technique. An expected bimodal distribution was obtained, where, theoretically, micro-pores correspond to voids inside an aggregate of bentonite and macro-pores are related to pores between aggregates. The difference between the final value of intruded mercury and the total void ratio in the cumulative curves (Figure 12) suggests that there are several void sizes which cannot be filled by mercury. These voids correspond to pores with a diameter smaller than 5.5 nm and large fissures identified by µ-CT observations. Consequently, it would be convenient to complete this MIP results with nitrogen gas adsorption (BET) technique in future investigations. The PSD curve of the powder of bentonite at its initial state was also obtained. The micro-pores of a single pellet and that of the powder are similar. For the macro-pores, the mean entrance is much larger than the obtained value for a pellet of bentonite. This value corresponds to the voids between grains of bentonite.

X-ray computed microtomography (µ-CT) observations revealed fissures at the upper part of the pellet of bentonite (sections I and II presented in Figure 4 and sections I, II and III in Figure 5) as well as non-swelling elements which could influence the swelling potential of the material. For the section I in Figure 4, located at the upper spherical pole of the pellet, there is a

predominant grey level with some deviations. At the border of the section an element of high density (white) is distinguished. Furthermore, several fissures are observed, confirming that the pellet had already swollen during storage at the laboratory.

For section II (Figure 4), located at the upper part of the pellet, more fissures are observed at the edge of the pellet, as well as elements of high density (white pixels observed everywhere). Based on those observations, the following remarks could be made: (i) pellets swell from the border to the centre (layers in contact with the atmosphere will swell, inducing fissures) and (ii) fissures observed at section I (Figure 4), located at the upper spherical pole of the pellet, could be due to the fabrication process combined to swelling.

For sections III and IV (Figure 4), located at the medium level and the lower spherical pole respectively, no more fissures are observed, but several elements of high density can still be identified. This suggests that the internal structure of a pellet of bentonite is not homogeneous. In addition to the existence of high density elements, different grey levels in the clayey part of the pellet are observed. The same conclusions can be extracted from the vertical sections I, II and III (Figure 5).

5. Conclusion

The µ-CT investigation of the microstructure of a pellet of bentonite provided interesting complementary features that could not be identified by MIP and SEM observations. Heterogeneous features were observed in the internal structure of the pellet, consisting in a heterogeneous density distribution of the clay minerals and in the presence of several high density elements. Furthermore, several fissures were observed at the upper pole of the pellet. This heterogeneity of a single pellet was confirmed by SEM and EDS observations, where several inclusions of non-swelling elements were observed (quartz, pyrite and calcite). The dimensions of these inclusions are not negligible, indicating that this could have an influence on the swelling potential of the pellet.

The MIP tests carried out on a pellet and powder of MX80 bentonite revealed some similarity between both materials, which is not surprising since the powder was fabricated by crushing pellets of bentonite. This similarity consisted on a double porosity and a comparable value of the mean size diameter of the micro-pores. The complementary information provided by µ-CT observations evidenced that macro-pores found by MIP results are due to voids between fissures observed at the upper pole of the pellet and cracks observed at the top and the bottom. A difference is observed when comparing the final value intruded by mercury and the total void

ratio in the cumulative curves, which corresponds to micro-pores with a diameter smaller than 5.5 nm and large fissures observed by µ-CT observations on the upper part of the pellet. Thus, in order to have a good understanding of the microstructure of bentonite-based materials, it is important to carry out these complementary observations together with MIP, SEM + EDS results. The µ-CT observations obtained from a pellet/powder bentonite mixture revealed a heterogeneous initial distribution of both materials within the sample. Thus, it can be concluded that this mixture is characterized by a double heterogeneity: at a microscopic level, a heterogeneous structure inside a pellet of bentonite, and at a macroscopic level, a heterogeneous distribution of pellets and powder. The investigation of this initial heterogeneity is important to understand the long-term evolution of the sealing for larger scale systems. Initially, the system is characterized by a heterogeneous distribution of dry density, so an anisotropic swelling will be attended. Future investigations should be conducted in order to study the heterogeneity of the material at the final state.

References

ANDRA, 2005, Dossier (2005). Evolution phénoménologique du stockage géologique.Rapport Andra no. C.RP.ADS.04.0025, France.

Mokni, N., and Barnichon, J.D. (2016). Hydro-mechanical analysis of SEALEX *in situ* tests- Impact of technological gaps on long term performance of repository seals. *Engineering Geology,* 205, pp. 81-92.

Alonso, E.E., Romero, E. and Hoffmann, C., (2011). Hydromechanical behavior of compacted granular expansive mixtures: experimental and constitutive study. *Géotechnique*, 61(4), pp.329–344.

Barnichon, J.D., Dick, P. and Bauer, C., (2012). The SEALEX *in situ* experiments : Performance tests of repository seals. *Harmonising Rock Engineering and the Environment - Qian and Zhou (eds) Taylor and Francis Group, London*, pp.1391–1394.

Delage, P., Marcial, D., Cui, Y. J. and Ruiz, X., (2006). Ageing effects in a compacted bentonite: a microstructure approach. *Géotechnique*, 56(5), pp.291–304.

Delage, P., Audiguier, M., Cui, Y.J. and Howat, M.D., (1996). Microstructure of a compacted silt. *Canadian Geotechnical Journal*, 33, pp.150–158.

Dereeper, B., Volckaert, G., Imbert, C., and Villar, M.V. (2001). Pellets/powder mixture of bentonite for backfill and sealing of HLW repositories. *Adadchi, K., Fukue, M. (Eds.), Clay Science for Engineering. Balkema, Rotterdam*, pp.487–490.

Van Geet, M., Volckaert, G. and Roels, S., (2005). The use of microfocus X-ray computed tomography in characterising the hydration of a clay pellet/powder mixture. *Applied Clay Science*, 29(2), pp.73–87.

Gens, A., and Alonso, E.E., (1992). A framework for behavior of unsaturated expansive clays. *Canadian Geotechnical Journal*, 29, pp.1013–1032.

Hoffmann, C., Alonso, E.E. and Romero, E., (2007). Hydro-mechanical behavior of bentonite pellet mixtures. *Physics and Chemistry of the Earth*, 32(8-14), pp.832–849.

Hoffmann Jauge, C.A., (2005). Caracterización hidromecánica de mezclas de pellets de bentonita. Estudio experimental y constitutivo. Available at: http://www.tdx.cat/handle/10803/6235 [Accessed July 13, 2015].

Imbert, C., and Villar, M.V., (2006). Hydro-mechanical response of a bentonite pellets/powder mixture upon infiltration. *Applied Clay Science*, 32(3-4), pp.197–209.

Lloret, A., Villar, M.V., Sanchez, M., Gens, A., Pintado, X. and Alonso, E.E., (2003). Mechanical behavior of heavily compacted bentonite under high suction changes. , (1), pp.27–40. Available at: http://dx.doi.org/10.1680/geot.53.1.27.37258.

Management Swedish Nuclear Fuel and Waste, (2002). Äspö Hard Rock Laboratory. Annual Report 2001.

Ridler, T.W. Calvard, S., (1978). Picture Thresholding Using an Iterative Slection Method. *IEEE Transactions on Systems, Man and Cybernetics*, 8(8), pp.630–632.

Ridley, A., Zdravkovic, L. and Monroy, R., (2010). Evolution of microstructure in compacted London Clay during wetting and loading. *Géotechnique*, 60(2), pp.105–119.

Romero, E., Della Vecchia, G. and Jommi, C., (2011). An insight into the water retention properties of compacted clayey soils. *Géotechnique*, 61(4), pp.313–328.

Saba, S., Romero, E., *et al*., 2014. *Hydro-mechanical* behavior *of bentonite-sand mixture used as sealing materials in radioactive waste disposal galleries*. Université de Paris Est.

Saba, S., Barnichon, J. D., Cui, Y. J., Tang, A. M. and Delage, P., (2014). Microstructure and anisotropic swelling behavior of compacted bentonite/sand mixture. *Journal of Rock Mechanics and Geotechnical Engineering*, 6(2), pp.126–132.

Salo, J.-P. and Kukkola, T., (1989). Bentonite pellets, an alternative buffer material for spent fuel canister deposition holes. *Workshop "Sealing of Radioactive Waster Repositories"*. *Braunschweig*.

Sugita, Y., Chijimatsu, M. and Suzuki, H., (2005). Fundamental properties of bentonite pellet for Prototype Repository Project. *In: Alonso, E. E., Ledesma, A. (Eds.), Advances in Understanding Engineered Clay Barriers. A. A. Balkema Publishers, Leiden*, pp.293–299.

Wang, L., (2012). Micromechanical experimental investigation and modelling of strain and damage of argillaceous rocks under combined hydric and mechanical loads.

Wang, Q., Cui, Y. J., Tang, A. M., Barnichon, J. D., Saba, S. and Ye, W. M., (2013). Hydraulic conductivity and microstructure changes of compacted bentonite/sand mixture during hydration. *Engineering Geology*, 164, pp.67–76.

Wang, Q., Cui, Y. J., Tang, A. M., Li, X. L. and Ye, W. M., (2014). Time- and density-dependent microstructure features of compacted bentonite. *Soils and Foundations*, 54(4), pp.657–666.

Water retention properties and microstructure changes of a bentonite pellet upon wetting/drying; application to radioactive waste disposal

Agustín Molinero Guerra[1,2], Pierre Delage[1], Yu-Jun Cui[1*], Nadia Mokni[2], Anh Minh Tang[1], Patrick Aimedieu[1], Frédéric Bernier[3], Michel Bornert[1]

[1]Ecole des Ponts ParisTech, Laboratoire Navier/CERMES, Marne La Vallée, France
[2]Institut de Radioprotection et de Sûreté Nucléaire (IRSN), Fontenay-aux-Roses, France
[3]Agence Fédérale de Contrôle Nucléaire (AFCN), Belgique

Abstract: Like bricks of compacted bentonite/sand mixtures, mixtures made up of pellets and powder of bentonite are considered as a possible material to make the sealing plugs used to fill up galleries and ensure long-term water tightness in deep radioactive waste disposal. Pellets/bentonite mixtures have a low permeability, high swelling capacity, good radionuclide retention capability and operational advantages in terms of placement in the galleries. Following a previous in-depth characterisation of bentonite pellets/powder mixture conducted in the same group, an investigation of the water retention properties and microstructure changes of a bentonite pellet submitted to wetting/drying cycles under free swelling conditions was carried out by means of Mercury Intrusion Porosimetry (MIP) and X-ray microtomography. A complete description of the changes in water content, void ratio and degree of saturation of the pellet was provided. Data showed that the free swelling of the pellet is due to the combined effect of both crack propagation at macro-scale, and the swelling of bentonite grains, governed by hydration mechanisms along the smectite faces at nano-scale. Significant development of a crack network is observed between 38 and 9 MPa. For suctions below 9 MPa, there is a significant decrease of the platelet thickness and an increase in the disorder of the platelet assembly, resulting in an average MIP entrance pore radius increasing to 0.4 μm within the expanded bentonite grains.

1. Introduction

Sealing plugs made of powder/pellets bentonite mixture are considered as a possible option to close the galleries excavated for deep geological radioactive waste disposal. Powder/pellets

bentonite mixtures have low permeability, high swelling capacity and high radionuclide retardation properties. They are also easy to store, transport and install in the galleries and allow for reduced gaps between the host rock and the seal once hydrated. The high-density of both the pellets and the powder grains allows obtaining a high final dry density of the seal once hydrated and, as a result, an adequate swelling pressure. When installed in the gallery, powder/pellet bentonite mixtures are initially unsaturated. They are afterwards hydrated under constrained volume due to the infiltration of pore water from the host rock, generating a swelling pressure that enables sealing the gallery by filling all pre-existing inter-grains and inter-pellets voids.

Many investigations have been carried out on the hydro-mechanical behavior of engineered barriers made up of either compacted pure bentonite or compacted bentonite/sand mixtures in the context of radioactive waste disposal (e.g. Pusch 1982; Graham *et al*., 1989; Komine & Ogata, 1994, 1999; Dixon *et al*., 1996; Alonso *et al.,* 2005; Wang *et al.,* 2013, 2014; Saba *et al.,* 2014; Sun *et al.,* 2014). These investigations have been completed by microstructure investigations carried out using mercury intrusion porosimetry (MIP), scanning electron microscopy (SEM, ESEM, e.g. Cui *et al*., 2002, Agus & Schanz 2005, Delage *et al*., 2006; Montes *et al*., 2001, Saba *et al*., 2014, Seiphoori *et al*., 2014) and X-ray computed microtomography (μ-CT, Kozaki *et al.*, 2001; Kawaragi *et al*., 2009).

An alternative to the use of engineered barriers made up of bricks of compacted bentonite or sand/bentonite mixtures is that of high-density pellets, or pellets/bentonite powder mixtures. Compared to bricks, the pellets have the advantage of much easier transportation and setting up into the galleries. They also allow for reduced technical voids at interfaces between the canisters or at the top of the gallery. Figure 1 shows as an example of the concept developed by Nagra, the Swiss agency for the management of radioactive waste, in which the canisters are placed on compacted bricks prior to being surrounded by pellets.

The swelling capacity of pellets has been investigated by various authors including Imbert & Villar (2006) who performed a series of infiltration tests on a 50/50% FoCa bentonite pellets/powder mixture at different dry densities. They concluded that, once full saturation was reached, the mixture became homogeneous with a swelling pressure equal to that of a bentonite powder compacted at same dry density. The changes in micro-fabric during hydration of the same mixture at a dry unit weight of 1.36 Mg/m^3 have been investigated by Van Geet *et al*. (2005) by using X-ray computed microtomography (X-Ray μCT). They observed a progressive

decrease in the density of the pellets during wetting, leading to a final homogenisation of the mixture at complete saturation.
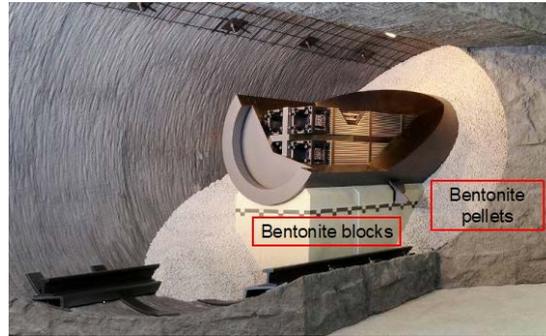
Figure 1. Nagra concept, based on bentonite blocks and bentonite pellets.

Rather few studies have been conducted on the hydro-mechanical behavior of bentonite pellets. Sugita *et al.* (2005) performed a characterisation of hydraulic, swelling and thermal properties of MX80 bentonite pellets by means of a full scale experiment called the Prototype Repository Project (PRP), carried out in the Aspoe underground research laboratory (Svemar & Pusch 2000) in Sweden. The purpose of their study was to validate some assumptions with respect to the numerical simulation of the engineered barrier system (EBS) in the PRP. They concluded that the mass of pellets could be assimilated to a homogeneous high density block in numerical simulations. Hoffmann *et al.* (2007) characterized the hydro-mechanical behavior of mixtures of compacted pellets at different dry densities considered within the framework of the EB project (Schuster *et al.*, 2014). They determined the pore size distribution of mixtures of pellets of different sizes compacted at different densities, evidencing three main groups of pores, i.e. the inter-aggregate, intra-aggregate and inter-pellets pores, respectively. The pore size density function of a single pellet was also determined, with two pore populations (intra-aggregate and inter-aggregate pores). Karnland *et al.* (2008) investigated the swelling pressure and hydraulic conductivity of Wyoming bentonite materials under three configurations: granulated material (maximum grain size of approximately 10 mm) without any pre-treatment, granulated material compacted into pellets and a mixture of 70% bentonite and 30% sand. They confirmed the findings of Imbert & Villar 2006 on a 50/50 bentonite powder/pellet mixture - at the same density there is no significant difference after hydration in terms of final swelling pressure and hydraulic conductivity, between the bentonite pellets and the granulated bentonite material.

Following a previous work in which the initial state of a bentonite pellets was investigated in details (Molinero-Guerra *et al.*, 2017) this work aims at investigating the water retention properties and the microstructure changes of a bentonite pellet under wetting/drying paths. The

33

changes in microstructure of samples submitted to various controlled suctions by means of the vapor control technique were investigated by MIP tests carried out on freeze-dried specimens, complemented by X-ray µCT observations.

2. Materials and methods

2.1. Material studied

The pellet is made up of bentonite from Wyoming (USA) with high smectite content (80%) and some inclusions of non-clayey minerals (quartz – 4% of the total mass, muscovite – 4% of the total mass, pyrite – less than 1% of the total mass, and some elements of calcite). The pellets were provided by the Laviosa-MPC company, under the commercial name Expangel SP7, but it is commonly named by another commercial name, MX80. The cation exchange capacity (CEC) is 98 meq/100g, with Na+ as major exchangeable cation (52 meq/100g, with also 1.2 meq/100g for K, 10 meq/100g for Mg and 37 meq/100g for Ca). The liquid limit is 560%, the plastic limit is 62% and the unit mass is 2.77 Mg/m^3 (Saba 2013).

Pellets were industrially produced the Laviosa-MPC company by compacting bentonite powder into a mould of 7 mm in diameter and 7 mm in height. Compaction was performed at a water content of 6±1% by applying instantaneously the compaction effort, resulting in a pellet dry density ρ_d = 2.06±0.06 Mg/m^3, corresponding to a void ratio e = 0.30±0.07. The pellets were stored in the laboratory in a hermetic plastic box at 20°C. The initial suction (s = 135 ± 3 MPa) was measured in the laboratory with a chilled mirror dew point tensiometer (Decagon WP4C), corresponding to an initial water content w = 7.25%, slightly higher than the fabrication one, due to further hydration after fabrication. Figure 2 shows the photo of a 7.14 mm high and 7.27 mm diameter pellet. It has a quasi-cylindrical shape with two spherical poles on top and bottom.

Figure 2. Pellet at initial state.

2.2. Experimental methods

The determination of the water retention properties under free swelling conditions was carried out by measuring the water content of pellets under suction controlled by vapor equilibrium, by placing the pellets in desiccators containing saturated saline conditions. The changes in water content of the pellets were made by placing the pellet in desiccators containing either distilled water (for the wetting path) or a saturated saline solution (Table 1, for the drying path). The sample was periodically taken out of the desiccator for measuring suction and weight.

Table 1. Saline solutions used for suction control for the vapor equilibrium technique

Solution	Relative humidity at 20°C (%)	Suction (MPa)
$LiCl$	15	261.5
K_2CO_3	44	113.2
$Mg(NO_3)_2$	55	82.4
$NaCl$	76	37.8
$(NH_4)_2SO_4$	83.5	24.9
KNO_3	93.7	9

The water content of the pellets was determined by oven-drying at 105°C for a period of 24 hours. The specimen's volume was determined by hydrostatic weighing waxed specimens into water (see Wan *et al.*, 2013). The void ratio, degree of saturation, dry density and volumetric deformation of the samples were calculated from their volume, mass and water content.

The pore size distribution (PSD) curve were obtained on freeze-dried samples using an Autopore IV 9500 mercury intrusion porosimeter (Micromeritics) that operates at a maximum pressure of 230 MPa, corresponding to a minimum entrance diameter of 0.00542 µm. Instantaneous freezing was carried out by plunging the pellet in slushy nitrogen (-210°C) obtained by previously submitting it to vacuum (Delage *et al.*, 2006). In such conditions, there is no nitrogen boiling around the samples when plunging them into nitrogen, resulting in quick freezing and good microstructure preservation with no ice expansion. In a standard fashion, the pore size distribution was interpreted assuming parallel, cylindrical non intersecting pores.

The microstructure investigation was completed by X-ray µ-CT observations. The X-ray sources parameters were 80kV and 40 µA. Voxel size was 4.41 µm. The samples were scanned using 1440 projections equally spread on 360°. After the reconstruction, 1298 horizontal slices were calculated (16 bit images; 1644 x 1292 pixels).

The reliability of the method of hydrostatic weighing waxed specimen to determine their volume was checked by using μ-CT so as to make sure that no wax infiltrated swollen specimens presenting cracks. Figure 3 presents a vertical slice of a waxed pellet of bentonite after hydration and swelling under a suction of 1 MPa, showing the presence of significant cracks in swollen bentonite. One can observe that there are no gaps between the pellet and wax and no infiltration of wax into the cracks connected to the sample surface, showing the validity of the method.
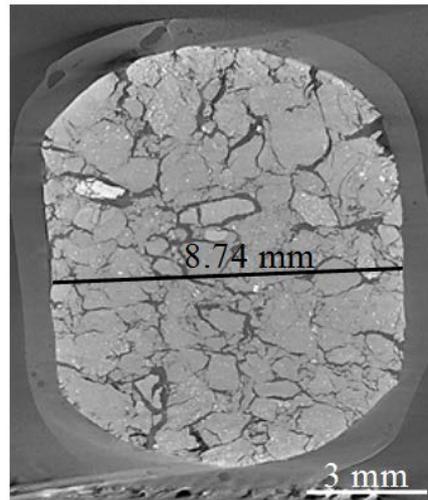
Figure 3. Vertical section of a waxed pellet of bentonite at 1 MPa of suction.

2.3. Test programme

The first series of suction controlled tests (group A, Table 2, P0 – P11) was aimed at determining the wetting (points P0 to P9) and drying (points P10 and P11) paths, starting from initial state P0 ($s = 135 \pm 3$ MPa, $w = 7.25\%$, $\rho_d = 2.06 \pm 0.06$ Mg/m^3). The pellet wetted under 0 MPa (P9) did not reach the imposed suction after 20 days, with a suction of 0.8 MPa measured by using the Decagon WP4 chilled mirror tensiometer.

In the second series of tests (group B, Table 1, P12 to P17), the pellets were first hydrated by submitting them during 12 days to a 100% relative humidity in a desiccator containing distilled water (path I). WP4 suction measurements showed that they reached a suction of 2.3 MPa.

The pellets were then dried (path II) to various suctions between 4.2 (P12) and 262 MPa (P17).

The water content and dry density of the samples of groups A and B were determined at equilibrium. MIP tests were performed on specimens of groups A (P0, P1, P2, P3, P4, P5, P6, P7, P8, P9, P10 and P11). In addition, X-ray observations were performed on specimens P0 (initial state, $s = 135.5$ MPa), P6 ($s = 9$ MPa), P4 ($s = 38$ MPa) and P8 ($s = 1$ MPa).

Table 2. Test programme

	Sample	Path (imposed suction in MPa)		At equilibrium	
		I	II	Water content (%)	Degree of saturation
A	P0	Initial state 135.5		6 - 7.25	54.5 – 66.1
	P1	113		7.9	53.5
	P2	82		9.4	63.4
	P3	40		15.6	63.1
	P4	38		16	64.1
	P5	25		16	60.7
	P6	9		24.6	63
	P7	4.2		31	63
	P8	1		43.5	61
	P9	0.8		45.4	71.8
	P10	149		6.3	45.2
	P11	262		3	25.9
B	P12	2.3	4.2	34.5	55.3
	P13	2.3	9	27.7	56.5
	P14	2.3	38	18.3	57.2
	P15	2.3	82.4	16.04	61.4
	P16	2.3	113	10.5	65.1
	P17	2.3	262	5.96	46.3

3. Experimental results

3.1. Water retention behavior

The changes in water content over time along path I are shown in Figure 4 for group A. The data show that in most cases, equilibrium was achieved after 10 days except for sample P9 at zero suction.
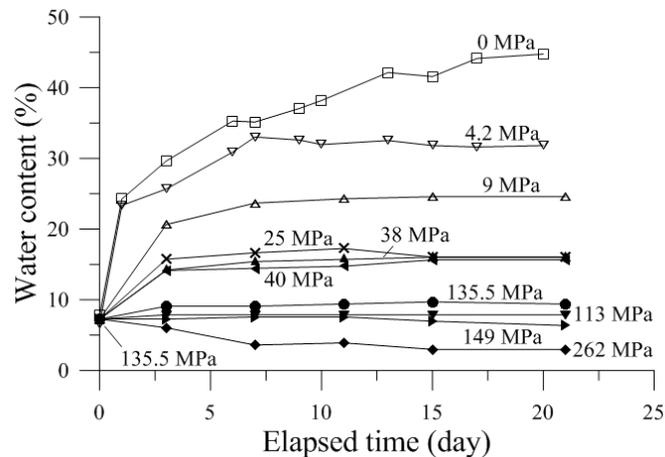
Figure 4. Water content versus elapsed time during path I for group A.

For group B, an equilibrated water content of 35±2% was reached after 12-day hydration. Figure 5, that presents the subsequent changes in water content along drying path II, shows that the drying phase is significantly faster than the wetting one, with equilibrium reached after 2 days, compared to the 10-day long equilibration period along the wetting path.
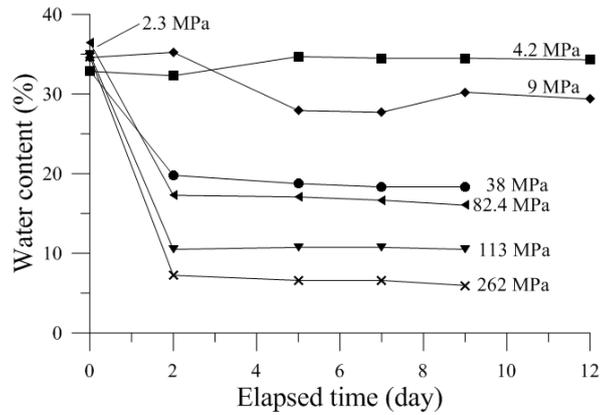
Figure 5. Water content versus elapsed time during path II for group B.

The water retention curve expressed in terms of water content versus suction is shown in Figure 6 for the points from controlled suctions. Given that the points correspond to different pellets, some dispersion is observed, particularly between the points at 40 and 39 MPa (that are satisfactorily close) and that at 25 MPa, with almost the same water content of 16% (whereas it should be larger). The wettest points at 0.8 and 1 MPa are in good correspondence with a maximum water content of 45.4%. Again, along the wetting path, the point at 4.2 MPa has a water content of 31% close to that at 2.3 MPa. It is however possible to draw averages curves to represent both the wetting and drying paths, with a slight hysteresis, including at the highest suction (262 MPa), where the point dried from the wetted state ($w = 6.0\%$) is above that from initial state ($w = 3.0\%$).
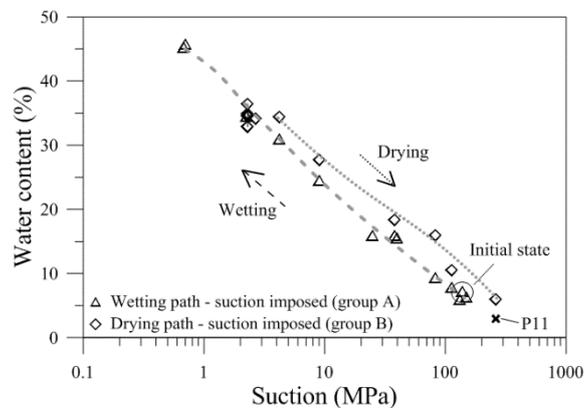
Figure 6. Water content versus suction for all the specimens.

The results obtained by the suction controlled method are shown in Figure 7 in terms of i) degree of saturation versus water content (Figure 7a) and suction (Figure 7b), ii) void ratio versus water content (Figure 7c) and suction (Figure 7d) and iii) volumetric strain versus water content (Figure 7e) and suction (Figure 7f). Figure 7b shows that, for the points of group A along the wetting path, the degree of saturation increased from 55.3% to 60% when decreasing suction from 135.5 MPa (initial state) to 82 MPa; it stabilized afterwards at approximately 60% at lower suctions This feature, also described in Gatabin *et al.* (2016), reflects that swelling (see Figure 7e) compensates the increase in water content, keeping constant the ratio *Vw/Vp* (in which *Vw* is the volume of water and *Vp* the total pore volume). This trend is confirmed by the linear shape of the e/w curve observed in Figure 7c, given that the void ratio *e = Vp/Vs* (with *Vs* the volume of the solid phase, constant) is proportional to *Vp* and *w* proportional to *Vw*.
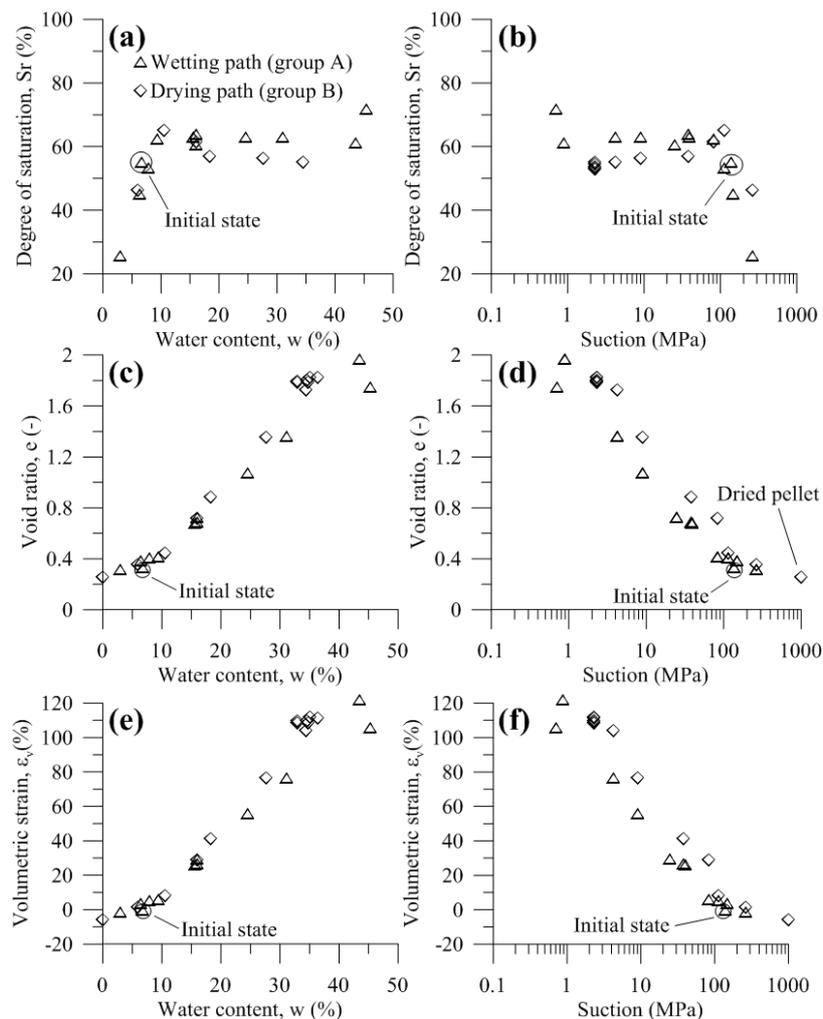
Figure 7. Volumetric behavior obtained by suction-controlled method: (a) Degree of saturation versus water content, (b) Degree of saturation versus suction, (c) void ratio versus water content, (d) void ratio versus suction, (e) volumetric strain versus water content, (f) volumetric strain versus suction.

The changes in void ratio and in volumetric strain with respect to water content (Figure 7c and e) and suction (Figure 7d and f) confirm the significant swelling of the pellet at low suction: 120% swelling at 0.8 MPa suction, with a water content increase from 7.3% to 45.4%.

The points previously wetted to 2.3 MPa (Group B, path II) stabilise at smaller degree of saturation (around 56%) when suction is increased from 4.2 to 39 MPa. The degree of saturation increases afterwards to a maximum value of 65.1% at 113 MPa, prior to decreasing to 46.3% once dried at 262 MPa. Observation of Figure 7d shows a monotonic decrease in water content with increased suction, except for the point at 113 MPa that exhibits a void ratio smaller than expected, explaining the peak in degree of saturation.

3.2. Microstructure changes during hydration

3.2.1. Mercury intrusion porosimetry

The results of MIP tests on samples P0-1 and P0-2 (initial state, 135 MPa suction), P10 (dried at 149 MPa suction) and P11 (dried at 262 MPa suction) are presented in Figure 8. Tests P0-1 and P0-2, made in order to investigate repeatability issues and possible differences between pellets, provide similar PSD curves, illustrating good repeatability and comparable pellets. In all cases, a difference between the maximum void ratio intruded by mercury and the total void ratio of the pellets is observed in the cumulative curves (Figure 8a). The total porosities of all pellets are similar except for P10 (s = 149 MPa) that has a slightly larger total porosity (0.39 compared to values around 0.34). In the case of heavily compacted smectite bearing materials, the porosity that is not intruded at the highest mercury pressure, called here infra-porosity, is related to small pores with entrance diameter smaller than 4 nm (Delage *et al.*, 2006). The nature of these pores will be commented in more details later on. The comparison of the curves shows that the various high suctions imposed here (135, 149 and 262 MPa) have no significant effect on the pore size distribution of the pellets, that are defined by a pore population with an average entrance diameter of 11.9 nm for samples at 135 MPa and 149 MPa and 10.7 nm for the pellet at 262 MPa. Cumulative and density functions curves also show a pore population at diameters around 4 – 5 µm that represents 6.8%, 5.06%, 5.2% of the total porosity, for pellets at 135 MPa, 149 MPa and 262 MPa respectively.

Figure 9 presents the pore size distribution curves of pellets hydrated from initial state (135.5 MPa) to suctions higher than or equal to 25 MPa along the wetting path: P1 (113 MPa), P2 (82 MPa), P3 (40 MPa), P4 (38 MPa) and P5 (25 MPa). The curves show that the average entrance

pore radius stays 10.7 nm at 113 MPa, whereas it increases up to 14.9 to 16.6 nm for suctions equal to or smaller than 82 MPa. Also, the pore population around 4 – 5 µm, previously observed at large suctions, is still observed at suctions of 113 and 82 MPa with comparable percentage of the total porosity (7.0% and 10.9%, respectively).
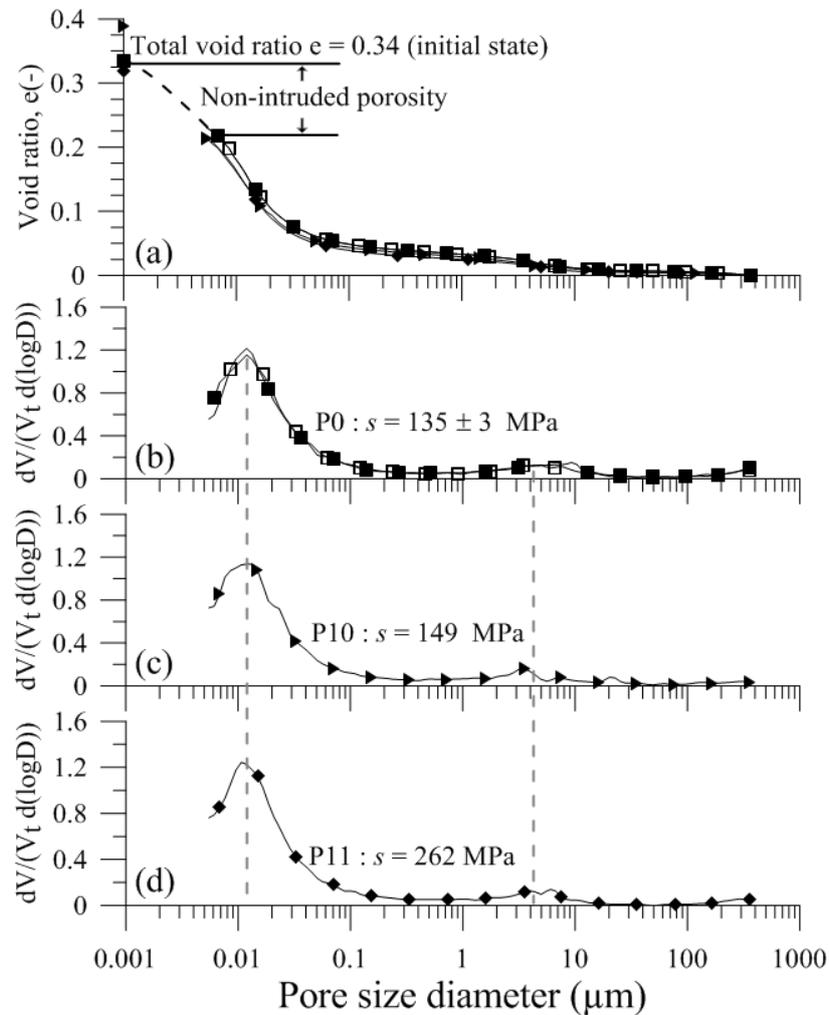
Figure 8. MIP tests results for P0, P10 and P11.

At lower suctions (40 MPa and below), the average diameter of large pores significantly increases to 30 – 40 µm, corresponding to a proportion of the total porosity of 8.3% for the pellet at 40 MPa.

Summarizing, two kinds of cumulative curves are observed, showing no significant swelling between the initial state and states at suction larger than 82 MPa, whereas swelling due to the developments of pores in the range 10 – 40 µm is observed between 82 and 25 MPa.

F presents the pore size distribution curves of pellets submitted to suctions equal to or lower than 25 MPa along the wetting path (P5 at 25 MPa, P6 at 9 MPa, P7 at 4.2 MPa, P8 at 1 MPa

and P9 at 0.8 MPa). Whereas cumulative curves at 25 and 9 MPa remain comparable to that of the former series, the curve at 4.2 MPa looks like a transition towards the curves at lower suction, with a decrease in the peak previously observed at 19 nm and the development of pores with a diameter up to 400 nm. At very low suction (1 and 0.8 MPa), no significant porosity is observed below 100 nm. The significant swelling is due to the development of pores with average diameters of 290 nm (suction 1 MPa) and 400 µm (suction 0.8 MPa), corresponding to 42.3% and 56.6% of the total porosity, respectively.
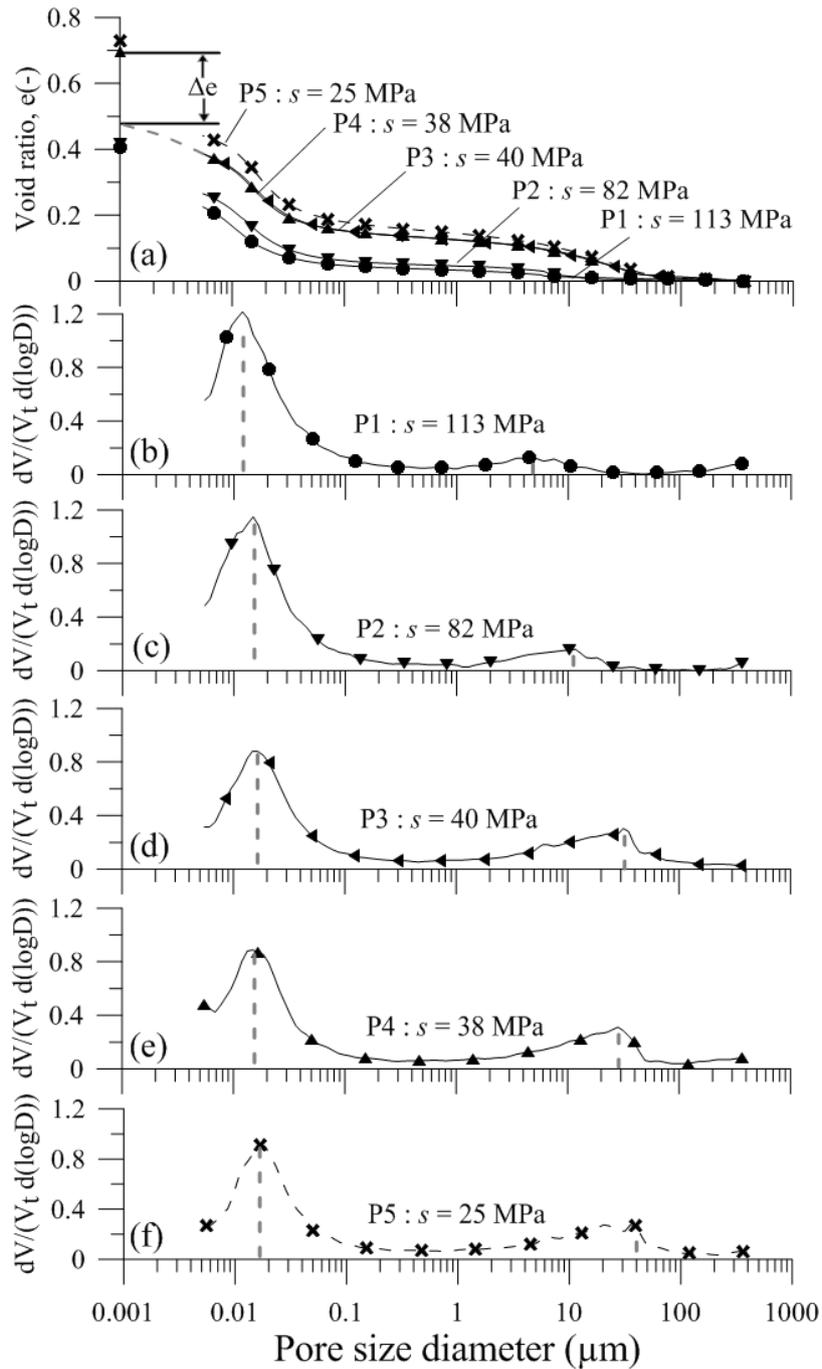
Figure 9. MIP tests results for P1-P5.
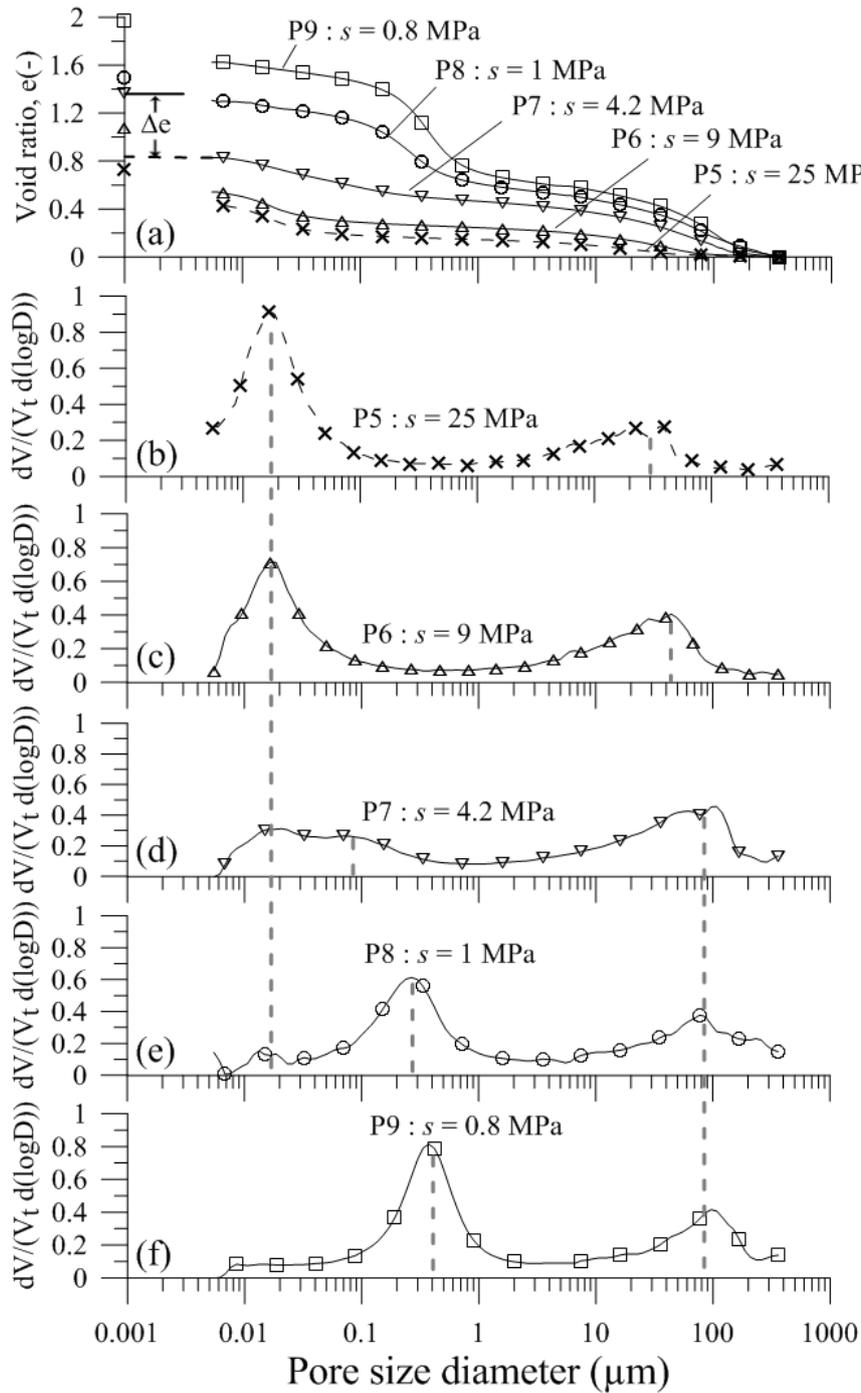
Figure 10. MIP tests results for P5-P9.

3.2.2. X-Ray computed microtomography

X-Ray computed microtomography data are presented in Figures 11 and 12. Figure 11 shows two horizontal sections (I, II) of pellet P0 at initial state (unit weight of 2.12 Mg/m3 and suction 135 MPa) together with that of pellet P4 equilibrated under a suction of 38 MPa, with a smaller unit weight 1.64 Mg/m3 due to swelling (also illustrated by the changes in diameter from 7.27

to 7.44 mm, and in height from 7.14 to 8.15 mm). Figure 12 presents two horizontal sections of pellet P6 at 9 MPa suction (1.33 Mg/m3) together with that of pellet P8 at 1 MPa suction (unit weight 0.93 Mg/m3). The changes in diameter (7.92 mm at 9 MPa and 8.74 mm at 1 MPa from 7.27 mm at the initial state) and height (9.29 mm at 9 MPa and 10.54 mm at 1 MPa from 7.14 mm) of the pellets are also indicated.
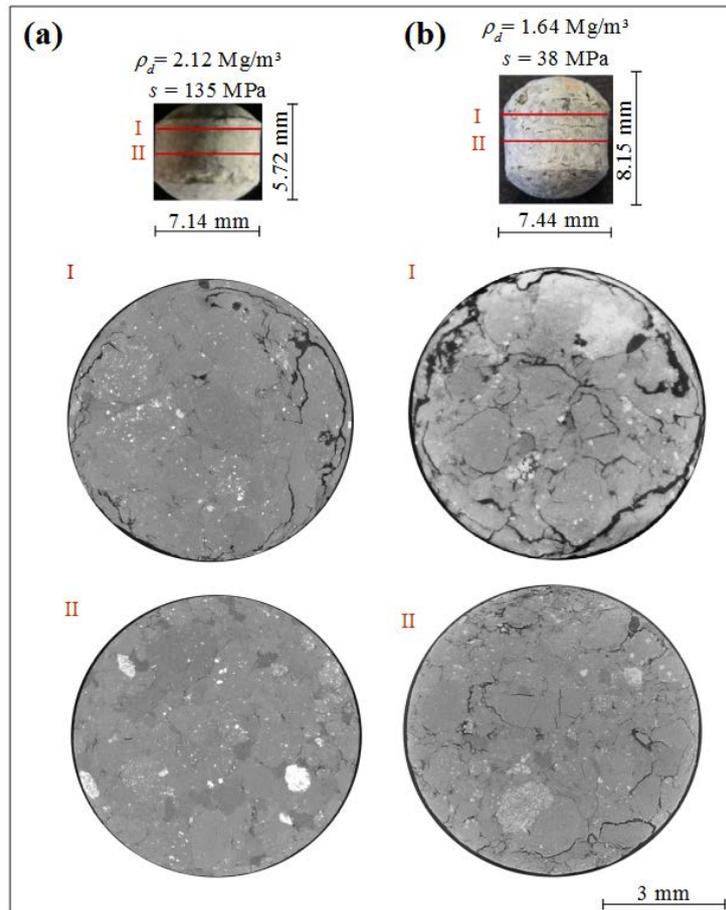
Figure 11. X-ray computed microtomography (μ-CT) observations – horizontal section: (a) 135 MPa (P0); (b) 38 MPa (P4).

Figure 13 compares the results of the volumetric strains obtained by hydrostatic weighing with wax to that calculated with the radial and axial strains. A good agreement is obtained for pellets at 9 and 38 MPa. However, at 1 MPa suction, the volumetric strain obtained by hydrostatic weighing is higher than that calculated from strains. This difference could be due to the fact that, unlike for samples at higher suctions, the two volume measurements at 1 MPa suction (hydrostatic weighing and size measurement) were not made on the same specimen.

A significant anisotropy in swelling is observed from size measurements, with axial swelling ε_a significantly larger than radial swelling ε_r, with a ratio $\varepsilon_a/\varepsilon_r$ of 6.1 at 38 MPa, 3.4 at 9 MPa and 2.4 at 1 MPa. This anisotropic response is linked to the fabrication process of a pellet, in

which bentonite powder grains are instantaneously compacted in a mould in one dimensional conditions, by increasing the axial stress, with no radial strain allowed. This results in an oriented structure with preferential sub-horizontal orientation of the particles that enhance swelling perpendicular to the smectite platelets.
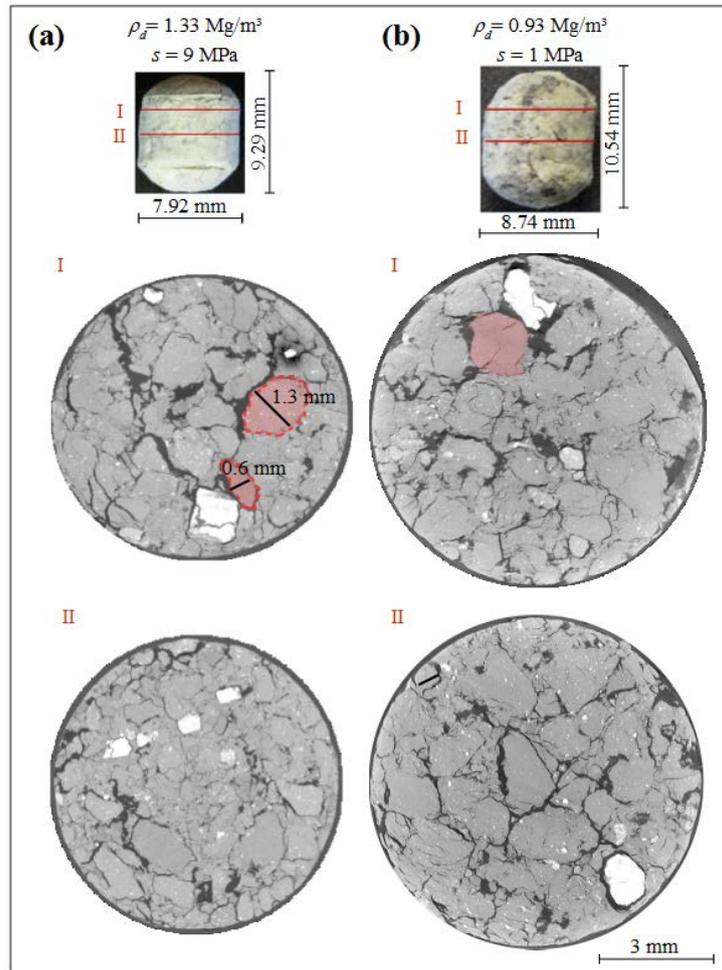
Figure 12. X-ray computed microtomography (µ-CT) observations – horizontal section: (a) 9 MPa (P6); (b) 1 MPa (P8).

Inspection of the sections of pellet P0 at initial state (Figure 11, s = 135 MPa) shows, in upper section I, some cracks located close to the perimeter of the pellet, with an average thickness of 25.5 µm. These cracks are no longer visible in the middle section II. Cracks are also observed in pellet P4 hydrated at 38 MPa. They are also more apparent in section I compared to middle section II. Compared to the initial state, more cracks are observed in the middle section at 38 MPa.

For pellet P6 hydrated at 9 MPa suction (F), the same phenomenon is observed, with more apparent cracks in the upper section I (average thickness of cracks 110 µm). Cracks observed

in the middle section II result from the swelling and separation of bentonite grains (see two delimitated grains with their dimensions located at Figure 12).
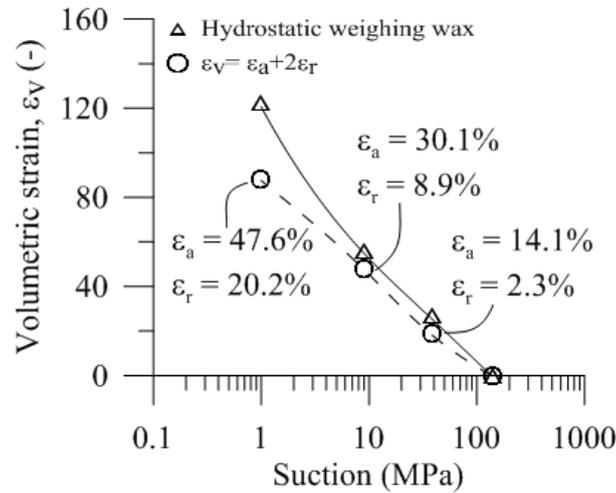
Figure 13. Volumetric strain obtained by hydrostatic weighing wax compared to that calculated with the radial and axial strain.

Within the crack network, the grey levels of the continuous areas of compacted bentonite are comparable, evidencing reasonably constant density. However, this grey level cannot be directly related to the density of the pellet. Note that white sections correspond to crystals of higher density (calcite, quartz or pyrite, see Molinero-Guerra *et al*., 2016 for more details).

Sections of pellet P8, hydrated at 1 MPa of suction, clearly reveal apparent cracks on both sections (I and II). Some cracks inside bentonite grains are also observed (see the grain delimitated with a red contour, section I). The deformability of the pellet is also evidenced in section I, where a change of the initial circular section is observed.

3D reconstructions of pellets at initial state, and hydrated at 38, 9 and 1 MPa, as well as the crack network of a region of interest taken in the centre of the pellets, are presented in Figure 14, providing a global view of the global changes of the pellets, as well as in their vertical sections. Compared to the photo at initial state (Figure 14a, described in detail in Molinero Guerra *et al*., 2016) that exhibits a rather homogeneous and compact mass with only some cracks at the top, the hydration at 38 MPa (Figure 14b) evidences the development of some disconnected cracks around and inside the pellet, particularly at the top. The aperture of the cracks has been determined based on the number of pixels contained in it. That of external cracks is between 76.8 and 122.4 µm at the top, and between 37.9 and 84.8 µm close to the bottom.

As observed in the sections of Figure 14c, the aspect of the pellet hydrated and swelled under 9 MPa suction (volumetric swelling of 55.8%) is quite different, showing that swelling is due for a significant part to the development of an interconnected crack network, further evidenced by the 3D reconstruction of cracks. As commented above, the bentonite pieces comprised within the crack network have comparable density. Their average size is comprised between 44.2 µm and 246.4 µm. The appearance of the solid phase of the pellet under 1 MPa (volumetric swelling of 88.1%, Figure 14d) is not that different from that under 9 MPa, the difference is more apparent in the crack network, with more cracks and more interconnection between them. The average size of the cracks is comprised between 171 µm and 487 µm.

An attempt was made to run X-Ray µ-CT observations on sample hydrated at 0.8 MPa; but the sample, close to full hydration, became weak and soft, not far from a slurry, and it was not possible to handle it safely to perform the test.
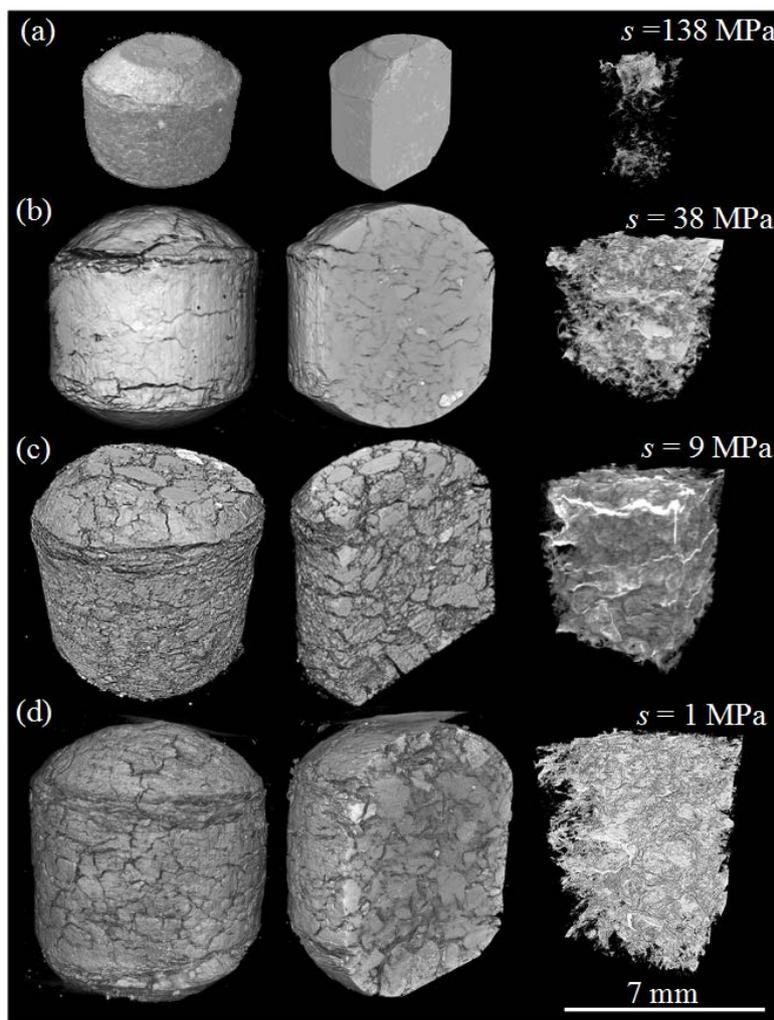

Figure 14. X-ray computed microtomography (µ-CT) observations – 3D reconstruction image and network of cracks: (a) P0 – initial state ; (b) P4 – $s = 38$ MPa; (c) P6 – $s = 9$ MPa; (d) P8 – $s = 1$ MPa.

4. Discussion

X-Ray µCT provide some complementary information at larger scale on the pellet microstructure, with respect to MIP data. The observation at initial state (suction of 135 MPa) evidences some circular cracks close to the edge, on the top section of the pellet, likely a consequence of stress release after the pellet manufacturing by rapid compacting. These cracks apparently play a role during the release of suction down to 38 MPa, with an enlargement of the circular cracks on the top section, and some development of internal cracks. Obviously, cracks favour the penetration of water vapor within the pellets. Internal cracks are more frequent at lower suctions (9 and 1 MPa), they develop between bentonite grains that are sometimes affected by internal cracks. The swelling of the pellet is hence due to the combined action of crack propagation (better observed by using X-Ray µCT) and grain expansion (quantified by MIP).

Referring to the PSD curves of Figures 8, 9 and 10, X-Ray µ-CT data indicate that the large pore populations observed in MIP above 10 µm correspond to cracks. MIP curves confirm that the crack network is not very developed at initial state (135 MPa), at which MIP data indicate that 6.8% of the total porosity has access diameters between 2 and 10 µm. This pore population is observed in the 3D crack reconstruction of Figure 14a.

As seen in the PSD curves, a distinction can be made between the curves at initial state, 113 and 82 MPa with that at 40 and 25 MPa with respect to the development of the large pores between 4 and 100 µm observed in the curves at 40 and 25 MPa. As indicated by X-Ray µCT, this is related to the development of a more apparent cracks network observed in Figure 14b, c, d. The images show that the interconnection between the cracks is more evident at 9 MPa, whereas the difference in PSD between 25 and 9 MPa is not straightforward apart from the shift of the peak in density function from 30 to 40 µm (Figure 10b and c). At lower suctions (4.2, 1 and 0.8 MPa), the peak shifts toward 80 µm (Figure 10d, e and f), in link with the increase in cracks interconnection observed at 1 MPa suction in the X-Ray µCT data of Figure 14d.

The changes in PSD curves in the small pore range are governed by different phenomena at a different scale, with average pore diameters of 11 nm at initial state and at a suction of 262 MPa. Applying higher suctions along the drying path has no effect on this pore population, as also observed in the decrease from 135 to 113 MPa suction. The intruded porosity is the same (0.22) at suctions between 262 and 113 MPa, and it slightly increases at 0.26 at 82 MPa, prior to reaching 0.38 at 40 MPa.

These features can be interpreted based on findings on the hydration mechanisms of smectites, that come from investigations on pure smectites (e.g. Mooney *et al*., 1952; Méring & Glaeser 1954; Norrish 1954) and have been extended to compacted smectite (Saiyouri *et al*., 2000, 2004, Delage 2007). As recalled in Figure 15, the inter-basal spacing of smectites, illites and interlayer illite–smectite minerals (all minerals made up of an octahedral layer comprised between two tetrahedral layers) is equal to 9.6 Å. During hydration, the inter-basal spacing of smectites is known to increase in an orderly fashion due to the successive adsorption of layers of water molecules. X-Ray diffraction techniques demonstrated that, during hydration, the successive adsorption of one, two or three layers of water molecules along the smectite minerals corresponded to interlayer spacing of 12.6, 15.6 and 18.6 Å, respectively (corresponding to an equivalent thickness of 3 Å for an individual layer of water molecules). Another important result (see for instance Ben Rhaiem *et al*., 1987; Bérend *et al*., 1995; Cases *et al*., 1997; Saiyouri *et al*., 2004; Ferrage *et al*., 2005, 2007) is that the number of layers adsorbed depends on the relative humidity (or suction) imposed during hydration. As an example, Saiyouri *et al*. (2004) observed, in a compacted MX 80 Wyoming montmorillonite specimen, that one layer of water molecules was adsorbed at suctions larger than 50 MPa, two layers between 50 and 7 MPa, and three layers below 7 MPa, with a fourth layer adsorbed at low suctions smaller than 0.1 MPa. This mechanism is illustrated in Figure 15. Saiyouri *et al*. (2004) also observed during hydration a constant decrease in thickness of the smectites platelets starting from stacks made up of around 300 layers down do around 10 layers at suction smaller than 9 MPa. Actually, it was also shown that this reduction in platelets thickness at low suction also corresponded to a larger disorder of the microstructure of the compacted bentonite due to the exfoliation of the aggregates.

In this framework, it seems convenient to analyse PSD curves by using the simplified brick model that consists in considering that the well-organized pore diameter distribution around an average diameter observed at suctions larger than 9 MPa provides an estimation of the average thickness of the clay platelets. The data of Figure 15 indicate that, with one layer adsorbed at large suctions of various hundreds of MPa, the thickness of the smectite layer is equal to 12.6 Å, providing an average thickness of the platelet of 11 nm, corresponding to a number of 9 layers per platelets.

The diagram of Figure 15 indicates an increase from 1 to 2 layers adsorbed when suction is decreased below 50 MPa. With 2 layers of water molecules, providing an inter basal spacing of 15.6 Å at 40 MPa, a thickness of 14 nm can be calculated at suction between 50 and 7 MPa.

This value is reasonably comparable with the value of 14.9 – 16.6 nm obtained from the PSD curve by using the brick model for suctions between 40 and 9 MPa.

Figure 15. Interlayer distance vs. suction pressure for smectites (after Saiyouri *et al*., 2004).

The combined use of MIP and X-Ray µCT investigations, combined to an interpretation based on the hydration mechanisms of smectites hence helps better understand the changes in microstructure of a bentonite pellet submitted to change in suction through the vapor phase. It confirms that the developments of cracks contributes in a significant manner to the swelling of the pellet, whereas 1, 2 and 3W adsorption mechanisms along the smectite mineral at the nanometre level is relevant to identify the simultaneous intra-platelet swelling mechanism.

5. Conclusion

To better understand the water retention properties of pellets of MX80 bentonite used as engineered barriers and plugs in some concepts for radioactive waste disposal at great depth, the change in microstructure of a pellet submitted to suction changes was investigated at small scale by means of MIP tests on freeze-dried specimens, complemented at larger scale by X ray µ-CT observations carried out on intact specimens.

Along the drying path at suctions larger than the initial one (135 MPa), MIP does not evidence any significant change in pore size distribution, and it is likely that cracks, that are not very apparent at 135 MPa, do not further develop. The tiny changes in microstructure observed are linked to the mechanisms of water adsorption at nano-scale along the smectite faces that are governed, at suctions of several hundreds of MPa, by 1W adsorption and a constant inter-basal distance of 12.6 Å. The average entrance pore radius at initial and drier states is related to the average thickness of the 1W hydrated smectite platelets, with no evidence of inter-aggregate

pores of larger size. This suggests that the powder grains are very closely packed together within pellets, as already observed in Molinero-Guerra *et al.* (2016).

Along the wetting path, swelling is due to the combined effect of crack propagation at the macro-scale, and of the swelling of bentonite grains that is governed by the hydration mechanisms of smectite at nano-scale, with 2W hydration at suctions between 82 and 9 MPa. In this suction range, the changes in average entrance diameter are not very significant in MIP, and both MIP and X ray μ-CT evidence the role played by crack propagation in swelling, with significant development of a crack network between 38 and 9 MPa. The application of suctions below 9 MPa is known to result in 3W hydration in smectites, corresponding to a significant decrease of the platelet thickness and to an increase in the disorder of the platelet assembly

Saiyouri *et al.* 2004). At low suction, hydrated smectites are known to be made up of thin platelets of around 10 layers (Tessier 1990, Saiyouri *et al.*, 2004), with open card house structures that may explain the large entrance diameter observed in the MIP investigation conducted in this work, that evidenced an increase in average entrance pore radius up to 0.4 μmwithin the expanded bentonite grains. Both X ray μ-CT and MIP also indicate that the crack network significantly develops.

Cracks are hence suspected to play an important role in the propagation of water vapor into the pellets during hydration and swelling. Given that the *in situ* hydration of pellets in deep radio-active disposal in claystones will occur at the contact between some pellets and the low permeability host rock through a very small flux of liquid water, vapor transfers through the inter-pellets porosity might play a significant role, at least at the beginning of hydration phase.

The investigations carried out in this work showed that the hydration of an individual pellet under free swelling conditions occurred within a period of time of 20-30 days, which provides an idea on the time scale involved, at least in ideal conditions. Of course, free swelling conditions will only hold as far as all the inter-pellets porosity is not filled by the expansion of deformable hydrating pellets. Once the continuity of the vapor phase stopped, it is likely that liquid hydration will become more significant and will govern the hydration kinetics.

It seems that the hydration mechanism of the mass of pellets should be investigated in more details by numerically modelling vapor phase transfers and the transition towards liquid water transfers. In the regard, the hydration boundary conditions at the interface between the pellets and the host rock should require further attention, together with the effects of the development of cracks and their subsequent closure after swelling.

Acknowledgements

References

Agus, S. S. & Schanz T., (2005). Effect of shrinking and swelling on microstructures and fabric of a compacted bentonite-sand mixture. *Proceedings of the international conference on problematic soils*, Cyprus, 2, 543–550.

Alonso, E.E., Romero, E., Hoffmann, C., & Garcia-Escudero, E., (2005). Expansive bentonite-sand mixtures in cyclic controlled-suction drying and wetting. *Engineering Geology*, 81(3), pp.213–226.

Alonso, E.E., Romero, E. & Hoffmann, C., (2011). Hydromechanical behavior of compacted granular expansive mixtures: experimental and constitutive study. *Géotechnique*, 61(4), pp.329–344.

Ben Rhaïem, H., Pons, C.H. & Tessier, D., (1987). Factors affecting the microstructure of smectites. Role of cation and history of applied stresses. Pp. 292?297 in: Proceedings of the International Clay Conference, Denver, 1985 (L.G. Schultz, H. Van Olphen & F.A. Mumpton, editors). The Clay Minerals Society, Bloomington IN.

Bérend, I., Cases, J.M., François, M., Uriot, J.P., Michot, L., Masion, I.A. & Thomas, F., (1995). Mechanism of adsorption and desorption of water vapor by homoionic montmorillonites: 2. TheLi+,Na+,K+, Rb+and Cs+-exchangedforms.ClayClayMiner.43, 324–336.

Cases, J.M., Berend, I., Besson, G., Francois, M., Uriot, J.P., Thomas, F., Poirier, J.E., (1992). Mechanism of adsorption and desorption of water vapor by homoionic montmoril- lonite. 1. The sodium-exchanged form. Langmuir 8, 2730–2739.

Cui, Y. J., Loiseau, C., & Delage, P., (2002). Microstructure changes of a confined swelling soil due to suction controlled hydration. Proc. 3rd Int. Conf. on Unsaturated Soils, Recife 2, 593–598.

Delage, P.,, Marcial, D., Cui, Y. J. & Ruiz, X., (2006). Ageing effects in a compacted bentonite: a microstructure approach. *Géotechnique*, 56(5), pp.291–304.

Delage, P., (2007). Microstructure Features in the Behavior of Engineered Barriers for Nuclear Waste Disposal. In *Experimental Unsaturated Soils Mechanics*, *Proc Int. Conf. on Mechanics of Unsaturated Soils,* 11-32, T. Schanz ed., Weimar, Germany, Springer.

Dixon D. A. Gray M. N. & Graham J., (1996). Swelling and hydraulic properties of bentonites from Japan, Canada and the USA. Environmental Geotechnics 1, 43-48.

Ferrage, E., Lanson, B., Sakharov, B.A. & Drits, V.A., (2005). Investigation of smectite hydration properties by modeling experimental X-ray diffraction patterns: part I. Montmoril- lonite hydration properties. Am. Mineral. 90, 1358–1374.

Ferrage, E., Kirk, C.A., Cressey, G., & Cuadros, J., (2007). Dehydration of Ca-montmorillonite at the crystal scale. Part 2. Mechanisms and kinetics. Am Mineral 92(7):1007-1017.

Gatabin, C., Talandier, J., Collin, F., Charlier, R. & Dieudonné, A. C., (2016). Competing effects of volume change and water uptake on the water retention behavior of a compacted mx-80 bentonite/sand mixture. Applied Clay Science 121–122, 57–62.

Graham, J., Saadat, F., Gray, M. N., Dixon, D. A., & Zhang, Q. Y., (1989). Strength and volume change behavior of a sand-bentonite mixture. Canadian Geotechnical Journal 26, No. 2, 292- 305.

Hoffmann, C., Alonso, E.E. & Romero, E., (2007). Hydro-mechanical behavior of bentonite pellet mixtures. *Physics and Chemistry of the Earth*, 32(8-14), pp.832–849.

Imbert, C. & Villar, M.V., (2006). Hydro-mechanical response of a bentonite pellets/powder mixture upon infiltration. *Applied Clay Science*, 32(3-4), pp.197–209.

Karnland, O., Nilsson, U., Weber, Hanspeter, W., & Wersin, P., (2008). Sealing ability of Wyoming bentonite pellets foreseen as buffer material - Laboratory results. *Physics and Chemistry of the Earth*, 33(SUPPL. 1), pp.472–475.

Kawaragi, C., Yoneda, T., Sato, T. & Kaneko, K., (2009). Microstructure of saturated bentonites characterized by X-ray CT observations. *Engineering Geology*, 106(1-2), pp.51–57.

Komine, H., & Ogata, N., (1994). Experimental study on swelling characteristics of compacted bentonite. Canadian geotechnical journal 31 , No. 4, 478-490.

Kozaki, T., Suzuki, S., Kozai, N., Sato, S., & Ohashi, H., (2001). Observation of Microstructures of Compacted Bentonite by Microfocus X-Ray Computerized Tomography (Micro-CT). *Journal of Nuclear Science and Technology*, 38(8), pp.697–699.

Méring, J. & Glaeser, R., (1954). Sur le rôle de la valence des cations échangeables dans la montmorillonite. Bulletin de la Société Francaise de Minéralogie et Cristallographie, 77, 519−530.

Molinero-Guerra, A., Mokni, N., Delage, P., Cui, Y. J., Tang, A. M., Aimedieu, P., Bernier, F., & Bornert, M., (2016). In-depth characterisation of a mixture composed of powder/pellets MX80 bentonite. *Applied Clay Science*.

Montes G., Duplay J. & Martinez L., (2001). Study of bentonite swelling : qualitative and quantitative analysis using ESEM and digital image analysis program. 12th International Clay Conference, july 22-28, Bahia Blanca, Argentina.

Mooney, R. W., Keenan, A. C. & Wood, L. A., (1952). Adsorption of water vapor by montmorillonite. II. Effect of exchangeable ions and lattice swelling as measured from X-ray diffraction, J Amer Chem Soc 74:1371–1374.

Norrish, K., (1954). The swelling of montmorillonite. Discussions of the Faraday Society 18, 120–134.

Pusch, R. (1982). Mineral-water interactions and their influence on the physical behavior of highly compacted Na bentonite. Canadian Geotechnical Journal, 19(3): 381–387. doi:10.1139/t82-041.

Schuster, K., Furche, M., Velasco, M., Gaus, I., Trick, T., Garcia-Siñeriz, J. L., Rey, M., Schulte, F., Sanchez Herrero, S., Tietz, T. & Mayor, J. C., (2014). *Long-term Performance of Engineered Barrier Systems PEBS Engineered Barrier Emplacement Experiment in Opalinus Clay: "EB" Experiment.*

Saba, S., (2013). *Comportement hydromécanique différé des barrières ouvragées argileuses gonflantes*. PhD thesis, Ecole des Ponts ParisTech -Université de Paris Est.

Saba, S., Barnichon, J. D., Cui, Y. J., Tang, A. M. & Delage, P.,(2014). Microstructure and anisotropic swelling behavior of compacted bentonite/sand mixture. *Journal of Rock Mechanics and Geotechnical Engineering*, 6(2), pp.126–132.

Saiyouri N., Hicher P.Y., Tessier D. (2000). Microstructural approach and transfer water modelling in highly compacted unsaturated swelling clays, Mech. Cohesive Frictional Mater 5:41–60.

Saiyouri, N., Tessier, D. & Hicher, P.Y., (2004). Experimental study of swelling in unsaturated compacted clays. *Clay Minerals*, 39(4), pp.469–479.

Seiphoori, A., Ferrari, A. & Laloui, L., (2014). Water retention behavior and microstructural evolution of MX-80 bentonite during wetting and drying cycles. *Géotechnique*, 64(9), pp.721–734.

Sugita, Y., Chijimatsu, M. & Suzuki, H., (2005). Fundamental properties of bentonite pellet for Prototype Repository Project. *In: Alonso, E. E., Ledesma, A. (Eds.), Advances in Understanding Engineered Clay Barriers. A. A. Balkema Publishers, Leiden*, pp.293–299.

Sun, W., Sun, D., Fang, L. & Liu, S., (2014). Soil-water characteristics of Gaomiaozi bentonite by vapor equilibrium technique. *Journal of Rock Mechanics and Geotechnical Engineering*, 6(1), pp.48–54.

Svemar, C. & Pusch, R., (2000). Project description FIKW-CT-2000-00055, SKB International Progress Report IPR-00-30.

Tessier, D. (1990). *Matériaux argileux: Structure, Propriétés et Applications* (ed. A. Decarreau), Vol.1, 387–445. Paris: Société Française de Minéralogie et Cristallographie.

Van Geet, M., Volckaert, G. & Roels, S., (2005). The use of microfocus X-ray computed tomography in characterising the hydration of a clay pellet/powder mixture. *Applied Clay Science*, 29(2), pp.73–87.

Wan, M., Delage, P., Tang, A. M. & Talandier, J., (2013). Water retention properties of the Callovo-Oxfordian claystone. *International Journal of Rock Mechanics and Mining Sciences*, 64, pp.96–104.

Wang, Q., Cui, Y. J., Tang, A. M., Barnichon, J. D., Saba, S. & Ye, W. M., (2013). Hydraulic conductivity and microstructure changes of compacted bentonite/sand mixture during hydration. *Engineering Geology*, 164, pp.67–76.

Wang, Q., Cui, Y. J., Tang, A. M., Li, X. L. & Ye, W. M., (2014). Time- and density-dependent microstructure features of compacted bentonite. *Soils and Foundations*, 54(4), pp.657–666.

Chapter 2

Hydro-mechanical characterization of the pellets/powder mixture

INTRODUCTION

This chapter aims at studying the water retention, swelling and compressibility properties of the 80/20 pellet/powder MX80 bentonite mixture. Firstly, the water retention curve (WRC) was determined by following a wetting path under constant-volume conditions using a specially designed cell with vapor exchange allowed in all directions. Results were compared to that of a single pellet of bentonite swelling under free swelling conditions. Secondly, a series of suction controlled oedometer tests were performed to investigate the compressibility properties of the mixture. The swelling behavior of the mixture following a wetting-drying path was also studied in oedometer. Finally, the swelling pressure was investigated using both constant-volume and swell-consolidation methods.

The results are presented in this chapter in the form of an article submitted to "Engineering Geology".

Characterization of water retention, compressibility and swelling properties of a pellet/powder bentonite mixture

Agustín Molinero Guerra[1,3], Yu-Jun Cui[1], Yong He[2], Pierre Delage[1], Nadia Mokni[3], Anh Minh Tang[1], Patrick Aimedieu[4], Michel Bornert[1], Frédéric Bernier[5]

[1]Ecole des Ponts ParisTech, Laboratoire Navier, France
[2]Central South University, School of Geosciences and Info-Physics, China
[3]Institut de Radioprotection et de Sûreté Nucléaire (IRSN), France
[4]Laboratoire Navier, UMR 8205, ENPC, IFSTTAR, CNRS, UPE, France
[5]Agence Fédérale de Contrôle Nucléaire (AFCN), Belgium

Abstract: The water retention, compressibility and swelling properties of a pellet/powder bentonite mixture was investigated in the laboratory. Vapor equilibrium technique was used for suction control. The water retention property was determined under constant-volume condition using a specially designed cell allowing vapor exchange in all directions; suction controlled oedometer tests were carried out for the compressibility investigation; both constant-volume and swell-consolidation methods were applied for the swelling pressure determination. Comparable results were found for water retention property of the pellet/powder mixture determined under constant-volume condition and the pellet under free swelling condition for suctions higher than 4 MPa, suggesting that physico-chemical suction prevails on capillary suction and moreover the swell of clay particle can be accommodated by the existing macro-pores. On the contrary, at lower suctions, the constant-volume conditions define a clear lower water retention capacity for the mixture, suggesting the disappearance of macro-pores. Oedometer compression curves revealed a different behavior for low and high suctions: at high suctions, the volume change behavior is governed by the pellets rearrangement combined with pellets crushing upon loading. By contrast, at low suctions, the mixture lost its initial granular structure during suction decrease; thus, the volume change behavior is similar to a compacted bentonite. Compared to a compacted bentonite, the pellet/powder bentonite shows a lower yield stress. A lower value of swelling pressure was found with the constant-volume method, indicating the limitation of the swell-consolidation method in determining soil swelling pressure.

Keywords: pellet/powder bentonite mixture; laboratory testing; initial heterogeneity; water retention; swelling; compressibility.

1. Introduction

The design of most deep geological depositories for high level radioactive wastes (HLW) is based on the multi-barrier concept which involves the natural host rock and engineered barriers (Sellin and Leupin, 2013). In this design concept, bentonite-based materials are used to construct buffers, backfills and seals of disposal galleries and access shafts to ensure isolation of the waste from the environment. In particular, mixtures made up of bentonite powder and pellets are considered as a promising candidate sealing material because of its particular properties: in addition to their low permeability, high swelling capacity and high radionuclide migration retardation properties, the pellet/powder mixture exhibits operational advantages in terms of emplacement and absence of technological gaps between the host rock and the seal. Once installed in the repository, the pellet/powder mixture will be submitted to both hydraulic and mechanical loadings: infiltration of pore water from the host rock and mechanical confinement imposed by the convergence of the surrounding rocks. In this context, to ensure the stability of the storage structure thus the safety of the disposal system, it is of paramount importance to well understand the hydro-mechanical behavior of unsaturated bentonite pellet/powder mixture. For this purpose, the French Institute for Radiation Protection and Nuclear Safety (IRSN) has launched the SEALEX project, which consists of a series of *in situ* experiments in the Underground Research Laboratory (URL) in Tournemire, France (Mokni and Barnichon, 2016; Mokni *et al.*, 2016). This project aims at investigating the long-term hydraulic performance of sealing systems in normal and critical scenarios, with different core configurations (precompacted or *in situ* compacted sand/bentonite mixtures, pellet/powder bentonite mixtures). In parallel to the *in situ* experiments, mock-up tests were also carried out (Wang *et al.*, 2012; Saba *et al.*, 2014; Mokni *et al.*, 2016). A relevant result from these investigations is the relationship between the swelling pressure and the dry density of bentonite (Börgesson *et al.*, 1996; Dixon *et al.*, 1996; Lloret *et al.*, 2003; Karnland *et al.*, 2008; Gens *et al.*, 2011; Villar *et al.*, 2012; Wang *et al.*, 2013; Saba *et al.*, 2014; Schanz & Al-Badran, 2014).

Few investigations have been undertaken on the hydro-mechanical behavior of pellet/powder bentonite mixture in the laboratory. Hoffmann *et al.* (2007) performed different tests on compacted granular Febex bentonite mixtures at different dry densities considered within the Engineered Barrier (EB) project (Schuster *et al.*, 2014). An important finding was the progressive decrease of water permeability induced by the clogging of the large inter-pellet pores due to granule swelling and the development in time of both swelling strain and pressure upon wetting. Imbert and Villar (2006) investigated the hydro-mechanical behavior of a 50/50

FoCa bentonite pellet/powder mixture by a series of infiltration tests. They concluded that the mixture became homogeneous with a swelling pressure equal to that of a bentonite powder compacted at the same dry density once full saturation was reached.

In this study, the water retention, swelling and compressibility properties of a 80/20 pellet/powder MX80 bentonite mixture were investigated. Firstly, the water retention curve (WRC) was determined by following a wetting path under constant-volume conditions using a specially designed cell with vapor exchange allowed in all directions. This curve was compared to that of a single pellet of bentonite swelling under free swelling conditions. Secondly, a series of suction controlled oedometer tests were performed to investigate the compressibility properties of the mixture. The swelling behavior of the mixture after following a wetting-drying path was also studied in oedometer. Finally, the swelling pressure was investigated using both constant-volume and swell-consolidation methods. Emphasis was put on the size of samples due to the strong heterogeneous nature of the material with large pellets.

2. Materials and methods

2.1. Materials

The investigated material is a mixture of pellet/powder MX80 bentonite at a proportion of 80/20 in dry mass. The MX80 bentonite comes from Wyoming, USA. It was provided by the Laviosa-MPC company under the commercial name Expangel SP7 for pellets and SP30 for the powder. The MX80 bentonite has a smectite content of 80%, other non-clayey inclusions being quartz, calcite and pyrite. The cation exchange capacity (CEC) is 98 meq/100g, with Na+ as major exchangeable cation, with a value of 52 meq/100g (1.2 meq/100g for K, 10 meq/100g for Mg and 37 meq/100g for Ca). The liquid limit is 560%, the plastic limit is 62% and the unit mass is 2.77 Mg/m^3 (Saba *et al.*, 2014).

Pellets were produced in the Laviosa-MPC company by compacting instantaneously powder of MX80 bentonite in a mould of 7 mm in diameter and 7 mm in height (Laviosa Minerals). A zoom on a single pellet is shown in Figure 1. The fabrication water content was $w = 6\pm1\%$ and the dry density $\rho_d = 2.06\pm0.06$ Mg/m^3, corresponding to$\rho\rho$ a void ratio $e = 0.30\pm0.07$. The pellets were stored in the laboratory in a hermetic plastic box at 20°C. The initial suction ($s = 135 \pm 3$ MPa) was measured in the laboratory with a chilled mirror dew point tensiometer (Decagon WP4C), at an initial water content $w = 7.25\%$ (determined after oven-drying at 105°C for 24 h), slightly higher than the fabrication one due to the water adoption from air after fabrication (Molinero Guerra *et al.*, 2016).
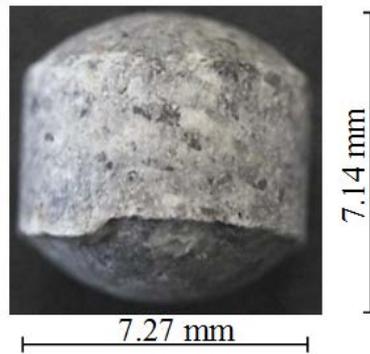
Figure 1. Pellet at its initial state.

The MX80 bentonite powder was produced by crushing pellets. An initial water content of 3.17% was found in the laboratory after oven-drying at 105°C for 24 h, corresponding to an initial suction s = 190.9 MPa (measured with a chilled mirror dew point tensiometer – Decagon WP4). More details about the initial state of the material can be found in Molinero Guerra *et al.* (2016).

2.2. Sample preparation

All the results presented in this work were obtained by performing laboratory tests on the pellet/powder bentonite mixture. The mixture was prepared by following the first protocol presented in Molinero Guerra *et al.* (2016) to obtain a relatively homogeneous pellet/powder distribution. It consists in filling the cell by packets corresponding to one layer of pellets spread over the base of the cylinder and to add the corresponding amount of powder, respecting the proportion of 80-pellets/20-powder. The global dry initial density of the mixture is 1.49 Mg/m^3.

In order to better understand the initial pellet/powder distribution, microfocus X-ray computed tomography observations were made on the mixture at its initial state. A vertical slice is presented in Figure 2. The dimensions of the observed sample are 120 mm in height and 60 mm in diameter. It appears that even though a special protocol was followed, it is difficult to perfectly control the homogeneity of the sample. Indeed, the grains of powder are not uniformly distributed within the sample, and inter-pellet voids can be clearly identified. The sample, placed between two porous stones, presents larger inter-pellet voids at the top porous stone and no grains of powder are observed in this zone. Therefore, this material is characterized by a strong heterogeneity at its initial state, which may be an important aspect to take into account while analysing the global hydro-mechanical behavior of the sample.

The samples used for the present study were prepared in the same manner, but have a height of 35 mm. This height corresponds to 5 times the height of a single pellet and it is believed that such dimensions constitute a representative volume of pellet/powder mixture. Note that this ratio of sample size to maximum grain size was also adopted by Duong *et al*. (2013) when investigating the mechanical behavior of a mixture of coarse and fine soils.
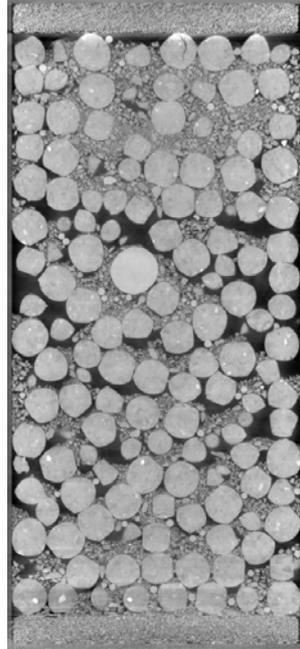

Figure 2. Vertical slice on the investigated pellet/powder bentonite mixture obtained by µ-CT observations - Resolution: 50 µm/voxel.

2.3. Experimental methods

1.1.1. Water retention properties

The water retention curve (WRC) of the pellet/powder bentonite mixture under constant-volume conditions was determined on samples of 50 mm in diameter and 35 mm in height, with a dry density of 1.49 Mg/m^3. A special device presented in Figure 3 was designed for this purpose. The pellet/powder mixture is placed into a rigid stainless steel cell that is designed to allow vapor exchanges not only through the two metallic porous disks on both top and bottom of the sample, but also through a cylindrical porous disk on the lateral surface of the sample. This design is expected to significantly accelerate the hydration of the sample by vapor equilibrium technique, essential for low-permeability materials like the studied swelling MX80 bentonite. Table 1 presents the different salt solutions used for controlling suctions at 20°C. The mass of sample was regularly measured. In a standard fashion, equilibrium was considered once the mass stabilized. Several samples were taken from the different pellet/powder mixtures

once equilibrium was reached to measure both the water content by oven drying and the suction with a chilled mirror dew point tensiometer (Decagon, WP4).
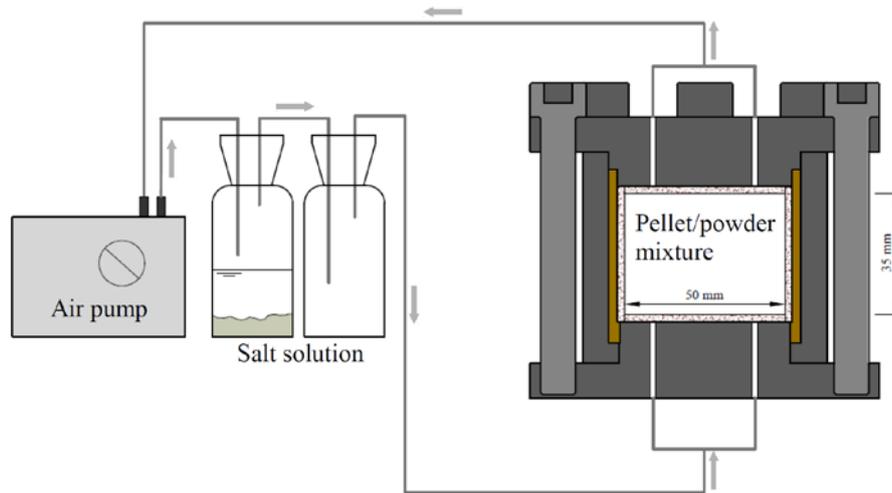
Figure 3. Schematic view of the special cell designed for determining the water retention curve under constant-volume conditions.

In parallel, the water retention curve under free swelling conditions for a single pellet of bentonite was obtained. To this end, pellets were hydrated under several values of suction from their initial state by vapor equilibrium technique. Table 2 presents the test program as well as water content and degree of saturation values at equilibrium (Pi denotes pellets and Mi represents the pellet/power mixture). For the pellet/powder mixture, zero suction was applied by injecting distilled water.

Table 1. Salt solutions and corresponding suctions.

Solution	Suction (MPa)
LiCl	262
MgCl₂	149
K₂CO₃	113.2
Mg(NO₃)₂	82
NaNO₃	30
NaCl	38
(NH₄)₂SO₄	25
KNO₃	9
K₂SO₄	4.2
Distilled water	0

Table 2. Test program for investigating water retention properties.

Sample	Condition	Path (imposed suction in MPa)	At equilibrium	
			Water content (%)	Degree of saturation
P0	Free swelling	Initial state 135.5	6 - 7.25	54.5 – 66.1
P1	Free swelling	113	7.9	53.5
P2	Free swelling	82	9.4	63.4
P3	Free swelling	40	15.6	63.1
P4	Free swelling	38	16	64.1
P5	Free swelling	25	16	60.7
P6	Free swelling	9	24.6	63
P7	Free swelling	4.2	31	63
P8	Free swelling	1	43.5	61
P9	Free swelling	0.8	45.4	71.8
P10	Free swelling	149	6.3	45.2
P11	Free swelling	262	3	25.9
M1	Constant volume	0	34.3	98.1
M2	Constant volume	4	31.7	90.7
M3	Constant volume	6	22.5	64.3
M4	Constant volume	9	20.5	58.8
M5	Constant volume	25	18.8	53.8
M6	Constant volume	82	12.7	36.4

1.1.1. *Compresibility properties – suction controlled oedometer tests*

Controlled suction oedometer compression tests were performed on samples of 35 mm in height and 50 mm in diameter by circulating vapor at controlled relative humidity through the base of the sample as shown in Figure 4 (tests SCO1, SCO2 and SCO3 presented in Table 3). A high pressure oedometer was used allowing application of vertical stresses as high as 50 MPa (Marcial *et al.*, 2002). As opposed to other suction values, zero suction was imposed by circulating pure water. Vertical strain was monitored using a digital micrometer (accuracy ± 0.001 mm).

Prior to compression, time was allowed until swelling stabilized (equilibrium was considered when the vertical displacement was lower than 0.01 mm during 8 hours) under the imposed value of suction and a low vertical stress of 0.1 MPa. Three tests were carried out under three different suctions (0 MPa, 9 MPa and 138 MPa).
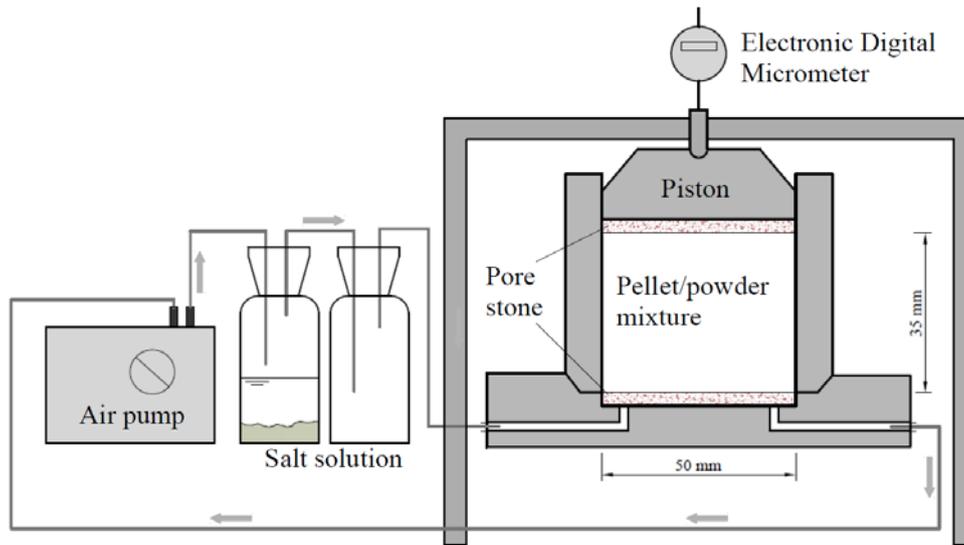
Figure 4. Experimental setup for suction-controlled oedometer tests.

Table 3. Test program for investigating the compressibility and swelling properties of pellet/powder bentonite mixture.

Test No.	Hydration system	Imposed suction (MPa)	Investigated property	Method
SCO1	Vapor transfer	138	Compressibility	-
SCO2	Vapor transfer	9	Compressibility	-
SCO3	Injected distilled water	0	Compressibility and swelling	Swell-consolidation
SCO4	Injected distilled water and vapor transfer	$0 \rightarrow 262$	Swelling	-
CV1	Injected synthetic water	0	Swelling	Constant-volume

1.1.2. Swelling properties

Three tests, SCO3, SCO4 and CV1 presented in Table 3 were performed in order to study the swelling properties of the pellet/powder bentonite mixture. Both the constant-volume and swell-consolidation methods were applied to determine the swelling pressure (Figure 5). To apply the constant-volume method (path 0-1), the device presented in Figure 6 was used. The constant-volume cell includes three parts: (i) the bottom part which contains a porous stone and a drainage system; (ii) the middle cell (70 mm in inner diameter) which prevents any radial swelling, with two air outlets; (iii) the top part including a total pressure sensor to monitor the axial swelling pressure. The water inlet was connected to a water reservoir, flooding the pellet/powder mixture. The saturation water used was synthetic water having the same chemical composition as the pore water of the Callovo-Oxfordian claystone from the ANDRA underground research laboratory in Bure (Table 5). In the swell-consolidation method (path 0-

2-3), the sample was hydrated under a low vertical pressure of 0.1 MPa until full swelling was achieved. Then, it was compressed following a standard consolidation test procedure. The pressure needed to compress the specimen back to its initial volume is defined as the swelling pressure of the material (Basma *et al.*, 1995; Abdullah and Mhaidib, 1998, 1999; Agus, 2005, Wang *et al.* 2012).
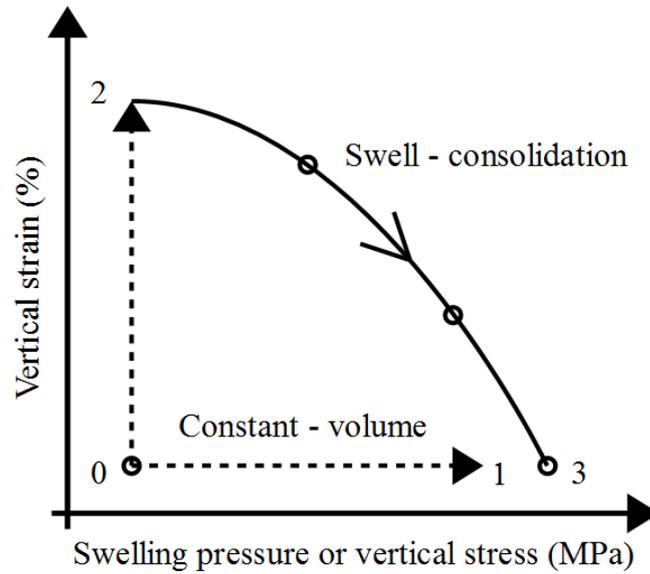

Figure 5. Swell-consolidation and constant-volume methods used to determine the swelling pressure.
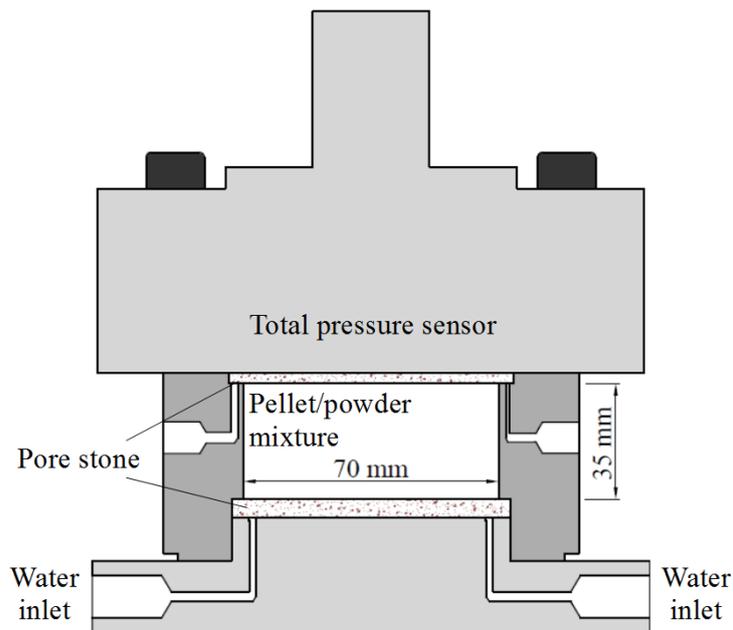
Figure 6. Constant-volume cell for swelling pressure determination.

Table 5. Chemical composition of the used synthetic water.

Components	NaHCO₃	Na₂SO₄	NaCl	KCl	CaCl₂ 2H₂O	MgCl₂O6H₂O	SrCl₂6H₂O
Mass (g) per litre of solution	0.28	2.216	0.615	0.075	1.082	1.356	0.053

3. Experimental results

3.1. Water retention curve

Figure 7 displays the evolution of water content with time for the pellet/powder mixture equilibrated at different suctions presented in Table 2. It is observed that the special cell designed allows the samples to reach water content stabilisation quite quickly. This is because with the specially designed cell (Figure 3), the sample was completely surrounded by porous stones, which accelerates the vapor exchange process. For all imposed suctions, the water content was stabilized after 30 days of hydration, except for 4 MPa and 82 MPa. For $s = 4$ MPa, some technical problems occurred during the test, and a constant water content value was found after 80 days. It is suspected that, at this low suction, the hydration system failed after a certain time due to water condensation in the pipes – cleaning intervention was necessary to solve the problem. For suction $s = 82$ MPa, it seems that water content was constant after 30 days; nevertheless, it continued increasing slightly up to 90 days. For this value of suction, several problems were found during wetting in the hydration system (blockage of the vapor circulation system) and regular interventions were needed.
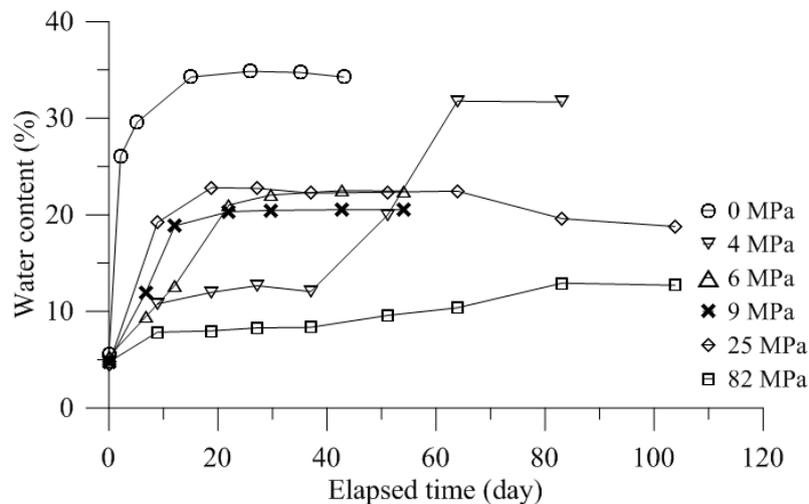

Figure 7. Evolution of water content with time for the pellet/powder bentonite mixture submitted to different suctions under constant-volume conditions.

The water retention curves under constant (pellet/powder mixture) and free swelling conditions (pellet) for a wetting path are presented in Figure 8 in terms of water retention versus suction. It appears that pellet and mixture have comparable water retention properties when suction is higher than 4 MPa, suggesting that the physico-chemical suction prevails on the capillary suction: the effect of capillary suction can be ignored facing the physico-chemical suction because otherwise the mixture should have a lower suction with its lower global density (Yahia-Aissa, 1998). In addition, in the case of mixture, the existing macro-pores can accommodate the swells of clay particles. When suction is lower than 4 MPa, it appears that the mixture has a lower water retention capacity under constant-volume conditions since its water content at zero suction is 34.3% (see Table 2 also). This suggests the disappearance of macro-pores in the mixture. Figure 9 presents the suctions measured by chilled mirror dew point tensiometer versus the imposed values by either vapor equilibrium technique (for non-zero suctions) or injecting distilled water (for zero suction) for the pellet/powder mixture. Some differences were found between the measured suction after equilibrium and the imposed value by vapor equilibrium technique, in particular for zero suction. This could be due to the stress release while dismantling the specimen, which makes suction increase within the mixture. This effect seems more pronounced in the case of zero suction due to the highest swelling pressure developed, which enhances the stress release effect.
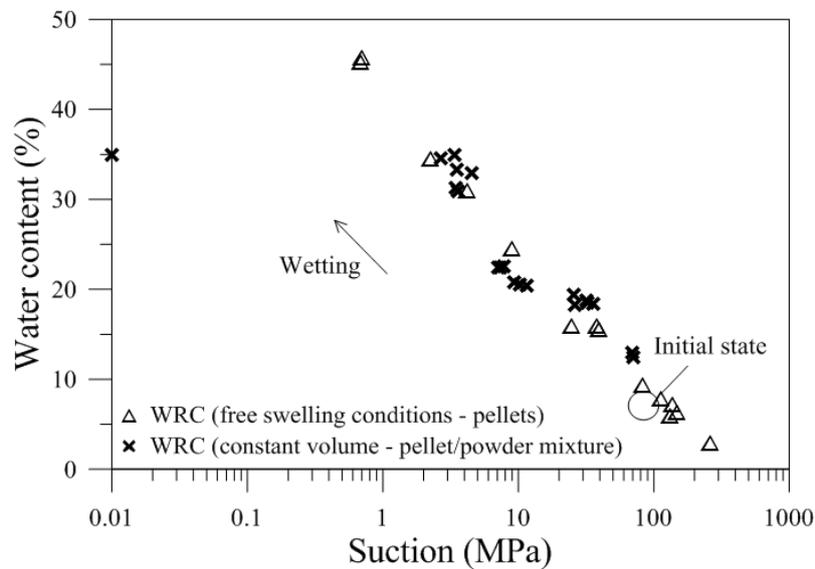

Figure 8. Water retention properties under free swelling conditions (pellets, samples P0-P11 in Table 2) and constant-volume conditions (pellet/powder mixture, samples M1-M6 in Table 2).
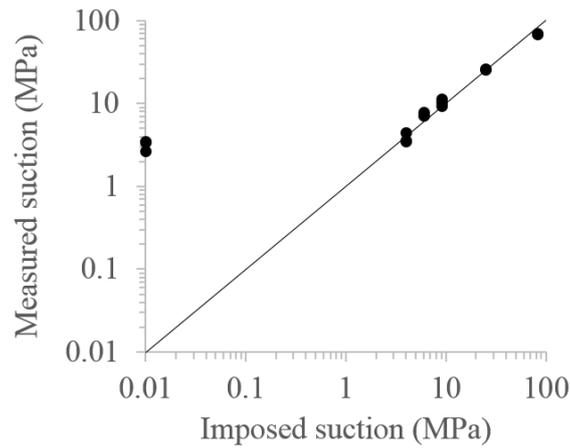
Figure 9. Imposed suctions by vapor equilibrium technique versus measured suction after equilibrium for the pellet/powder bentonite mixture.

3.2. Controlled suction compression tests (SCO1, SCO2 and SCO3)

Figure 10 presents the evolution of volumetric strain with time for tests SCO1, SCO2 and SCO3. In these tests, the samples were equilibrated at 138 MPa, 9 MPa and 0 MPa suctions, respectively. Prior to compression, a vertical stress of 0.1 MPa was applied while imposing suction. In test SCO3, the pellet/powder mixture was hydrated by injecting distilled water to impose zero suction. Equilibrium was reached after 53 days, with a value of 21.1% of volumetric strain, corresponding to a void ratio of $e = 1.25$. The volumetric strain once equilibrium was reached is higher than the value obtained by Wang *et al.* (2011) for compacted bentonite/sand mixture: 18% ($e = 0.97$). This is due to the higher swelling capacity of compacted bentonite pellets. In test SCO2 for 9 MPa suction applied by vapor equilibrium technique, equilibrium was achieved after 43 days, with a volumetric strain of 8.9% ($e = 1.02$). Note that a constant-volumetric strain was reached between 320 h and 430 h. This is due to a problem in the hydration system that needed an intervention of cleaning. After 430 h, the specimen continued swelling until reaching equilibrium. In test SCO1, no suction was imposed as 138 MPa corresponds to the initial state of the pellet/powder mixture; a period of 5 days was considered prior to loading in this case. Once equilibrium was reached, samples were submitted to compression at constant suction. Pressure was increased gradually until reaching 12.8 MPa for the three tests. Under this pressure, the values of volumetric strain of -7.27% ($e = 0.72$), -10.59% ($e = 0.66$) and -23.34% ($e = 0.42$) were recorded for specimens equilibrated at 0 MPa, 9 MPa and 138 MPa of suction, respectively. The unloading process is also shown in this figures. The values of final volumetric strain of 0.62% ($e = 0.87$), -8.39% ($e = 0.7$) and -22.33%

(e = 0.44) were recorded for specimens equilibrated at 0 MPa, 9 MPa and 138 MPa, respectively.
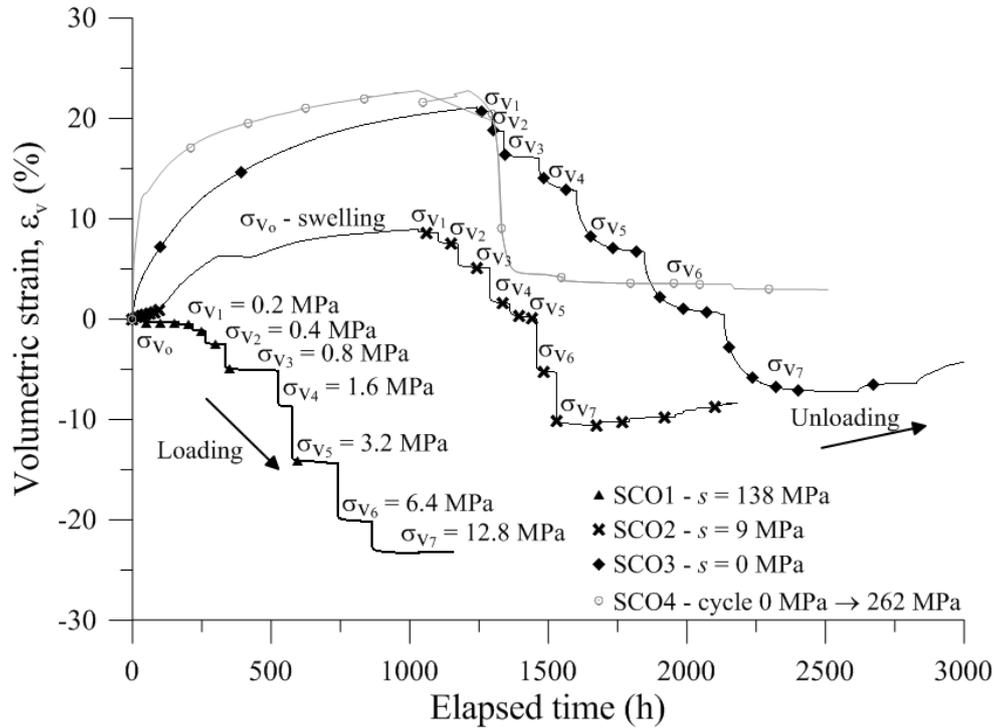

Figure 10. Evolution of the volumetric strain with time in the oedometer tests SCO1, SCO2 and SCO3.

Test SCO4 was designed to study the volume change behavior upon wetting/drying in oedometer. In this case, the pellet/power mixture was submitted to a wetting-drying cycle at a constant vertical stress of 0.1 MPa. In the first phase, the specimen was hydrated by injecting distilled water during 52 days to reach equilibrium at zero suction (comparable to the 53 days for test SCO3). A volumetric strain of 22.8% (e = 1.28) was found at equilibrium. Then, a suction of 262 MPa was imposed to the mixture. The volumetric strain decreased drastically, reaching a value of 4.8% (e = 0.87) after 57.3 days. A final value of 3% (e = 0.84) was observed after 96.3 days.

Once equilibrated at the imposed suctions, the pellet/powder mixtures were submitted to compression at constant suctions. Results are displayed in Figure 11 in terms of specified volume v with respect to vertical net stress. The initial specified volume is different for all the tests due to different swells under different suctions. In a standard fashion, the compression curves are characterized by an initial linear part with low compressibility (that can be considered as the pseudo-elastic domain) followed by a second part with higher compressibility (that can be considered as the plastic domain). Finally, the third part, corresponding to the

unloading, exhibits the same trend as the elastic domain, as only elastic deformations are expected. For test SCO3 where a suction of 0 MPa was applied, the unloading path can also be considered as bi-linear, in agreement with that identified by Cui *et al*. (2013) for Ypresian clays (YPClay).
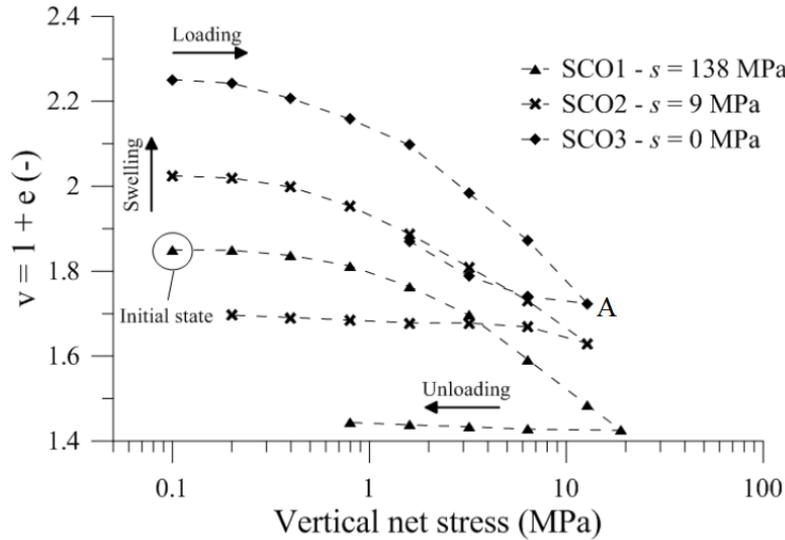
Figure 11. Specific volume versus vertical stress for tests SCO1, SCO2 and SCO3.

The evolution of the yield stress with suction is presented in Figure 12, together with the values obtained by Marcial *et al*. (2003) and Wang *et al*. (2013) for compacted pure bentonite and compacted bentonite/sand mixture respectively. A good coincidence is observed for compacted pure bentonite and the pellet/powder mixture at zero suction. For other values of suction, in a standard fashion, the yield stress increases as suction increases. However, this phenomenon is not clear for the pellet/powder mixture: a much lower yield stress value is obtained. This point will be discussed later.
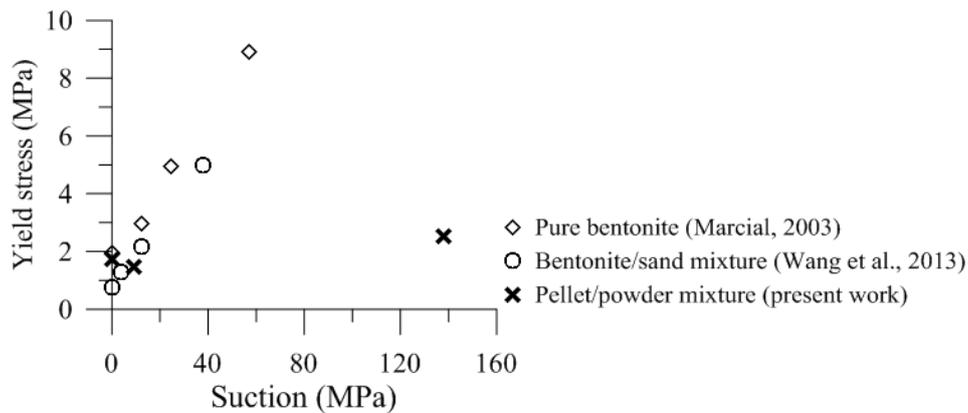
Figure 12. Changes in yield stress with suction.

The swelling pressure of the pellet/powder mixture can be determined by the swell-consolidation method using the results from test SCO3. As it was explained previously, the swelling pressure of the material corresponds to the vertical stress needed to compress the sample to its initial volume. The obtained value is $\sigma_s = 7.1\ MPa$ ($e = 0.859$).

3.3.   Swelling under constant-volume conditions (CV1)

The swelling behavior of the pellet/powder bentonite mixture under constant-volume conditions was investigated by following the evolution of the axial swelling pressure while hydration (test CV1 in Table 3). Results are displayed in Figure 13. Two rates of increase of axial swelling pressure can be distinguished from the beginning of the hydration process: the first one corresponds to a period from the beginning of the hydration up to 20 days, when swelling pressure reaches a value of 0.43 MPa. Then, the pressure continues increasing at a different rate, until 45 days of hydration. At this moment, the swelling pressure reaches 0.8 MPa. Afterwards, a slight increase is observed, finally reaching 0.87 MPa after 440 days. Nevertheless, it can be observed that the swelling pressure continues increasing, which means that the sample is not completely in equilibrium, even though the rate of increase is quite low compared to those observed before. The value of pressure observed after 440 days (0.87 MPa) is significantly lower than the value obtained by applying the swell-consolidation method on the consolidation curve (7.1 MPa). It is also important to mention that based on the relationship obtained by Wang *et al.* (2013) between the dry density of bentonite and the swelling pressure, a value of 4.15 MPa of swelling pressure is found at a dry density of 1.49 Mg/m^3. These differences will be also discussed later in the discussion section.
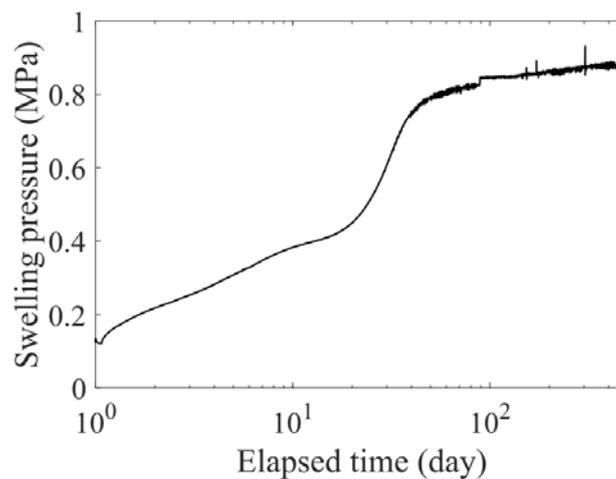

Figure 13. Evolution of axial swelling pressure with time in test CV1.

4. Discussion

The water retention curves (following a wetting path) obtained for the pellet/powder mixture under constant-volume conditions and a single pellet of bentonite under free swelling conditions revealed that, for low suctions, the water retention property of bentonite depends strongly on the confining conditions (Yahia-Aissa *et al*., 2001; Cui *et al*., 2008; Ye *et al*., 2009). Nevertheless, for high suctions both curves become comparable. This is because at high suctions, the exfoliation of clay particles from the aggregates into inter-aggregate pores caused by hydration is moderate and can be accommodated by the existing macro-pores.

The investigation of the swelling properties of the pellet/powder bentonite mixture by following the swell-consolidation and constant-volume method revealed different values of swelling pressure: the swell-consolidation method provided 7.1 MPa, whereas a value of 0.87 MPa was found with the constant-volume method. The results obtained by Wang *et al*. (2013) also revealed higher swelling pressures with the swell-consolidation method and the authors explained that by the coupling between the microstructure deformation and the macrostructure deformation, combined to the effect of friction.

Cui *et al*. (2013) carried out oedometer tests with loading/unloading/reloading on natural stiff Ypresian clays (YPClay). They concluded that each unloading/reloading curve can be satisfactorily considered as bi-linear with a small and a larger slope separated by a threshold vertical stress. This stress was confirmed to be the swelling pressure corresponding to the void ratio just before the unloading or reloading. By applying this approach to the pellet/powder mixture at zero suction (SCO3), with the consideration of the unloading path as bilinear, a swelling pressure of 4.2 MPa (threshold vertical stress) is obtained, corresponding to a void ratio $e = 0.72$ (dry density $\rho_d = 1.61$ Mg/m^3, point A in Figure 11). This value is comparable with that estimated by the method of Wang *et al*. (2013), showing clearly that the true swelling pressure of the mixture must be lower than that determined by the swell-consolidation method because the value corresponds to the point separating the two parts of unloading curve, thus below the compression curve.

The results from test SCO4 allow the reversibility of swelling of the pellet/powder mixture to be investigated. After wetting under zero suction, the sample was dried by imposing $s = 262$ MPa. Results showed a drastic decrease of volumetric deformation, reaching a final value of 3%. This suggests that plastic swelling deformation occurred upon wetting under zero suction, as shown in Figure 14. This is due to: (i) the plastic deformations developed at a microstructural

level combined to (ii) the evolution of the granular structure towards a homogeneous specimen. Compared to test SCO3, a slightly higher volumetric strain was reached in test SCO4, suggesting a certain effect of the pellet/powder distribution that is specific for each sample. The final points of tests SCO1, SCO2 and SCO3 appears well aligned, defining a wetting line. This line is below the drying line estimated from test SCO4. The difference between the two lines is larger at higher suction.
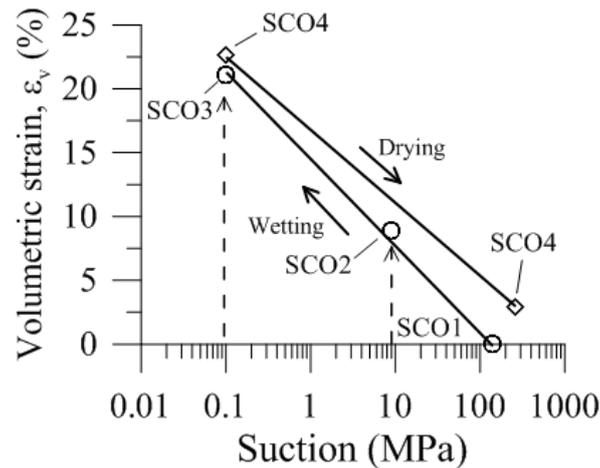

Figure 14. Volumetric strains measured at different suctions after equilibrium at the imposed suction for the different tests.

Further analysis of the swelling pressure evolution with time displayed in Figure 13 revealed the processes governing the structural changes of the pellet/powder mixture while wetting. At the very beginning of the test, the observed swelling pressure and the corresponding rate of increase are due to the pellets located at the top of the sample, where the suction is still high. After a period of 20 days, a second rate of increase higher than the first one is observed. The reason is that water has arrived to pellets located at the top of the sample at this state; thus, the involved pellets start swelling and the pressure increases accordingly. It is suspected that all inter-pellet voids are filled with swollen bentonite after 40 days of hydration, as the rate of increase of swelling pressure decreases. However, the value is not equal to zero, meaning that the specimen is not homogeneous. Taking into account the relationship proposed by Wang *et al.* (2013) between the swelling pressure and the dry density of bentonite, a final value of 4.15 MPa of swelling pressure is found. To reach this value, much more time is necessary.

The investigation of the compressibility properties of the mixture revealed the common elastic and plastic deformations for all suctions. Results shows lower values of the yield stress compared to pure bentonite mixtures except the yield stress corresponding to zero suction (Marcial, 2003). This is because, for non-zero suctions, the pellet/powder mixture has not

completely lost its initial granular mixture; thus, the deformations are essentially governed by the rearrangement and crushing of pellets while loading. These deformations are of plastic nature. However, in the case of zero suction, the mixture has entirely lost its granular structure; thus, the volume change behavior is comparable to that of a common compacted bentonite. This phenomenon can be also observed by analyzing the evolution of volumetric strain with time: at 138 MPa and 9 MPa of suctions, the volumetric strains decrease almost instantaneously while loading; however, at zero suction, the decrease rate of volumetric strain is clearly lower than those observed at other suctions, because the pellets have lost their granular structure at zero suction.

5. Conclusion

The water retention, compressibility and swelling properties of a 80-pellet/20-powder bentonite mixture were investigated through the water retention tests under free (pellet) and constant-volume (mixture) conditions, suction controlled oedometer tests and hydraulic tests on samples at a dry density of 1.49 Mg/m3.

The new cell designed for the WRC determination under constant-volume condition allowed the hydration process to be significantly accelerated - 50 days were necessary to saturate the pellet/powder mixture in the oedometer cell, while only 23 days was needed with this new system.

Similar water retention properties were observed for pellet/powder mixture under constant-volume condition and pellet under free swelling condition at suction higher than 4 MPa, indicating that physico-chimical suction prevails on capillary suction, the effect of the latter being negligible; in addition, the swell of clay particles was accommodated by existing macro-pores in the mixture. On the contrary, at lower suctions, constant-volume condition defined a lower water retention capacity because of the disappearance of macro-pores in that case.

The investigation of the compressibility properties revealed lower values of yield stress than the common pure bentonite mixtures, except for the specimen hydrated at zero suction. This is due to the granular structure in the case of non-zero suction where the volume change behavior is governed by the rearrangement and crushing of pellets, and the loss of the granular structure in the case of zero suction.

The irreversibility of the volumetric strain was confirmed by imposing a wetting-drying cycle to the pellet/powder mixture under constant loading. This is due to the combination of plastic

deformations developed at a microstructural level and the evolution of the granular structure towards a homogeneous specimen.

Different swelling pressure values were obtained by applying different methods. A higher swelling pressure was obtained with the swell-consolidation method. Further analysis based on the method proposed by Cui *et al*. (2013) showed that the swell-consolidation systematically overestimates swelling pressure because for a given density the swelling pressure must be lower than the corresponding pressure on the consolidation curve.

References

Abdullah, I., Mhaidib, A., (1998). Prediction of swelling potential of an expansive shale. Proceedings Of The Second International Conference On unsaturated soils. 27–30 August. Beijing, China, vol. 1.

Abdullah, I., Mhaidib, A., (1999). Swelling behavior of expansive shales from the middle region of Saudi Arabia. Geotechnical and Geological Engineering 16 (4), 291–307.

Agus, S., (2005). An Experimental study on hydro-mechanical characteristics of com- pacted bentonite-sand mixtures. PhD thesis. Weimar.

Basma, A.A., Al-Homoud, A.S., Husein, A., (1995). Laboratory assessment of swelling pres- sure of expansive soils. Applied Clay Science 9 (5), 355–368.

Börgesson, L., Karnland, O. and Johannesson, L. E., (1996). Modelling of the physical behavior of clay barriers close to water saturation. Engineering Geology 41, No. 1–4, 127–144.

Cui, Y.J., Tang, A.M., Loiseau, C., Delage, P., (2008). Determining the unsaturated hydraulic conductivity of a compacted sand–bentonite mixture under constant-volume and free-swell conditions. Physics and Chemistry of the Earth, Parts A/B/C 33 (Suppl. 1), S462–S471.

Cui, Y. J., Nguyen, X. P., Tang, A. M., and Li., X. L., (2013). An Insight into the Unloading/reloading Loops on the Compression Curve of Natural Stiff Clays. Applied Clay Science 83-84: 343–48.

Dixon, D. A., Gray, M. N. and Graham, J., (1996). Swelling and hydraulic properties of bentonites from Japan, Canada and the USA. Environmental Geotechnics 1, 43–48.

Duong, T. V., Tang, A. M., Cui, Y. J., Trinh, V. N., Dupla, J. C., Calon, N., Canou, J., and Robinet, A. (2013). Effects of fines and water contents on the mechanical behavior of interlayer soil in ancient railway sub-structure, *Soils Found.*, vol. 53, no. 6, pp. 868–878.

Gens, A., Vallejan, B., Sánchez, M., Imbert, C., Villar, M.V. and Van Geet, M., (2011). Hydro mechanical Behavior of a Heterogenous Compacted Soil: Experimental Observations and Modelling.

Hoffmann, C., Alonso, E.E. & Romero, E., (2007). Hydro-mechanical behavior of bentonite pellet mixtures. Physics and Chemistry of the Earth, 32(8-14), pp.832–849.

Imbert, C. & Villar, M.V., (2006). Hydro-mechanical response of a bentonite pellets/powder mixture upon infiltration. *Applied Clay Science*, 32(3-4), pp.197–209.

Karnland, O., Nilsson, U., Weber, H., Wersin, P., (2008). Sealing ability of Wyoming bentonite pellets foreseen as buffer material – laboratory results. Physics and Chemistry of the Earth, Parts A/B/C 33, S472–S475.

Lloret, A., Villar, M. V., Sánchez, M., Gens, A., Pintado, X. and Alonso, E. E., (2003). Mechanical behavior of heavily compacted bentonite under high suction changes. Géotechnique 53, No. 1, 27–40.

Marcial, D., Delage, P., Cui, Y.J., (2002). On the high stress compression of bentonites. Canadian Geotechnical Journal 39, 812–820.

Marcial, D., (2003). Comportement hydromécanique et microstructural des matériaux de barrière ouvragée, thèse. ENPC Paris, France.

Mokni, N. & Barnichon, J.D., (2016). Hydro-mechanical analysis of SEALEX *in situ* tests-Impact of technological gaps on long term performance of repository seals. Engineering Geology, 205, pp. 81-92.

Mokni, N., (2016). Analysis of hydro-mechanical behavior of compacted bentonite/sand mixture using a double structure formulation. Environ Earth Sci (2016) 75: 1087.

Molinero-Guerra, A., Mokni, N., Delage, P., Cui, Y. J., Tang, A. M., Aimedieu, P., Bernier, F. and Bornert, M., (2016). In-depth characterisation of a mixture composed of powder/pellets MX80 bentonite. Applied Clay Science,135, pp. 538-546.

Saba, S., Cui, Y.J., Tang, A.M., and Barnichon, J.D., (2014). Investigation of the swelling behavior of compacted bentonite–sand mixture by mock-up tests. Canadian Geotechnical Journal, 51(12), pp.1399–1412.

Sellin, P., and Leupin, O. X., (2013). The use of clay as an engineered barrier in radioactive-waste management – a review. Clays and Clay Minerals 61, No. 6, 477–498.

Schanz, T. and Al-Badran, Y., (2014). Swelling pressure characteristics of compacted Chinese Gaomiaozi bentonite GMZ01. Soils and Foundations 54, No. 4, 748–759.

Schuster, K., Furche, M., Velasco, M., Gaus, I., Trick, T., Garcia-Siñeriz, J. L., Rey, M.,Schulte, F., Sanchez Herrero, S., Tietz, T. & Mayor, J. C., (2014). Long-term Performance of Engineered Barrier Systems PEBS Engineered Barrier Emplacement Experiment in Opalinus Clay: "EB" Experiment.

Villar, M. V., Gómez-Espina, R. and Guitiérrez-Nebot, L., (2012). Basal spacings of smectite in compacted bentonite. Applied Clay Science 65–66, 95–105.

Wang, Q., Tang, A. M., Cui, Y. J., Delage, P., and Gatmiri, B., (2012). Experimental study on the swelling behavior of bentonite/claystone mixture. Eng. Geol., vol. 124, no. 1, pp. 59–66.

Wang, Q., Tang, A.M., Cui, Y.J., Barnichon, J.D. and Ye, W.M., (2013). A comparative stud on the hydro-mechanical behavior of compacted bentonite/sand plug based on laboratory and field infiltration tests. Eng. Geol. 162, 79–87.

Yahia-Aissa, M. (1999). Comportement hydromécanique d'une argile gonflante fortement compactée. PhD thesis, Ecole Nationale des Ponts et Chaussées, CERMES, Paris, France (in French).

Yahia-Aissa,M., Delage, P., Cui, Y.J., (2001). Suction–water relationship in swelling clays. Clay Science for Engineering. In: Adachi, K., Fukue,M. (Eds.), Proceedings of the IS-Shizuoka International Symposium on Suction, Swelling, Permeability and Structure of Clays. Shizuoka, Japan Balkema, pp. 65–68.

Ye, W.M., Cui, Y.J., Qian, L.X., Chen., B., (2009). An experimental study of the water transfer through confined compacted gmz bentonite. Engineering Geology 108 (3–4), 169–176.

Chapter 3

Physical modelling – investigation of the HM behavior by mock-up tests

INTRODUCTION

Laboratory mock-up tests were performed on samples at 1/10th of that in SEALEX project with similar boundary conditions (hydration under constant-volume conditions through the top and bottom of the sample). Two cells were designed: the first one allows monitoring the radial swelling pressure and the relative humidity at different positions within the sample, as well as the global axial swelling pressure. The volume of injected water was also monitored during the test. The second one was specially designed to allow μ-CT observations of the pellet/powder mixture while wetting. It consists of a transparent PMMA cell. Only the global axial swelling pressure was monitored for this cell.

The first part of this chapter aims at studying the hydro-mechanical behavior of a 80/20 pellet/powder mixture fabricated by following a special protocol detailed in the first chapter of this work. A deep analysis of the radial swelling pressure evolution as well as the axial swelling pressure was performed, together with the relative humidity. In the second part of the chapter, the structural changes of a pellet/powder bentonite mixture fabricated by following the same protocol mentioned previously was investigated by means of μ-CT observations. An estimation of the evolution of density of the mixture while wetting was performed, and a qualitative analysis of the swelling behavior was conducted. Moreover, different configurations were considered in order to investigate the influence of the pellet/powder distribution on the hydro-mechanical response of the material. The first sample was fabricated by following the protocol detailed previously, which ensures a relatively homogeneous pellet/powder distribution. The second sample was specially fabricated to study a strong heterogeneous pellet/powder distribution: the top half part of the cell was composed only by pellets of bentonite. However, all inter-pellet voids were filled by bentonite grains in the bottom half part of the specimen. Finally, a comparison was made between the SEALEX *in situ* experiment and the laboratory mock-up tests.

This chapter is organised in the form of an article submitted to "Engineering Geology" for the first part, and "Applied Clay Science" for the second and "Canadian Geotechnical Journal" for the last part.

Investigation of the hydro-mechanical behavior of a pellet/powder MX80 bentonite mixture using an infiltration column

Agustín Molinero Guerra[1,2], Yu-Jun Cui[1*], Nadia Mokni[2], Pierre Delage[1], Michel Bornert[1], Patrick Aimedieu[3], Anh Minh Tang[1], Frédéric Bernier[4]

[1]Ecole des Ponts ParisTech, Laboratoire Navier/CERMES, Marne La Vallée, France
[2]Institut de Radioprotection et de Sûreté Nucléaire (IRSN), Fontenay-aux-Roses, France
[3]Laboratoire Navier, UMR 8205, ENPC, IFSTTAR, CNRS, UPE, Champs-sur-Marne 77455, France
[4]Agence Fédérale de Contrôle Nucléaire (AFCN), Belgium

Abstract: Non-compacted pellet/powder bentonite mixtures are considered as candidate sealing plug materials in geological disposals of radioactive waste. Due to its nature, this mixture is characterized by a heterogeneous porosity network, which is responsible for its complex hydro-mechanical (HM) behavior. The French Institute of Radioprotection and Nuclear Safety (IRSN) has investigated this mixture within the SEALEX project. Both *in situ* large-scale and laboratory small-scale experiments were carried out. This paper presents the results of a small-scale mock-up test at 1/10th scale of the *in situ* experiments, in which the pellet/powder mixture has been saturated from both sides (top and bottom of the specimen). Both swelling pressure and relative humidity were monitored at several positions of the specimen. Different responses from the sensors were found, depending on the local porosity as well as the evolution of the hydration front. The HM response of the mixture is strongly conditioned by the initial pellet/powder distribution, which depends on the protocol followed for the specimen preparation. After 800-day hydration, an anisotropy was found between the axial and the radial swelling pressures, due to the presence of larger void at the top of the sample and the friction at the cell wall. The estimated density gradient was heterogeneous after 800-day hydration due to the initial heterogeneous porosity distribution, combined with the effect of friction and the non-saturation of the mixture. The evolution of injected water with time revealed that the sample was not saturated after 800-day hydration.

Keywords: pellet/powder bentonite mixture; heterogeneous porosity network; mock-up test; swelling pressure; relative humidity; density profile.

1. Introduction

Powder/pellet bentonite mixtures are considered as one of the candidate sealing materials for deep underground radioactive waste repositories thanks to their favourable properties: high swelling capacity, high radionuclide migration retardation properties and operational advantages: easy to manufacture and install (especially in vertical shafts). Once installed in the gallery, the pellet/powder bentonite mixture is initially unsaturated. Then, the saturation process starts under constrained volume condition due to the infiltration of pore water from the host rock, generating a swelling pressure that allows filling the voids within the mixture. Due to its nature, these mixtures are characterized by an initial heterogeneous porosity distribution (Molinero Guerra *et al*., 2016), which results in a complex hydro-mechanical behavior during the saturation process. It is therefore essential to investigate this swelling behavior in order to validate the material for the sealing plug in the underground radioactive waste disposal.

In this context, the Institute of Radioprotection and Nuclear Safety (IRSN, France) has launched the SEALEX (SEALing performance Experiments) project, within which the work presented here was conducted. The purpose of this project is to investigate the long-term hydraulic performance of sealing systems in normal and critical scenarios, as well as different core compositions and configurations (mixture composed of bentonite pellets with bentonite powder or of sand with bentonite powder, precompacted or *in situ* compacted). Figure 1 presents the layout of the experiments.
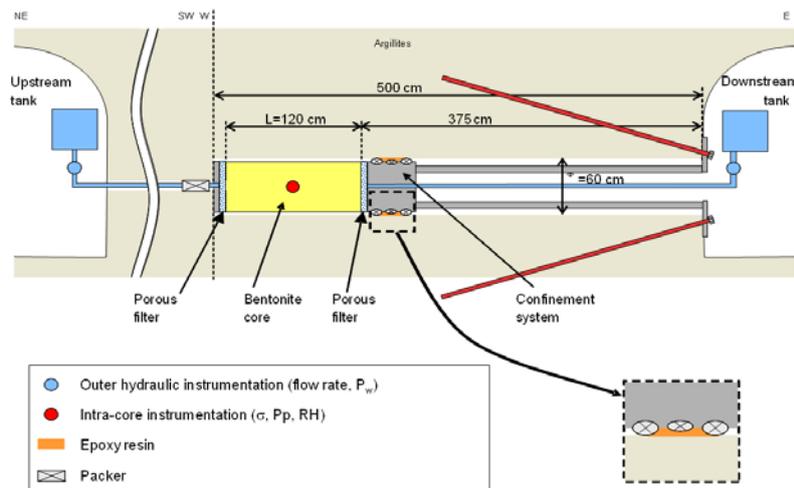

Figure 1. Layout of the SEALEX *in situ* tests (after Mokni *et al*., 2016).

The hydro-mechanical behavior of different configurations of sealing plugs has been investigated at both laboratory and field scales (Wang *et al*., 2012; Saba *et al*., 2014; Mokni *et al*., 2016). An important result from these investigations is the relationship between the swelling

pressure and the dry density of bentonite (Börgesson *et al*., 1996; Dixon *et al*., 1996; Lloret *et al*., 2003; Karnland *et al*., 2008; Gens *et al*., 2011; Villar *et al*., 2012 ; Wang *et al*., 2013; Saba *et al*., 2014; Schanz & Al-Badran, 2014). These relationships were derived on the basis of the measured axial swelling pressure of the investigated materials. However, few investigations have been carried out on the radial swelling of the studied sealing plug (Saba *et al*., 2014). Therefore, it is fundamental to further investigate the complex patterns governing the swelling behavior of the initially heterogeneous mixture of pellet/powder of bentonite in order to ensure that this repository configuration design meets the performance targets.

The swelling capacity of pellet/powder bentonite mixtures was investigated by Imbert & Villar (2006) through a series of infiltration tests on a 50/50 pellet/powder FoCa bentonite compacted at different dry densities. After full saturation, the swelling pressure was found analogous to that of a specimen of powder compacted at the same dry density. Van Geet *et al*. (2005) studied the hydration process of a 50/50 pellet/powder FoCa bentonite mixture by X-ray computed tomography. The results showed the progressive decrease of the density of pellets and the apparent homogenisation after saturation. Other sealing plug configurations were investigated by mock-up tests. Wang *et al*. (2013) and Saba *et al*. (2014) studied a compacted MX80 bentonite/sand mixture (with a proportion of 70/30 in dry mass). Saba *et al*. (2014) investigated the anisotropy of swelling pressure of compacted bentonite/sand mixture. µCT observations revealed that the material was looser in the radial direction than in the axial one. The homogenisation process of a granular material made of highly compacted bentonite pellets (granular buffer material, GBM) was investigated by Garcia-Siñeriz *et al*. (2015) under the context of the EB (engineered barrier) experiment. Upon dismantling, a gradient of density and water content was found within the GBM, probably due to the initial heterogeneity of the material (Villar, 2013).

No investigations have been carried out on the swelling of non-compacted pellet/powder bentonite mixtures. This is however crucial in the design of sealing plugs for deep radioactive waste disposal, because the initial heterogeneous distribution of porosity of these configurations might result in an anisotropy of swelling. Therefore, this study aims at investigating the HM behavior of this kind of mixture by simulating the SEALEX *in situ* experiments at a small scale (1/10, resulting in 60 mm in diameter and 120 mm in height). Radial swelling pressure at different positions, as well as axial swelling pressure and relative humidity were monitored during hydration from both sides (top and bottom of the sample). The volume of injected water was also recorded during the test.

2. Investigated material

The soil studied is a mixture of pellet/powder MX80 bentonite at a proportion of 80/20 in dry mass. The bentonite investigated comes from Wyoming, USA. It was provided by the Laviosa-MPC company under the commercial name Expangel SP7 for pellets and SP30 for the powder. The MX80 bentonite has a smectite content of 80%, other minerals being quartz, calcite and pyrite. The cation exchange capacity (CEC) is 98 meq/100g, with Na+ as major exchangeable cation (52 meq/100g, with also 1.2 meq/100g for K, 10 meq/100g for Mg and 37 meq/100g for Ca). The liquid limit is 560%, the plastic limit is 62% and the unit mass is 2.77 Mg/m^3 (Saba *et al*., 2014).

Pellets of bentonite were produced by Laviosa-MPC Company by compaction of a powder of MX80 bentonite in a mould of 7 mm in diameter and 7 mm in height. Compaction was performed at a water content of 6±1% by applying instantaneous compaction effort, resulting in a pellet dry density ρ_d = 2.06±0.06 Mg/m^3, corresponding to a void ratio e = 0.30±0.07. The pellets were stored in the laboratory in a hermetic plastic box at 20°C. The initial suction (s = 135 ± 3 MPa) was measured in the laboratory with a chilled mirror dew point tensiometer (Decagon WP4C), at an initial water content w = 7.25%, slightly higher than the fabrication one, due to further hydration after fabrication (Molinero Guerra *et al*., 2016).

The MX80 bentonite powder was produced by crushing pellets. An initial water content of 3.17% was found in the laboratory after drying at 105°C for 24h, corresponding to an initial suction s = 190.9 MPa (measured with a chilled mirror dew point tensiometer – Decagon WP4). More details about the initial state of the material can be found in Molinero Guerra *et al*. (2016).

The saturation water used in the test is synthetic water having the same chemical composition as the pore water of the Callovo-Oxfordian claystone from the ANDRA underground research laboratory in Bure (Table 1). The water was obtained by mixing the chemical components with distilled water until full dissolution.

Table 1. Chemical composition of the synthetic water

Components	NaHCO$_3$	Na$_2$SO$_4$	NaCl	KCl	CaCl$_2$ 2H$_2$O	MgCl$_2$O6H$_2$O	SrCl$_2$6H$_2$O
Mass (g) per litre of solution	0.28	2.216	0.615	0.075	1.082	1.356	0.053

2.1. Microstructural features of the material

Results of mercury intrusion porosimetry (MIP) tests for a pellet of bentonite at its initial state are presented in Figure 2. A pore population with an average entrance diameter of 11.9 nm is detected, as well as a second one at diameters around 4 – 5 µm that represents the 6.8% of the total porosity. For the pellet/powder mixture, macro-voids existing between pellets and power grains will play an important role in the HM behavior. The investigated material is characterized by a multimodal porosity network with a heterogeneous distribution of the porosity within the sample. The latter was demonstrated by a qualitative analysis of a vertical slice obtained by carrying out µ-CT observations of a pellet/powder bentonite mixture prepared by following the same protocol as the investigated specimen in the mock-up test (Figure 3). This feature is crucial since it conditions the overall HM behavior of the material.
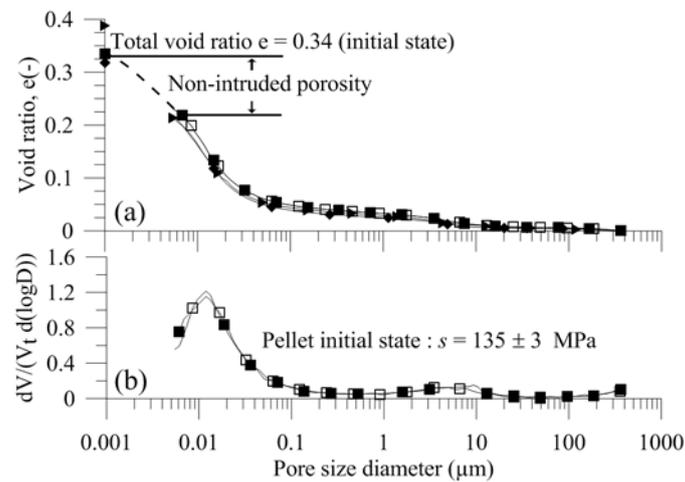

Figure 2. MIP tests results for a pellet of bentonite at its initial state.
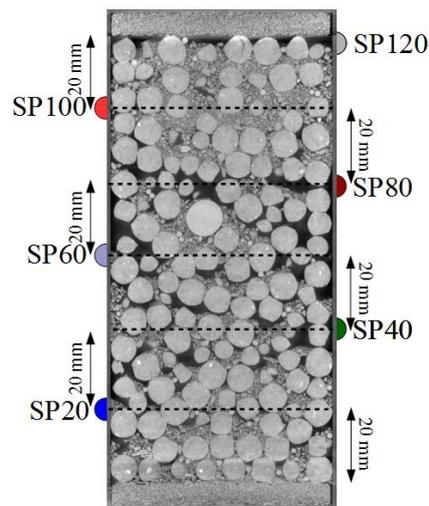
Figure 3. Vertical section of the investigated pellet/powder bentonite mixture obtained by µ-CT observations. Resolution: 50 µm/voxel.

3. Experimental methods

3.1. Experimental set-up

The layout of the small-scale infiltration cell (mock-up test cell) is presented in Figure 4. The dimensions correspond to 1/10 of the *in situ* SEALEX experiments (60 mm in diameter and 120 mm in height). The confined saturation conditions for the pellet/powder bentonite mixture are ensured by a rigid structure that keeps a zero radial displacement and a piston blocked by a screw, which prevents any axial displacement. The material is saturated from both sides (top and bottom), simulating the SEALEX *in situ* experiments. The sample is placed between two pore stones and two filter papers. The bottom and the upper bases are equipped with a water inlet and an air outlet. The air outlet is needed to evacuate the air that is present in the base and in all the system near the inlets. Mechanical valves are mounted and sealed at the faces of both inlets, allowing the entrance of water and the evacuation of air. Flexible water hoses are connected to the valves. The side serving as a water inlet is connected to a burette and to a water tank, allowing the volume of injected water to be measured during hydration. Six total pressure sensors are installed in the cell (SP20, SP40, SP60, SP80, SP100 and SP120), which allow the measurement of the radial swelling pressure at different positions (h = 20, 40, 60, 80, 100 and 120 mm from the bottom side). Figure 3 presents the pellet/powder mixture together with the position of the radial swelling pressure sensors. A force transducer is installed under the cell base, which monitors the axial swelling pressure. In this study, the relative humidity is also recorded by five relative humidity sensors (RH31, RH51, RH71, RH91 and RH111) placed at different heights in the cell (h = 31, 51, 71, 91 and 111 mm, see Figure 4), allowing the evolution of suction to be monitored while hydration.

3.2. Sample preparation and test procedure

The sample was prepared directly into the cell that was already placed on the tray of the force transducer with the radial sensors screwed to the cell. The pellet/powder mixture was obtained by following the first protocol proposed in Molinero Guerra *et al.* (2016), which allows a homogeneous sample to be obtained. It was to fill the cell by packets corresponding to one layer of pellets spread over the base of the cylinder and to add the corresponding amount of powder (taking into account the proportion 80% pellets – 20% powder in dry mass). Figure 3 presents a vertical section of the pellet/powder mixture obtained by microfocus X-ray computed tomography observations on a sample at its initial state, together with the positions of the swelling pressure sensors. The global dry density is 1.49 Mg/m^3.
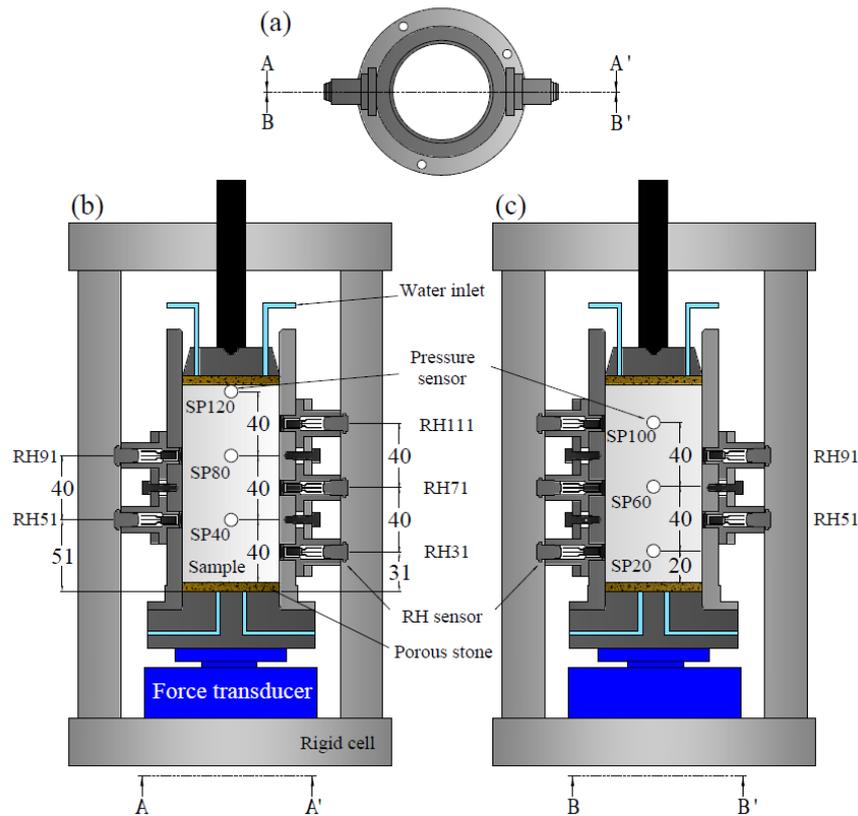
Figure 4. Layout of the mock-up test cell (a) seen from above; (b) section A-A'; (c) section B-B'.

Once the sample was prepared, the two stainless steel plates were fixed with three rods. The central screw was adjusted to ensure the constant volume conditions. The test was started by opening the water inlet valves. At the beginning of the test, air in the base or in the piston was evacuated by opening the air outlet valve until no air bubble was observed in the pipes. Synthetic water was injected by both the top and the bottom of the sample, as the SEALEX *in situ* experiments. Radial and axial swelling pressures, as well as relative humidity were recorded automatically by a data logger. The volume of injected water was also controlled while hydration by two graduated burettes connected to the hydration system. No water pressure was applied during the saturation process.

4. Results

4.1. Investigation of the swelling pressure

The evolution of the swelling pressure with a zoom on the first 15 days is observed in Figure 5. A different rate of increase is identified for each sensor. For sensor SP100, located at 100 mm

from the bottom (and 12 mm from the top hydration front), an initial fast increase of the swelling pressure is observed, reaching a peak value of 2.15 MPa, then a decrease until 1.5 MPa, and finally an increase to reach stabilisation at about 2.5 MPa. This phenomenon occurs during the first hours of hydration. For other sensors, the rates of increase are similar, being the sensor located at 20 mm from the bottom (SP20) the one who exhibits a higher swelling pressure after 15 days (1.5 MPa), because of its proximity to the front of hydration. The difference in the increase rate depends on the evolution of the hydration front as well as the local porosity of the material characterized by an initial heterogeneous distribution of macroporosity. After a few hours, water reaches sensor SP40. This sensor presents a negative rate at the beginning of the test, which could be interpreted as a collapse of the material at this level due to the presence of larger voids. The evolution of SP60 indicates that water arrived after 4 days of hydration.
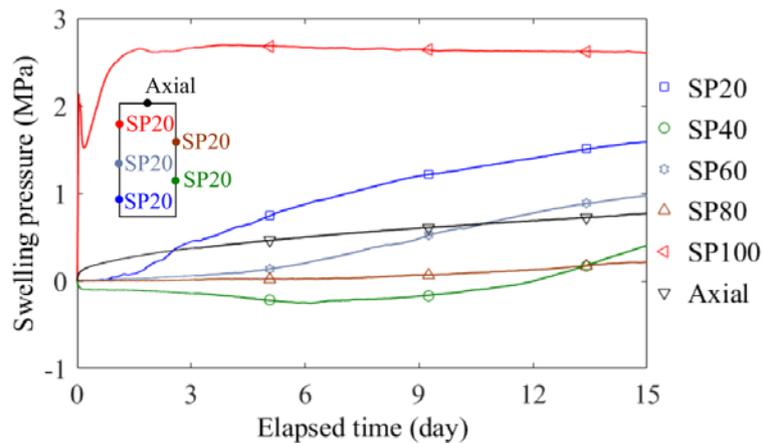

Figure 5. Evolution of the swelling pressure with time after 15 days of hydration.

Figure 6 presents the evolution of swelling pressure during 200-day hydration. The lowest swelling pressure and increase rate are observed for sensor SP120, located at the top of the sample. This is because, at this level, the sensor is in contact with the porous stone (see Figure 3), thus the response does not correspond to the behavior of the soil. For the sensors located at the middle position (SP40, SP60, SP80 and SP100), the increase rate and the swelling pressure depend not only on the distance to the hydration front, but also on the local porosity defined by the pellets/power grains distribution. A common value of about 2.5 MPa of swelling pressure is reached after 60 days of hydration except for SP20. Afterwards, sensors SP40, SP60 and SP80 exhibit the same increase rate until 110 days of hydration, where a stabilized swelling pressure is reached. At 120 days, SP80 presents an increase in swelling pressure which stabilizes again at 135 days of hydration. Sensor SP100 presents a different response: an

increase of swelling pressure is observed after 60 days, with a value almost constant, and then at 93 days it increases again to reach a constant value (the same increase is observed for SP40, SP60 and SP80), lower than the swelling pressures from other radial sensors (except that at 120 mm, which value is the lowest as it was explained previously). It should be noted that the swelling pressures after 200 days are different for all the sensors. This phenomenon will be discussed later. The axial swelling pressure corresponds to the global pressure transmitted to the piston, and its value is lower than those from other sensors. However, no consistent comparison can be made with the radial rates since in the latter case the pressures are measured locally. The rate of increase of the axial swelling pressure cannot be compared to the radial rates as the force transducer measures a global force and not the local total pressure.
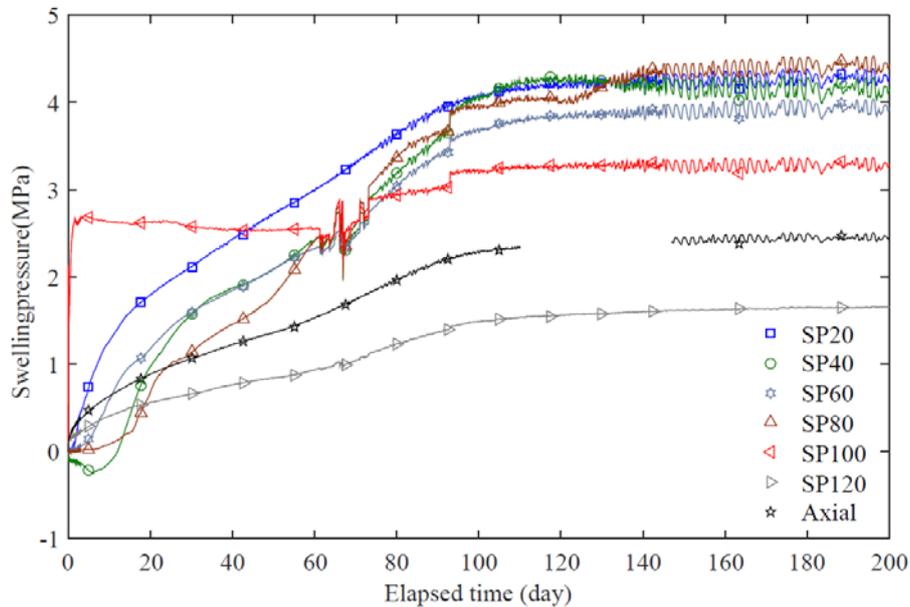

Figure 6. Evolution of the swelling pressure with time after 200 days of hydration.

According to the cell design (Figure 4), the swelling pressure of the material is transmitted to the upper piston, and then the force is transmitted to the force transducer. Therefore, two phenomena should be considered to interpret the measured axial swelling pressure: (i) the local porosity at the top of the sample, which is higher due to the presence of larger voids (see Figure 3, where the porous stone is in contact with some pellets at the top of the sample but there is no powder at this level) and (ii) the effect of friction. These two combined phenomena might explain the lower value of swelling pressure.

The evolution of the swelling pressures for 845-day hydration is shown in Figure 7. Some oscillations are observed after 200 days of hydration. These oscillations could be due to

electrical problems, even if the response of the sensors has been corrected with respect to the electrical voltage. After 700 days of hydration, a common value of about 4 MPa of swelling pressure is reached for sensors SP20, SP40, SP60 and SP80. Sensor SP100 still remains at a lower value, slightly higher than 3 MPa, as well as the axial pressure (2.5 MPa).
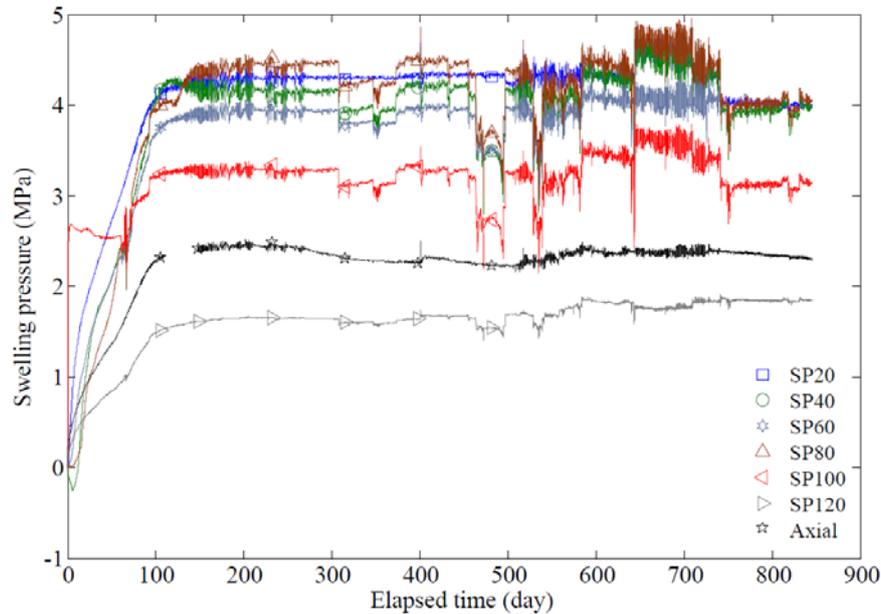

Figure 7. Evolution of the swelling pressure with time after 845 days of hydration.

Figure 8 presents the swelling pressure profiles at a time interval of 5 days. As it was explained before, the swelling pressure at 120 mm is not representative because the sensor is in contact with the porous stone at this level. At the bottom of the sample, the increasing rate of swelling pressure is lower because there might not be preferential arrangement of pellets at this level. After 50 days of hydration, the lowest value of swelling pressure is at 60 mm, which corresponds to the farthest position from the hydration front. These heterogeneous swelling pressure values depend on the local porosity of the material, which is controlled by the initial pellet/powder distribution within the sample. The profiles of swelling pressure every 100 days are shown in Figure 9. An increase of the swelling pressure is observed at 40 mm, 60 mm and 80 mm due to the evolution of the hydration front and the consequent swelling of the material at these levels. A heterogeneity of the final value of swelling pressure is observed after 800 days of hydration, with a mean value slightly higher than 4 MPa.
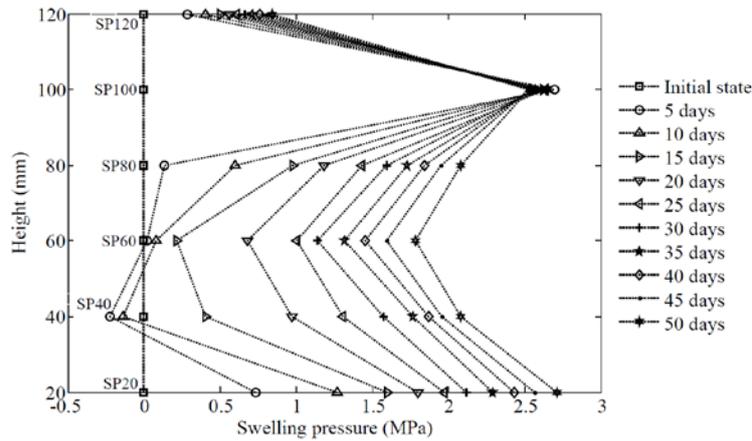
Figure 8. Swelling pressure profiles at different times (every 5 days).
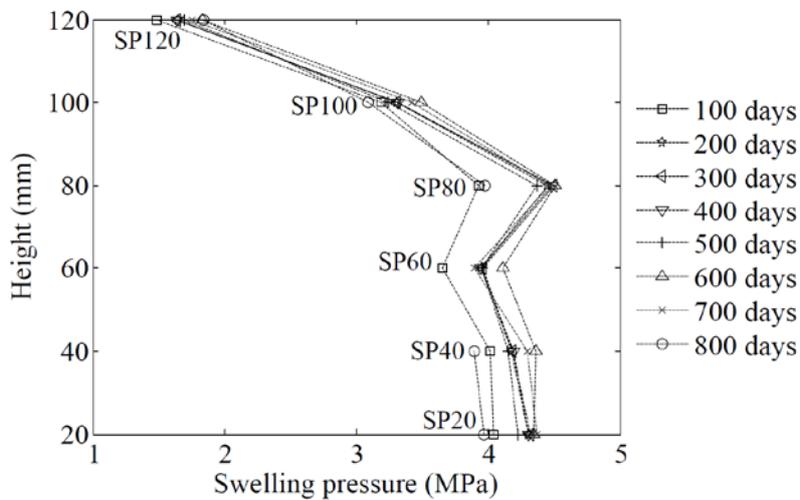
Figure 9. Swelling pressure profiles at different times (every 100 days).

4.2. Investigation of the relative humidity

The evolution of the relative humidity with time is shown in Figure 10. Starting at 36.7% relative humidity corresponding to 138 MPa of suction, the curves show different rates for different sensors. Those located close to the front of hydration (RH31 and RH111) present the highest rates, and a value of 100% is reached after 15 days for RH111 and 20 days for RH31. Sensor RH111, located at 9 mm from the top hydration front, presents the highest rate because of the effect of gravity and the presence of voids at this level of the sample (Figure 3), which creates preferential paths for injected water. For sensors RH51 and RH91 the increase rate is similar, and saturation is reached after 45 days of hydration. Sensor RH71, located at 29 mm from the top hydration front, exhibits the lowest increase rate, with a value of 100% reached after almost 50-day hydration. The response of the sensors located at an intermediate position in the sample (RH51, RH71 and RH91) depends on the evolution of the hydration front.
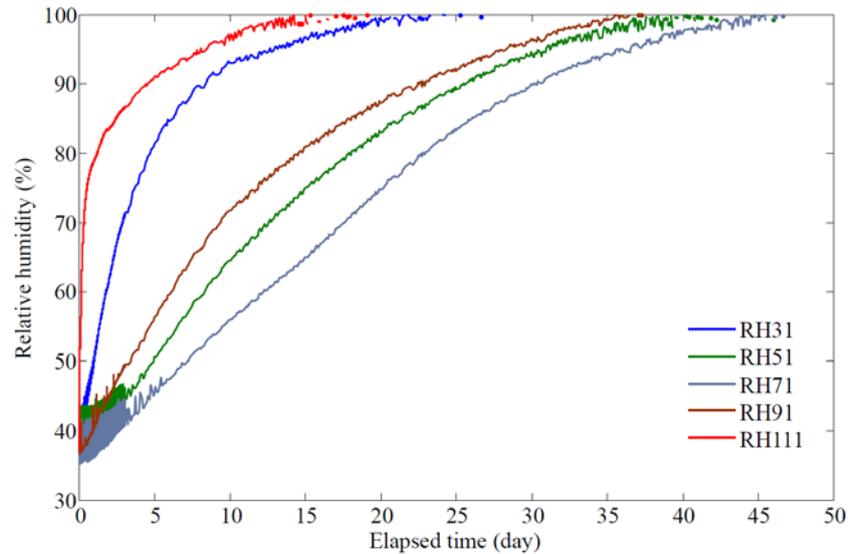
Figure 10. Evolution of the relative humidity with time.

The total volume of water injected while hydration, as well as the volume injected by the top and the bottom are presented in Figure 11. At the beginning of the test, the rate of increase is comparable for the top and bottom injection. However, a higher volume is injected by the top due to the existence of larger voids (Figure 3) combined with the gravity effect. The infiltration by the top of the specimen is controlled by the water level of the burette which hydrates the sample by the top. The volume of water injected by the top of the sample increased instantaneously after 125 days of hydration due to a manipulation of the burette connected to the hydration system; the water level was adjusted to the top of the cell. After 700 days of hydration, the volumes injected by the bottom and the top are 78.2 cm^3 and 128.2 cm^3 respectively. The total volume injected during the test is 206.4 cm3. As it can be observed, the rate of increasing is still positive after 700 days of hydration. This suggests that the sample is not entirely saturated after 700 days of hydration.

The profiles of relative humidity at a time interval of 5 days are presented in Figure 12. At the beginning of the test, before hydration, different values are observed for every sensor (around 40% of relative humidity). This is because the initial suction is not homogeneous within the sample, thus the results depend on the local relative humidity. Then, while wetting, an instantaneously increase is observed at 31 mm and 111 mm, due to the proximity of the hydration front. The evolution of other sensors depends on the evolution of the hydration front. A total saturation (corresponding to a value of relative humidity of 100%) is observed after 40-day hydration. However, it was observed that the rate of injected water is still positive after 700-day hydration. This means that the measured relative humidity value of 100% after 40 days

corresponds to the saturation of the large pores, and it does not represent the full saturation of the sample.
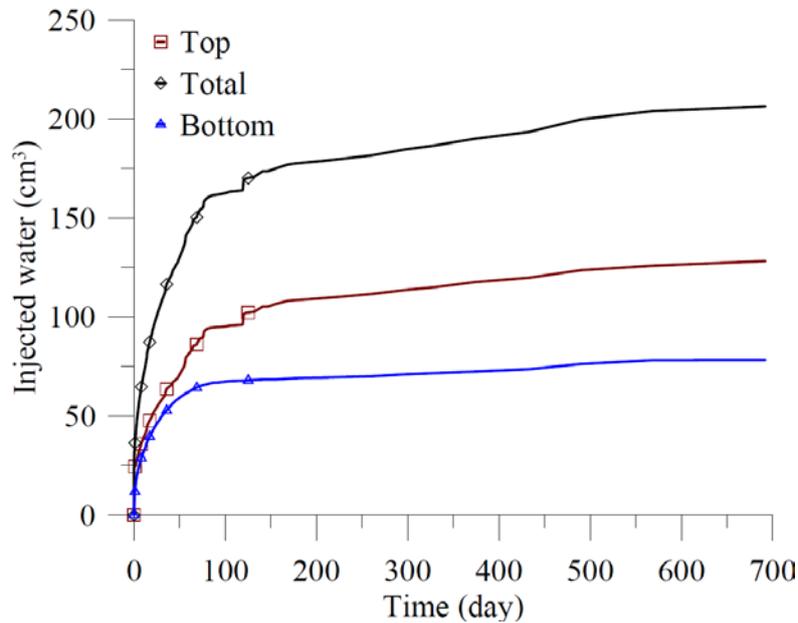
Figure 11. Evolution of the injected water with time during hydration.
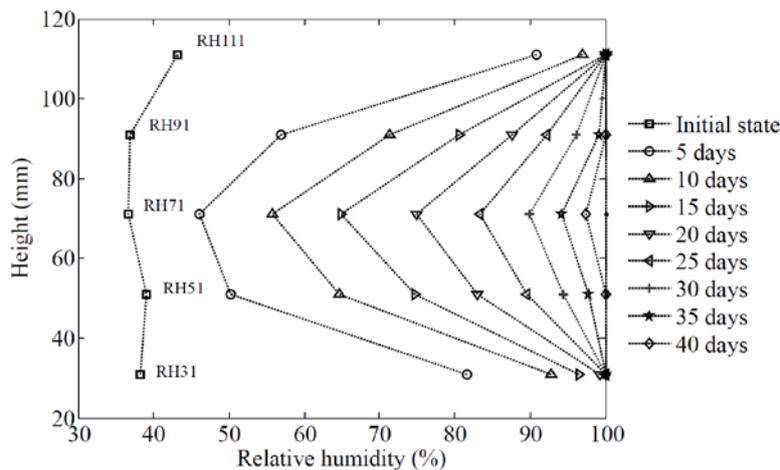
Figure 12. Relative humidity profiles at different times (every 5 days).

5. Discussion

The anisotropy of swelling pressure observed in this investigation can be interpreted based on two key features: (i) the dependence of the swelling pressure on the dry density of bentonite and (ii) the initial heterogeneous distribution of the material. The swelling pressure evolution of the sensor located at 100 mm (SP100) during the first 200 days (Figure 5) is due to the presence of larger voids at this level, as it is observed in Figure 3. A peak is observed at the beginning of the hydration process. This peak and consequent temporary drop corresponds to the reorganization of the microstructure of the soil induced by the collapse of the larger voids,

95

so inter-pellet voids (Alonso *et al*., 2011; Gens *et al*., 2011). During hydration, pellets start swelling and filling the larger voids between them. This kind of response can be associated to the limit between two layers of pellets with powder of bentonite located in the inter-pellet voids, as it can be observed in Figure 3 at 100 mm. The heterogeneous distribution of pellets and powder within the sample plays an important role in the creation of these larger voids.

Figure 13 displays the evolution of swelling pressure with suction for sensors SP40, SP60, SP80 and SP100. As the positions of the RH sensors and SP sensors are not the same, an interpolation of the evolution of the suction is carried out in order to estimate the suction at the same level as the SP sensors. These calculations were not carried out for sensor SP20 as there is no RH sensors between the bottom hydration front and SP20. For sensor SP100, from the initial state (point A), a sudden increase of the swelling pressure is observed until a value of suction of 120 MPa. Then, a peak is observed (point B) due to the reorganization of the microstructure of the soil induced by the collapse of the macropores (inter-pellets voids). Then, the swelling pressure increases while wetting again until a constant value is reached (2.5 MPa) before saturation. It is worth noting that the calculated suctions using RH measurements correspond to the local macro structural suctions prevailing locally at the measured point. Unfortunately, the RH sensors do not allow the measurement of the evolution of suction at the microstructural level which might experience a delay in saturation.

For other sensors (SP40, SP60 and SP80 in Figure 13) this behavior is not observed. The shape of the wetting path depends on the local density of the material, which depends on the pellet/powder structural distribution at the corresponding position as well as the vicinity of the hydration front. The increase rate of swelling pressure of sensor SP40 is negative at the beginning of the test, which might be due to a reorganization of the macrostructure at this level. The behavior is different compared to sensor SP100 as no swelling is observed before the collapse. The rate of increase of swelling pressure for SP40 is the lowest for the four sensors, indicating that the material has a low dry density at this level. This response can be associated to the limit of two layers of pellets with no grains of powder between the pellets. This distribution can be observed in Figure 3 at 40 mm. For sensor SP60, a decrease in suction is observed with no swelling before 50 MPa suction. It is believed that there is a concentration of bentonite powder grains in the vicinity of this sensor with no pellets (this kind of distribution can be observed in Figure 3 between SP20 and SP60). Therefore, bentonite grains swell but no pressure is registered by the sensor until suction reaches 50 MPa due to its loose structure. For sensor SP80, swelling pressure increases with a rate higher than SP60, but no collapse of the

macrostructure is observed. No constant value of swelling pressure is observed for both sensors under a certain value of suction, as it was observed for sensor SP100, indicating that the structure of the mixture is still changing at this state of the hydration process. After 700 days, a common value of 4 MPa of swelling pressure is observed for radial sensors except SP100, which value is slightly higher than 3 MPa.

Based the initial average dry density of the mixture (1.49 Mg/m3) and the relationships between axial swelling pressure and dry density derived by Karnland *et al*. (2008) and Wang *et al*. (2012), the final value of the axial swelling pressure can be estimated. It ranges from 4.15 MPa to 4.66 MPa. The lower measured value (2.5 MPa) is due to: (i) the friction of the material with the cell while swelling (Saba *et al*., 2014), which is transmitted to the force transduced and (ii) the material preparation protocol, which results in a concentration of macrovoids at the top of the sample, where the porous stone is in contact with some pellets without powder grains between them (Figure 3). Moreover, the vicinity of each radial sensor to the material is observed clearly in Figure 3, which might be due to the sample preparation process, in which the cell is filled by packets corresponding to one layer of pellets spread over the base of the sample (see for instance Molinero Guerra *et al*., 2016).
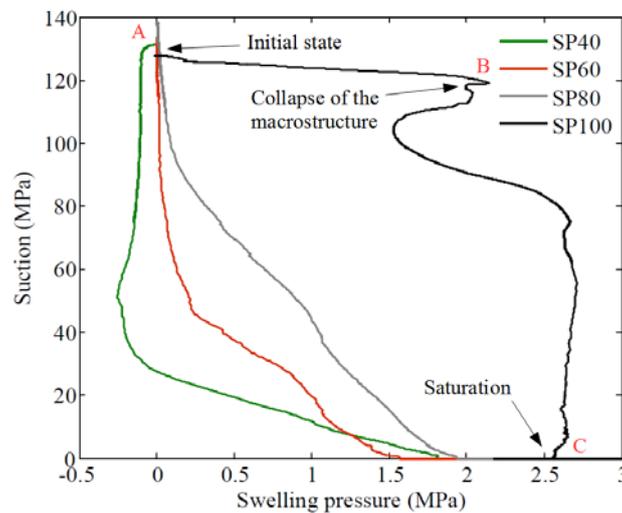
Figure 13. Suction versus swelling pressure at different positions.

Figure 14 displays the profiles of dry density obtained using the exponential relationship derived by Wang *et al*. (2012). A gradient of dry density is observed along the sample due to the initial heterogeneous distribution of macroporosity, the non-saturation of the sample after 800 days of hydration, and the effect of friction.
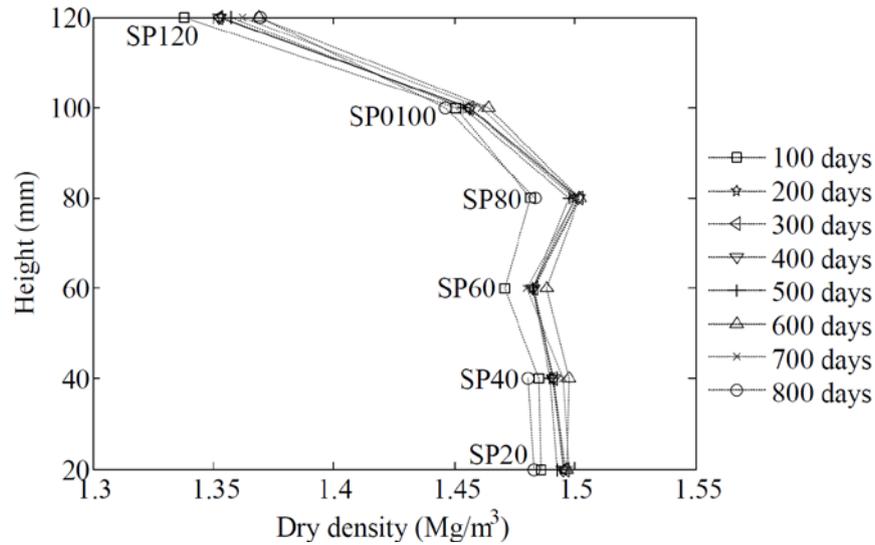
Figure 14. Dry density versus height at different times (every 10 days).

The total volume of injected water is 206.4 cm^3 after 700 days of hydration. However, taking into account the dry density of the material, the theoretical injected volume when the mixture is saturated should be 155 cm^3. This difference is due to the increase in water density while hydration (Jacinto *et al.*, 2012; Marcial 2011). A water density of 1.316 Mg/m^3 is obtained in this work from the theoretical volume of injected water and the measured value. Marcial (2011) obtained a water density of 1.02 Mg/m^3, 1.27 Mg/m^3 and 1.57 Mg/m^3 for a sample of compacted MX80 bentonite at a dry density of 1.354 Mg/m^3, 1.691 Mg/m^3 and 1.952 Mg/m^3 respectively. It is worth noting that the water in the interlayer zone of expansive clays has several features which are quite different from those of free water. This increase in water density, which depends on the relative humidity, can be partially associated with the predominant exchangeable cations in the clay, and the difference in the interaction mechanisms between each cation and the interlayer water (Jacinto *et al.*, 2012).

6. Conclusions

In the context of the SEALEX project (IRSN), a small-scale test (1/10) was performed in order to investigate the HM behavior of pellet/powder MX80 bentonite mixture. The swelling pressure at different positions in the sample allowed better understanding the complex swelling behavior of this heterogeneous material.

The evolution of the radial swelling pressure for the different positions are due to the local porosity of the material combined to the evolution of the hydration front. Local porosities depend strongly on the initial heterogeneous distribution of pellets and powder within the sample. A collapse of the material is observed at the sensor located at 100 mm due to the

presence of larger voids at this level, corresponding to the limit between two layers of pellets with some bentonite powder grains between them. At 40 mm from the bottom, a collapse is found at the beginning of the test with no previous swelling, due to the reorganization of the macro structure at this level. This behavior could be related to the limit between two layers of pellets without powder grains between them. For the rest of the sensors, no collapse is observed because there are no macrovoids in the vicinity of the sensors.

The anisotropy observed between radial and axial swelling pressure is due to the presence of larger voids at the top of the sample, where the top pore stone contacts with some pellets without no powder grains between them, as well as the friction of the material with the cell while swelling. Note that the effect of friction could be much more significant in field scale. Moreover, it is believed that the sample is more compact radially than axially due to the fabrication process, which can greatly affect the pellet/powder distribution, and consequently the HM behavior of the material.

The evolution of radial swelling pressure depends on the pellet/powder distribution. Different responses can be obtained even if the same protocol is followed. The final dry density profile is not entirely homogeneous at the end of test due to the initial heterogeneous distribution of porosities combined to the effect of friction and the non-saturation of the mixture.

 During the saturation process, a difference was observed between the measured volume of injected water and that estimated by considering the total porosity. This difference is firstly explained by changes in water density, as it was concluded by Jacinto *et al*. (2012) and Marcial (2011). The water density depends on the relative humidity, and it is associated with the predominant exchangeable cations in the clay, and the difference in the interaction mechanisms between each cation and the interlayer water. This dependence should be considered in the investigation on the performance of sealing plugs with bentonite-based materials.

References

Alonso, E.E., Vaunat, J. and Gens, A., (1999). Modelling the mechanical behavior of expansive clays. Engineering Geology, 54(1-2), pp.173–183.

Alonso, E.E., Romero, E. and Hoffmann, C., (2011). Hydromechanical behavior of compacted granular expansive mixtures: experimental and constitutive study. Géotechnique 61 (4), 329–344.

Börgesson, L., Karnland, O. and Johannesson, L. E., (1996). Modelling of the physical behavior of clay barriers close to water saturation. Engineering Geology 41, No. 1–4, 127–144.

Dixon, D. A., Gray, M. N. and Graham, J., (1996). Swelling and hydraulic properties of bentonites from Japan, Canada and the USA. Environmental Geotechnics 1, 43–48.

Garcia-Siñeriz, J. L., Villar, M. V., Rey, M., and Palacios, B., (2015). "Engineered barrier of bentonite pellets and compacted blocks: State after reaching saturation," Eng. Geol., vol. 192, pp. 33–45.

Gens, A. and Alonso, E.E., (1992). A framework for behavior of unsaturated expansive clays. Canadian Geotechnical Journal, 29, pp.1013–1032.

Gens, A., Vallejan, B., Sánchez, M., Imbert, C., Villar, M.V. and Van Geet, M., (2011). Hydro-mechanical Behavior of a Heterogenous Compacted Soil: Experimental Observations and Modelling.

Hoffmann, C., Alonso, E.E. and Romero, E., (2007). Hydro-mechanical behavior of bentonite pellet mixtures. Physics and Chemistry of the Earth, 32(8-14), pp.832–849.

Imbert, C. and Villar, M.V., (2006). Hydro-mechanical response of a bentonite pellets/powder mixture upon infiltration. Applied Clay Science, 32(3-4), pp.197–209.

Jacinto, a. C., Villar, M.V. and Ledesma, A., (2012). Influence of water density on the water-retention curve of expansive clays. Géotechnique, 62(8), pp.657–667.

Josa, a., Alonso, E.E. and Gens, A., (1991). Discussion: A constitutive model for partially saturated soils. Géotechnique, 41(2), pp.273–275.

Karnland, O., Nilsson, U., Weber, H., Wersin, P. and (2008). Sealing ability of Wyoming bentonite pellets foreseen as buffer material – laboratory results. Physics and Chemistry of the Earth, Parts A/B/C 33, S472–S475.

Lloret, A., Villar, M. V., Sánchez, M., Gens, A., Pintado, X. and Alonso, E. E., (2003). Mechanical behavior of heavily compacted bentonite under high suction changes. Géotechnique 53, No. 1, 27–40.

Marcial, D., (2011). A simple method to consider water density changes in the calcualtion of the degree of saturation of swelling clays. In Unsaturated Soils: Proceedings of the Fitth International Conference on Unsaturated Soils, Barcelona, Spain, 6-8 september 2010. pp. 473-478.

Mokni, N. and Barnichon, J.D., (2016). Hydro-mechanical analysis of SEALEX *in situ* tests - Impact of technological gaps on long term performance of repository seals. Engineering Geology, 205, pp.81–92.

Molinero-Guerra, A., Mokni, N., Delage, P., Cui, Y. J., Tang, A. M., Aimedieu, P., Bernier, F. and Bornert, M., (2016). In-depth characterisation of a mixture composed of powder/pellets MX80 bentonite. Applied Clay Science,135, pp. 538-546.

Saba, S., (2014). Hydro-mechanical behavior of bentonite-sand mixture used as sealing materials in radioactive waste disposal galleries. Université de Paris Est.

Saba, S., Cui, Y.J., Tang, A.M., and Barnichon, J.D., (2014). Investigation of the swelling behavior of compacted bentonite–sand mixture by mock-up tests. Canadian Geotechnical Journal, 51(12), pp.1399–1412.

Schanz, T. and Al-Badran, Y., (2014). Swelling pressure characteristics of compacted Chinese Gaomiaozi bentonite GMZ01. Soils and Foundations 54, No. 4, 748–759.

Van Geet, M., Volckaert, G. and Roels, S., (2005). The use of microfocus X-ray computed tomography in characterising the hydration of a clay pellet/powder mixture. Applied Clay Science, 29(2), pp.73–87.

Villar, M. V., Gómez-Espina, R. and Guitiérrez-Nebot, L., (2012). Basal spacings of smectite in compacted bentonite. Applied Clay Science 65–66, 95–105.

Villar, M.V., (2013). EB experiment. Contribution of CIEMAT to EB dismantling report. Physical state of the bentonite. EC Contract 249681 PEBS. Informe Técnico CIEMAT/DMA/ 2G210/04/2013 (Madrid, 21 pp.).

Wang, Q., Tang, A.M., Cui, Y.J., Delage, P. and Gatmiri, B., (2012). Experimental study on the swelling behavior of bentonite/claystone mixture. Eng. Geol. 124, 59–66. http://dx. doi.org/10.1016/j.engeo.2011.10.003

Wang, Q., Tang, A.M., Cui, Y.J., Barnichon, J.D. and Ye, W.M., (2013). A comparative study on the hydro-mechanical behavior of compacted bentonite/sand plug based on labora- tory and field infiltration tests. Eng. Geol. 162, 79–87.

Analyses of the structural changes of a pellet/powder bentonite mixture upon wetting by X-ray computed microtomography

Agustín Molinero Guerra[1,2], Patrick Aimedieu[1], Michel Bornert[1],Yu-Jun Cui[1], Anh Minh Tang[1*], Zhao Sun[3], Nadia Mokni[2], Pierre Delage[1], Frédéric Bernier[4]

[1]Ecole des Ponts ParisTech, CNRS, IFSTTAR, Laboratoire Navier/CERMES, Marne La Vallée, France
[2]Institut de Radioprotection et de Sûreté Nucléaire (IRSN), Fontenay-aux-Roses, France
[3]Tongji University, China
[4]Agence Fédérale de Contrôle Nucléaire (AFCN), Belgium

Abstract: Pellet/powder bentonite mixture is one of the candidate materials for sealing plugs in geological disposal of high-level radioactive waste, whose hydro-mechanical behavior can be strongly influenced by its initial heterogeneity. This paper presents an investigation on the structure changes of this mixture, occurring in the saturation process by means of X-ray computed micro-tomography. The test was performed in an infiltration column (60 mm in inner diameter and 120 mm in height). Water was injected to the two ends of the column and the changes of the sample morphology are followed during a period of 100 days of saturation. The first qualitative analysis shows that the initially heterogeneous structure turned into an apparent homogeneous mixture, with no more air-filled inter-pellet voids after 100 days of hydration. The density field of the specimen at various moments was determined allowing quantitative assessment of the morphology change. Digital Image Correlation (DIC) technique was also used to determine the vertical displacement field of the bentonite powder. The highest displacements correspond to the positions where air-filled inter-pellet voids are dominant.

Keywords: pellet/powder bentonite mixture; X-ray computed microtomography; initial heterogeneity; Digital Image Correlation; water saturation; homogeneisation.

1. Introduction

In the context of deep geological disposal, non-compacted pellet/powder bentonite mixtures are considered as candidate sealing materials thanks to their high swelling capacity and high radionuclide migration retardation properties, as well as their operational advantages: they are easy to transport, install, and allow gaps between the rock and the seal to be minimized. Firstly, this unsaturated mixture is installed in the gallery. Then, water coming from the host rock starts saturating the mixture under almost constant-volume conditions. The swollen mixture will fill different voids and generate swelling pressure, ensuring the sealing of the storage system. Previous investigation carried out by Molinero Guerra *et al.* (2016) shows that this mixture is characterized by an initial heterogeneous distribution of pellets and powder, with presence of

102

inter-pellet voids within the mixture. Obviously, this initial state can greatly influence the saturation process and the corresponding structure changes. As a result, the overall hydro-mechanical behavior will change during the saturation process. Therefore, to properly assess the safety of the underground radioactive waste disposal, it is of paramount importance to well understand the microstructure change of the mixture in the course of hydration.

In this context, the Institute of Radioprotection and Nuclear Safety (IRSN, France), as a part of the overall research and development program that aims at providing scientific background of disposal safety, has launched the SEALEX (SEALing performance EXperiments) project, within which this work has been conducted. It consists in a series of *in situ* tests carried out in IRSN's Underground Research Laboratory (URL – Tournemire, France) (Barnichon & Deleruyelle, 2009; Mokni & Barnichon, 2016) and small-scale tests conducted in the laboratory (Wang *et al*., 2012; Saba *et al*., 2014). In the current project, the long-term hydraulic performance of sealing systems has been studied, in normal and altered conditions as well as different core configurations (sand/bentonite mixtures, pellets/powder mixtures). This work is focused on a pellet/powder mixture with a proportion of 80/20 in dry mass, at a target dry density of 1.49 Mg/m^3.

The hydro-mechanical behavior of engineered barriers composed of compacted bentonite/sand mixtures or compacted pure bentonite has been extensively investigated (e.g. Pusch 1982; Graham *et al*., 1989; Komine & Ogata, 1994; Dixon *et al*., 1996; Alonso *et al*., 2005; Wang *et al*., 2013b, 2014; Saba *et al*., 2014; Sun *et al*., 2014). However, few studies have been carried out on the mixture of pellet and powder of bentonite. Imbert & Villar (2006) performed infiltration tests on a pellet/powder bentonite mixture. The obtained swelling pressure was analogous to that of a specimen of compacted powder at the same dry density. Van Geet *et al*. (2005) investigated the hydration process of a pellet/powder bentonite mixture by X-ray computed tomography. A progressive decrease of the pellets density and an apparent homogenous sample after saturation were observed. Garcia-Siñeriz *et al*. (2015) studied the homogenization process of a material made of compacted bentonite pellets through experiment on engineered barrier (EB). Upon dismantling, a gradient of density and water content was still found within the mixture because of the initial heterogeneity of the material (Villar, 2013).

Few works have been carried out on the homogenization process of a granular buffer material (GBM) while wetting, even though this is crucial while validating this kind of materials as sealing material for deep underground radioactive waste disposal. The present work is thus

conducted to investigate the structural changes of a pellet/powder bentonite mixture. Firstly, the sealing capacity of the mixture and its structural evolution during saturation are studied qualitatively. Second, Digital Image Correlation (DIC) technique is applied to calculate the displacement field within the sample. Finally, the evolution of the axial swelling pressure while wetting is investigated. The results obtained provides helpful elements in assessing the hydromechanical performance of seals/plugs made up of this kind of bentonite mixtures.

2. Material and methodology

2.1. Pellet/powder MX80 bentonite mixture

The soil studied is a mixture of pellet/powder MX80 bentonite at a proportion of 80/20 in dry mass. The bentonite investigated comes from Wyoming, USA. It was provided by the Laviosa-MPC Company under the commercial name Expangel SP7 for pellets and SP30 for the powder. The MX80 bentonite has a smectite content of 80%, other minerals being quartz, calcite and pyrite. The cation exchange capacity (CEC) is 98 meq/100g, with 52 meq/100g, for Na, 1.2 meq/100g for K, 10 meq/100g for Mg and 37 meq/100g for Ca. The liquid limit is 560%, the plastic limit is 62% and the unit mass is 2.77 Mg/m^3 (Saba *et al*. 2014).

Cylindro-spherical pellets of bentonite were produced by compacting commercial bentonite powder in a mold of 7 mm in diameter and 7 mm in height. The initial suction ($s = 135 \pm 3$ MPa) was measured in the laboratory with a chilled mirror dew point tensiometer (Decagon WP4C), corresponding to an initial water content $w = 5\%$ - 7%. The initial void ratio of the pellets is $e = 0.235 – 0.278$ and its degree of saturation is $Sr = 54.5\% – 66.1\%$. The bentonite powder was produced by crushing pellets. An initial water content of 3.17% was found in the laboratory, corresponding to an initial suction $s = 191$ MPa.

Table 1. Chemical composition of the synthetic water.

Components	NaHCO$_3$	Na$_2$SO$_4$	NaCl	KCl	CaCl$_2$ 2H$_2$O	MgCl$_2$O6H$_2$O	SrCl$_2$6H$_2$O
Mass (g) per litre of solution	0.28	2.216	0.615	0.075	1.082	1.356	0.053

The saturation fluid was obtained by mixing the chemical components presented in Table 1 with distilled water until full dissolution. The resulting synthetic water has the same chemical composition as the pore water of the Callovo-Oxfordian claystone from the underground research laboratory in Bure (Wang *et al*., 2013a).

2.2. Experimental set-up

A special set-up was designed to carry out X-ray computed microtomography (μ-CT) observations on the pellet/powder mixture while wetting. The layout is presented in Figure 1a. It consists in a transparent PMMA (PolyMethyl MethAcrylate) cell of 60 mm of inner diameter and 120 mm of height (corresponding to 1/10th scale of the SEALEX *in situ* tests). It is worth noting that using a 30 mm-thick cylinder PMMA allows resisting the mechanical stresses originating from the specimen swelling and minimizing X-ray absorption/diffusion through the testing device. The specimen is placed between two porous stones and filter papers, placed at its top and bottom. The confined saturation condition for the pellet/powder bentonite mixture is ensured by the rigid PMMA cell and a top piston which prevents axial displacement. The material is saturated from both sides (top and bottom), simulating the SEALEX *in situ* experiments. The axial swelling pressure is monitored during the test with a force transducer. The base and top are both equipped with an inlet of water and an outlet of air. Figure 1b shows the PMMA cell positioned inside the microtomograph. The cell is connected to two reservoirs (situated at the top and bottom of the sample) allowing water infiltration.
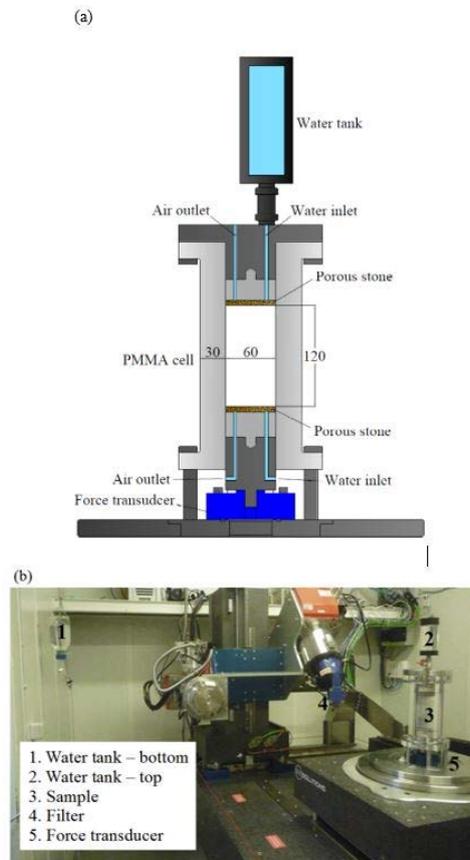

Figure 1. Photography of the experimental set-up inside the x-ray microtomograph device (b) and layout of the cell (a).

2.3. Sample preparation and test protocol

The pellet/powder mixture was prepared by following the first protocol proposed in Molinero Guerra *et al*. (2016), which ensures a homogeneous pellet/powder distribution within the sample at the target dry density (1.49 Mg/m^3). It consists in filling the cell by packets corresponding to one layer of pellets spread over its base and by adding the corresponding amount of powder (considering the proportion 80-pellet/20-powder in dry mass). Two elements were added while preparing the specimen. It consisted of two glass spheres whose diameter was 10 mm and whose density was 2.60 Mg/m^3. Both have been used as reference elements for subsequent quantitative analyses. The attenuation of these two materials remains stable during the hydration process, as their composition does not change while wetting. Secondly, they do not absorb water. For this reason, their associated grey levels in the obtained pictures do not change during the test. Therefore, these two spheres, along with the PMMA cell, allow: (i) normalizing the attenuation of the obtained pictures, ensuring that the grey level values of these materials are constant during the test, and (ii) estimating the evolution of the apparent density of the mixture while wetting. Moreover, some reference elements of 1500 PMMA spheres of 1.6 mm diameter were randomly distributed within the sample during the preparation process. The purpose is to carry out quantitative analyses of bentonite powder displacement by DIC technique.

A preliminary study was carried out to estimate the beam hardening artefact, which leads to grey level variations from the centre of the cylinder to the border, even for homogeneous samples whose grey levels patterns should be flat (Herman, 1979). In order to reduce this artifact, it was decided to add an external copper filter plate (thickness: 1.5 mm) on the window of the X-ray generator (see Figure 1). The general experiment scheme consisted in scanning the pellet/powder mixture while wetting at different times during the saturation process. This resulted in a kind of incremental scans occurring during the hydration process: several µ-CT observations were carried out at different times until an apparent homogeneous mixture was observed.

The very first step of the test consisted in opening the water inlet valves. Consequently, air inside the system was evacuated by opening the air outlet valve until no air bubble could be observed anymore in the outlets. Water was injected through both the top and bottom of the sample, as in the SEALEX *in situ* experiments. Axial swelling pressure was recorded automatically by a force transducer and a numerical data logger.

µ-CT scans were performed using an "Ultratom" microtomograph (RX Solutions, France). Images were acquired and reconstructed using the software Xact (RX Solutions), which uses back filtered projection technique. The source is a microfocus X-ray tube Hamamatsu L10801 and the imager a Paxscan Varian 2520V (pixels: 1960 x 1536, 127 µm, square shape). The X-ray source parameters were 160 kV and 120µA, and voxel size was 50 µm. The samples were scanned using 5760 projections in helical mode. Each scan took 19 h. After reconstruction, 2800 horizontal slices were calculated (16 bit images, 1499 x 1499 pixels^2).

A first qualitative analysis was performed, based on the observations of the pellet/powder bentonite mixture while wetting. Then, quantitative analyses were carried out in order to further investigate the structural evolution of the mixture. These analyses were based on: (i) the investigation of the attenuation of the material at different positions while wetting, and (ii) the DIC technique, which allowed calculating the displacements of PMMA spheres placed inside the sample.

DIC is a full-field measurement technique that basically consists in comparing two pictures at two different stages and calculating a displacement field. In the present case, it was used while hydrating the sample. A detailed description of this technique can be found in Sutton *et al*. (2009) and Bornert *et al*. (2012). The procedure that was used in this work can be summarized as follows. Firstly, a grid of correlation points, which correspond in this case to the PMMA spheres, is generated. Each point is considered as a correlation cube. In this work, the correlation windows were cubes whose lateral dimension was 30 pixels. Secondly, the correlation procedure was performed. It consists in finding the most similar domain in the deformed image for each correlation window of the reference image. A correlation coefficient is calculated, which measures the similarity of grey levels between correlation windows in the reference image and in the image after swelling. This coefficient is optimized to measure the displacements between the two stages.

3. Results

3.1. Qualitative analysis of the swelling behavior

The behavior of the pellet/powder mixture was firstly investigated by carrying out a qualitative analysis of the µ-CT observations at different heights of the column. Figure 2 displays several horizontal sections corresponding to different positions (10, 20, 30, 60, 90, and 110 mm from the bottom) at different times (initial state – before hydration, 11, 27 and 56 days after hydration).

Initially, the mixture has a heterogeneous distribution of pellets and powder. At 10 mm from the bottom, pellets are distributed quasi uniformly. At 20, 30 and 60 mm the air-filled inter-pellets voids are more dominant than the bentonite powder in these voids. At 10 mm from the top (110 mm of height), a homogeneous distribution of pellets comparable to that observed at 10 mm from the bottom is observed. It can be also observed that the powder distribution in each horizontal cross section is not homogeneous. This pellet/powder distribution depends strongly on the protocol followed to produce the specimen. These results confirm that pellet and powder distribution in the mixture is heterogeneous in spite of adopting a careful preparation procedure in the laboratory. In-depth characterization of a mixture composed of powder/pellets bentonite can be found in Molinero Guerra *et al*. (2016).
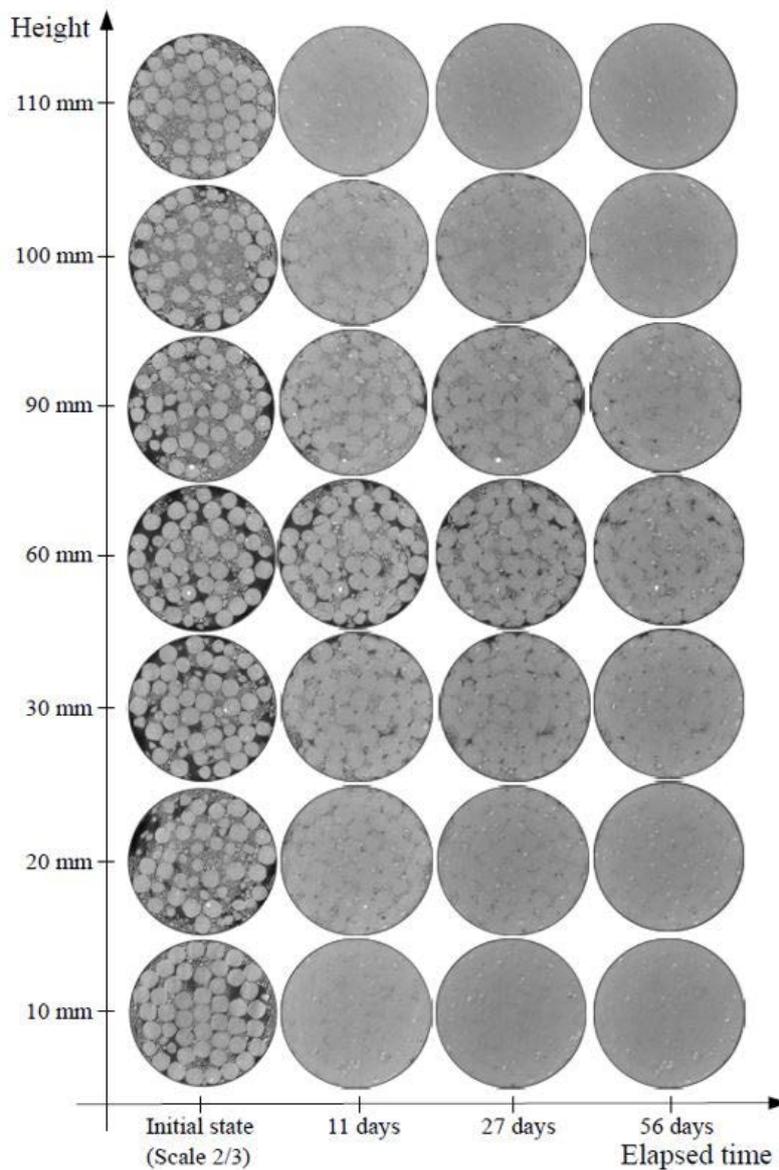

Figure 2. Horizontal sections of the sample at different times and positions.

108

After 11 days of hydration, a quasi-homogeneous mixture is observed at 10 mm from the top and bottom. Pellets have almost lost their initial geometry and no more inter-pellet voids can be observed. Accordingly, sections located at 20 mm from the hydration fronts show an almost homogeneous mixture; however, the pellets are still noticeable, as well as small residual air-filed inter-pellet voids which are not completely sealed by powder grains swelling. For the sections located at 30 mm and 90 mm from the bottom, pellets can be clearly identified even though swelling has already started. For the section located in the middle of the specimen (60 mm of height), the only remarkable changes compared to the initial state are some cracks developed inside some pellets, whose nature will be discussed later. At this section, it seems that the pellets in contact to the cell start swelling earlier than the pellets located near the central axis of the specimen. This could be explained by larger air-filled inter-pellet voids existing in the zone close to the cell wall, which may be a preferential path for moisture transfer.

After 27 days of hydration, the granular structure disappears at 20 mm and 100 mm, even though some contours can be still identified. At 30 mm and 90 mm from the bottom, pellet contours can be distinguished clearly. At 60 mm, swelling starts for all the pellets. 56 days after the beginning of the test, a completely homogeneous mixture is observed at 10, 20 and 110 mm. At 100 mm, the material is homogeneous, but an air-filled inter-pellet void is observed at the contact with the cell. For the sections located at 30 mm and 90 mm, the material has lost its granular structure but some pellet contours as well as air-filled inter-pellet voids can be observed. Air-filled inter-pellet voids are still identified at the furthest position from the hydration front.

These observations can be further completed in Figure 3, in which a vertical section located at the same position is presented at different times. The results confirm the observation on horizontal slides; air-filled inter-pellet voids are dominant in the zone between the bottom and 90-mm height. Above this zone, bentonite powder is more dominant in the inter-pellet voids. At the initial state, the top of the mixture is characterized by the presence of larger air-filled voids between the pellet and the porous stone, most probably due to segregation in the fabrication process. After 2 days of hydration, these voids are completely sealed due to their vicinity to the hydration front, so the material at this level swells quickly. It can be deduced from sections corresponding to 2 days and 4 days after hydration that the evolution of the top hydration front is quicker than the bottom. Afterwards, as was observed from the horizontal slices, the evolution of both hydration fronts is similar. The initial structure loses its granular nature while wetting; air-filled inter-pellet voids are still visible after 56 days of hydration, even

though the pellets located at the furthest position from both hydration fronts have already swollen at this time. An apparently global homogeneous sample is observed after 100 days of hydration. At this time, almost all the air-filled inter-pellet voids have been completely sealed.

The qualitative analysis of the behavior of the pellet/powder mixture was completed with the 3D reconstructions of the mixture at different times presented in Figure 4. It is observed that the initial granular structure becomes an apparently homogeneous bentonite mixture after 100 days of hydration, where all the voids air-filled inter-pellet voids have been sealed.
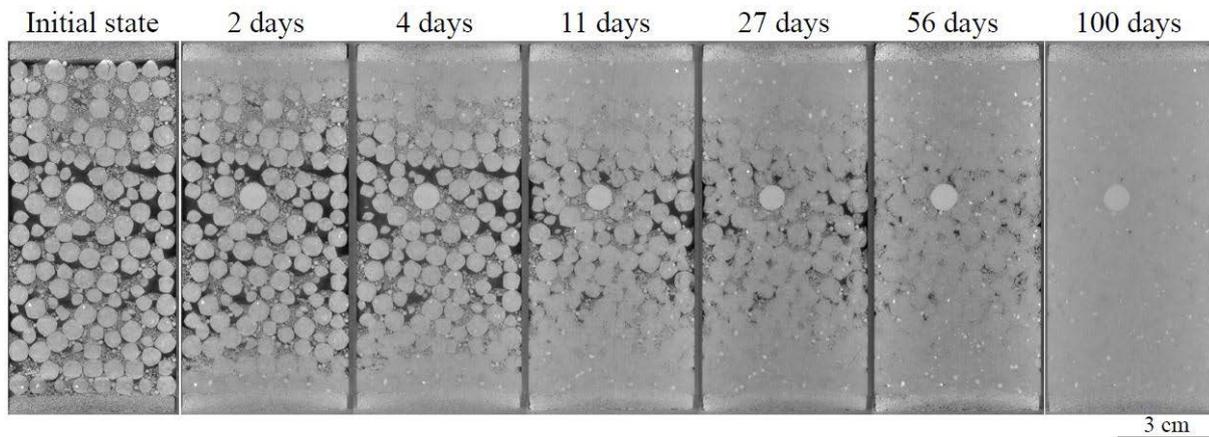
Figure 3. Vertical sections of the pellet/powder mixture while wetting.
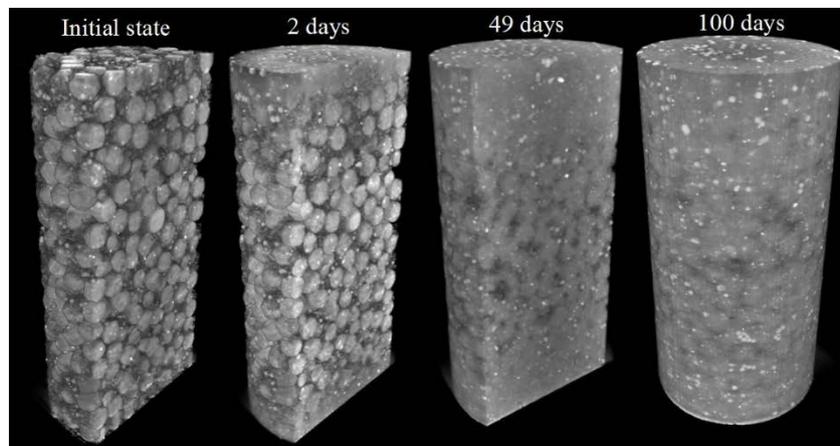
Figure 4. X-ray computed microtomography (µ-CT) observations – 3D reconstruction image.

The initial heterogeneous pellet/powder bentonite mixture is characterized by a granular structure with powder grains distributed within the inter-pellet voids. This distribution depends strongly on the protocol followed for the specimen preparation. From a first qualitative analysis of the results, it is observed that pellets progressively lose their granular structure while wetting. This depends on the evolution of the hydration front: pellets located at the top and bottom of

the sample lose rapidly their structure, leading to an apparently homogeneous structure where their initial shape as well as the inter-pellet voids have disappeared. To better understand the transition between the initial state and the final one, a zoom on an assembly of the pellets in contact to the cell at 60 mm from the bottom hydration front is presented in Figure 5. Initially, high-density pellets can be observed with several powder grains between them. After 11 days of hydration, some cracks have developed within the pellets due to the decrease of suction. As was observed by Molinero Guerra *et al*. (2016), cracks are already part of the initial state of the pellet; they appeared during the storage in the laboratory combined to the fabrication process of a single pellet. Those cracks cannot be observed in this work, due to the insufficient resolution of the µ-CT observations (50 µm/voxel) as compared to the resolution that was used to study a single pellet (4.4 µm/voxel); however, it is most probable that they were already present at the initial state and opened while wetting. After 27 days, more cracks are observed, as well as the decrease of the inter-pellet voids due to swelling. Then, pellets start losing their granular structure. After 56 days, pellets can be still identified even if they have almost lost their initial granular structure; some air-filled inter-pellet voids are observed, which are sealed definitively after 100 days of hydration. Therefore, the evolution of the structure of a single pellet is characterized by the development of cracks combined to the swelling of its components. From this qualitative analysis, an apparently homogeneous mixture was observed after 100 days of hydration. From this zoom, it can be also observed that pellets in contact to the cell start swelling earlier than those located near the central axis of the specimen. Therefore, voids between pellets and the cell constitute a preferential path during the hydration process.
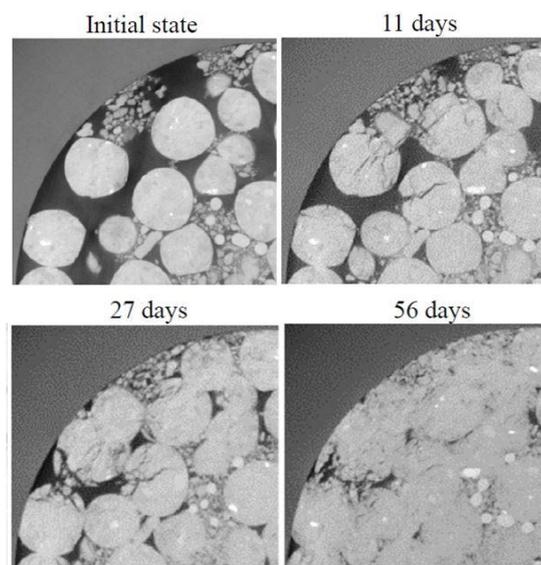

Figure 5. Zoom at 60 mm from the bottom.

Van Geet *et al*. (2004) investigated the homogenization process of a pellet/powder mixture by performing an analysis of the µ-CT results. They noticed the decrease of the pellet density while wetting and the final homogenization at complete saturation. In the present work, several positions within the sample were investigated in order to ensure the total homogenization at the studied resolution, as well as the sealing of all air-filled voids within the mixture.

3.2. Quantitative analysis of the behavior

3.2.1. Evolution of the axial swelling pressure

The evolution of the axial swelling pressure during wetting was monitored during the test thanks to a force transducer installed at the bottom of the sample (see Figure 1). Results are presented in Figure 6 for the 160 days of hydration. Due to the design of the cell, this value corresponds to the average force transmitted to the porous stone at the bottom of the sample. A plateau of 3 MPa was reached after 100 days of hydration. It can be noted that, an apparent homogenous material was observed by µ-CT at this date (see Figure 3).

Based on the relationships between axial swelling pressure and dry density obtained by Karnland *et al*. (2008) and Wang *et al*. (2012) and on the average dry density of the mixture (1.49 Mg/m^3), the axial swelling pressure value can be estimated. It should range from 4.15 MPa to 4.66 MPa. The lower value obtained in this work (3.00 MPa) revealed a looser structure in the vertical direction, which may be related to the fabrication process.
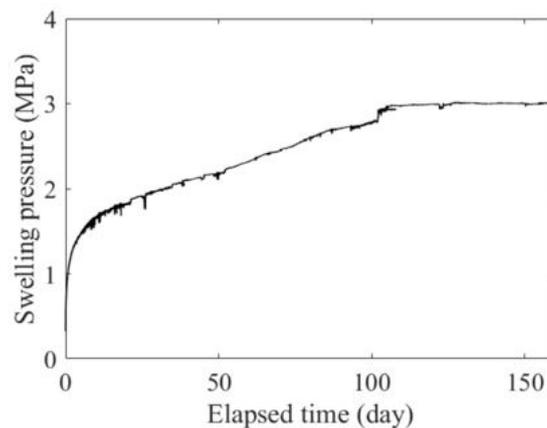

Figure 6. Evolution of the axial swelling pressure of the mixture.

3.2.2. Investigation of the density evolution

Further investigations have been conducted on the behavior of the pellet/powder mixture. Firstly, a preliminary grey level normalization of the obtained pictures was performed. To this end, the same grey level was imposed to the voxels corresponding to PMMA and glass for all the steps during the test. Indeed, these grey level values must remain constant during hydration.

112

Once this first normalization was achieved, an estimation of the apparent density of the bentonite was carried out. A linear relationship was established between the normalized grey levels and the apparent density of the material. The adopted procedure is based on the work presented by Van Geet *et al.* (2005), in which the linear attenuation coefficients were converted into density values.


$$GL = 0.0019d^2 + 0.3473d + 118.24$$
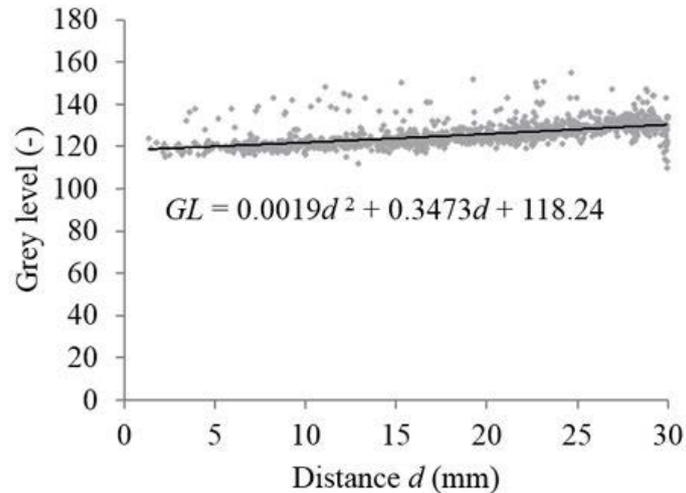
Figure 7. Grey level of PMMA spheres network.

The subsequent step consisted in verifying the absence of residual beam hardening effects. To this end, PMMA spheres were used in order to investigate the grey level of the voxel corresponding to the center of each sphere at 100 days of hydration, which should be constant. Figure 7 shows the grey level of these spheres along the radial direction (zero distance corresponds to the central axis of the specimen). As one can observe, the grey level of the center of the spheres is not constant and slightly increases with the distance to the central axis of the specimen (the high grey level values observed correspond to voxels which are not perfectly centered into the corresponding sphere). This means that there are some residual beam hardening effects even though a filter made of cooper was used to avoid them. Therefore, a correction was applied in order to avoid these artefacts. For this purpose, the least square fit presented in Figure 7 was used to normalize the grey levels. Three different grey profiles located at 10, 60 and 110 mm are displayed in Figures 8, 9 and 10, respectively. They correspond to μ-CT observations carried out on the sample after 100 days of hydration. These profiles are represented before and after applying this correction. It appears that without correction, higher values of attenuation are observed at the edges of the specimen, which may be explained a priori as a gradient of density within the sample. Nevertheless, after applying the correction, a constant value of grey level for the three distributions can be observed. This means that, at the

studied resolution (50 µm/voxel) the sample seems homogeneous after 100 days of hydration as no gradient densities are observed. The same medium grey level value (120) is observed at 10, 60 and 110 mm from the bottom hydration front after correction.
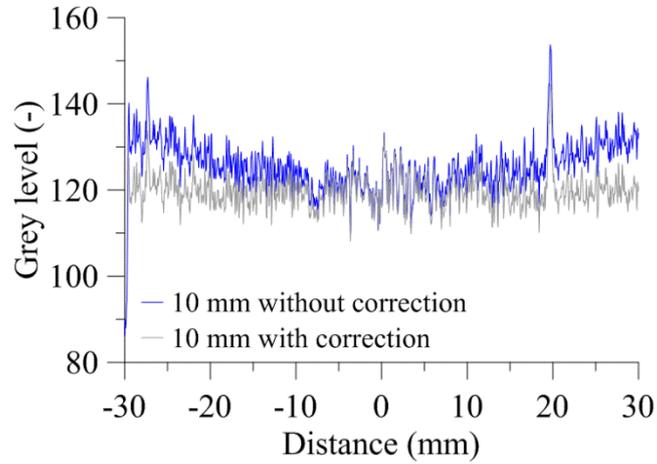

Figure 8. Grey level distribution at 10 mm from the bottom.
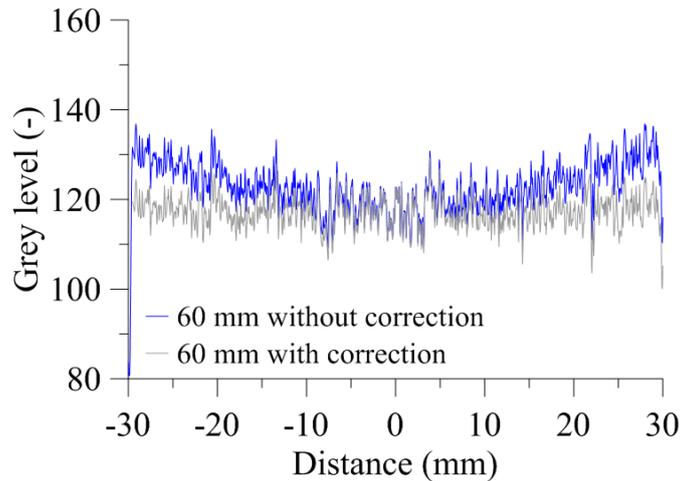
Figure 9. Grey level distribution at 60 mm from the bottom.
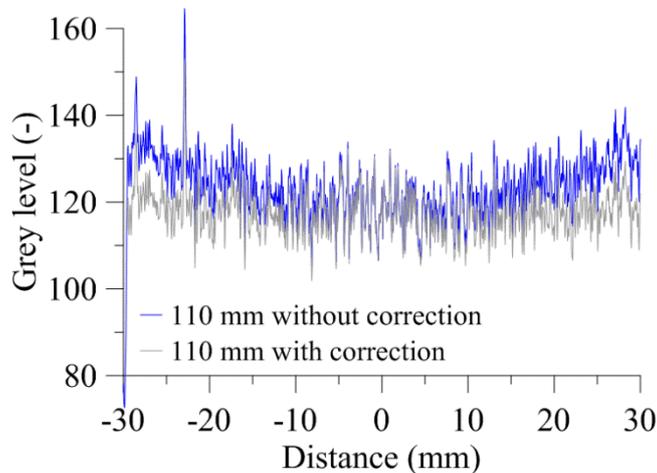

Figure 10. Grey level distribution at 110 mm from the bottom hydration front.

The evolution of apparent density field in a vertical section is shown in Figure 11. From the initial state of the material until four days of hydration, higher density pellets can be distinguished within the sample (except those located near the hydration fronts) with air-filled inter-pellet voids between them. After four days of hydration, all pellets are affected by the evolution of the hydration front, resulting in the progressive decrease of their density.
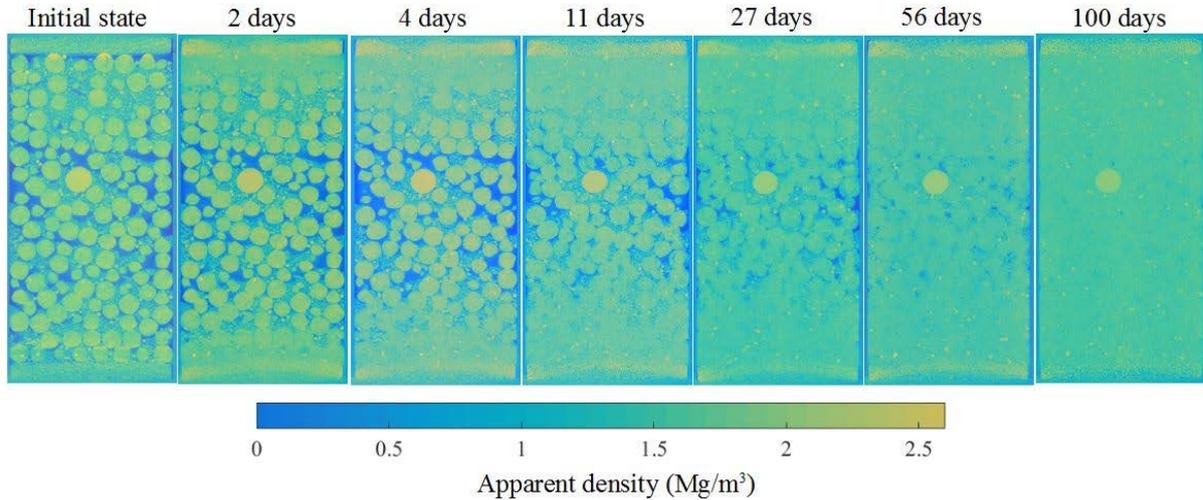

Figure 11. Apparent density field at various times.

3.2.3. Investigation of the displacement field of the bentonite powder

DIC technique has been used to calculate the displacement field of PMMA spheres added to the sample during the fabrication process. Figure 12 presents the results, which correspond to vertical displacements occurring during the first 100 days of hydration (the arrow indicates the positive displacement sense). For each location (height), the displacements of spheres located at ±10 mm in the vertical direction were considered, and finally the medium value was calculated.

The results show a sudden displacement of 0.2 – 0.4 mm of the PMMA spheres towards the bottom after 2 days of hydration for the locations at 30, 50, 70 and 110 mm. Actually, these locations correspond to the zone were air-filled inter-pellet voids are dominant (Figures 2 and 3). Hydration induces swelling of the material at the two ends, increasing the swelling pressure (Figure 6), and provokes pellets re-arrangement. The movement of pellets would then induce the movement of bentonite powder and PMMA spheres located in the inter-pellet voids. As air-filled inter-pellet voids are dominant in these zones, bentonite powder and PMMA spheres would tend to move downward because of the gravity. This phenomenon is less visible at 10 mm for the bottom because the bottom partly restricts this movement. At 90 mm, a heave is

observed during the first 2 days of hydration. First, the downward displacement of PMMA spheres should be limited in this zone because bentonite powder is relatively dominant in the inter-pellet voids (see Figures 2 and 3). Second, material in this zone would tend to heave to fill the initial gap at the top (see Figure 3).

The above phenomena continue generally with the same trends until 11 days of hydration. After this date, the movement of the PMMA sphere is negligible until 49 days of hydration. Between 49 days and 56 days of hydration, a sudden downwards movement was found at all the levels (except at 10 mm from the bottom). This movement would be explained by an accidental shock during the installation of the cell; the cell was removed from the micro-tomograph during the hydration and put back to its positions only during the scan. This explanation could be also used for the general downward displacement between 56 days and 100 days of hydration.
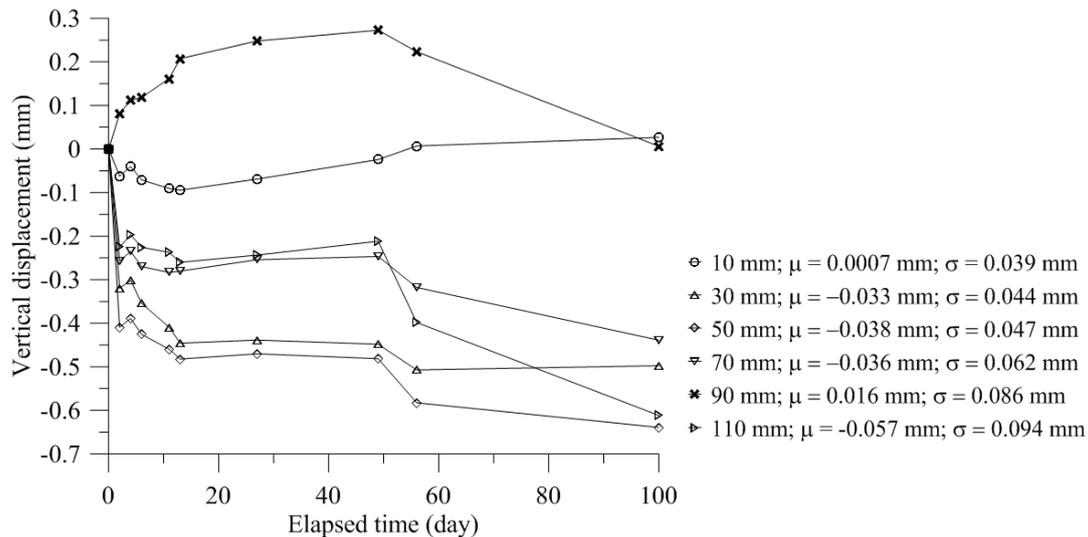

Figure 12. Vertical displacements obtained by Digital Image Correlation Technique (DIC) based on the PMMA spheres network while wetting.

4. Conclusions

The wetting-induced structure changes of a pellet/powder mixture have been investigated in this work by µ-CT observations. Both qualitative and quantitative analyses were carried out.

The results show that the initial mixture is a heterogeneous granular material. The pellet and powder distribution depends strongly on the followed protocol to fabricate it. While wetting the top and bottom sides, the granular structure is quickly lost in the vicinity of both hydration fronts. Pellets lose their structure and the mixture becomes an apparently homogeneous material, with no more air-filled inter-pellet voids. For the rest of the sample, this process depends on the evolution of the hydration front. An estimation of the evolution of density while

hydration was carried out; a homogeneous pellet/powder mixture was observed after 100 days of hydration at the studied resolution (50 µm/voxel). These results allow understanding the structural changes occurring while wetting for SEALEX *in situ* tests.

Vertical displacements of PMMA spheres mixed with bentonite powder reveals downward movement of the sphere at the beginning of the hydration. This phenomenon, induced by the gravity, is more dominant in the zone having large air-filled inter-pellet voids.

The axial swelling pressure (3.00 MPa) observed was lower than the expected value. This was explained by the initial heterogeneous of morphology of the mixture.

References

Alonso, E.E., Romero, E., Hoffmann, C., & Garcia-Escudero, E., (2005). Expansive bentonite-sand mixtures in cyclic controlled-suction drying and wetting. *Engineering Geology*, 81(3), pp.213–226.

Bornert, M., Hild, F., Orteu, J.-J. and Roux, S. (2012). Chapter 6: digital image correlation. In: Full-field measurements and identification in solid mechanics. Grediac, M. & Hild, F. (Eds), Wiley-ISTE, 496 pages

Dixon D. A. Gray M. N. & Graham J., (1996). Swelling and hydraulic properties of bentonites from Japan, Canada and the USA. Environmental Geotechnics 1, 43-48.

Barnichon, J.D., Deleruyelle, F., (2009). Sealing Experiments at the Tournemire URL. EUROSAFE.

Garcia-Siñeriz, J. L., Villar, M. V., Rey, M., and Palacios, B., 2015. "Engineered barrier of bentonite pellets and compacted blocks: State after reaching saturation," Eng. Geol., vol. 192, pp. 33–45.

Graham, J., Saadat, F., Gray, M. N., Dixon, D. A., & Zhang, Q. Y., (1989). Strength and volume change behavior of a sand-bentonite mixture. Canadian Geotechnical Journal 26, No. 2, 292- 305.

Herman, G.T. (1979). Correction for beam hardening in computed tomography. Physicsin Medicine andBiology, 24, 81.

Imbert, C. & Villar, M.V., (2006). Hydro-mechanical response of a bentonite pellets/powder mixture upon infiltration. *Applied Clay Science*, 32(3-4), pp.197–209.

Komine, H., & Ogata, N., (1994). Experimental study on swelling characteristics of compacted bentonite. Canadian geotechnical journal 31 , No. 4, 478-490.

Molinero-Guerra, A., Mokni, N., Delage, P., Cui, Y. J., Tang, A. M., Aimedieu, P., Bernier, F., Bornert, M., (2016). In-depth characterisation of a mixture composed of powder/pellets MX80 bentonite. Applied Clay Science (135), 538 – 546.

Mokni, N. & Barnichon, J.D., (2016). Hydro-mechanical analysis of SEALEX *in situ* tests- Impact of technological gaps on long term performance of repository seals. Engineering Geology, 205, pp. 81-92.

Pusch, R. (1982). Mineral-water interactions and their influence on the physical behavior of highly compacted Na bentonite. Canadian Geotechnical Journal, 19(3): 381–387. doi:10.1139/t82-041.

Saba, S., Cui, Y.J. and Barnichon, J.D., (2014). Investigation of the swelling behavior of compacted bentonite–sand mixture by mock-up tests. Canadian Geotechnical Journal, 51(12), pp.1399–1412.

Sun, W., Sun, D., Fang, L. & Liu, S., (2014). Soil-water characteristics of Gaomiaozi bentonite by vapor equilibrium technique. *Journal of Rock Mechanics and Geotechnical Engineering*, 6(1), pp.48–54.

Sutton, M.A., Orteu, J.J., and H. Schreier., H., (2009). Image correlation for shape, motion and deformation measurements: basic concepts, theory and applications. Springer Science & Business Media.

Van Geet, M., Volckaert, G. & Roels, S., (2005). The use of microfocus X-ray computed tomography in characterising the hydration of a clay pellet/powder mixture. *Applied Clay Science*, 29(2), pp.73–87.

Villar, M.V., 2013. EB experiment. Contribution of CIEMAT to EB dismantling report. Physical state of the bentonite. EC Contract 249681 PEBS. Informe Técnico CIEMAT/DMA/2G210/04/2013 (Madrid, 21 pp.).

Wang, Q., Tang, A.M., Cui, Y.J., Delage, P., Gatmiri, B., (2012). Experimental study on the swelling behavior of bentonite/claystone mixture. Eng. Geol. 124, 59–66. http://dx. doi.org/10.1016/j.engeo.2011.10.003.

Wang, Q. & Cui, Y.J., Tang, A.M., Delage, P., Gatmiri, B. and Ye, WM., (2013a). Long-term effect of water chemistry on the swelling pressure of a bentonite-based material. Applied Clay Science. 87. 10.1016/j.clay.2013.10.025.

Wang, Q., Cui, Y. J., Tang, A. M., Barnichon, J. D., Saba, S. & Ye, W. M., (2013b). Hydraulic conductivity and microstructure changes of compacted bentonite/sand mixture during hydration. *Engineering Geology*, 164, pp.67–76.

Wang, Q., Cui, Y. J., Tang, A. M., Li, X. L. & Ye, W. M., (2014). Time- and density-dependent microstructure features of compacted bentonite. *Soils and Foundations*, 54(4), pp.657–666.

Impact of initial structural heterogeneity on long term swelling behavior of MX80 bentonite pellet/powder mixtures

Agustín Molinero Guerra[1,2], Nadia Mokni[2*],Yu-Jun Cui[1], Pierre Delage[1], Anh Minh Tang[1],

Patrick Aimedieu[1], Frédéric Bernier[3], Michel Bornert[1]

[1]Ecole des Ponts ParisTech, Laboratoire Navier/CERMES, Marne La Vallée, France
[2]Institut de Radioprotection et de Sûreté Nucléaire (IRSN), Fontenay-aux-Roses, France
[3]Agence Fédérale de Contrôle Nucléaire (AFCN), Belgium

Abstract: In order to better understand the results from the *in situ* tests carried out in the Tournemire Underground Research Laboratory (URL) by the French Institute of Radiation Protection and Nuclear Safety in the SEALEX project, the hydro-mechanical behavior of a pellet/powder MX80 bentonite mixture at a dry density of 1.49 Mg/m3 was investigated in the laboratory by means of μ-CT observations and laboratory small scale infiltration tests. Radial and axial swelling pressures as well as relative humidity were monitored while wetting. Two configurations were considered: the first one was a pellet/powder mixture with a proportion of 80/20 in dry mass prepared following a specific protocol allowing the initial structural heterogeneity to be minimised; the second one was specially designed to study a strong heterogeneous pellet/powder distribution: the half bottom part of the specimen corresponds to a mixture in which all inter-pellet voids are filled with powder grains (66.7-pellets/33.3-powder), but the half top part is filled with only pellets of bentonite. It was observed that the evolution of radial swelling pressure depends on the heterogeneous distribution of pellets/powder. When comparing the axial swelling pressures in the two configurations, it appeared that the axial swelling pressure also strongly depends on the distribution of pellets/powder. Finally, a comparison was made between the *in situ* and the mock-up tests. A factor scale of 30 was found when comparing the injected volume of water during wetting.

Keywords: pellet/powder bentonite mixture; X-ray computed microtomography; initial heterogeneity; long term behavior.

1. Introduction

Bentonite-based materials are considered in many countries as buffer/backfill/seal material in deep geological nuclear waste disposal. To ensure the safety functions of the deep geological repository, it is crucial to well understand the hydro-mechanical behavior of buffers/backfills/seals made up of this kind of materials at different scales, in particular, the swelling behavior upon welling. In this context, the Institute of Radiation protection and

Nuclear Safety (IRSN) has launched SEALEX project to investigate the long-term hydraulic performance of sealing systems in normal and critical scenarios, as well as different core compositions. A series of *in situ* experiments have been performed in IRSN's Underground Research Laboratory (URL – Tournemire, France) (Mokni & Barnichon, 2016; Mokni, 2016). This work focuses on the last one in which a mixture of pellets and powder of bentonite with a proportion of 80/20 in dry mass was investigated. Based on the design of the *in situ* experiments, two laboratory mock-up tests (1/10th scale) were performed aiming at studying the hydro-mechanical behavior and the structure changes of the material during hydration.

The hydro-mechanical behavior of different configurations of sealing plugs has been investigated at both laboratory and field scales (Mokni & Barnichon, 2016; Mokni, 2016, Wang *et al*., 2012, 2013; Saba *et al*., 2014). The relationship between swelling pressure and bentonite dry density of the material is an important result from these investigations (Börgesson *et al*., 1996; Dixon *et al*., 1996; Lloret *et al*., 2003; Imbert and Villar, 2006; Karnland *et al*., 2008; Gens *et al*., 2011; Villar *et al*., 2012; Wang *et al*., 2013; Saba *et al*., 2014; Schanz & Al-Badran, 2014). However, this relationship was mainly established based on the axial swelling pressure of the bentonite-based materials, and a few results of radial swelling pressure were considered for this purpose. Additionally, very few experiments focused on the evolution of dry density heterogeneity upon hydration and its influence on the swelling behavior. Furthermore, few investigations have been conducted on the hydro-mechanical behavior of bentonite pellet/powder mixture which is one of candidate sealing materials (Imbert and Villar, 2006; Van Geet *et al*. 2005; Molinero *et al*. 2016). This material, consisting of a mixture of low-density bentonite powder and highly compacted bentonite pellets, is obviously highly heterogeneous in its initial state. Molinero *et al*., (2016) demonstrated that preparing samples of a mixture of MX80 bentonite pellet/powder at the same target dry density with the same fabrication protocol does not ensure an initial homogenous structural distribution. The degree and distribution of heterogeneity might vary during hydration; thus, the average dry density might be not sufficient to characterize its final state. Another important characteristic of the bentonite mixture is the multimodal nature of its porous network which governs its overall hydro-mechanical properties.

The aim of this work is to investigate the effect of initial heterogeneous structural distributions on the swelling capacity and microstructural evolution of the bentonite pellet/powder mixture upon hydration. To account for possible structural heterogeneities resulting from the installation process in real disposal repositories, two configurations were considered. In the first

configuration, the specimen consists of a mixture of MX80 bentonite pellet and powder with a proportion of 80/20 in dry mass, similarly to the SEALEX *in situ* test. Special effort has been made to minimize initial structural heterogeneities. In the second configuration, a highly heterogeneous specimen, with half consisting of MX80 bentonite pellet and half of MX80 bentonite pellet/powder mixture was tested. The results of the small scale tests are presented along with the results of *in situ* SEALEX test. Comparison of the small scale laboratory tests and the *in situ* experiments provides useful information regarding the test scale effect.

2. Materials

The studied soil is a mixture of MX80 bentonite pellet and powder (80/20 in dry mass). The bentonite investigated comes from Wyoming, USA. It was provided by the Laviosa-MPC company under the commercial name Expangel SP7 for pellets and SP30 for the powder. The MX80 bentonite has a smectite content of 80% with some inclusions of crystals (quartz, calcite and pyrite). The cation exchange capacity (CEC) is 98 meq/100g, with Na+ as major exchangeable cation (52 meq/100g, with also 1.2 meq/100g for K, 10 meq/100g for Mg and 37 meq/100g for Ca). The liquid limit is 560%, the plastic limit is 62% and the unit mass is 2.77 Mg/m^3 (Saba *et al*. 2014).

Pellets of bentonite were produced by Laviosa-MPC company by compacting a powder of MX80 bentonite in a mould of 7 mm in diameter and 7 mm in height. Compaction was performed at a water content of 6±1% by applying instantaneously the compaction effort, resulting in a pellet dry density ρ_d = 2.06±0.06 Mg/m^3, corresponding to a void ratio e = 0.30±0.07. The pellets were stored in the laboratory in a hermetic plastic box at 20°C. The initial suction (s = 135 ± 3 MPa) was measured in the laboratory with a chilled mirror dew point tensiometer (Decagon WP4C), corresponding to an initial water content w = 7.25%, slightly higher than the fabrication one, due to further hydration after fabrication.

The MX80 bentonite powder was produced by crushing pellets. An initial water content of 3.17% was found in the laboratory after drying at 105°C for 24h, corresponding to an initial suction s = 190.9 MPa (measured with a chilled mirror dew point tensiometer – Decagon WP4).

3. Methods

3.1. Description of SEALEX *in situ* test

The last SEALEX *in situ* performance test namely PT-N4 has been performed, aiming at investigating the long term homogenisation of seals composed of the mixture of MX80 bentonite pellets and powder. When installing the experiment, a horizontal borehole (0 ± 2°), with a 60 cm diameter and 540 cm long was prepared by excavation in the Tournemire URL of IRSN, located in a Mesozoic sedimentary basin on the western edge of the French Causses. The bentonite-based core with a total length of 120 cm consists of a granular mixture of bentonite pellets and powder in a ratio of 80/20 (in dry mass). The bentonite core was constructed using an auger conveyor; vibration was applied through the auger itself in order to achieve the target dry density of 1.49 Mg/m^3.

The core was confined between two fixed stainless steel lids, namely upstream and downstream lids, which provided both hydraulic and mechanical closures (Figure 1). The lids consist of a stainless steel circular plate and a cylindrical stainless steel tube welded all around its periphery. It has a series of three rubber inflatable cushions (O-ring) all around and passing for the hydration tubings. The hydration at both sides of the lids (upstream and downstream) are based on special geotextile mats fed with water distribution tubes. The reduction in thickness of the mats due to the swelling of the buffer is limited to 4 MPa. The hydration system is equipped with a water distribution panel fed by a weighed stainless steel water tank connected with inflow lines to both hydration surfaces (downstream and upstream). The confining system consists of a support tube inserted into the cylindrical tube of the downstream lid up to rest against the circular plate and of a closure plate (1400 mm in diameter) placed at the outer face of the borehole and secured by four bolts anchored to the rock.
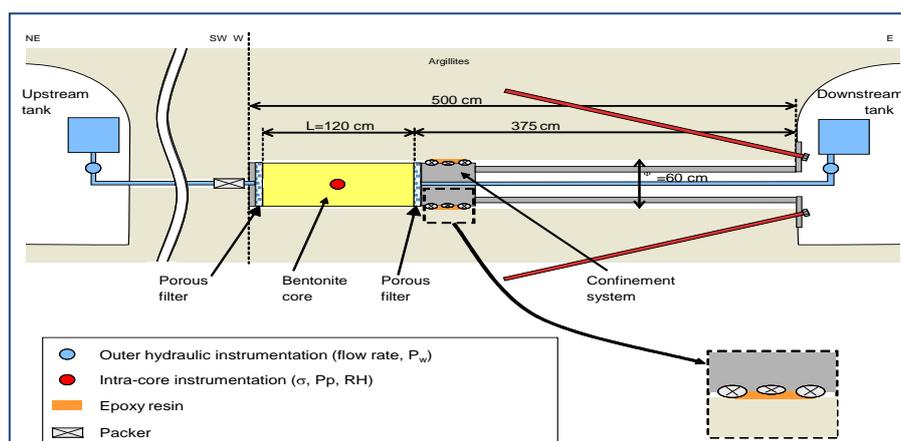

Figure 1. Layout of the SEALEX *in situ* test (Modified from Mokni *et al*., 2016).

In order to avoid potential flow paths along cables and sensors, and thereby, to limit the disturbance of the clay core as much as possible, wireless sensors were used. Three types of

sensors were installed within the seal: 5 total pressure cells (Kulite BG-1-0234-6 MPa), 8 pore pressures sensors (Kulite ETM-200-375-1 MPa) and 8 relative humidity sensors (commercially-available Sensirion SHT75) (Figure 2). Three total pressure sensors were installed on the surface of the core at 60 cm from the downstream saturation face in order to measure the radial swelling pressure. Two total pressure sensors were installed at 0 and 120 cm from the downstream saturation face to measure axial swelling pressure. Hydration was performed by injecting synthetic water with the same chemical composition as the pore water of the Callovo-Oxfordian claystone from the ANDRA underground research laboratory in Bure (Table 1). Injection was carried out using a counter pressure of 0.2 MPa during few hours, and then the backward pressure was released.
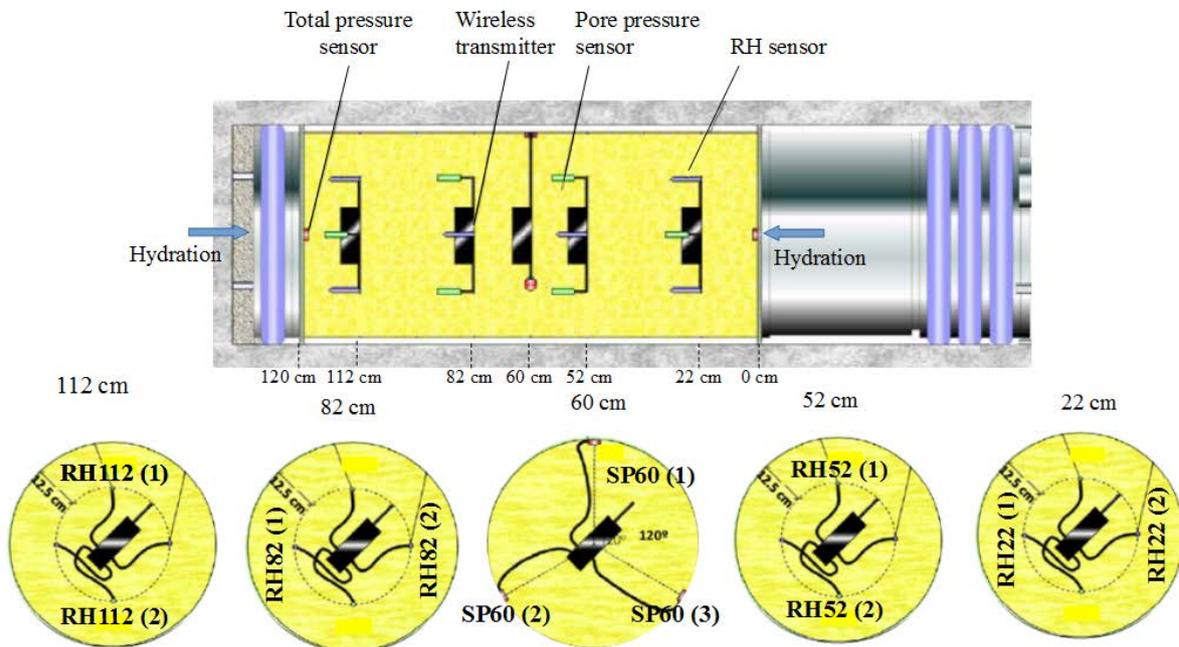
Figure 2. Distribution of the relative humidity and swelling pressure sensors in the seal of SEALEX test.

Table 1. Chemical composition of the synthetic water.

Components	$NaHCO_3$	Na_2SO_4	NaCl	KCl	$CaCl_2$ $2H_2O$	$MgCl_2O6H_2O$	$SrCl_26H_2O$
Mass (g) per litre of solution	0.28	2.216	0.615	0.075	1.082	1.356	0.053

3.2. Experimental mock-up tests

Mock-up tests to Investigate hydro-mechanical behavior *of the mixture*

Two identical small-scale infiltration cells (mock-up tests, Figure 3) were designed in order to investigate the hydro-mechanical behavior of the mixture. The dimensions correspond to 1/10 of *in situ* SEALEX experiments (60 mm in diameter and 120 mm in height). The confined saturation conditions for the pellet/powder bentonite mixture are ensured by a rigid structure and a piston blocked by a screw. The material was saturated from both sides (top and bottom) as in the SEALEX *in situ* experiment. Six total pressure sensors were installed in the cell (SP20, SP40, SP60, SP80, SP100 and SP120), which allowed the measurement of the radial swelling pressures at different positions (h = 20, 40, 60, 80, and 100 from the bottom side). A force transducer was installed under the cell base, monitoring the axial swelling pressure. The relative humidity was also recorded by using five relative humidity sensors (RH31, RH51, RH71, RH91 and RH111) placed at different heights in the cell (h = 31, 51, 71, 91 and 111 mm, see Figure 3).
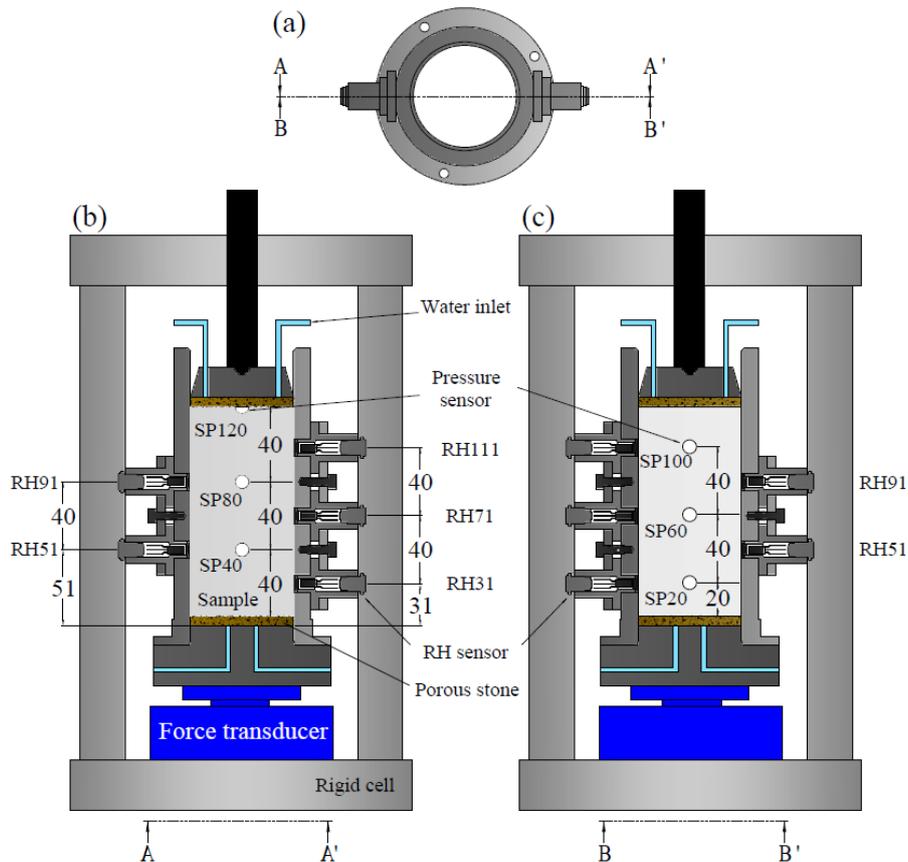

Figure 3. Layout of the mock-up test cell (a) top view; (b) section A-A'; (c) section B-B'.

Mock-up tests to investigate microstructural evolution of the mixture

The evolution of the microstructural distribution of the material upon hydration was investigated by means of Microfocus X-ray Computed Tomography observations (μ-CT). A special set-up consisting of a transparent PMMA (Polymethyl methacrylate) cell was designed (Figure 4). It has 60 mm of inner diameter and 120 mm of height, which corresponds to 1/10th scale of the SEALEX *in situ* tests. The mixture is prepared inside the cell, between two pore stones and filter papers. The rigid PMMA cell (30 mm thick) and the blocked piston ensures a constant-volume hydration condition. The mixture is saturated from both top and bottom sides, as in the SEALEX *in situ* experiments.
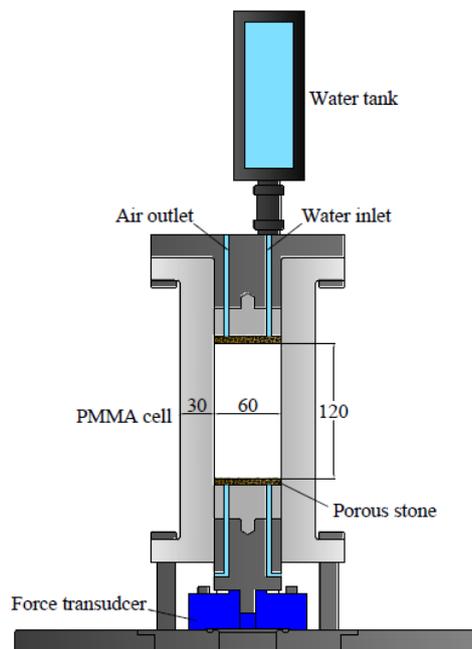
Figure 4. Layout of the transparent PMMA cell.

μ-CT scans were carried out on both mixtures at initial state and during hydration by using an "Ultratom" microtomograph (RX Solutions, France). Images were reconstructed using the software Xact (RX Solutions). The source is a microfocus X-ray tube Hamamatsu L10801 and the imager is a Paxscan Varian 2520V (1960 x 1536 pixel^2, 127 µm size).

The X-ray source parameters were 160 kV and 120µA; the voxel size was 50 µm. The samples were scanned using 5760 projections in helical mode. After reconstruction, 2800 horizontal slices were obtained (16 bit images, 1499 x 1499 pixel^2). An external metal filter consisting of a 1.5mm thickness cooper plate was used in the μ-CT source. This filter allows reducing the low energy photon component of the X-ray beam, reducing the beam hardening effect.

3.3. Sample preparation and protocol adopted in the mock-up tests

To account for possible structural heterogeneities resulting from the installation process in real disposal conditions, two configurations were considered at the same global dry density of 1.49 Mg/m³. In the first configuration, the specimen (sample 1) consists of a mixture of MX80 bentonite pellet and powder with a proportion of 80/20 in dry mass, similarly to SEALEX *in situ* test. A special preparation protocol was adopted to minimize initial structural heterogeneities (Molinero Guerra *et al*., 2016). It consists in filling the cell by packets corresponding to one layer of pellets spread over the base of the cylinder and by adding the corresponding amount of powder (taking into account the proportion 80% pellets – 20% powder in dry mass) (Figure 5a). In the second configuration, a highly heterogeneous specimen (sample 2) consisting of a mixture of MX80 bentonite pellet and powder prepared at different proportions was tested (Figure 5b). In this case, the half bottom part of the cell was filled with a 66.7% pellet/33.3% powder mixture (proportions in dry mass) – corresponding to a dry density of 1.79 Mg/m³, to ensure that all inter-pellet voids are filled with powder. On the contrary, the top half of the cell was filled with only pellets of bentonite at a dry density of 1.19 Mg/m³. The latter case simulates possible defects that might results from *in situ* installation process.
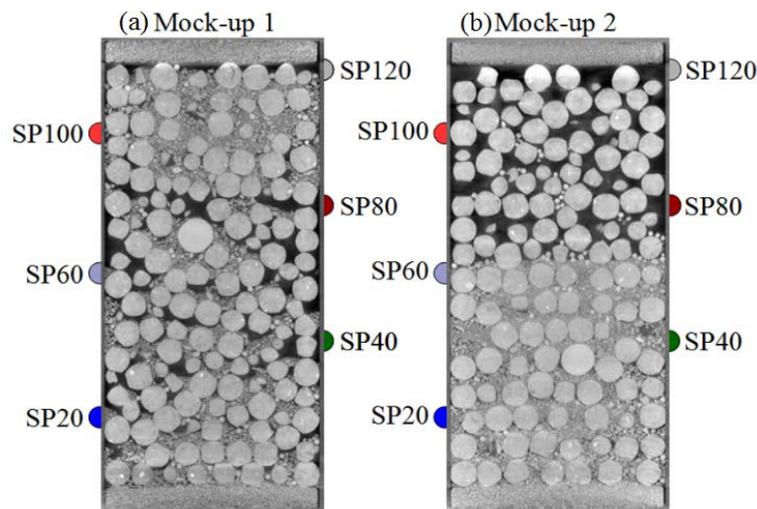

Figure 5. µ-CT observations of the investigated mixture for (a) mock-up 1 and (b) mock-up 2.

All the tests (mock-up and µ-CT tests) started by opening the water inlet valves. At the beginning, air in the base or in the piston was evacuated by opening the air outlet valve until no air bubble was observed in the pipes. Water was then injected through both the top and the bottom of the sample. Values of radial and axial swelling pressure as well as relative humidity

were recorded automatically by a data logger. The volume of injected water was also monitored during hydration.

4. Experimental results

Mechanical results

Figure 6 displays the swelling pressure evolution of the two investigated samples (sample 1 and 2) after 300 days of hydration. Two distinct hydro-mechanical responses can be identified for both mixtures. For sample 1 (Figure 6a), the pattern of behavior is very similar in all positions (except at SP 100). The swelling pressure increases at different rates depending on the distance to the hydration front, then reaches a nearly stationary value after 200 days. Nevertheless, a negative rate is observed at the beginning of the hydration process at SP40. This negative rate can be related to a rearrangement of the material structural distribution at this zone at the beginning of the hydration process. After 300 days, the highest radial swelling pressure (4.6 MPa) is measured at SP80 located at 40 cm from the top hydration face. At SP60 the magnitude of the swelling pressure is lower and reaches 3.8 MPa after 300 days. At SP100 located at 20 mm from the top hydration front, the swelling pressure increases very rapidly and reaches a peak of about 2.1 MPa (a zoom is presented in Figure 7). After about 5 hours a significant decrease of the swelling pressure occurs, to a minimum value of 1.5 MPa. The swelling pressure increases again at slower rate and reaches a value of 2.55 MPa after 60 days. Afterwards, the swelling pressure increases and is stabilized at 3.3 MPa after 200 days. The peak occurrence followed by a decrease corresponds to the reorganisation of the microstructure characterized by the collapse of the macrospores between the bentonite grains. It is worth noting that the horizontal swelling pressure measurements are strongly influenced by the local microstructural distribution at the vicinity of the sensors. The non-peak occurrence at SP40, SP60, and SP80 suggest that the sensors were placed in zones where high density pellets are tightly arranged with few or no grains of bentonite powder in between of them. Similar trends were observed for the axial swelling pressure. However, in this case no macrostructural collapse is observed, indicating that collapse in some zone is compensated by the non-collapsing behavior of other zones.

A different pattern of behavior is observed for the highly heterogeneous mixture (sample 2, Figure 6b). At SP20 located within the denser bottom part of the mixture, a fast increase of the swelling pressure is observed at the beginning of the test, reaching a peak value of 6.1 MPa. Then, it decreases until a value of 3.6 MPa after 75 days of hydration. Swelling pressure

increases slightly between 150 and 300 days of hydration, being 3.8 MPa the highest value. On the contrary, at SP40 the swelling pressure increases gradually, and then reaches a nearly stationary value after 100 days.
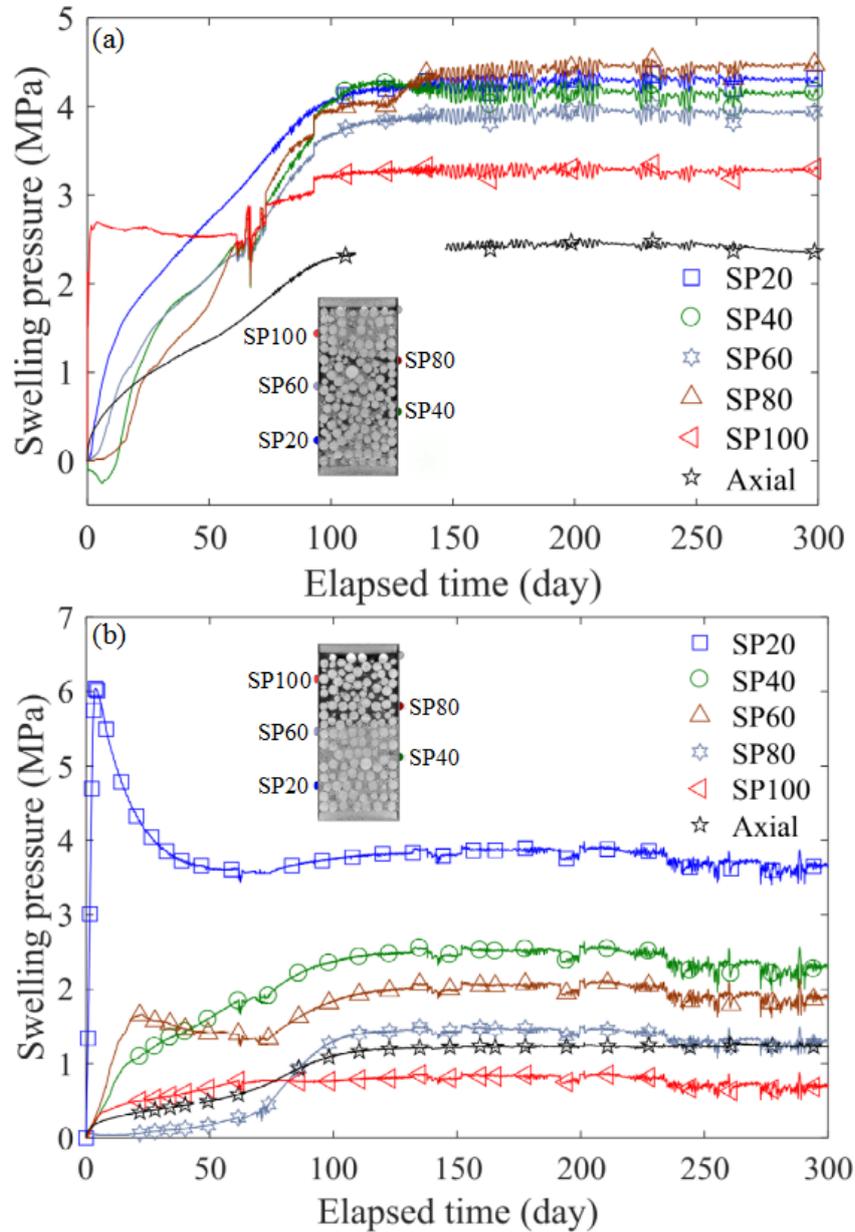

Figure 6. Evolution of swelling pressure with time – results of mock-up tests - for (a) sample 1 with a proportion of 80-pellet/20-powder and (b) sample 2: proportion of 65-pellet/35-powder for the lower half and 100-pellet/0-powder for the upper half.

At SP60 located at the limit between the denser and the looser part of sample 2, a fast increase of swelling pressure is recorded, with a rate higher than that at SP40, until reaching a peak at 1.6 MPa. Then, the swelling pressure decreases slowly to a value of 1.2 MPa. After 72 days, an increase is observed again with the same rate as at SP40. After 300 days of hydration, a swelling pressure of 2 MPa is measured.
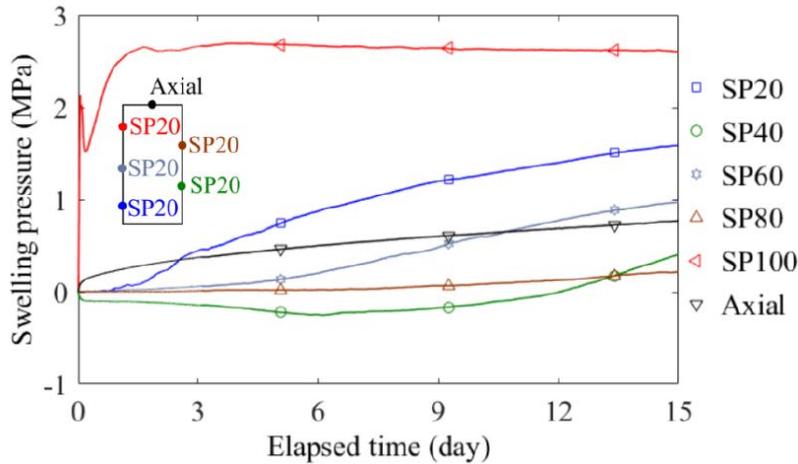
Figure 7. Evolution of the swelling pressure in sample 1 – zoom on the first 15 days.

The lowest swelling pressure increase rate and magnitude are observed at SP80 and SP100 respectively, located at the upper looser part of sample 2 (1.19 Mg/m^3), at 40 and 20 cm form the upper hydration front. At SP80, the radial swelling pressure increases very slowly until reaching a value of 0.3 MPa after 75 days of hydration. Then, an increase of swelling pressure is observed until 100 days, where an almost constant value of 1.2 MPa is reached. The lowest swelling pressure magnitude is recorded at SP100 where a value of about 0.6 MPa is reached after 60 days and remains constant till 300 days. For all sensors, after 230 days a fluctuation is observed for all sensors, which could be due to problems in the system acquisition during the test.

For the axial swelling pressure, as in sample 1, it increases slowly and reaches a nearly stationary value after almost 100 days. However, in this case the magnitude of the swelling pressure in lower (1.1 MPa in this case against 2.3 MPa for sample 1).

Figure 8 displays the profiles of swelling pressure at different times for both samples. For sample 1 (Figure 8a), the curves have a quasi-parabolic shape with a symmetry at 60 mm. This trend is not observed for the highly heterogeneous sample 2 (Figure 8b). In this case, the highest swelling pressure value is reached at the bottom of the mixture, in the denser part of the specimen. Figure 9 displays the swelling pressure profiles after 300 days of hydration for both samples. A relatively constant radial swelling pressure is observed for sample 1, in the range from 3.3 to 4.4 MPa. On the contrary for the highly heterogeneous sample 2, the swelling pressure tends to decrease from the bottom to top. The highest value is observed at 20 mm from the bottom hydration face, where the sample has a high initial density of 1.79 Mg/m^3.
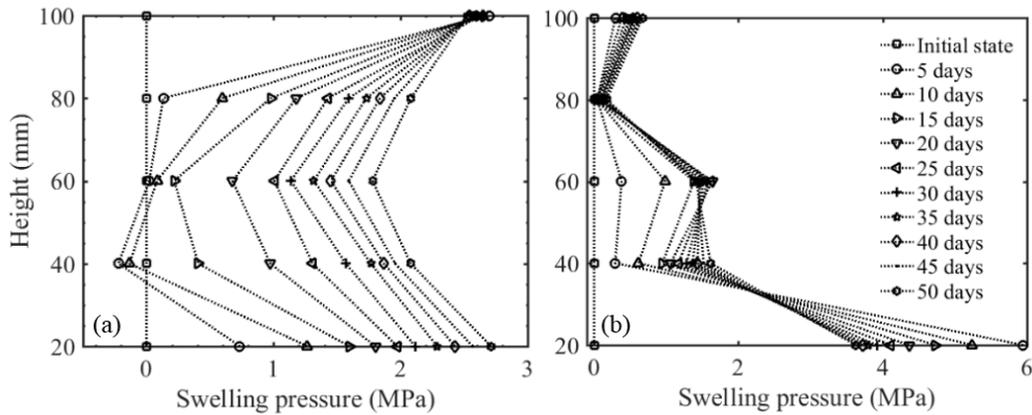
Figure 8. Radial swelling pressure profiles in (a) sample 1 and (b) sample 2.
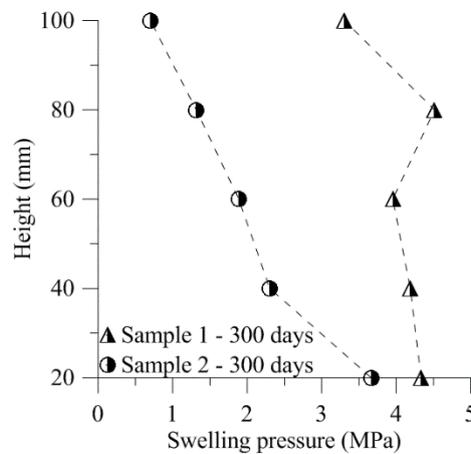
Figure 9. Radial swelling pressure profiles after 300 days of hydration in samples 1 and 2.

Hydraulic results

Figure 10 shows the evolution of Relative Humidity (RH) measured at different distances from the hydration faces for both samples. For sample 1 (Figure 10a), once hydration started, the relative humidity at RH31 located at 31 mm from the bottom hydration face and at RH111 located at 9 mm from the top hydration face increases rapidly and reaches 100% after 20 and 13 days respectively. The relative humidity located at 49 cm from the top hydration (corresponding to sensor RH 71) face started to increase after about 45 days, indicating that the increasing rate of RH is dependent on the distance from the wetting ends.

For sample 2 (Figure 10b), two patterns of behavior can be distinguished. For sensors RH71, RH91 and RH111 located within the upper looser part of the sample, RH increases instantaneously at the beginning of the test, reaching 100% for RH91 and RH111 and 80% for RH71. Then, a decrease is observed for the three sensors until 92%, 87% and 58% for RH111, RH91 and RH71, respectively. Subsequently, RH increases again until saturation at 4, 30 and

40 days for RH111, RH91 and RH71 respectively. Different trends are observed at RH51 and RH 31 located within the denser bottom part of sample 2. At these sensors RH increases progressively until reaching 100% after 20 (RH 31) and 40 days (RH 51), respectively.
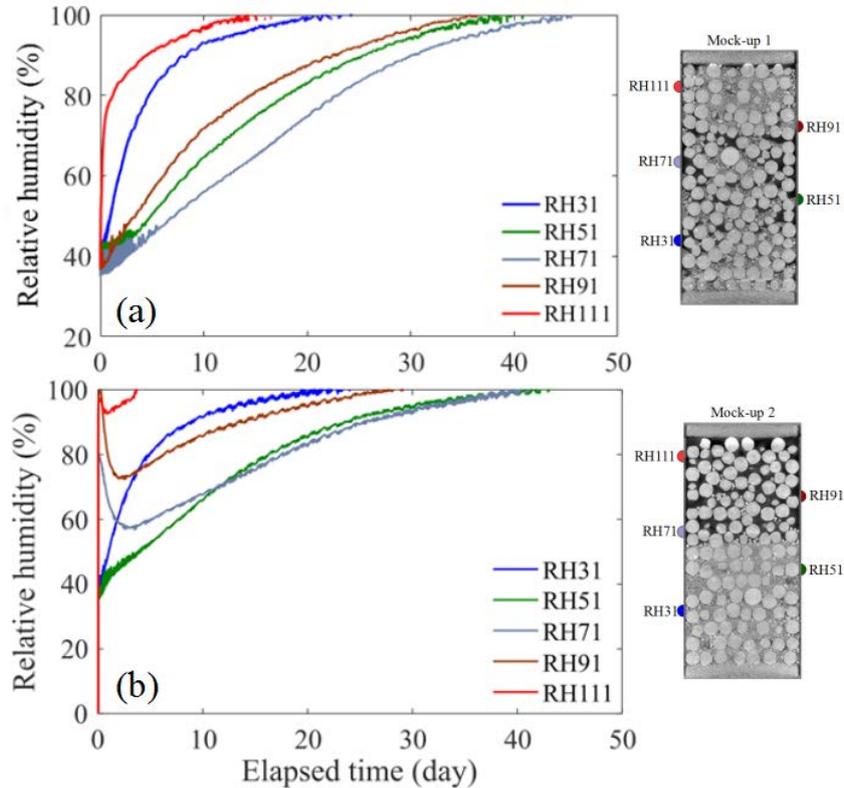

Figure 10. Evolution of relative humidity in (a) sample 1 and (b) sample 2.

The volume of injected water is displayed in Figure 11 for both samples. The top and bottom volumes of injected water were measured separately during the saturation process. In both cases, a higher volume is injected though the top due to the presence of larger voids at this level combined with the gravity effect. Additionally, larger water volumes were injected through the top and bottom for sample 2.

After 300 days, the total volume of injected water is 184.6 cm3 for sample 1 and 230.4 cm^3 for sample 2. These volumes are higher than the theoretical water volume (155 cm^3) calculated by considering a global dry density of 1.49 Mg/m^3.
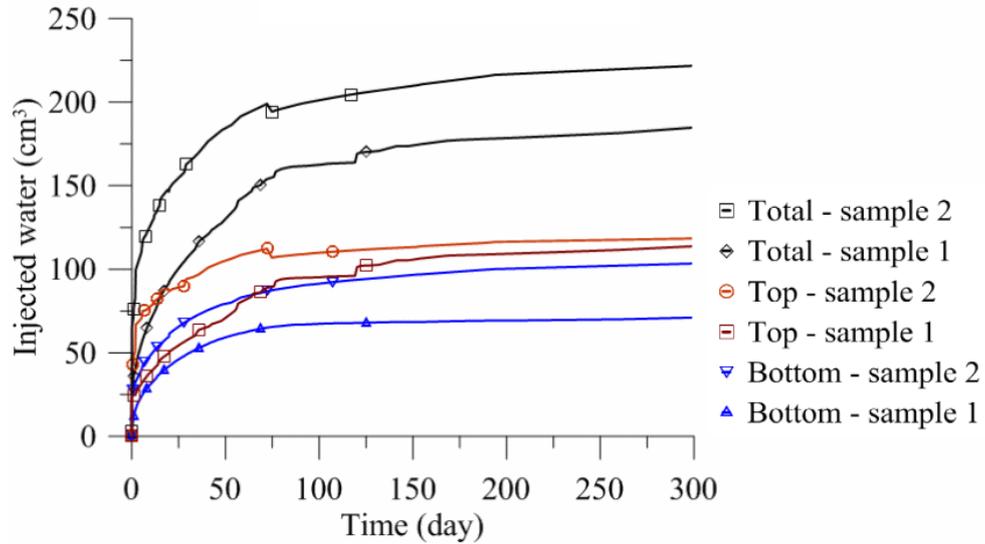
Figure 11. Volumes of injected water into sample 1 and sample 2 while hydration.

Microstructural observations

The microstructural evolution during hydration was investigated by µ-CT observations on two MX 80 bentonite pellet and powder samples (named sample 1a and sample 2a). Sample 1a was prepared similarly as sample 1 and sample 2a was prepared similarly as sample 2 with high initial heterogeneity.
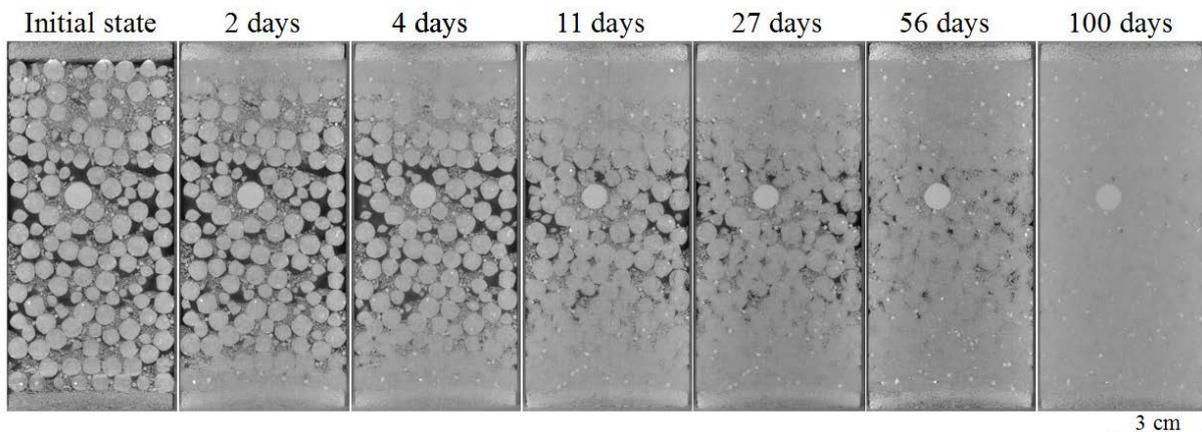

Figure 12. Evolution of the patterns of vertical sections of sample 1a while wetting.

Figure 12 shows the vertical µ-CT sections of sample 1a at different times. The initial state shows the presence of larger voids between the pellet and the porous stone at the top of the mixture, most probably due to segregation during the sample fabrication. Note also the presence of large inter-pellet voids which are not filled with powder, particularly in the peripheral part of the specimen. After 2 days of hydration, the top large inter-pellets voids are completely sealed due to the vicinity to the hydration front. During hydration, the poly-disperse assembly

132

of the highly compacted pellets and powder is progressively lost. Inter-pellet voids are still observed after 56 days of hydration, even though the pellets located at the furthest position from both hydration fronts have already swollen at this time. An apparently global homogeneous sample is observed after 100 days of hydration. At this time, almost all the voids are completely sealed.

Figure 13 shows a zoom of an assembly of pellets located at the middle of sample 1a. These observations allow better understanding the pellets structural changes during hydration. After 11 days of hydration, liquid water has not reached this section but hydration is ensured by vapor transfer. Several cracks can be observed within the pellets. These cracks will play the role of preferential paths for vapor transfer during saturation. After 27 days, new cracks are observed and the pellets are progressively degraded. The initial granular structure is almost lost after 56 days but some inter-pellet voids are still observed.
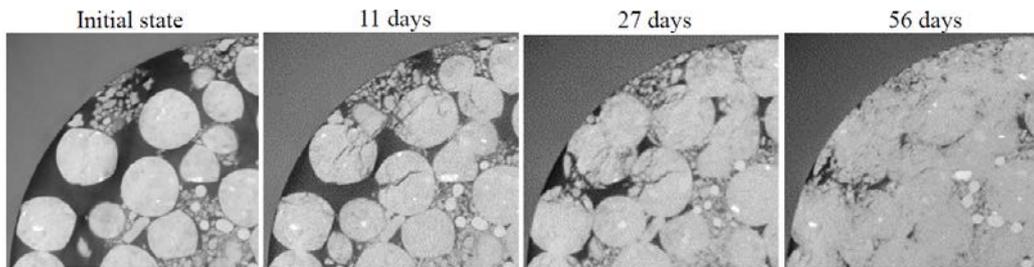

Figure 13. Zooms at 60 mm from the bottom of the sample1a at different times.

Figure 14 shows the vertical μ-CT sections of the highly heterogeneous sample 2a during wetting. A clear distinction can be observed between the top and bottom halves of the sample. For the 100-pellt/0-powder mixture (situated between 60 mm and 120 mm from the bottom hydration front), the initial granular structure completely disappears after 1 day of hydration. Pellets shape can be hardly distinguished; but several large voids can still be observed. After 40 days, the voids are almost sealed by swollen bentonite. A view of the structural evolution of the mixture at a horizontal section located within the looser upper part of the sample at 110 mm from the bottom hydration front is shown in Figure 15. Initially, an assembly of pellets with larger inter-pellet voids not filled with powder can be observed. After 30 min of hydration, the shape of pellets is completely lost as they swell instantaneously. After 90 min of hydration, all voids are completely sealed, resulting in an apparently homogeneous bentonite mixture.

For the denser lower part of sample 2a (66.7-pellet/33.3-powder), only pellets in contact with the bottom porous stone start swelling after 1 day of hydration, but no significant changes are observed in the rest of the sample (Figure 14). Unlike the looser upper part of the sample where

133

the material was rapidly inundated with water, for the denser lower part it is suspected that saturation occurs by advection of liquid water and diffusion of vapor. After 5 days, a homogenous saturated bentonite layers is formed at the bottom boundary of the sample. At this layer, large macro voids are invaded by the swollen bentonite and the hydraulic conductivity becomes very low, favoring the saturation of the remaining unsaturated zones by vapor transfer. Interestingly, the material located at the limit between the denser and looser part (at 60 mm from the bottom) starts swelling rapidly after 5 days since it is also hydrated by water coming from the looser part. Significant changes are observed after 35 days. In the looser part, most inter-pellets voids are already sealed, while in the denser part an increase of the thickness of the outer apparently homogenous bentonite layer is observed. However, after 40 days, several inter-pellets voids are still identified in the looser part; but they are progressively sealed, as it is observed within the outer layer closer to the hydration front (Figure 15). Simultaneously, at the denser part of the sample, the pellet shape can be still noticeable. Unfortunately, the μ-CT observations were stopped at 40 days.
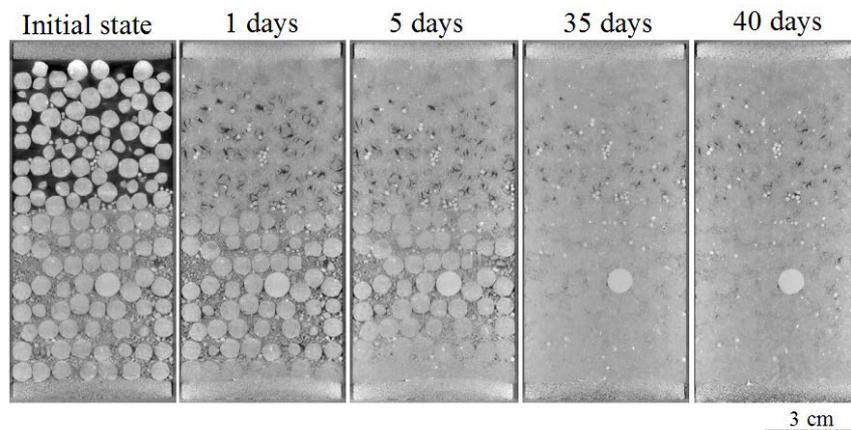

Figure 14. Evolution of the patterns of vertical sections of sample 2a upon wetting.
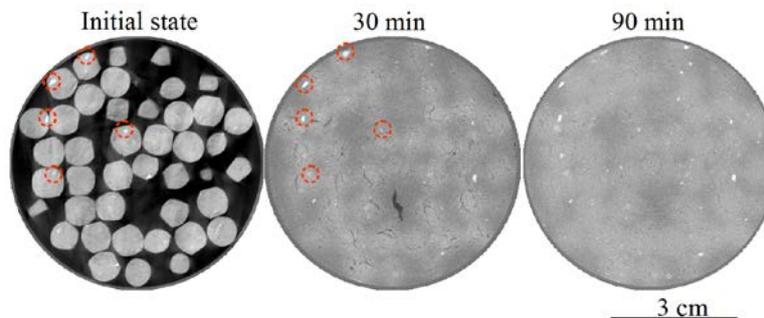
Figure 15. Horizontal sections at 110 mm from the bottom of sample 1a. White points within the section correspond to the high density materials inserted into the mixture for image calibration.

5. Comparative analysis and discussions

Since no information is available about the structural distribution of the bentonite pellet/powder mixture in SEALEX *in situ* test PTN4, comparison of the latter to both mock up tests, allows better interpretation of PTN4 results. The mock up tests are considered as extreme cases since they were performed on a highly heterogeneous sample (sample 2) and on an ideally prepared sample (sample 1) (specific preparation protocol to minimize the heterogeneities as much as possible).

Injected volume of water

The flooding phase in PTN4 was performed in 2 steps: First, a back pressure of 0.2 MPa was applied, in 2 hours. Second, the back pressure was removed, and the upper level of the water in the tank was constantly maintained at 1m above the axis of the borehole (i.e. 1 m water head). Figure 16 shows the evolution of injected water volume over time. Interestingly, a backward flow into the tank induced by bentonite swelling is observed. After a slight increase in rate during the first months, the water intake slowed down to a very low rate and reached 95 L after 780 days. A close examination of the hydration system revealed the presence of entrapped air within the hydration lines which prevented further water intake. Purging of the tubings allowed for further water intake. A total amount of 125 L of synthetic water was injected into the system after 1400 days.
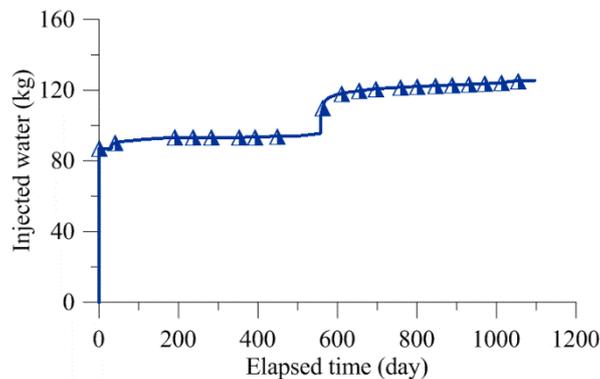

Figure 16. Injected volume of water in the SEALEX *in situ* test PTN4.

In order to compare the evolution curves at different scales (PTN4 versus mock up tests), the water volumes were normalized considering the maximum water volume that can be injected in both mock up and *in situ* tests (158 l for PTN4, 0.158 l for mock up tests). Assuming that the *in situ* test is an intermediate case in between the two extreme cases studied in the laboratory

(mock up 1 and 2), an up scaling time scale ratio of 30 (*in situ*/mock up tests) was found from the normalized water volume (Figure 17).
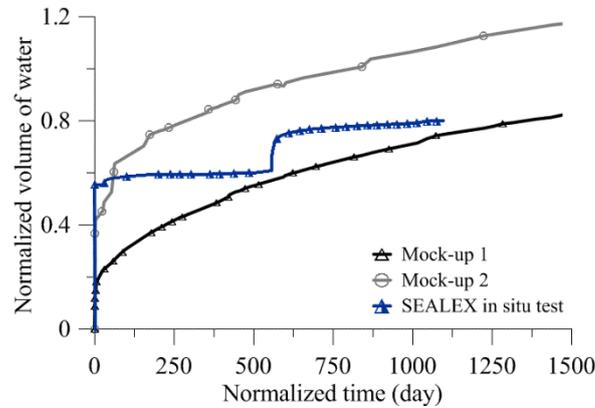

Figure 17. Normalized volume of injected water for both the laboratory and *in situ* tests.

Even though both mock up test samples were prepared at the same mean dry density, larger injection rate and water volume were observed in sample 2. At the beginning of the test, the injection rate is higher for sample 2 because the permeability is higher in the looser upper part of the sample. The difference between injected water volume in sample 2 and the theoretical value may be related to the low water density (1.00 Mg/m^3) considered. This value can be much higher for high plasticity materials as the MX80 (Marcial, 2003; Villar and Lloret, 2004; Lloret and Villar, 2007; Jacinto *et al*., 2012).

Relative humidity evolution

In PTN4, 8 relative humidity sensors were installed in the bentonite core at 22, 52, 82 and 112 cm from the downstream hydration face (Figure 2). Sensors RH52 (1, 2) placed at 52 cm from the downstream lid was malfunctioning since the beginning of the hydration phase. Additionally, data from several operating sensors were not available during several time periods due to a temporary problem in the data acquisition units. The variations with time of relative humidity measured at different sections are displayed in Figure 18. *In situ* data are compared to those from both mock up tests using time scale factor of 30. Once the hydration started, at sensors RH22 (1,2) and RH112 (1,2) located at 22 and 112 cm from downstream hydration face in PTN4, the relative humidity increased progressively and reached 95% after 450 days. A faster RH increasing rate is observed in both mock up tests at sensor RH22 located closer to the bottom and top hydration faces, respectively. This difference is mainly attributed to the different sensors positioning within the *in situ* and laboratory tests. Indeed, in the mock up tests RH sensors were located at the interface between the sample and the cell, where there is almost no

bentonite powder filling the inter-pellets voids (Figure 12 and Figure 14), while in the *in situ* test RH sensors were installed in the bentonite-based core at a distance of about 12.5 cm from the host rock.

Different evolution trends are observed at RH82 (1,2) (Figure 18c). Similarly to RH71 and RH 91 located within the looser upper part in sample 2, a fast increase of RH is observed at the beginning of hydration until reaching 100%, prior to a rapid drop. Then, RH increases again gradually. This suggests that the structural distribution of the bentonite-based core at the vicinity of the RH sensors is comparable to the upper looser part in sample 2. Since no powder exists in this zone, this behavior can be associated to structural changes of the granular pellets during wetting: initially, water comes instantaneously through the inter-pellet voids, which leads to rapid RH increases. Then, the pellets lose their initial granular structure due to swelling, and fill the inter-pellet voids (Figure 15). Therefore, the RH sensors are in contact with the swollen bentonite, which suction is initially higher than that prevailing within the inter-pellets voids upon water inundation. This value will increase gradually during the saturation process.
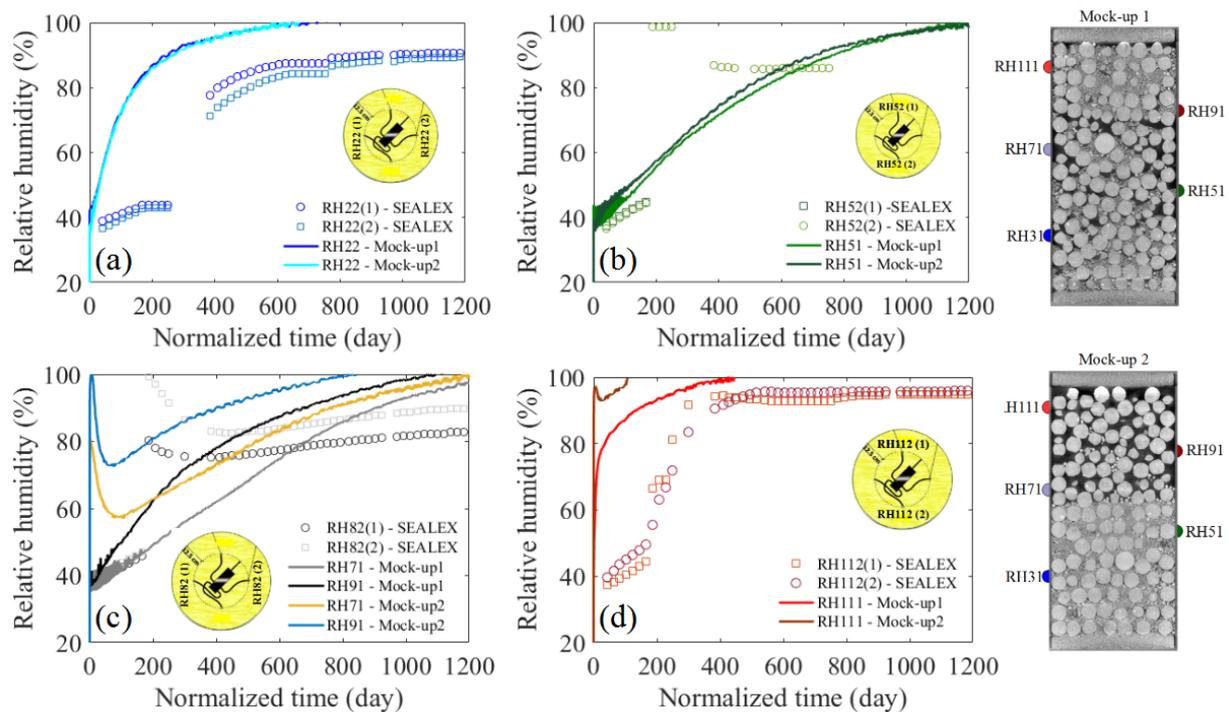

Figure 18. Comparison of relative humidity results between SEALEX *in situ* results and mock-up tests. (a) RH22; (b)RH52 for SEALEX test and RH51 for mock-up tests; (c) RH82 for mock-up tests, RH71 and RH91 for mock-up tests; (d) RH112 for SEALEX test, RH111 for mock-up tests.

The µ-CT observations of sample 1 (Figure 12) revealed that after 56 days in the central zone of the sample pellets were clearly distinguishable, indicating that pellets swelling and hydration

are still progressing. Nevertheless, RH measurements suggests full saturation of the mixture after almost 45 days (Figure 10a). This indicates that the saturation of the highly compacted pellets (2.2 Mg/m^3) is a slower process. This phenomenon was identified as water transfer between the macrostructure and the microstructure, the rate being controlled by several microstructural parameters (e.g. Gens *et al*, 2011, Alonso *et al*, 2011).

Swelling pressure evolution

The *in situ* radial and axial swelling pressure evolutions are depicted in Figure 19 and Figure 20 respectively, together with the normalized curves of mock up tests. Figure 19 compares the evolution of PTN4 radial swelling pressure measured by three total pressure sensors installed on the surface of the bentonite core at 60 cm from the downstream saturation face. It is observed that the swelling pressures increased over time at different rates, depending on the sensors positions. The highest swelling pressure increasing rate is measured at sensor SP60 (1) located on the top of the radial cross section. The value reached at 1200 days is almost 2.4 MPa. On the contrary, the same lower swelling pressure evolutions rates are recorded at SP60 (2) and SP60 (3) and lower values are reached after 1200 days of hydration (1.3 MPa at SP60 (2) and 1.2 MPa SP60 (3)). The measured differences suggest a heterogeneous structural distribution within the *in situ* mixture core, resulting from the field installation process adopted. This observation is confirmed when comparing the radial swelling pressures measured at the same position in both mock up tests: different swelling pressure increasing rates and magnitudes were measured even though both tested samples were fabricated at the same global dry density (1.49 Mg/m^3).

Figure 20 shows the evolution of axial swelling pressure measured by a sensor placed at the downstream hydration face in PTN4. No reliable data have been provided by the total pressure sensor at 120 cm, at the upstream hydration face. The plot shows that the swelling pressure increased at a constant rate and reached 1.4 MPa after 1200 days. Lower values are obtained in the laboratory mock up tests. This difference is closely related to the measurement methods. In the *in situ* test, the sensors placed at upstream and downstream measured the axial swelling pressures locally, while in the mock up tests, the force transducer installed under the cell base ensure the measurement of the global axial swelling pressure.
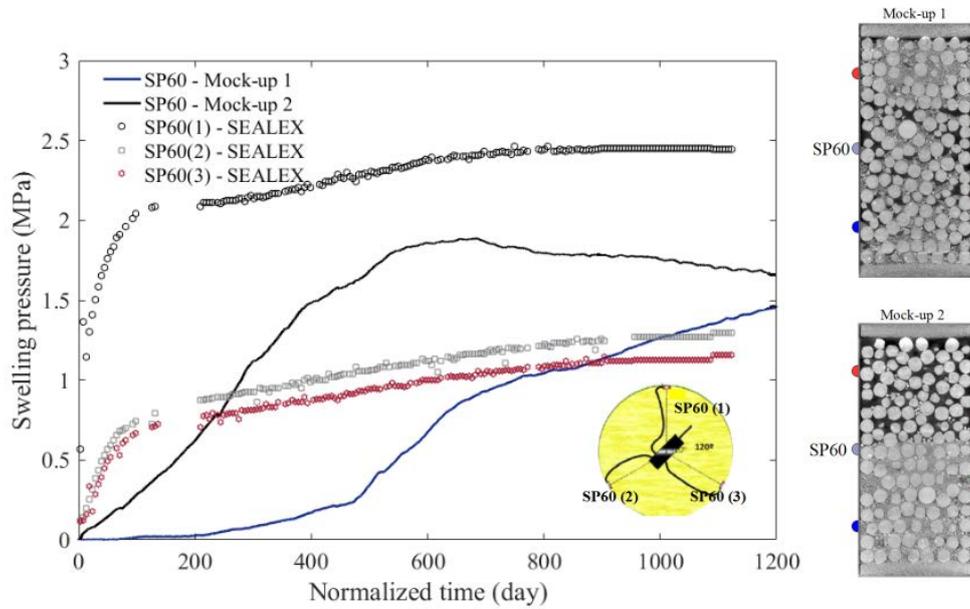
Figure 19. Comparison of swelling pressure results at 60 mm from the bottom hydration front for SEALEX *in situ* test and mock-up 1 test.
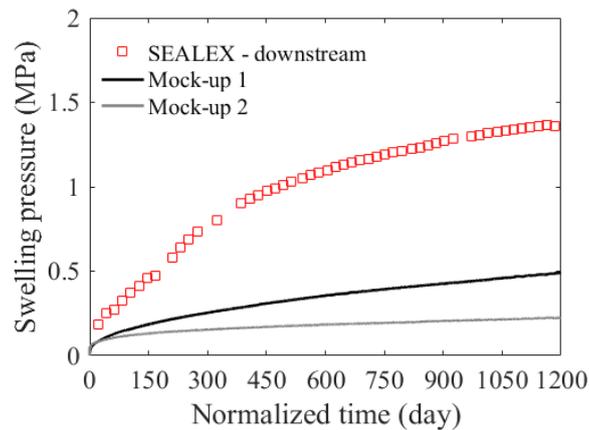

Figure 20. Comparison of axial swelling pressure between SEALEX *in situ* test and mock-up 1 test.

No peaks of swelling pressure are observed in the *in situ* test, while this particular behavior characterized by a peak occurrence followed by a decrease of the swelling pressure are observed in the mock up tests: at sensors SP100 (mock-up 1) and SP20 (mock-up 2), suggesting the appearance of local collapse of the macrospores between the bentonite grains in the latter case (Alonso *et al*., 2011; Gens *et al*., 2011). The non-peak occurrence in PTN4 suggests that the sensors were placed in zones where high density pellets are tightly arranged with a few or no grains of bentonite powder in between.

For both *in situ* and laboratory tests, the final values of axial swelling pressure are lower than those measured radially. A high anisotropic coefficient Ca (defined as the horizontal swelling pressure divided by the axial pressure) ranging from 1.25 and 1.65 is obtained for mock up 1 (Figure 21). For mock up 2 (sample 2), the values of Ca range from 0.5 to 2.9. This strong anisotropy is obviously induced by the highly heterogeneous structural distribution in sample 2. Similarly in PTN4, significant Ca values are obtained (Figure 21), confirming that the installation process greatly influenced the structural distribution of the mixture. Different values are obtained for the three sensors located at 60 mm as their responses are different. The values are near one for SP60(1) and SP60(2) and between the two mock-up tests for SP60(3). This suggests that high heterogeneity exists in several zones PTN4, where pellets are assembled with no or few bentonite powder filling the inter-pellets large voids.
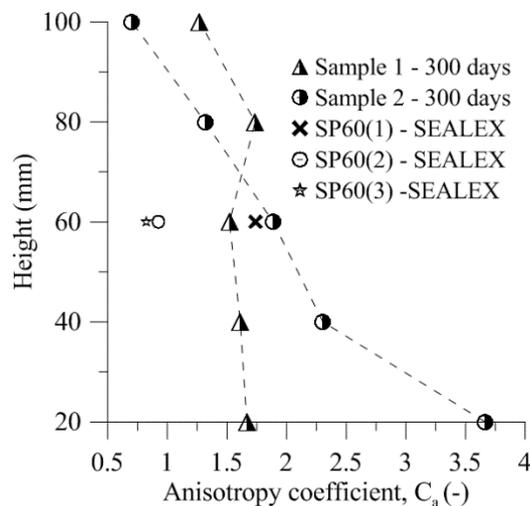

Figure 21. Anisotropy coefficient Ca for mock-up tests and *in situ* SEALEX test.

References

Aitemin, 2012. "SEALEX Project (Tests of Seal Performance): Implementation of *in situ* tests at the Tournemire Experimental Station LOT 2 : Dispositif de confinement / étanchéité , FEASIBILITY AND PERFORMANCE TEST FOR EMPLACEMENT OF Prepared for : IRSN, France.

Alonso, E.E., Romero, E. and Hoffmann, C., (2011). Hydromechanical behavior of compacted granular expansive mixtures: experimental and constitutive study. Géotechnique 61 (4), 329–344.

Barnichon, J.D., Dick, P., Bauer, C., (2012). In: Qian, Zhou (Eds.), The SEALEX *In situ* Experiments: Performance Test of Repository Seals. Harmonising Rock Engineering and the Environment. Taylor & Francis Group, London, pp. 1391–1394 (ISBN 978-0- 415- 80444-8).

Börgesson, L., Karnland, O. and Johannesson, L. E., (1996). Modelling of the physical behavior of clay barriers close to water saturation. Engineering Geology 41, No. 1–4, 127–144.

Dixon, D. A., Gray, M. N. and Graham, J., (1996). Swelling and hydraulic properties of bentonites from Japan, Canada and the USA. Environmental Geotechnics 1, 43–48.

Gens, A., Vallejan, B., Sánchez, M., Imbert, C., Villar, M.V. and Van Geet, M., (2011). Hydro-mechanical Behavior of a Heterogenous Compacted Soil: Experimental Observations and Modelling.

Imbert, C. and Villar, M.V., (2006). Hydro-mechanical response of a bentonite pellets/powder mixture upon infiltration. Applied Clay Science, 32(3-4), pp.197–209.

Jacinto, A.C., Villar, M.V., Ledesma, A., (2012). Influence of water density on the water-retention curve of expansive clays. Geotechnique 62 (8), 657–667.

Karnland, O., Nilsson, U., Weber, H. and Wersin, P., (2008). Sealing ability of Wyoming bentonite pellets foreseen as buffer material – laboratory results. Physics and Chemistry of the Earth, Parts A/B/C 33, S472–S475.

Lloret, A., Villar, M. V., Sánchez, M., Gens, A., Pintado, X. and Alonso, E. E., (2003). Mechanical behavior of heavily compacted bentonite under high suction changes. Géotechnique 53, No. 1, 27–40.

Lloret, A., Villar, M., (2007). Advances on the knowledge of the thermo-hydro- mechanical behavior of heavily compacted FEBEX bentonite. Physics and Chemis- try of the Earth 32, 701–715.

Marcial, D., (2003). Comportement hydromécanique et microstructural des matériaux de barrière ouvragée. (PHD thesis) École Nationale des Ponts et Chaussées, Paris, France.

Mokni, N. & Barnichon, J.D., (2016). Hydro-mechanical analysis of SEALEX *in situ* tests-Impact of technological gaps on long term performance of repository seals. Engineering Geology, 205, pp. 81-92.

Mokni, N., (2016). Analysis of hydro-mechanical behavior of compacted bentonite/sand mixture using a double structure formulation. Environ Earth Sci (2016) 75: 1087. https://doi.org/10.1007/s12665-016-5872-2.

Molinero-Guerra, A., Mokni, N., Delage, P., Cui, Y. J., Tang, A. M., Aimedieu, P., Bernier, F., & Bornert, M., (2016). In-depth characterisation of a mixture composed of powder/pellets MX80 bentonite. *Applied Clay Science*.

Saba, S., Cui, Y.J. and Barnichon, J.D., (2014). Investigation of the swelling behavior of compacted bentonite–sand mixture by mock-up tests. Canadian Geotechnical Journal, 51(12), pp.1399–1412.

Schanz, T. and Al-Badran, Y., (2014). Swelling pressure characteristics of compacted Chinese Gaomiaozi bentonite GMZ01. Soils and Foundations 54, No. 4, 748–759.

Van Geet, M., Volckaert, G. and Roels, S., (2005). The use of microfocus X-ray computed tomography in characterising the hydration of a clay pellet/powder mixture. Applied Clay Science, 29(2), pp.73–87.

Villar, M.V., Lloret, A., (2004). Influence of temperature on the hydro-mechanical behav- iour of a compacted bentonite. Applied Clay Science 26 (1–4), 337–350.

Villar, M. V., Gómez-Espina, R. and Guitiérrez-Nebot, L., (2012). Basal spacings of smectite in compacted bentonite. Applied Clay Science 65–66, 95–105.

Wang, Q., Tang, A.M., Cui, Y.J., Barnichon, J.D. and Ye, W.M., (2013). A comparative study on the hydro-mechanical behavior of compacted bentonite/sand plug based on labora- tory and field infiltration tests. Eng. Geol. 162, 79–87.

Wang, Q., Tang, A.M., Cui, Y.J., Delage, P. and Gatmiri, B., (2012). Experimental study on the swelling behavior of bentonite/claystone mixture. Eng. Geol. 124, 59–66. http://dx. doi.org/10.1016/j.engeo.2011.10.003.

Chapter 4

Constitutive and numerical modelling

INTRODUCTION

An important aspect of the bentonite pellet/powder mixture is the multimodal nature of its porous network, which governs the hydro-mechanical behavior. This feature has been considered in several HM models (e.g. Gens & Alonso, 1992, Alonso *et al.* 1999, Sanchez *et al.* 2005, Gens *et al.*, 2011, Alonso *et al*, 2011). Nevertheless, the initial heterogeneities and the damage behavior have not been taken into account yet.

In this chapter, a HM model which considers the initial heterogeneity of pellets/powder distribution within the mixture and its multimodal nature has been developed. Furthermore, the model accounts for the transient microstructural features characterizing the evolution of bentonite pellets upon wetting. This model has been used to simulate the mock-up test presented in the previous chapter with a mixture sample fabricated by following a special protocol. Model parameters were determined based on the results obtained from the extensive laboratory tests on a single pellet and on the pellets/powder mixture. Results demonstrate the performance of this model in describing the hydro-mechanical behavior of bentonite pellets/powder mixtures with high initial microstructural heterogeneities. In particular, the evolution of dry density gradient and the anisotropic swelling behavior were satisfactorily modelled.

This chapter is presented in the form of an article submitted to "Géotechnique".

Modelling the long term hydro-mechanical behavior of a bentonite pellet/powder mixture with consideration of initial structural heterogeneities

Nadia Mokni[2*], Agustín Molinero Guerra[1,2], Yu-Jun Cui[1*], Pierre Delage[1], Patrick Aimedieu[1], Michel Bornert[1], Anh Minh Tang[1]

[1]Ecole des Ponts ParisTech, Laboratoire Navier/CERMES, Marne La Vallée, France
[2]Institut de Radioprotection et de Sûreté Nucléaire (IRSN), Fontenay-aux-Roses, France

Abstract: The aim of this paper is to investigate the long term hydro-mechanical behavior of highly heterogeneous MX80 bentonite pellet/powder mixture (80/20 in dry mass) envisaged as sealing material in deep geological repositories. In spite of the operational advantages related to the use of the mixture, structural heterogeneities resulting from the installation process constitutes a matter of concern and require special approaches to adequately describe the material behavior during hydration. In this study, a double structure formulation taking into account the initial structural heterogeneity of the material as well as pellets damage upon wetting is proposed. The formulation is applied to the modelling of a 1/10 mock-up of SEALEX large scale tests. Hydraulic and mechanical parameters are determined from an extensive laboratory program carried out on a single pellet of bentonite and on the pellet/powder mixture. To ensure an adequate analysis of the test, the initial heterogeneous structural distribution of the material is determined by image analysis of Microfocus X-ray Computed Tomography observations. The model allows the anisotropic swelling behavior of the mixture to be satisfactorily reproduced when accounting for the spatial variation of the material initial porosity. In particular, the long term hydromechanical behavior of the mixture can be well described. Detailed analysis of the modelling results demonstrate the existence of dry density gradients at long term and their influence on swelling pressure anisotropy.

Keywords: anisotropy; clays; expansive soils; finite-element modelling.

1. Introduction

Most European concepts for high-level radioactive waste disposal involve bentonite-based materials as buffers, backfills and seals of disposal galleries and access shafts to ensure isolation and containment of the waste from the biosphere. Swelling pressures of buffers, backfills and seals are key functions for the safe deep geological repository. One of the major roles of swelling is to ensure that the buffer is self-sealing and closes technological gaps and macro-

voids. It is well documented that the swelling pressure depends principally on the dry density of material (Imber and Villar, 2006). Accordingly, a relatively small change in density can induce significant changes in swelling pressure. That is why most of laboratory and large scale tests have focused on achieving the required average dry density. However, very few experiments have focused on the dry density heterogeneities in the course of hydration and their influence on swelling pressure. It is worth noting that this dry density homogenisation can last long time. For instance, while dismantling the Engineered Barrier emplacement experiment (EB) where two types of bentonite with different dry densities were emplaced (blocks and pellets of bentonite), some heterogeneity in terms of dry density and water content distributions were observed after almost ten years of hydration (Wieszorek *et al.*, 2017).

In order to investigate the long term homogenisation of bentonite-based seals, the French Institute of Radiation protection and Nuclear safety (IRSN) has launched SEALEX project which relies on a series of *in situ* experiments in IRSN's Underground Research Laboratory (URL - Tournemire, France) (Mokni & Barnichon, 2016; Mokni, 2016; Mokni *et al.*, 2016). Based on the design of the *in situ* experiments, laboratory mock-up tests (1/10th scale) were also performed aiming at investigating the distribution of dry density due to water saturation.

SEALEX *in situ* and mock-up tests were conducted on MX80 bentonite pellet/powder mixture which is one of the candidate sealing materials because of its low permeability, high radionuclide retardation capacity and its high swelling potential upon hydration (Pusch, 1979; Yong *et al.*, 1986; Villar, 2008). This material, corresponding to a mixture of bentonite powder and highly compacted bentonite pellets is obviously highly heterogeneous. The degree and distribution of heterogeneities will vary during hydration and the average dry density might be not sufficient to characterise its final state. Low density zones might remain within the buffer mixture, promoting advective transport of radionuclides in the long repository exploration period.

For long-term safety assessment of the repository, it is essential to predict the evolution and the final state of the initially heterogeneous seal and to evaluate the effects of remaining density gradients and swelling pressure differences within the emplaced mixture on the seal hydromechanical behavior. To this end, an appropriate constitutive Hydro-Mechanical (HM) model that accounts for spatial and temporal distributions of the relevant properties of the bentonite pellet/powder is fundamental.

Another important characteristic of the bentonite pellet/powder mixture is the multimodal nature of its porous network which governs all its hydromechanical properties. This aspect has been considered in several HM constitutive models (e.g. Gens & Alonso, 1992, Alonso *et al*. 1999, Sanchez *et al*. 2005, Gens *et al*., 2011, Alonso *et al*, 2011). However, the initial heterogeneities have been often neglected.

In this study, a HM model which takes into account the initial heterogeneous distribution and multimodal nature of the bentonite pellet/powder mixture is developed. Moreover, the model accounts for transient microstructural features characterising the high density bentonite pellets. A description of microstructural characteristics of the pellet/powder mixture is first made, providing a background for the model development. The proposed model is then outlined and used to the model the mock-up test. The model parameters were determined essentially based on the back analysis of laboratory test results. Special attention has been devoted to the swelling anisotropy features identified experimentally.

2. Insights into micro- and macro-structural features

Tested material

The investigated material is a mixture of pellets and powder of MX80 bentonite (Wyoming, USA) with a proportion of 80-pellets/20-powder in dry mass prepared at a dry density $\rho_d = 1.49$ Mg/m^3. It has a high smectite content (80%) with some inclusions of non-clayey minerals (quartz – 4% of the total mass, muscovite – 4% of the total mass, pyrite – less than 1% of the total mass, and some elements of calcite). The cation exchange capacity (CEC) is 98 meq/100g, with Na+ as major exchangeable cation. The liquid limit is 560%, the plastic limit is 62% and the unit mass is 2.77 Mg/m^3 (Saba *et al*., 2014a). Powder grains present a diameter between 0.8 mm and 2 mm. The initial suction of bentonite powder, $s = 190.9$ MPa, was measured with a chilled mirror dew point tensiometer (Decagon WP4).

Pellets were produced by compacting instantaneously bentonite powder into a mould of 7 mm in diameter and 7 mm in height at a water content of $6 \pm 1\%$ (resulting in a dry density $\rho_d = 2.12$ Mg/m^3, corresponding to a void ratio $e = 0.30 \pm 0.07$). Fig. 1 shows a pellet of bentonite at its initial state. It has a quasi-cylindrical shape with two spherical poles on top and bottom. The initial suction $s = 135.5$ MPa and the global initial suction of the mixture $s = 138$ MPa was measured in the laboratory also with WP4.
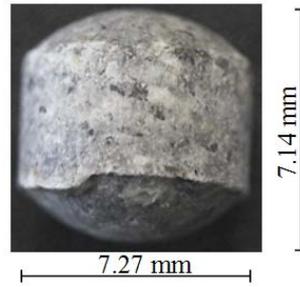
Fig. 1. Pellet at its initial state.

Microstructural characterization

The microstructure of a pellet of bentonite at initial state was investigated by means of Mercury Intrusion Porosimetry tests (MIP) (Fig. 2) combined with Microfocus X-ray Computed Tomography (µ-CT) observations (Fig. 3). At initial state, a monomodal distribution is observed corresponding to the micro-pores with a dominant peak at 11.9 nm (Fig. 2). Another pore population at diameters around 4-5 µm representing 6.8% of the total porosity is also identified. This population corresponds to cracks within the pellet. The network of cracks is also visible in Fig. 3a.
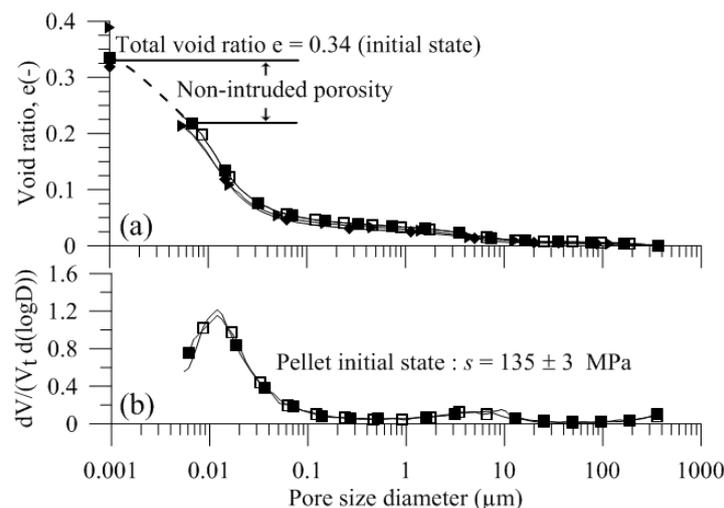

Fig. 2. MIP test results for a pellet of bentonite at its initial state.

Several Pore Size Distribution curves (PSD) (Fig. 4, 5 and 6) of pellets equilibrated at different suctions were determined, together with the µ-CT observations (Fig. 3). Interestingly, as suction decreases, two structural levels become distinguishable (Fig. 4, 5 and 6): the micro-pores correspond to intra-aggregate pores and have a size smaller than 3 µm; the macro-pores correspond to inter-aggregate pores and swelling-induced cracks and have a size greater than 3 µm. Here, the depression between the dominant peaks reported in the PSD functions at $s = 1$

MPa (Fig. 5) has been used as limiting entrance pore size separating micro- and macro-porosity (3 µm).
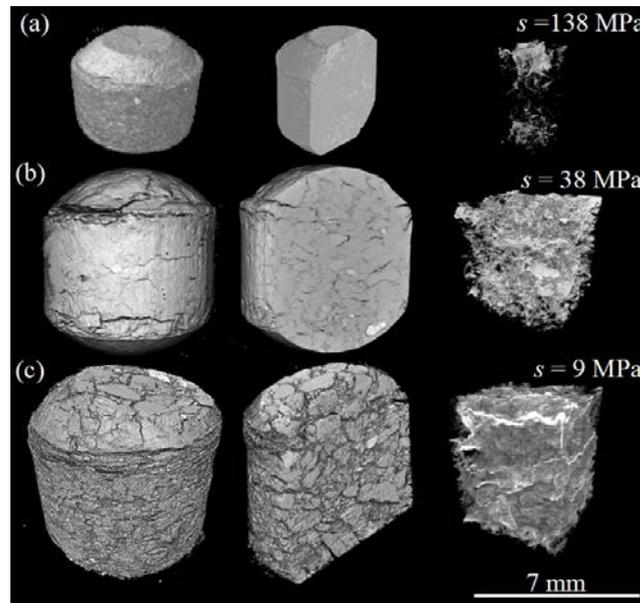
Fig. 3. X-ray computed microtomography (µ-CT) observations (4.41 µm/voxel) – 3D reconstruction image and network of cracks: (a) initial state; (b) s = 38 MPa; (c) s = 9 MPa; (d) s = 1 MPa.

µ-CT observations show that the cracks pattern is significantly developed for $s = 9$ and $s = 38$ MPa (Fig. 3), suggesting that pellets degradation and damage is dependent on suction. This is consistent with the observation of Wang *et al.* (2013) on highly compacted bentonite-based materials.

MIP tests were performed on the mixture prepared at a dry density $\rho_d = 1.49$ Mg/m^3 and saturated under constant-volume conditions. The PSD curves are shown in Fig. 7. Two structural levels can be distinguished: the micro-pores with an average size diameter of 14.9 nm which is in the range of the small pores detected within a single pellet of bentonite and macro-pores with an average size diameter of 49.3 µm corresponding to inter-aggregate pores and swelling-induced cracks with sizes greater than 3 µm.

X-ray computed microtomography observations were performed on the bentonite pellet/powder mixture prepared at $\rho_d = 1.49$ Mg/m^3 and $s = 138$ MPa using a special cell in polymethyl methacrylate (PMMA). The PMMA cell has 60 mm inner diameter and 120 mm height (1/10 SEALEX *in situ* tests, see Fig. 8). The objective here is to investigate the initial microstructural distribution of the mixture and its evolution during hydration. Three samples (samples 1, 2 and 3) was prepared by filling the cell by packets corresponding to one layer of pellets spread over

150

the base of the 60 mm diameter cylinder and by adding the corresponding amount of powder (80% pellets and 20% powder). This protocol allowed a relatively homogeneous mixture at the target dry density (Molinero *et al*., 2016).
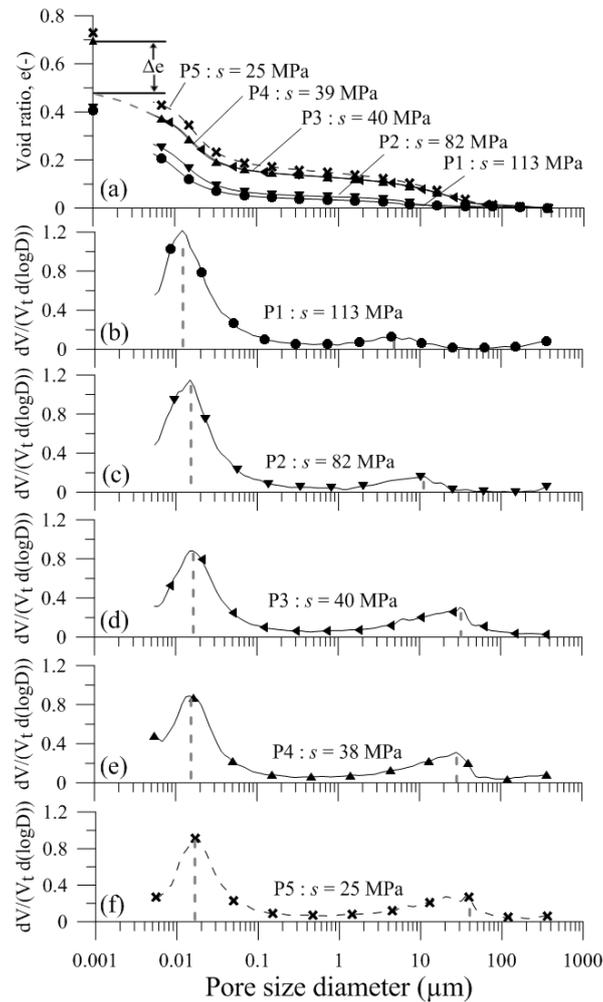

Fig. 4. MIP test results on a single pellet of bentonite equilibrated under suctions from 113 MPa to 25 MPa.

The vertical sections of the tested samples are shown in Fig. 9a. Several zones with inter-pellet voids without grains of powder are observed inside and at the top the sample in the three cases. Fig. 9b shows a zoom of an assembly of pellets located at 60 mm from the bottom hydration front in case of sample 1. After 11 days several cracks can be observed within the pellets constituting preferential paths for water infiltration. After 27 days, the cracks pattern develops inducing pellets degradation. After 56 days, the damaged swollen pellets invade the large inter-pellets macro-pores.
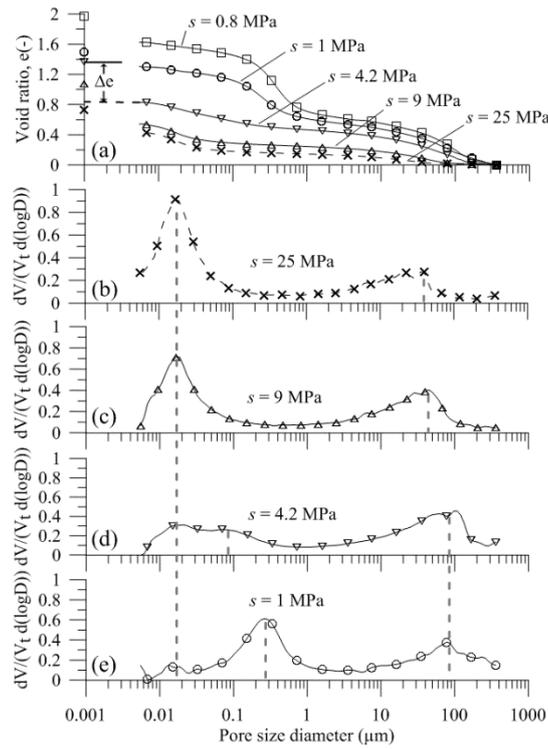
Fig. 5. MIP test results on a single pellet of bentonite equilibrated under suctions from 25 MPa to 1 MPa.
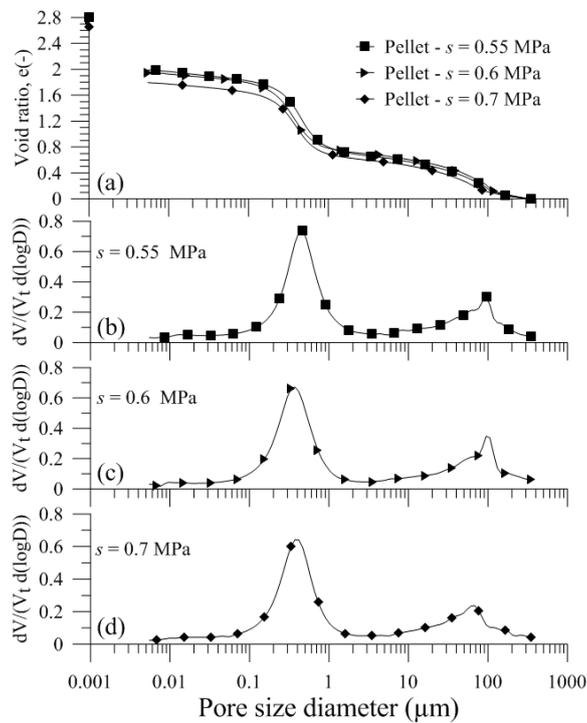

Fig. 6. MIP test results for pellets equilibrated at s = 0.55; 0.6 and 0.7 MPa.
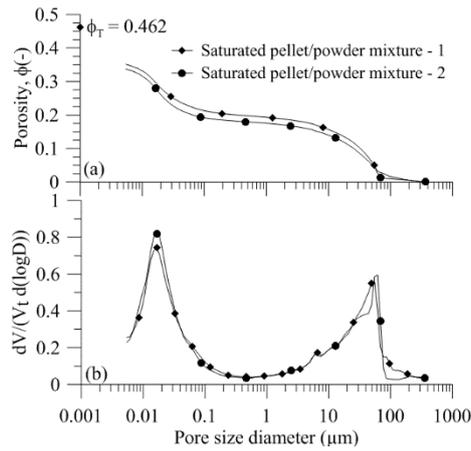
Fig. 7. MIP test results for two specimens of saturated pellet/powder mixture.
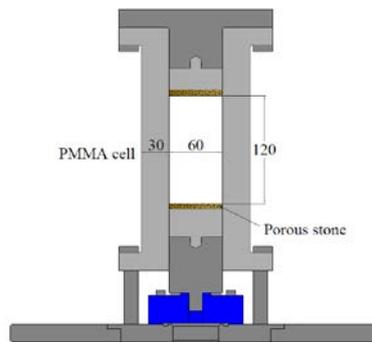

Fig. 8. Layout of the PMMA cell.
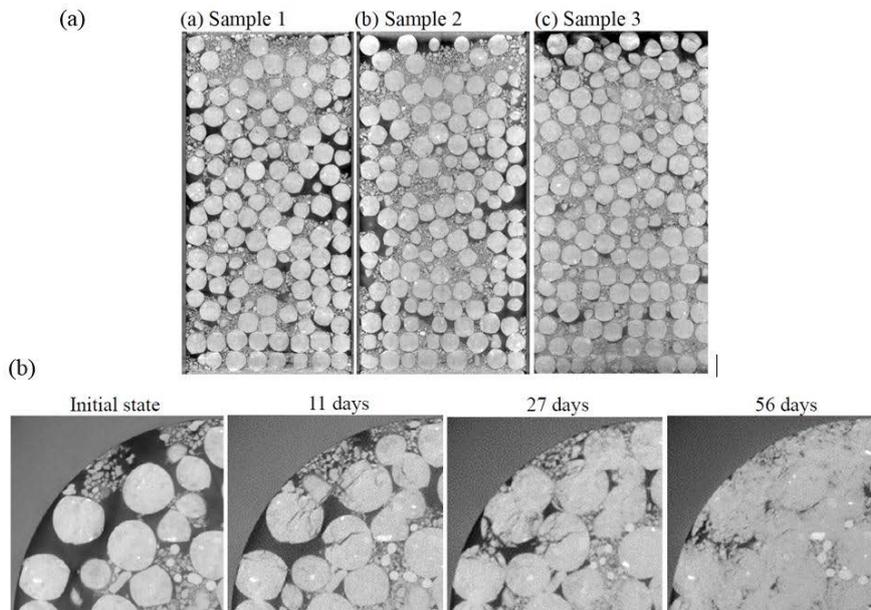
Fig. 9. (a) µ-CT observations (vertical slices) of three different pellet/powder bentonite mixtures (image's resolution is 50 µm/voxel). (b) Zoom at 60 mm from the bottom of the sample 1 at different times.

3. HM behavior of the mixture in 1/10 mock-up test

A 1/10 mock-up test was performed in order to investigate the long-term behavior of the bentonite pellet/powder mixture upon hydration. The layout of the small-scale infiltration stainless steel cell is presented in Fig. 10. The constant-volume conditions are ensured by a rigid structure. The material is saturated from both the top and the bottom.
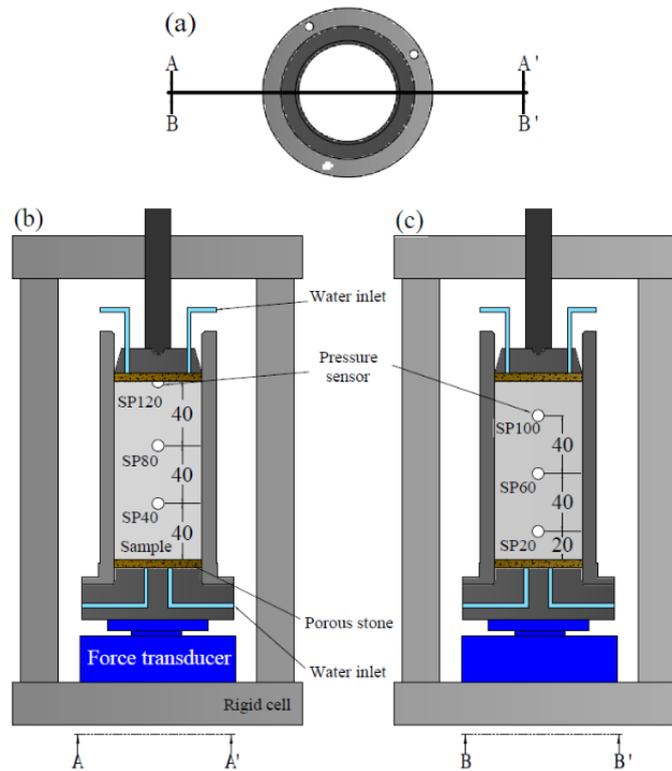

Figure 10. Layout of the small-scale mock-up test.

Six total pressure sensors measure the radial swelling pressure at different positions in the cell: h = 20, 40, 60, 80 and 100, namely SP20, SP40, SP60, SP80 and SP100, respectively. This configuration allows investigating the evolution of the swelling pressure at different positions, which is crucial for monitoring the evolution of dry density. A force transducer was installed under the cell base to monitor the axial swelling pressure. Due to the use of stainless steel cell, no µ-CT scans were possible for the initial state characterisation.

Fig. 11 shows the evolution of swelling pressure at different positions after 200 days of hydration. A heterogeneous evolution of swelling pressure is observed, which is due to the distance to the hydration front and the initial heterogeneous pellet/powder distribution. The difference observed between the radial and axial swelling pressure after 200 days of hydration could be attributed to the presence of larger inter-pellet voids at the top of the sample.

154
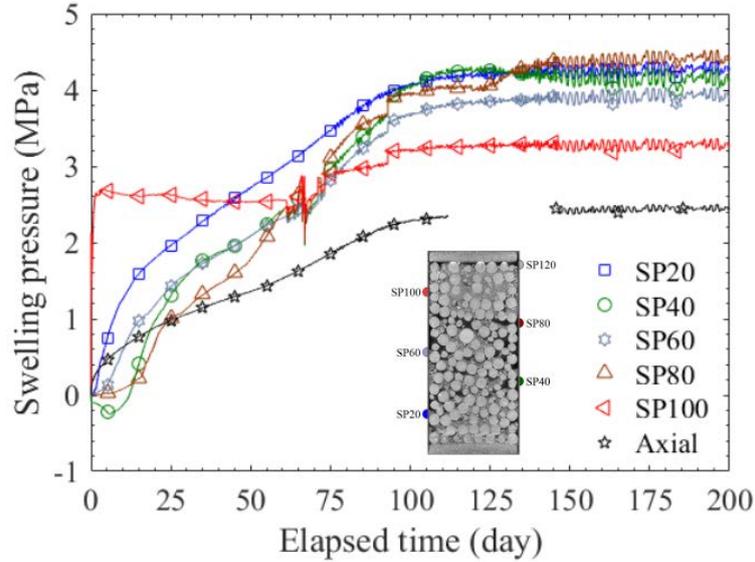
Fig. 11. Evolution of swelling pressure with time for the pellet/powder bentonite mixture after 200 days of hydration.

4. A double structure HM model accounting for initial heterogeneity and swelling damage

Mechanical constitutive equations

The model is based on the distinction within the material of two dominant pore levels (macro and micro pores). This distinction allows accounting for the phenomena that affect each pore level and the interaction between them (e.g. Gens & Alonso 1992; Alonso *et al*., 2011; Gens *et al*., 2011).

The macro-pores are considered to be partially filled with liquid phase. The macroscopic transport of liquid takes place in the macro-pores, which are called flowing pores. The total porosity is defined as the sum of macro-porosity ϕ_M and microporosity ϕ_m.

The basic idea of the model is the appropriate representation of the macro-porosity in each finite element assuming that the micro-porosity is homogenously distributed. The resulting field has the same mean porosity as the tested mixture. This allows accounting for the initial heterogeneous structural distribution. The spatial variations of total porosity and of dry density within the material are thus represented.

For each finite element a macroscopic volumetric deformation is computed form the mean macro void ratio e_M^{mean} (Alonso *et al*. 2006):

$$e_M^{mean} = \frac{\phi_M}{1-\phi_M} \qquad (1)$$

155

$$\varepsilon_v^M = -\frac{e_M - e_M^{mean}}{1 + e_M^{mean}} \tag{2}$$

To represent the mechanical behavior of the material, a double structure elasto-plastic model for expansive clays is adopted (e.g. Gens and Alonso 1992; Sanchez *et al.* 2005; Gens *et al.* 2011). The model considers deformations at macro- and micro-structural levels, and the coupling between them. The model assumes that for the macro-structural level, both elastic and plastic stains can develop as a result of stress and suction changes. The behavior of the macro-structural level is defined by the Barcelona Basic Model (BBM) (Alonso *et al.*, 1990).

Considering a heterogeneous distribution of macro-porosity, the hardening parameter is defined for each finite element as follows:

$$P_0^* = P_{0_{mean}}^* exp \left(\frac{1 + e_M^{mean}}{\lambda(s) - k} \varepsilon_v^M \right) \tag{3}$$

$$\lambda(s) = \lambda(0)\left[r + (1 - r)e^{-\beta s} \right] \tag{4}$$

where $\lambda(s)$ is the slope of the virgin consolidation line at suction s, $\lambda(0)$ is the slope of the virgin saturated consolidation line, p_o^* the saturated preconsolidation pressure, p_c a reference stress, r and β model parameters.

A fundamental assumption of the framework is that microstructural behavior is independent of the macrostructural state and only responds to changes in suction and stress at microstructural level. The mechanical behavior at microstructural level is controlled by mean effective stress defined as (e.g. Gens & Alonso 1992; Alonso *et al.*, 2011; Gens *et al.*, 2011):

$$\hat{p} = (p + s) \tag{5}$$

where p is the net stress and s is suction.

The line corresponding to the constant microstructural mean stress in plane (*p-s*) is referred to as neutral line (NL) since no microstructural deformation occur when the stress path moves on it (Fig 12a). The NL line divides the plane into two parts, defining two main generalized stress paths identified as: microstructural swelling (MS) when there is a decrease in $\hat{p}$ and microstructural compression (MC) when there is an increase in $\hat{p}$.
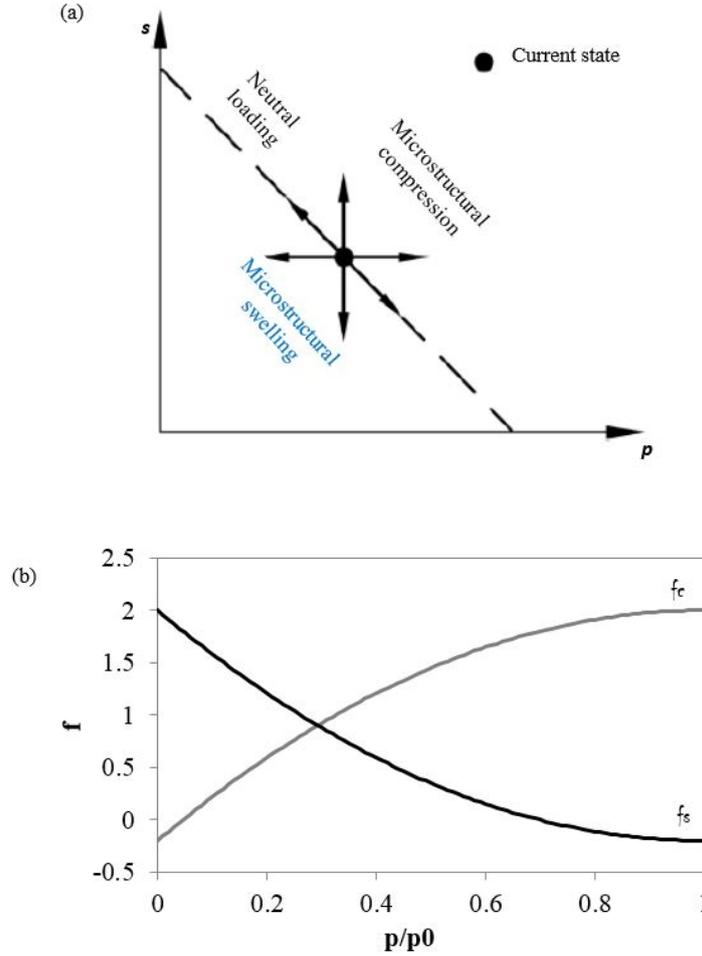
Fig. 12. Double structure deformation model for expansive clays: (a) microstructural model; (b) interaction functions.

In order to account for crack generation while wetting (Fig 3 and 9b), a damage coefficient D is defined as the ratio of generated porosity corresponding to cracks within a single pellet (pores with an average diameter higher than 3 µm) to the total porosity of the pellet at a given suction:

$$D(s) = \frac{\beta_d \, ln(\alpha_d s^2 + 1)}{(s + p_{atm})^{\beta_d / \alpha_d}} \qquad (6)$$

where α_d, β_d parameters of the model are, s is suction and p_{atm} is the atmospheric pressure.

The evolution of D as a function of suction is displayed in Fig. 13. Each point in Fig. 13 corresponds to a single pellet equilibrated from the initial state to a desired suction. The fitting curve using Equation 6 is also shown in the figure. The results show that D is dependent on the suction imposed. It increases with decreasing suction, reaching a maximum value at $s = 4$ MPa. At this stage the pellet has degraded and lost his initial geometry (Figure 9b) and no more cracks develop for lower suctions when reaching saturation.

157

The microstructural elastic volumetric strain incorporating pellets damage is expressed as:

$$d\varepsilon_{vm}^e = \frac{d\hat{p}}{K_m^*} = \frac{d(p+s)}{(1-D)K_m} \tag{7}$$

where e_m is the microstructural void ratio, $\hat{p}$ is the mean effective stress for microstructure, p is the net stress and s is the suction.
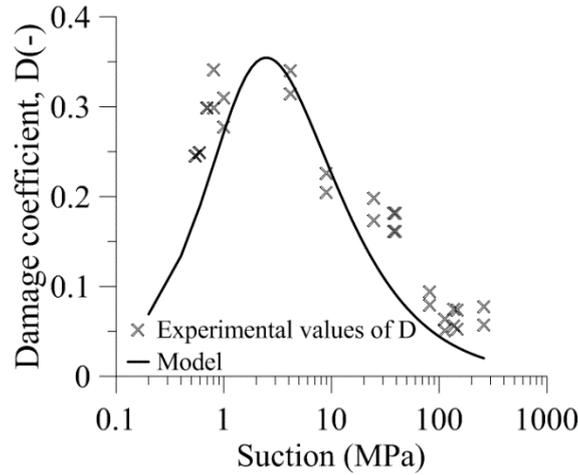

Fig. 13. Damage coefficient D - experimental results and model fitting.

The microstructural bulk modulus, K_m, is defined as:

$$K_m = \frac{1+e_m}{\kappa_m}(p+s) \tag{8}$$

where κ_m is a model parameter.

The measured and calculated (Equation 7) microstructural volumetric strain at different suction values are compared in Fig. 14 together with a model fitting at $D = 0$. Clearly, the non-consideration of damage ($D = 0$) fails in predicting the pellets swelling deformation.

The macrostructural deformations are affected by the microstructural deformations in an irreversible way (Gens and Alonso 1992). A hypothesis of the model is that the plastic deformations of the macrostructure induced by microstructural effects are proportional to the microstructural strain according to the interaction functions f_α. Two interaction functions f_α are defined in case of suction decrease (MS) and suction increase (MC) (Fig. 12b), respectively. In this study, the following form is used:

$$f_\alpha = f_{\alpha 0} + f_{\alpha i}\left(1 - \frac{p}{p_0}\right)^{n_\alpha} ; \quad \alpha = s(\text{swelling}), \quad c(\text{contraction}) \qquad (9)$$

The interaction functions depend on the ratio p/p_0, with p_0 as the yield mean net stress at the current macrostructural suction value.
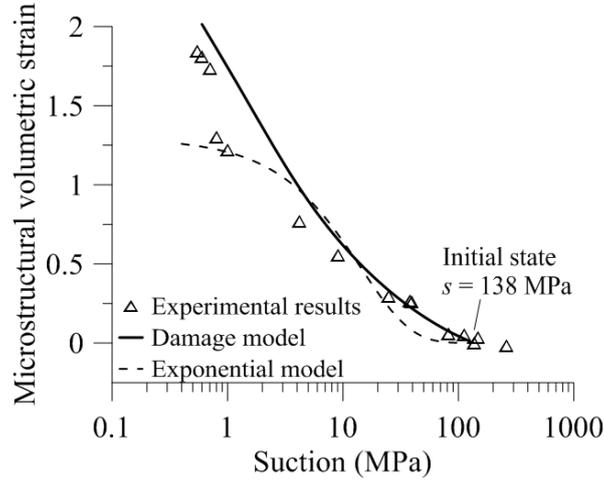

Fig. 14. Microstructural volumetric strain evolution upon wetting under free swelling conditions of MX80 bentonite pellets. Experimental data and the proposed damage model.

The total plastic macrostructural strain (ε_{vM}^p) is obtained as the sum of the inelastic deformations of microstructure through the interaction mechanism, and the plastic deformations (ε_{vLC}^p) induced when yielding of macrostructure takes place (when the stress path reaches the Loading Collapse, LC curve defined in BBM model):

$$d\varepsilon_{vM}^p = d\varepsilon_{vLC}^p + f_\alpha d\varepsilon_{vm}^e \qquad (10)$$

Hydraulic constitutive equations

The formulation assumes that the microstructural level is saturated even at relatively high suctions, which can be supported by the high affinity of the active clay minerals by water. The macro-pores are considered to be partially filled with the liquid phase. In this work, hydraulic equilibrium between the two continua is assumed.

Advective fluxes governed by Darcy's law, are expressed as function of macrostructural permeability:

$$q = -\frac{k_M k_{rM}}{\mu_M}(\nabla p + \rho_{wM} g \nabla z) \qquad (11)$$

where q is the mass liquid flow (with respect to the solid phase), k_M is macrostructural intrinsic permeability, k_{rM} is the relative permeability that expresses the effect of degree of saturation on global permeability, μ_M is the liquid viscosity, ρ_{wM} is water density and g is gravity.

The dependency of intrinsic permeability on macroporosity is assumed as:

$$k = k_0 \frac{\phi_M^3}{(1-\phi_M)^2} \frac{(1-\phi_0)^2}{\phi_0^3} \tag{12}$$

where ϕ_M is the macro-porosity and k_0 is the reference intrinsic permeability at a reference porosity ϕ_0.

The dependency of relative permeability on degree of saturation is expressed as:

$$k_{rM} = S_e^n \tag{13}$$

where n is a material parameter and S_e^n is the effective degree of saturation defined as:

$$S_e = \frac{S_r - S_{lr}}{S_{ls} - S_{lr}} \tag{14}$$

where S_r is the degree of saturation, S_{lr} is the residual degree of saturation and S_{ls} is the degree of saturation in saturated conditions.

The water retention model adopted for the macrostructure is a modification of the expression proposed by Van Genuchten (1978):

$$S_e = \frac{S_r - S_{rl}}{S_{sl} - S_{rl}} = \left(1 + \left(\frac{s}{P_0} \right)^{\frac{1}{1-\lambda}} \right)^{-\lambda} \tag{15}$$

where s is suction and P_0, λ are model parameters.

5. Modelling the 1/10 mock-up test

The numerical analysis has been performed with a modified version of Code_Bright (Olivella *et al*., 1996) which incorporates the double structure elasto-plastic model for heterogenous expansive clays and damage equations.

Determination of HM parameters

The HM parameters of the model were determined from a series of laboratory tests performed on the MX80 bentonite pellet/powder mixture (80-pellets/20-powder in dry mass).

The hydraulic parameters are summarized in Table 1. Variation of intrinsic permeability with porosity (Equation 12) have been derived from permeability tests performed on compacted MX80 bentonite compacted at different dry densities (Karland *et al.*, 2008 and Dixon *et al.* 1996). Fig. 15 shows the experimental measurements together with the model fitting (Equation 12). The reference intrinsic permeability adopted is $k_0 = 4.94 \times 10^{-21} \text{ m}^2$ for a reference macro-porosity $\phi_M = 0.269$.

Table 6. Hydraulic parameters.

| Constitutive law	Parameter	Units	Value
Retention curve $$S_e = \frac{S_l - S_{lr}}{S_{ls} - S_{lr}} = \left(1 + \left(\frac{P_g - P_l}{P_O}\right)^{\frac{1}{1-\lambda}}\right)^{-\lambda}$$	P_o λ S_{ls} S_{rl}	MPa - - -	4.026 0.26 1 0.01
Intrinsic permeability $$k_j = k_o \frac{\phi^3}{(1-\phi)^2} \frac{(1-\phi_o)^2}{\phi_o^3}$$	k_o ϕ_o ϕ_{min}	m^2 - -	4.94e-21 0.269 0.01
Relative permeability $$k_{rj} = S_{ej}^\lambda$$	λ S_{ls} S_{lr}	- - -	3 1 0.01

Fig. 15. Intrinsic permeability variation of MX80 pure bentonite with macroporosity: experimental results (Karland *et al.*, 2008 and Dixon *et al.* 1996) and model fitting.

The water retention curve under constant-volume conditions was obtained for the pellet/powder mixture prepared at a dry density of 1.49 Mg/m^3 , using a special set-up which allows imposing suctions to specimens of 50 mm diameter and 35 mm height by vapor transfer. The experimental results are displayed in Fig. 16, together with the model fitting (Equation 15).
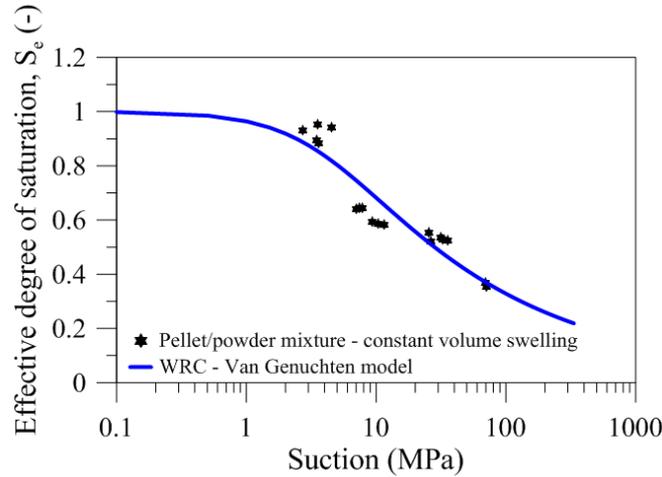

Fig. 16. Water retention curve of a MX80 bentonite pellet/powder mixture prepared at dry density of 1.49 Mg/m^3 under constant-volume conditions - experimental data and model fitting

The parameters for the mechanical behavior are summarized in Table 2. The microstructural volume deformation (Equation 7) has been calibrated using the experimental data on free swelling of single pellet at different suctions (Fig. 14). The microstructural parameter defining the microstructural bulk modulus used to calibrate the experimental data was estimated to κ_m = 0.06 (Fig. 14). The parameters for the damage description (Equation 6) were estimated at α_d = 0.58, β_d = 0.6 (Fig. 13).
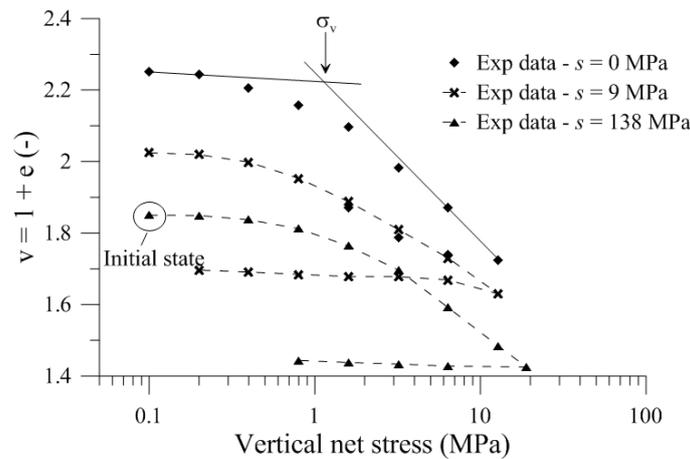

Fig. 17. Results from suction controlled oedometer tests on MX80 pellet/powder bentonite mixture (80/20) prepared at a dry density equal to 1.49 Mg/m^3.

The swelling and compressibility parameters for the macrostructure were determined using the results from suction-controlled oedometer tests. Three tests were performed on specimens of bentonite/pellet mixture prepared at $\rho_d = 1.49$ Mg/m^3 (Fig. 17). Each test consisted of a wetting path followed by a loading/ unloading path. The obtained results were used to derive the compressibility parameters (κ, λ) (Table 2).

Table 7. Mechanical parameters.

Constitutive law	Parameter	
Macrostructure		
Elastic part $d\varepsilon_{vM}^e = \left(\dfrac{\kappa}{1+e_M}\right)\dfrac{dp}{p} + \left(\dfrac{\kappa_s}{1+e_M}\right)\dfrac{ds}{s+p_{atm}}$	κ κ_s	0.028 0.001
Yield locus $p_0 = p_c\left(\dfrac{p_o^*}{p_c}\right)^{\frac{\lambda(0)-\kappa}{\lambda(s)-\kappa}}$ $\lambda(s) = \lambda(0)\left[r + (1-r)e^{-\beta s}\right]$	$p_o^*: MPa$ $p_c: MPa$ r $\lambda(0)$ $\beta: MPa^{-1}$	1.737 0.6 0.75 0.222 0.1
Microstructure		
Microstructural behavior $K_m^* = \dfrac{1+e_m}{\kappa_m}\hat{p}$	κ_m	0.04
Damage model $K_m^* = (1-D)K_m; D(s) = \dfrac{\beta_d \ln(\alpha_d s^2 + 1)}{(s+p_{atm})^{\frac{\beta_d}{\alpha_d}}}$	α_d β_d	0.58 0.6
Interaction function (micro-swelling) $f_s = f_{so} + f_{s1}\left(1 - \dfrac{p}{p_o}\right)^{n_s}$	f_{so} f_{s1} n_s	-0.3 2.19 2.4
Interaction function (macro-swelling) $f_c = f_{co} + f_{c1}\left(\dfrac{p}{p_o}\right)^{n_c}$	f_{co} f_{c1} n_c	-0.29 2.19 0.5

Geometry and boundary conditions

The 1/10 mock-up test is simulated using the proposed model outlined above and the hydro-mechanical parameters summarized in Tables 1 and 2. The HM coupled analysis has been performed on a 3-D finite element geometry (Fig. 18). A mechanical boundary condition restraining displacement is assigned at the outer surfaces of the model domain. A water pressure of 0 MPa is imposed at the top and the bottom of the geometry to simulate hydration of the sample.

163
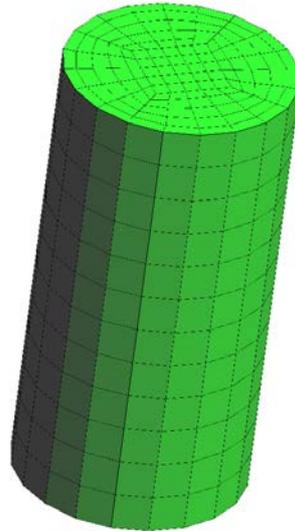
Fig. 18. Model geometry and mesh.

Estimation of the initial heterogeneous porosity field

Since no µ-CT observations were performed on the sample tested within the stainless steel mock up cell, estimations of initial heterogeneous porosity fields were undertaken by image analysis of µ-CT scans carried out on three MX80 bentonite pellet/ powder mixtures prepared at $\rho_d = 1.49$ Mg/m^3 and $s = 138$ MPa and tested within a PMMA mock up cell (**Erreur ! Source du renvoi introuvable.**). The technique of microfocus X-ray computed tomography uses X-ray projections of the same sample at many different angles allowing reconstructing a three-dimensional view of the sample. The visualized parameter is the linear X-ray attenuation coefficient represented as a grey level. This parameter depends on the density, the atomic number and the used Xray energy. The latter parameter is kept constant when scanning the bentonite at several time intervals. To derive correlation between mean grey levels and density (Fig. 19), reference elements with known density consisting of two glass spheres and an element of aluminium were introduced into the mixture of MX80 bentonite and pellets (Van Geet *et al*. 2005). To quantify porosity distribution, mean grey value corresponding to each finite element was calculated then converted into apparent density using the calibration presented in Figure 19.

Fig. 2 displays initial heterogeneous porosity fields of the three scanned samples. For the three cases, the experimental variograms are shown in Fig. 21. Covariance function was calculated along the sample axis to get insight into the impact of the preparation protocol (the samples were prepared by placing layer by layer the mixture into the cell) on porosity distribution.

A non-stationary variogram is obtained for sample 3. For samples 1 and 2 no spatial correlation is observed beyond 30 mm (sample 1) and 22 mm (sample 2), indicating a random distribution of porosity within the remaining domain of samples, which confirms that preparing samples at the same mean dry density with the same preparation protocol does not ensure similar spatial distribution of porosity within the mixture.
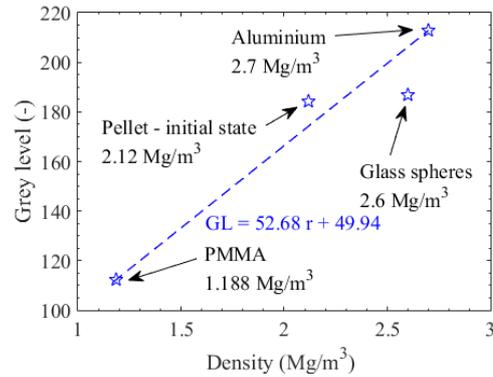

Fig. 19. Correlation plot between density and grey level obtained from the µ-CT observations.
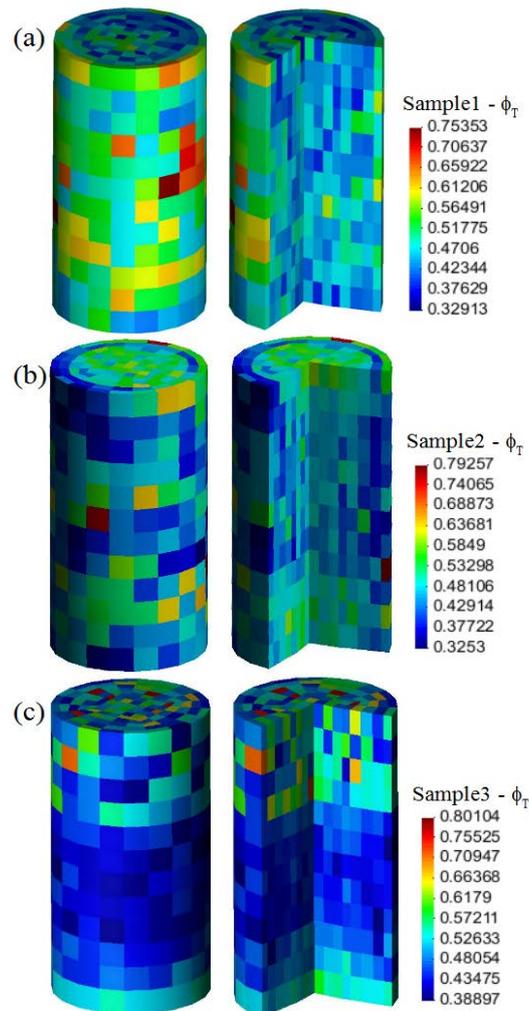

Fig. 20. Initial total porosity of the three samples.
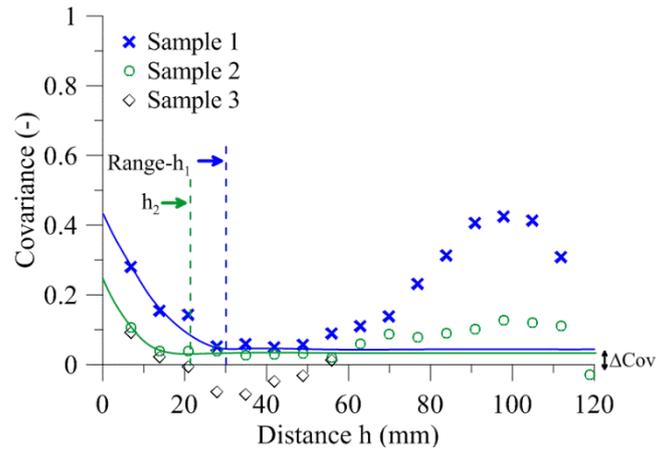
Fig. 21. Covariance of the total porosity following the vertical direction of the three investigated samples - variogram.

Modelling results

The estimated porosity fields were used to simulate the 1/10 mock-up test. The measured and predicted axial and radial swelling pressure evolutions for the three cases are displayed in Fig. . For completeness, the homogeneous case with no spatial variation of porosity (constant porosity equal 0.462) is compared to the results. Interestingly, the model predictions in case 1 (sample 1) appears to satisfactorily match the experimental results, except of sensor SP100. This indicates that the porosity field in this case corresponds to the best estimate of the structural distribution of the sample. In general, the rate and the magnitude of the swelling pressure are overestimated in cases 2, 3 and in the homogenous case. In spite of the highly heterogeneous structural distribution, the pattern of behavior is very similar in all positions (except at SP 100). The swelling pressure increases with different rates depending on the distance to the hydration front then reaches a nearly stationary value after 200 days. At SP100 located at 20 mm from the top hydration front, the swelling pressure increased very rapidly and reached a peak of about 2.1 MPa (Fig. 23). After about 5 hours a significant decrease of the swelling pressure occurred towards a minimum value of 1.5 MPa (Fig. 23). The swelling pressure increased again at slower rate and reached a value of 2.55 MPa after 60 days. Afterwards, the swelling pressure increased and stabilized at 3.3 MPa after 200 days (Fig. 22). The peak occurrence followed by a decrease of the swelling pressure corresponds to the reorganisation of the microstructure characterized by the collapse of the macrospores between the bentonite grains.
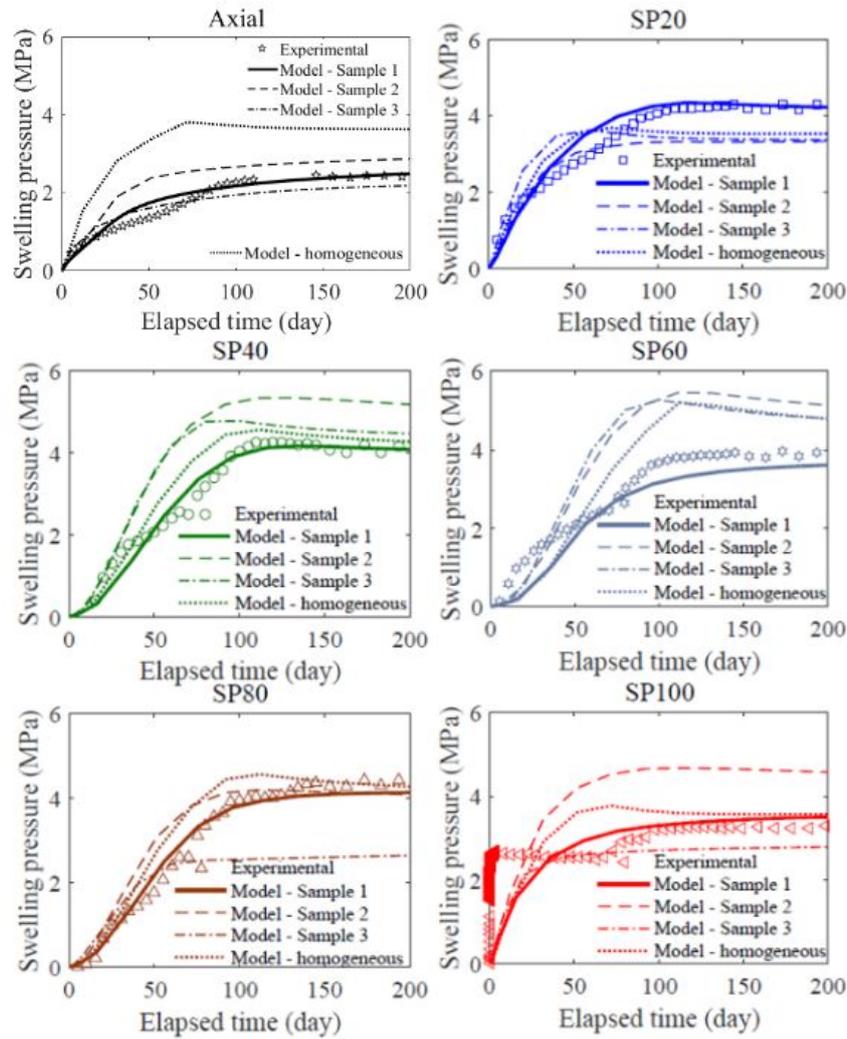
Fig. 22. Evolution of swelling pressure at different positions for the mock-up test together with model results of three different samples and a homogenous case.
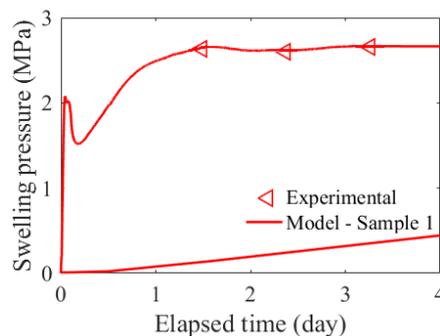
Fig. 23. Evolution of radial swelling pressure at SP100 during the first four days - experimental and modelling results.

The final values of radial swelling pressure are in the range of 3.3 to 4.4 MPa. It is worth noting that the radial swelling pressure measurements are strongly influenced by the local microstructural distribution at the vicinity of the sensors. The non-peak occurrence at SP40,

SP60, and SP80 suggest that the sensors were placed in zones where high density pellets are tightly arranged with a few or no grains of bentonite powder in between (Fig. 24). Similar trends were observed for the axial swelling pressure but with a lower final value of about 2.45 MPa. No macrostructural collapse is observed in this case indicating that collapse in some zones is compensated by the non-collapsing behavior of other zones.

The radial and axial swelling pressures are not identical. The final values of radial swelling pressure are in the range of 3.3 to 4.4 MPa while a lower final value of about 2.45 MPa is reached for the axial swelling pressure. A high anisotropic coefficient Ca ($C_a = p_h/p_v$) ranging from 1.25 to 1.65 is obtained. This anisotropy is a consequence of the highly heterogeneous microstructural distribution of the mixture.

As the modelling of case 1 appears to be the most satisfactory, interesting information might be obtained by analyzing in more detail some of the modelling results.
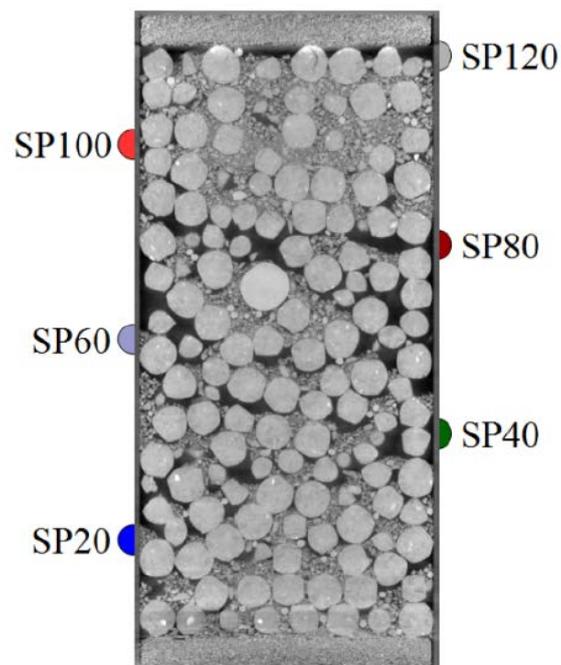
Fig. 24. Vertical section of sample 1 with the position of the radial swelling pressure sensors.

Fig. 25 displays the calculated macro- and micro-porosities at initial state and after 200 days along three radial lines at 20mm (R20), 60 mm (R60) and 100 mm (R100) from the bottom hydration face. Initially, different distributions of macro-porosity are observed along the three profiles with a concentration of large macro-pores at the sample boundary. Upon hydration there is a reduction of macro-spores while the microstructure is expanding. It has to be noted that the evolution of the macro-porosity results from two competitive phenomena. Cracking of

168

the pellets during swelling induces an increase of macro-pores. Simultaneously, the macro-pores are progressively invaded by the swollen bentonite particles. After 200 days, the macro-porosoty is reduced progressively, with a concentration of large macro-pores within the central zone at R20 and R100. On the contrary, at R60 although the difference between the central part and the boundary reduces, large macro-pores are still located at the sample boundary.
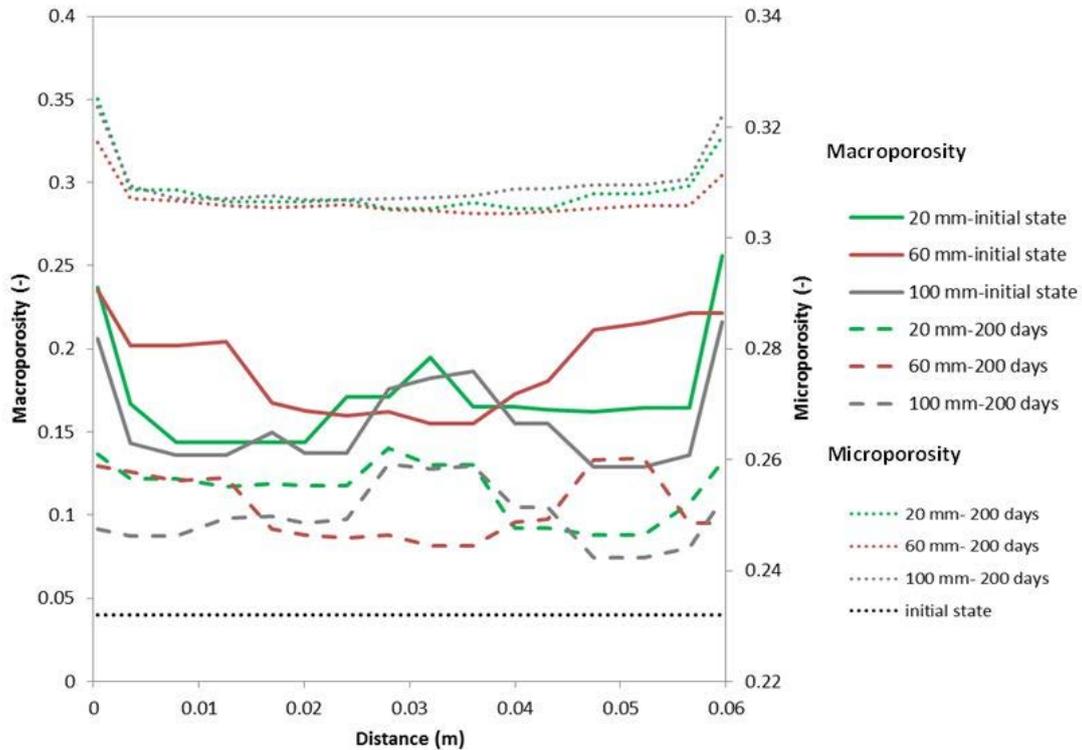
Figure 25. Profiles of macro- and micro-porosities for sample 1 at different positions and times.

In order to explore the long term homogenization of the mixture, the radial profiles (R20, R60 and R100) and distributions of dry density at different times (0, 200 and 5000 days) and sections are displayed in Figs. 26 and 27, respectively. A heterogeneous distribution of dry density is observed. For a given hydration time, at R20 and R60 and R100 low densities prevail at the outer boundaries due the concentration at this zone of large macro-pores (Fig. 25). Dry density increases progressively deeper within the sample with a minimum value toward the central zone. An inverse gradient is observed along R60 further from the hydration ends where dry density increases progressively toward the center of the sample. As saturation progresses, the density gradients decrease but, at 5000 days, there are still remaining differences over the cross-sections of the sample (Fig. 27). After 5000 days of hydration, along R20, ρ_d values range from 1.47 Mg/m^3 to 1.63 Mg/m^3, while along R60, ρ_d values range from 1.52 Mg/m^3 to 1.63 Mg/m^3.
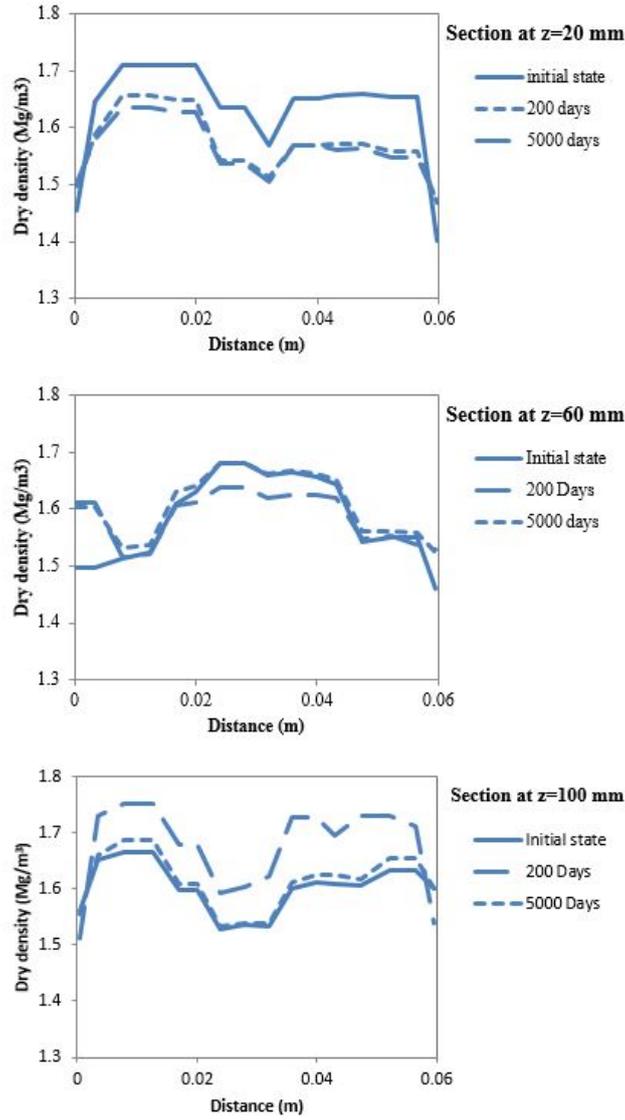
Fig. 26. Profiles of dry density for sample 1 at different positions after 200 days and 5000 days of hydration.
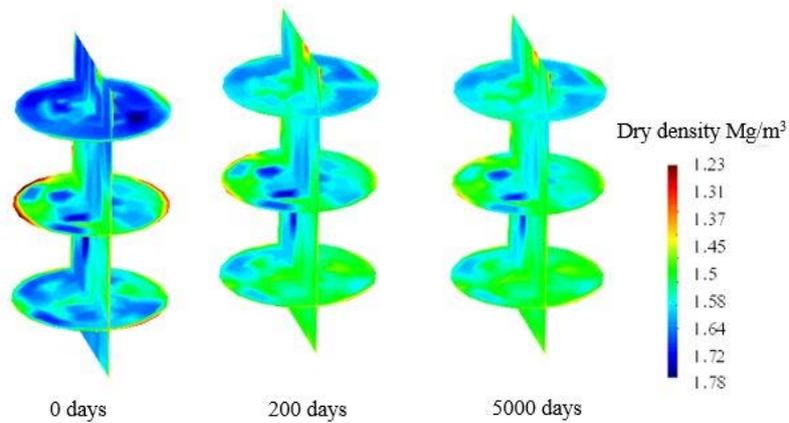
Fig. 27. Contours of dry density at different hydration times.

Interesting information on the hydration process can be obtained by analysing the impact of the heterogeneous structural distribution on intrinsic permeability (k). Fig. 28 shows the distributions of k at different times (0, 200 and 5000 days). At early hydration times, higher permeability is predicted at the outer boundaries of the sample due to the localisation of large macro-pores in this zone. This tendency is reversed when, under constant-volume conditions, the progressive clogging of macro-pores due to microstructural swelling leads to a potentially large reduction in intrinsic permeability, which significantly delays the mixture hydration. At long term (after 5000 days), the permeability gradients within the sample are reduced but still exist over the cross-sections of the sample (Fig. 28).
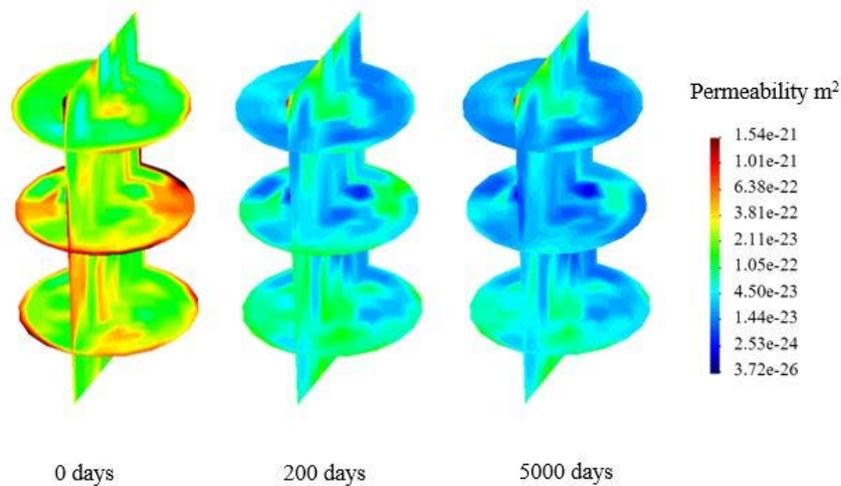
Fig. 28. Contours of permeability at different hydration times.

Mesh size effect

Porosity field estimation being linked to the model Finite Element (FE) mesh, three different mesh sizes have been considered to analyse their possible influence on modelling results. Two porosity distribution fields of sample 1 were determined by considering two different mesh sizes (coarser and more refined mesh than for case 1). Fig. 29 shows a horizontal section of sample 1 and the FE nodes corresponding to the two FE meshes.

Fig. depicts the evolution of swelling pressure for the two additional cases together with case 1. No significant differences are observed, indicating that the size mesh effect is negligible.
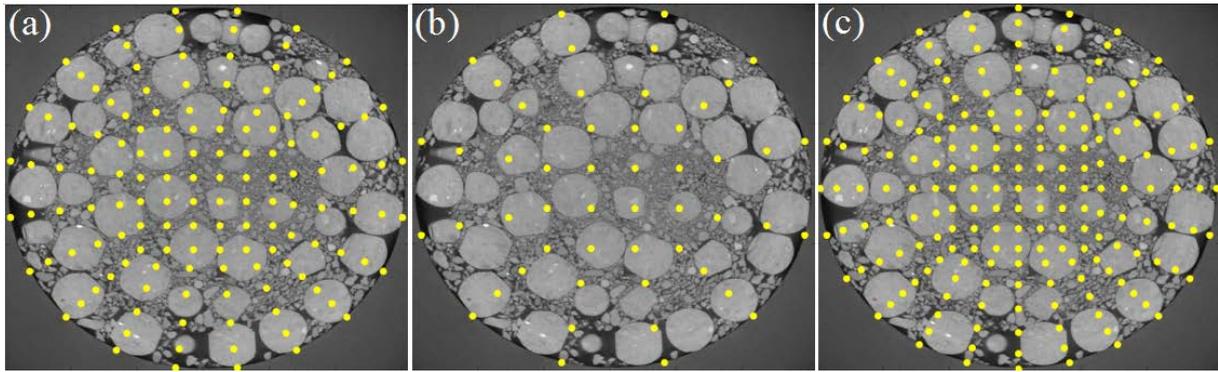
Fig. 29. Horizontal section of the sample 1 and finite element nodes corresponding to three finite element meshes used in the analysis.
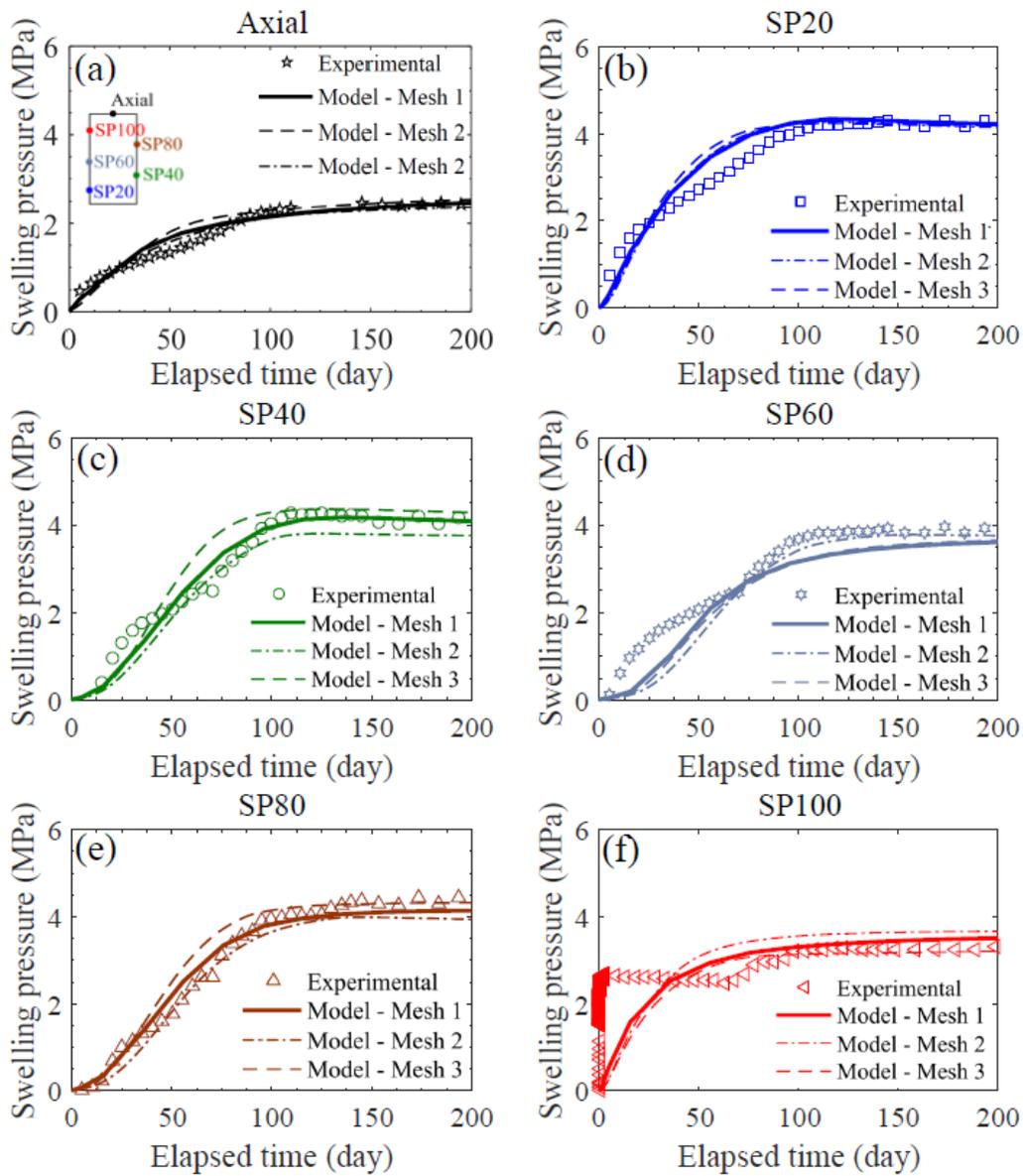
Fig. 30. Evolution of the swelling pressure at different positions with time -experimental data and model results with different mesh sizes.

6. Concluding remarks

The HM behavior of MX80 bentonite pellet/powder mixture (80/20 in dry mass) intended as sealing material in underground repositories for nuclear waste was analysed by using a double structure formulation which considers the initial heterogeneous structural distribution of the mixture and the pellets wetting-induced damage. The model parameters were determined based on the laboratory experimental results. The proposed model was then used to simulate a 1/10 scale mock-up test. In order to ensure a good representation of the test initial conditions, the initial heterogeneous distribution of bentonite pellets/powder mixture was appropriately estimated from μ-CT observations. The analysis carried out has demonstrated a number of interesting features.

The evolution rates of axial swelling pressure was significantly lower than the radial ones. This difference is attributed the initial heterogeneous structural distribution associated with the fabrication of the bentonite mixture sample. Model results demonstrated the long term heterogeneous distribution of dry density. As hydration progresses, even though a decrease in dry density gradients is observed, there are still remaining differences in dry density over the cross section of bentonite mixture after almost 13 years of hydration. The swelling anisotropy is found to be well preserved at long term. Additionally, the remaining dry density gradients induce differences in hydraulic conductivity which should be considered in the evaluation of long term performance.

References

Alonso, E.E., Gens, A., Josa, A., (1990). A constitutive model for partially saturated soils. Géotechnique 40 (3), 405–430.

Alonso, E.E., Gens, A., Josa A., (1999). Modelling the mechanical behavior of expansive clays. Eng Geol 54 :173-183.

Alonso, E.E., Olivella, S., Arnedo D., (2006). Mechanisms of gas transport in clay barriers.Journal of iberian geology 32 (2), 175-196.

Alonso, E.E., Romero, E. & Hoffmann, C., (2011). Hydromechanical behavior of compacted granular expansive mixtures: experimental and constitutive study. *Géotechnique*, 61(4), pp.329–344.

Barnichon, J.D., Deleruyelle, F., (2009). Sealing Experiments at the Tournemire URL. EUROSAFE.

Dixon, D.A., Gray, M.N., Graham, J., (1996). Swelling and hydraulic properties of bentonites from Japan, Canada and USA. In Proceedings of the second International Congress on Environmental Geotechnics, Osaka, Japan, pages 5–8.

Gens, A., Vallejan, B., Sánchez, M., Imbert, C., Villar, M.V., Van Geet, M., (2011). Hydrome- chanical Behavior of a Heterogenous Compacted Soil: Experimental Observations and Modelling

Gens, A. & Alonso, E.E., (1992). A framework for behavior of unsaturated expansive clays. *Canadian Geotechnical Journal*, 29, pp.1013–1032.

Imbert, C. & Villar, M.V., (2006). Hydro-mechanical response of a bentonite pellets/powder mixture upon infiltration. *Applied Clay Science*, 32(3-4), pp.197–209.

Karnland, O., Nilsson, U., Weber, H., and Wersin, P., (2008). Sealing ability of Wyoming bentonite pellets foreseen as buffer material-Laboratory results. *Physics and Chemistry of the Earth*, Parts A/B/C, 33:S472–S475.

Lloret, A., Villar, M.V., Sanchez, M., Gens, A., (2007). Advances on the knowledge of the thermo-hydro-mechanical behavior of heavily compacted "FEBEX" bentonite. Phys. Chem. Earth 32, 701–715.

Lloret, A., Villar, M.V., Sanchez, M., Gens, A., (2003). Mechanical behavior of heavily compacted bentonite under high suction changes. Geotechnique 53 (1), 27–40.

Molinero-Guerra, A., Mokni, N., Delage, P., Cui, Y. J., Tang, A. M., Aimedieu, P., Bernier, F., Bornert, M., (2016). In-depth characterisation of a mixture composed of powder/pellets MX80 bentonite. Applied Clay Science (135), 538 – 546.

Mokni, N. & Barnichon, J.D., (2016). Hydro-mechanical analysis of SEALEX *in situ* tests- Impact of technological gaps on long term performance of repository seals. Engineering Geology, 205, pp. 81-92.

Mokni, N., (2016). Analysis of hydro-mechanical behavior of compacted bentonite/sand mixture using a double structure formulation. Environ Earth Sci (2016) 75: 1087. https://doi.org/10.1007/s12665-016-5872-2

Olivella, S., Gens, A., Carrera, J., Alonso, E.E., (1996). Numerical formulation for a simulator (CODE_BRIGHT) for the coupled analysis of saline media. Eng. Comp. 13, 87–112.

Pusch, R., (1979). Highly compacted sodium bentonite for isolating rock-deposited radio-active waste products. Nucl. Technol. 45 (2), 153–157 (United states).

Saba, S., Delage, P., Lenoir, N., Cui, Y.J., Tang, A.M., Barnichon, J.D., (2014). Further insight into the microstructure of compacted bentonite/sand mixture. Eng. Geol. 168, 141–148.

Saba, S., Cui, Y.J. and Barnichon, J.D., (2014a). Investigation of the swelling behavior of compacted bentonite–sand mixture by mock-up tests. Canadian Geotechnical Journal, 51(12), pp.1399–1412.

Saba, S., (2014). *Hydro-mechanical* behavior *of bentonite-sand mixture used as sealing materials in radioactive waste disposal galleries*. Université de Paris Est.

Sanchez, M., Gens, A., Guimaraes, L., Olivella, S., (2005). A double structure generalized plasticity model for expansive materials. Int J Numer Anal Methods Geomech 29(8):751-787.

Van Geet, M., Volckaert, G. & Roels, S., (2005). The use of microfocus X-ray computed tomography in characterising the hydration of a clay pellet/powder mixture. *Applied Clay Science*, 29(2), pp.73–87.

Villar, M.V., Gómez-Espina, R., Campos, R., Barrios, I., Gutiérrez-Nebot, L., (2012). Porosity changes due to hydration of compacted bentonite. In: Manusco, C., Jommi, C., DÓnza, F. (Eds.), Unsaturated Soils: Research and Applications vol. 1. Springer, Berlin, pp. 137–144.

Villar, M.V., (2008). Thermo-hydro-mechanical characterisation of a bentonite from Cabo de Gata. A Study Applied to the Use of Bentonite as SealingMaterial in High Level Radioactive Waste Repositories. Publicación Técnica ENRESA 01/2002, Madrid (258 pp.).

Wang, Q., Tang, A.M., Cui, Y.J., Delage, P., Gatmiri, B., (2012). Experimental study on the swelling behavior of bentonite/claystone mixture. Eng. Geol. 124, 59–66. http://dx.doi.org/10.1016/j.engeo.2011.10.003.

WANG Q., TANG A.M., CUI Y.J., BARNICHON J.D. YE W.M. 2013. Investigation of the hydro-mechanical behavior of compacted bentonite/sand mixture based on the BExM model. Computer and Geotechnics 54, 46-52.

Wieczorek, K., Gaus, I., Mayor, J.C., Schuster, K., J. L. García-Siñeriz, J.C., and Sakaki, T., (2017). *In situ* experiments on bentonite-based buffer and sealing materials at the Mont Terri rock laboratory (Switzerland), Swiss J. Geosci., vol. 110, no. 1, pp. 253–268.

Yang D.Q., Alonso E.E., Rahardjo, H., (1998). Modelling volumetric behavior of an unsaturated expansive soil. In: 2nd international conference on unsaturated soils, Beijing, China, vol 2, pp 249-254.

Yong, R.N., Boonsinsuk, P.,Wong, G., (1986). Formulation of backfill material for a nuclear fuel waste disposal vault. Can. Geotech. J. 23 (2), 216–228.

Conclusions

CONCLUSIONS

The hydro-mechanical behavior of a pellet/powder MX80 bentonite mixture with a proportion 80/20 in dry mass has been investigated at different scales. The first part of this work consisted on characterizing the material at both micro- and macro-scales. To this end, several experiments were carried out, allowing an overall analysis of the HM behavior of a single pellet of bentonite and the mixture. Mercury Intrusion Porosimetry (MIP) tests combined with μ-CT observations of a single pellet at different suctions provided interesting results concerning the changes of microstructure occurring during wetting within a pellet. Water retention properties were also investigated in free-swell condition and in constant-volume condition using a specially designed cell that allows vapor exchanges in all directions. For the pellet/powder mixture, swelling pressure tests, water retention tests and suction controlled oedometer tests allowed studying different fundamental properties of the material. In parallel, two small scale (1/10) mock-up tests of the SEALEX *in situ* experiments were carried out. Two extreme cases were considered: a homogeneous pellet/powder mixture fabricated by following a special protocol, and a strong heterogeneous mixture. The purpose was to study the influence of the pellet/powder distribution on the HM behavior of the seal. Results were compared to the SEALEX *in situ* experiments. A special cell was designed in order to carry out μ-CT observations of these two mixtures and investigate the fabric evolution and structural changes while wetting. Finally, the experimental results on a single pellet of bentonite were used in order to develop a damage model which considers the fissures network observed while wetting. The mock-up tests were simulated by using a double porosity model (Barcelona Expansive Model, BExM), taking into account this new damage model together with the initial heterogeneous porosity network of the mixture. The following conclusions can be drawn from the work.

Microstructure and fabric changes

At initial state, a pellet of bentonite is characterized by a single pore population with an average entrance diameter of 11.9 nm. Another pore population at diameters around 4-5 μm develops while wetting. It corresponds to cracks within the pellet due to swelling. Therefore, along the wetting path, swelling of a single pellet is due to the combined effect of crack propagation at the macro-scale, with significant development between 38 and 9 MPa of suction, and of the swelling of bentonite grains, which is governed by the hydration mechanisms of smectite at nano-scale. The application of suctions below 9 MPa corresponds to a significant decrease of the platelet thickness and to an increase in the disorder of the platelet assembly.

178

µ-CT observations of the pellet/powder mixture revealed that the material is characterized by an initial granular structure with a heterogeneous pellet/powder distribution. While wetting, pellets in contact to the hydration fronts lose instantaneously its shape, becoming a homogeneous mixture. For the rest of the specimen, this process depends on the distance to the hydration front combined to the pellet/powder distribution. Fissures were observed within a pellet prior to losing their granular shape due to swelling. A homogeneous sample was observed after 100 days of hydration, where all the inter-pellet voids were completely sealed. Quantitative analysis of the results revealed the absence of density gradients within the specimen at the studied resolution (50 µm/voxel) after this long time hydration.

Water retention properties

Similar water retention properties were observed for pellet/powder mixture under constant-volume condition and pellet under free swelling condition at suctions higher than 4 MPa. This suggests that physico-chimical suction prevails on capillary suction, the effect of the latter being negligible. Moreover, the swell of clay particles was accommodated by existing macro-pores in the mixture. On the contrary, at lower suctions, constant-volume condition defined a lower water retention capacity because of the disappearance of macro-pores in this case.

Compressibility properties

Lower yield stress values than the common pure bentonite mixtures were found for the pellet/powder mixture, except for the specimen hydrated at zero suction. This is due to the granular structure for cases of non-zero suction, where the volume change behavior is governed by the rearrangement and crushing of pellets, and the loss of the granular structure in the case of zero suction.

Physical modelling – mock-up tests

The HM behavior of the pellet/powder mixture was investigated by terms of mock-up tests. The radial and axial swelling pressure, as well as relative humidity were measured during wetting. Two different specimens, fabricated at the same global dry density (1.49 Mg/m^3), were investigated: the first one was fabricated by following a special protocol, which ensures a homogeneous pellet/powder distribution, while the second one was designed to study a strong heterogeneous mixture, composed by a bottom denser part where all the inter-pellet voids were filled with powder grains, and a top loser part only made of pellets. Even if the global dry density is the same, different responses were obtained. The evolution of the radial swelling

pressure is strongly influenced by the local pellet/powder distribution combined with the distance to the hydration front. An anisotropy swelling behavior was identified in both tests, as the axial swelling pressure is lower than the radial one. This anisotropy is more pronounced in the case of heterogeneous sample, due to the higher initial heterogeneity in terms of dry density distribution within the mixture. Moreover, the axial swelling pressure was different for both tests even though they were fabricated at the same global dry density, which means that it depends also on the pellet/powder distribution.

Constitutive and numerical modelling

A new damage model which takes into account the fissures observed by µ-CT observations while wetting within a pellet of bentonite was developed. This new model considers that swelling of a single pellet is the combination of two phenomena, swelling of bentonite grains and development of fissures. It is based on the experimental results obtained by MIP tests combined to µ-CT observations on a single pellet while wetting. This new model was included into the well-known double porosity model BExM (Barcelona Expansive Model) to carry out numerical simulations of the mock-up test. In addition, the initial heterogeneous porosity distribution was considered, which allows correctly reproducing the heterogeneous swelling pressure evolution while wetting, as well as the anisotropy swelling.

This model will allow to understand the long term behavior of the SEALEX *in situ* experiments, as well as the existence of possible density gradients within the pellet/powder mixture, which is a crucial aspect in order to verify the safety of the storage.

References

REFERENCES

Abdullah, I., Mhaidib, A., (1998). Prediction of swelling potential of an expansive shale. Proceedings Of The Second International Conference On unsaturated soils. 27–30 August. Beijing, China, vol. 1.

Abdullah, I., Mhaidib, A., (1999). Swelling behavior of expansive shales from the middle region of Saudi Arabia. Geotechnical and Geological Engineering 16 (4), 291–307.

Agus, S. S. & Schanz T., (2005). Effect of shrinking and swelling on microstructures and fabric of a compacted bentonite-sand mixture. *Proceedings of the international conference on problematic soils*, Cyprus, 2, 543–550.

Aitemin, (2012). "SEALEX Project (Tests of Seal Performance): Implementation of *in situ* tests at the Tournemire Experimental Station LOT 2 : Dispositif de confinement / étanchéité , FEASIBILITY AND PERFORMANCE TEST FOR EMPLACEMENT OF Prepared for : IRSN, France.

Alonso, E.E., Gens, A., Josa, A., (1990). A constitutive model for partially saturated soils. Géotechnique 40 (3), 405–430.

Alonso, E.E., Vaunat, J. and Gens, A., (1999). Modelling the mechanical behavior of expansive clays. Engineering Geology, 54(1-2), pp.173–183.

Alonso, E.E., Romero, E., Hoffmann, C., & Garcia-Escudero, E., (2005). Expansive bentonite-sand mixtures in cyclic controlled-suction drying and wetting. *Engineering Geology*, 81(3), pp.213–226.

Alonso, E.E., Olivella, S., Arnedo D., (2006). Mechanisms of gas transport in clay barriers.Journal of iberian geology 32 (2), 175-196.

Alonso, E.E., Romero, E. and Hoffmann, C., (2011). Hydromechanical behavior of compacted granular expansive mixtures: experimental and constitutive study. *Géotechnique*, 61(4), pp.329–344.

ANDRA, 2005, Dossier (2005). Evolution phénoménologique du stockage géologique.Rapport Andra no. C.RP.ADS.04.0025, France.

Barnichon, J.D., Deleruyelle, F., (2009). Sealing Experiments at the Tournemire URL. EUROSAFE.

Barnichon, J.D., Dick, P. and Bauer, C., (2012). The SEALEX *in situ* experiments : Performance tests of repository seals. *Harmonising Rock Engineering and the Environment - Qian and Zhou (eds) Taylor and Francis Group, London*, pp.1391–1394.

Basma, A.A., Al-Homoud, A.S., Husein, A., (1995). Laboratory assessment of swelling pressure of expansive soils. Applied Clay Science 9 (5), 355–368.

Ben Rhaïem, H., Pons, C.H. & Tessier, D., (1987). Factors affecting the microstructure of smectites. Role of cation and history of applied stresses. Pp. 292?297 in: Proceedings of

the International Clay Conference, Denver, 1985 (L.G. Schultz, H. Van Olphen & F.A. Mumpton, editors). The Clay Minerals Society, Bloomington IN.

Bérend, I., Cases, J.M., François, M., Uriot, J.P., Michot, L., Masion, I.A. & Thomas, F., (1995). Mechanism of adsorption and desorption of water vapor by homoionic montmorillonites: 2. TheLi+,Na+,K+, Rb+and Cs+-exchangedforms.ClayClayMiner.43, 324–336.

Bestel, M., Gimmi, T., Glaus, M.A., Van Loon, L.R., Zamponi, M., Diamond, L.W. and Jurányi; F. (2013). Water distribution in Na- and Cs-Montmorillonite. Swiss Bentonite Metting, Bern, Switzerland.

Börgesson, L., Karnland, O. and Johannesson, L. E., (1996). Modelling of the physical behavior of clay barriers close to water saturation. Engineering Geology 41, No. 1–4, 127–144.

Bornert, M., Hild, F., Orteu, J.-J. and Roux, S. (2012). Chapter 6: digital image correlation. In: Full-field measurements and identification in solid mechanics. Grediac, M. & Hild, F. (Eds), Wiley-ISTE, 496 pages.

Cases, J.M., Berend, I., Besson, G., Francois, M., Uriot, J.P., Thomas, F., Poirier, J.E., (1992). Mechanism of adsorption and desorption of water vapor by homoionic montmoril- lonite. 1. The sodium-exchanged form. Langmuir 8, 2730–2739.

Cui, Y. J., Loiseau, C., & Delage, P., (2002). Microstructure changes of a confined swelling soil due to suction controlled hydration. Proc. 3rd Int. Conf. on Unsaturated Soils, Recife 2, 593–598.

Cui, Y.J., Tang, A.M., Loiseau, C., Delage, P., (2008). Determining the unsaturated hydraulic conductivity of a compacted sand–bentonite mixture under constant-volume and free-swell conditions. Physics and Chemistry of the Earth, Parts A/B/C 33 (Suppl. 1), S462–S471.

Cui, Y. J., Nguyen, X. P., Tang, A. M., and Li., X. L., (2013). An Insight into the Unloading/reloading Loops on the Compression Curve of Natural Stiff Clays. Applied Clay Science 83-84: 343–48.

Delage, P., Audiguier, M., Cui, Y.J. and Howat, M.D., (1996). Microstructure of a compacted silt. *Canadian Geotechnical Journal*, 33, pp.150–158.

Delage, P., Marcial, D., Cui, Y. J. and Ruiz, X., (2006). Ageing effects in a compacted bentonite: a microstructure approach. *Géotechnique*, 56(5), pp.291–304.

Delage, P., (2007). Microstructure Features in the Behavior of Engineered Barriers for Nuclear Waste Disposal. In *Experimental Unsaturated Soils Mechanics*, *Proc Int. Conf. on Mechanics of Unsaturated Soils,* 11-32, T. Schanz ed., Weimar, Germany, Springer.

Dereeper, B., Volckaert, G., Imbert, C., and Villar, M.V. (2001). Pellets/powder mixture of bentonite for backfill and sealing of HLW repositories. *Adadchi, K., Fukue, M. (Eds.), Clay Science for Engineering. Balkema, Rotterdam*, pp.487–490.

Dixon D. A. Gray M. N. & Graham J., (1996). Swelling and hydraulic properties of bentonites from Japan, Canada and the USA. Environmental Geotechnics 1, 43-48.

Duong, T. V., Tang, A. M., Cui, Y. J., Trinh, V. N., Dupla, J. C., Calon, N., Canou, J., and Robinet, A. (2013). Effects of fines and water contents on the mechanical behavior of interlayer soil in ancient railway sub-structure, *Soils Found.*, vol. 53, no. 6, pp. 868–878.

Ferrage, E., Lanson, B., Sakharov, B.A. & Drits, V.A., (2005). Investigation of smectite hydration properties by modeling experimental X-ray diffraction patterns: part I. Montmoril- lonite hydration properties. Am. Mineral. 90, 1358–1374.

Ferrage, E., Kirk, C.A., Cressey, G., & Cuadros, J., (2007). Dehydration of Ca-montmorillonite at the crystal scale. Part 2. Mechanisms and kinetics. Am Mineral 92(7):1007-1017.

Garcia-Siñeriz, J. L., Villar, M. V., Rey, M., and Palacios, B., (2015). Engineered barrier of bentonite pellets and compacted blocks: State after reaching saturation, Eng. Geol., vol. 192, pp. 33–45.

Gatabin, C., Talandier, J., Collin, F., Charlier, R. & Dieudonné, A. C., (2016). Competing effects of volume change and water uptake on the water retention behavior of a compacted mx-80 bentonite/sand mixture. Applied Clay Science 121–122, 57–62.

Gens, A., and Alonso, E.E., (1992). A framework for behavior of unsaturated expansive clays. *Canadian Geotechnical Journal*, 29, pp.1013–1032.

Gens, A., Vallejan, B., Sánchez, M., Imbert, C., Villar, M.V. and Van Geet, M., (2011). Hydro-mechanical Behavior of a Heterogenous Compacted Soil: Experimental Observations and Modelling.

Graham, J., Saadat, F., Gray, M. N., Dixon, D. A., & Zhang, Q. Y., (1989). Strength and volume change behavior of a sand-bentonite mixture. Canadian Geotechnical Journal 26, No. 2, 292- 305.

Herman, G.T. (1979). Correction for beam hardening in computed tomography. Physicsin Medicine andBiology, 24, 81.

Hoffmann Jauge, C.A., (2005). Caracterización hidromecánica de mezclas de pellets de bentonita. Estudio experimental y constitutivo.

Hoffmann, C., Alonso, E.E. and Romero, E., (2007). Hydro-mechanical behavior of bentonite pellet mixtures. *Physics and Chemistry of the Earth*, 32(8-14), pp.832–849.

IAEA (2009). Classification of radioactive waste. General safety guide. IAEA Safety Standards GSG-1, 68.

Imbert, C., and Villar, M.V., (2006). Hydro-mechanical response of a bentonite pellets/powder mixture upon infiltration. *Applied Clay Science*, 32(3-4), pp.197–209.

Jacinto, A.C., Villar, M.V. and Ledesma, A., (2012). Influence of water density on the water-retention curve of expansive clays. Géotechnique, 62(8), pp.657–667.

Josa, a., Alonso, E.E. and Gens, A., (1991). Discussion: A constitutive model for partially saturated soils. Géotechnique, 41(2), pp.273–275.

Karnland, O., Nilsson, U., Weber, Hanspeter, W., & Wersin, P., (2008). Sealing ability of Wyoming bentonite pellets foreseen as buffer material - Laboratory results. *Physics and Chemistry of the Earth*, 33(SUPPL. 1), pp.472–475.

Kawaragi, C., Yoneda, T., Sato, T. & Kaneko, K., (2009). Microstructure of saturated bentonites characterized by X-ray CT observations. *Engineering Geology*, 106(1-2), pp.51–57.

Komine, H., & Ogata, N., (1994). Experimental study on swelling characteristics of compacted bentonite. Canadian geotechnical journal 31 , No. 4, 478-490.

Kozaki, T., Suzuki, S., Kozai, N., Sato, S., & Ohashi, H., (2001). Observation of Microstructures of Compacted Bentonite by Microfocus X-Ray Computerized Tomography (Micro-CT). *Journal of Nuclear Science and Technology*, 38(8), pp.697–699.

Lloret, A., Villar, M.V., Sanchez, M., Gens, A., Pintado, X. and Alonso, E.E., (2003). Mechanical behavior of heavily compacted bentonite under high suction changes. , (1), pp.27–40.

Lloret, A., Villar, M.V., Sanchez, M., Gens, A., (2007). Advances on the knowledge of the thermo-hydro-mechanical behavior of heavily compacted "FEBEX" bentonite. Phys. Chem. Earth 32, 701–715.

Management Swedish Nuclear Fuel and Waste, (2002). Äspö Hard Rock Laboratory. Annual Report 2001.

Marcial, D., Delage, P., Cui, Y.J., (2002). On the high stress compression of bentonites. Canadian Geotechnical Journal 39, 812–820.

Marcial, D., (2003). Comportement hydromécanique et microstructural des matériaux de barrière ouvragée. (PHD thesis) École Nationale des Ponts et Chaussées, Paris, France.

Marcial, D., (2011). A simple method to consider water density changes in the calcualtion of the degree of saturation of swelling clays. In Unsaturated Soils: Proceedings of the Fitth International Conference on Unsaturated Soils, Barcelona, Spain, 6-8 september 2010. pp. 473-478.

Méring, J. & Glaeser, R., (1954). Sur le rôle de la valence des cations échangeables dans la montmorillonite. Bulletin de la Société Francaise de Minéralogie et Cristallographie, 77, 519−530.

Molinero-Guerra, A., Mokni, N., Delage, P., Cui, Y. J., Tang, A. M., Aimedieu, P., Bernier, F., & Bornert, M., (2016). In-depth characterisation of a mixture composed of powder/pellets MX80 bentonite. *Applied Clay Science*.

Mokni, N., (2016). Analysis of hydro-mechanical behavior of compacted bentonite/sand mixture using a double structure formulation. Environ Earth Sci (2016) 75: 1087. https://doi.org/10.1007/s12665-016-5872-2.

Mokni, N., and Barnichon, J.D. (2016). Hydro-mechanical analysis of SEALEX *in situ* tests-Impact of technological gaps on long term performance of repository seals. Engineering Geology, 205, pp. 81-92.

Montes G., Duplay J. & Martinez L., (2001). Study of bentonite swelling : qualitative and quantitative analysis using ESEM and digital image analysis program. 12th International Clay Conference, july 22-28, Bahia Blanca, Argentina.

Mooney, R. W., Keenan, A. C. & Wood, L. A., (1952). Adsorption of water vapor by montmorillonite. II. Effect of exchangeable ions and lattice swelling as measured from X-ray diffraction, J Amer Chem Soc 74:1371–1374.

NEA (2008). Moving forward with geological disposal of radioactive waste, a collective statement by the NEA Radioactive Waste Management Commitee (RWMC). Technical report, OECD – Nuclear Energy Agency.

Norrish, K., (1954). The swelling of montmorillonite. Discussions of the Faraday Society 18, 120–134.

OECD/NEA (1995). The environmental and ethical basis of geological disposal of long- lived radioactive wastes. ïA collective opinion of the Radioactive Waste Management Committee of the OECD Nuclear Energy Agency. Technical report, OECD – Nuclear Energy Agency.

Olivella, S., Gens, A., Carrera, J., Alonso, E.E., (1996). Numerical formulation for a simulator (CODE_BRIGHT) for the coupled analysis of saline media. Eng. Comp. 13, 87–112.

Pusch, R., (1979). Highly compacted sodium bentonite for isolating rock-deposited radioactive waste products. Nucl. Technol. 45 (2), 153–157 (United states).

Pusch, R. (1982). Mineral-water interactions and their influence on the physical behavior of highly compacted Na bentonite. Canadian Geotechnical Journal, 19(3): 381–387. doi:10.1139/t82-041.

Ridler, T.W. Calvard, S., (1978). Picture Thresholding Using an Iterative Slection Method. *IEEE Transactions on Systems, Man and Cybernetics*, 8(8), pp.630–632.

Ridley, A., Zdravkovic, L. and Monroy, R., (2010). Evolution of microstructure in compacted London Clay during wetting and loading. *Géotechnique*, 60(2), pp.105–119.

Romero, E., Della Vecchia, G. and Jommi, C., (2011). An insight into the water retention properties of compacted clayey soils. *Géotechnique*, 61(4), pp.313–328.

Saba, S., Delage, P., Lenoir, N., Cui, Y.J., Tang, A.M., Barnichon, J.D., (2014). Further insight into the microstructure of compacted bentonite/sand mixture. Eng. Geol. 168, 141–148.

Saba, S., Romero, E., *et al*., (2014). *Hydro-mechanical* behavior *of bentonite-sand mixture used as sealing materials in radioactive waste disposal galleries*. Université de Paris Est.

Saba, S., Cui, Y.J., Tang, A.M., and Barnichon, J.D., (2014). Investigation of the swelling behavior of compacted bentonite–sand mixture by mock-up tests. Canadian Geotechnical Journal, 51(12), pp.1399–1412.

Saba, S., Barnichon, J. D., Cui, Y. J., Tang, A. M. and Delage, P., (2014). Microstructure and anisotropic swelling behavior of compacted bentonite/sand mixture. *Journal of Rock Mechanics and Geotechnical Engineering*, 6(2), pp.126–132.

Saiyouri N., Hicher P.Y., Tessier D. (2000). Microstructural approach and transfer water modelling in highly compacted unsaturated swelling clays, Mech. Cohesive Frictional Mater 5:41–60.

Saiyouri, N., Tessier, D. & Hicher, P.Y., (2004). Experimental study of swelling in unsaturated compacted clays. *Clay Minerals*, 39(4), pp.469–479.

Salo, J.-P. and Kukkola, T., (1989). Bentonite pellets, an alternative buffer material for spent fuel canister deposition holes. *Workshop "Sealing of Radioactive Waster Repositories"*. *Braunschweig*.

Sanchez, M., Gens, A., Guimaraes, L., Olivella, S., (2005). A double structure generalized plasticity model for expansive materials. Int J Numer Anal Methods Geomech 29(8):751-787.

Schanz, T. and Al-Badran, Y., (2014). Swelling pressure characteristics of compacted Chinese Gaomiaozi bentonite GMZ01. Soils and Foundations 54, No. 4, 748–759.

Schuster, K., Furche, M., Velasco, M., Gaus, I., Trick, T., Garcia-Siñeriz, J. L., Rey, M., Schulte, F., Sanchez Herrero, S., Tietz, T. & Mayor, J. C., (2014). *Long-term Performance of Engineered Barrier Systems PEBS Engineered Barrier Emplacement Experiment in Opalinus Clay: "EB" Experiment.*

Seiphoori, A., Ferrari, A. & Laloui, L., (2014). Water retention behavior and microstructural evolution of MX-80 bentonite during wetting and drying cycles. *Géotechnique*, 64(9), pp.721–734.

Sellin, P., and Leupin, O. X., (2013). The use of clay as an engineered barrier in radioactive-waste management – a review. Clays and Clay Minerals 61, No. 6, 477–498.

Sugita, Y., Chijimatsu, M. and Suzuki, H., (2005). Fundamental properties of bentonite pellet for Prototype Repository Project. *In: Alonso, E. E., Ledesma, A. (Eds.), Advances in Understanding Engineered Clay Barriers. A. A. Balkema Publishers, Leiden*, pp.293–299.

Sun, W., Sun, D., Fang, L. & Liu, S., (2014). Soil-water characteristics of Gaomiaozi bentonite by vapor equilibrium technique. *Journal of Rock Mechanics and Geotechnical Engineering*, 6(1), pp.48–54.

Sutton, M.A., Orteu, J.J., and H. Schreier., H., (2009). Image correlation for shape, motion and deformation measurements: basic concepts, theory and applications. Springer Science & Business Media.

Svemar, C. & Pusch, R., (2000). Project description FIKW-CT-2000-00055, SKB International Progress Report IPR-00-30.

Tessier, D. (1990). *Matériaux argileux: Structure, Propriétés et Applications* (ed. A. Decarreau), Vol.1, 387–445. Paris: Société Française de Minéralogie et Cristallographie.

Van Geet, M., Volckaert, G. and Roels, S., (2005). The use of microfocus X-ray computed tomography in characterising the hydration of a clay pellet/powder mixture. *Applied Clay Science*, 29(2), pp.73–87.

Villar, M.V., Lloret, A., (2004). Influence of temperature on the hydro-mechanical behav- iour of a compacted bentonite. Applied Clay Science 26 (1–4), 337–350.

Villar, M.V., (2008). Thermo-hydro-mechanical characterisation of a bentonite from Cabo de Gata. A Study Applied to the Use of Bentonite as SealingMaterial in High Level Radioactive Waste Repositories. Publicación Técnica ENRESA 01/2002, Madrid (258 pp.).

Villar, M.V., Gómez-Espina, R., Campos, R., Barrios, I., Gutiérrez-Nebot, L., (2012). Porosity changes due to hydration of compacted bentonite. In: Manusco, C., Jommi, C., DÓnza, F. (Eds.), Unsaturated Soils: Research and Applications vol. 1. Springer, Berlin, pp. 137–144.

Villar, M. V., Gómez-Espina, R. and Guitiérrez-Nebot, L., (2012). Basal spacings of smectite in compacted bentonite. Applied Clay Science 65–66, 95–105.

Villar, M.V., (2013). EB experiment. Contribution of CIEMAT to EB dismantling report. Physical state of the bentonite. EC Contract 249681 PEBS. Informe Técnico CIEMAT/DMA/ 2G210/04/2013 (Madrid, 21 pp.).

Wan, M., Delage, P., Tang, A. M. & Talandier, J., (2013). Water retention properties of the Callovo-Oxfordian claystone. *International Journal of Rock Mechanics and Mining Sciences*, 64, pp.96–104.

Wang, L., (2012). Micromechanical experimental investigation and modelling of strain and damage of argillaceous rocks under combined hydric and mechanical loads.

Wang, Q., Tang, A.M., Cui, Y.J., Delage, P. and Gatmiri, B., (2012). Experimental study on the swelling behavior of bentonite/claystone mixture. Eng. Geol. 124, 59–66.

Wang, Q. & Cui, Y.J., Tang, A.M., Delage, P., Gatmiri, B. and Ye, WM., (2013). Long-term effect of water chemistry on the swelling pressure of a bentonite-based material. Applied Clay Science. 87. 10.1016/j.clay.2013.10.025.

WANG Q., TANG A.M., CUI Y.J., BARNICHON J.D. YE W.M. (2013). Investigation of the hydro-mechanical behavior of compacted bentonite/sand mixture based on the BExM model. Computer and Geotechnics 54, 46-52.

Wang, Q., Tang, A.M., Cui, Y.J., Barnichon, J.D. and Ye, W.M., (2013). A comparative study on the hydro-mechanical behavior of compacted bentonite/sand plug based on labora- tory and field infiltration tests. Eng. Geol. 162, 79–87.

Wang, Q., Cui, Y. J., Tang, A. M., Barnichon, J. D., Saba, S. and Ye, W. M., (2013). Hydraulic conductivity and microstructure changes of compacted bentonite/sand mixture during hydration. *Engineering Geology*, 164, pp.67–76.

Wang, Q., Cui, Y. J., Tang, A. M., Li, X. L. and Ye, W. M., (2014). Time- and density-dependent microstructure features of compacted bentonite. *Soils and Foundations*, 54(4), pp.657–666.

Wieczorek, K., Gaus, I., Mayor, J.C., Schuster, K., J. L. García-Siñeriz, J.C., and Sakaki, T., (2017). *In situ* experiments on bentonite-based buffer and sealing materials at the Mont Terri rock laboratory (Switzerland), Swiss J. Geosci., vol. 110, no. 1, pp. 253–268.

Yahia-Aissa, M. (1999). Comportement hydromécanique d'une argile gonflante fortement compactée. PhD thesis, Ecole Nationale des Ponts et Chaussées, CERMES, Paris, France (in French).

Yang D.Q., Alonso E.E., Rahardjo, H., (1998). Modelling volumetric behavior of an unsaturated expansive soil. In: 2nd international conference on unsaturated soils, Beijing, China, vol 2, pp 249-254.

Yahia-Aissa,M., Delage, P., Cui, Y.J., (2001). Suction–water relationship in swelling clays. Clay Science for Engineering. In: Adachi, K., Fukue,M. (Eds.), Proceedings of the IS-Shizuoka International Symposium on Suction, Swelling, Permeability and Structure of Clays. Shizuoka, Japan Balkema, pp. 65–68.

Ye, W.M., Cui, Y.J., Qian, L.X., Chen., B., (2009). An experimental study of the water transfer through confined compacted gmz bentonite. Engineering Geology 108 (3–4), 169–176.

Yong, R.N., Boonsinsuk, P.,Wong, G., (1986). Formulation of backfill material for a nuclear fuel waste disposal vault. Can. Geotech. J. 23 (2), 216–228.